

ANTI-OXIDANT AND ANTI-INFLAMMATORY COMPOUNDS FROM *Magnolia liliifera* (L.)
Baill. FLOWER AND *Dendrobium signatum* Rchb.f.



A Thesis Submitted in Partial Fulfillment of the Requirements
for the Degree of Master of Science in Chemistry
Department of Chemistry
FACULTY OF SCIENCE
Chulalongkorn University
Academic Year 2020
Copyright of Chulalongkorn University

สารออกฤทธิ์ต้านอนุมูลอิสระและต้านการอักเสบจากดอกมณฑา *Magnolia liliifera* (L.) Baill. และ
เอื้องเค้าก๊ว *Dendrobium signatum* Rchb.f.



วิทยานิพนธ์นี้เป็นส่วนหนึ่งของการศึกษาตามหลักสูตรปริญญาวิทยาศาสตรมหาบัณฑิต
สาขาวิชาเคมี ภาควิชาเคมี
คณะวิทยาศาสตร์ จุฬาลงกรณ์มหาวิทยาลัย
ปีการศึกษา 2563
ลิขสิทธิ์ของจุฬาลงกรณ์มหาวิทยาลัย

Thesis Title	ANTI-OXIDANT AND ANTI-INFLAMMATORY COMPOUNDS FROM <i>Magnolia liliifera</i> (L.) Baill. FLOWER AND <i>Dendrobium signatum</i> Rchb.f.
By	Mr. Prajak Khumploy
Field of Study	Chemistry
Thesis Advisor	Professor KHANITHA PUDHOM, Ph.D.

Accepted by the FACULTY OF SCIENCE, Chulalongkorn University in Partial
Fulfillment of the Requirement for the Master of Science

..... Dean of the FACULTY OF SCIENCE
(Professor POLKIT SANGVANICH, Ph.D.)

THESIS COMMITTEE

..... Chairman
(Professor VUDHICHAJ PARASUK, Ph.D.)

..... Thesis Advisor
(Professor KHANITHA PUDHOM, Ph.D.)

..... Examiner
(Associate Professor NATTAYA NGAMROJANAVANICH,
Ph.D.)

..... External Examiner
(Assistant Professor Wimolpan Rungprom, Ph.D.)

ประจักษ์ ชุมพลอย : สารออกฤทธิ์ต้านอนุมูลอิสระและต้านการอักเสบจากดอกมณฑา *Magnolia liliifera* (L.) Baill. และเอื้องคำกั่ว *Dendrobium signatum* Rchb.f.. (ANTI-OXIDANT AND ANTI-INFLAMMATORY COMPOUNDS FROM *Magnolia liliifera* (L.) Baill. FLOWER AND *Dendrobium signatum* Rchb.f.) อ.ที่ปรึกษาหลัก : ศ. ดร.ชนิษฐา พุดหอม

ในการศึกษาการแยกส่วนสกัดหยาบเอทิลแอสซิเทตจาก aerial parts ของเอื้องคำกั่ว *Dendrobium signatum* Rchb.f. สามารถแยกสารบริสุทธิ์ได้ 15 ชนิด (1-15) และ ส่วนสารสกัดหยาบเฮกเซนของดอกมณฑา *Magnolia liliifera* (L.) Baill สามารถแยกสารบริสุทธิ์ได้ 3 ชนิด (16-18) ได้แก่สารชนิดใหม่ในกลุ่ม microtoxane sesquiterpene, 7-hydroxydendroterpene B (2) และกลุ่ม α -pyrone, (-)-6*R*-signatone (4) ร่วมกับสารที่เคยค้นพบแล้วทั้งสิ้น 16 ชนิด ได้แก่ dendroxine (1), crystallin (3), dendrocandin B (5), dendrocandin I (6), 6"-de-*O*-methyl dendrofindlaphenol A (7), *p*-hydroxyphenylethyl-*p*-coumarate (8), 3,4-dihydroxy-5,4'-dimethoxybibenzyl (9), 3-methoxy-5-[2-(4-methoxyphenyl) ethyl]phenol (10), 4,4'-dihydroxy-3,5-dimethoxybibenzyl (11), naringenin (12), (2*S*)-homoeridodictyol (13), (2*S*)-homohesperetin (14), (-)-syringaresinol (15), (+) sesamin (16), (+) fargesin (17) และ (-) kobusin (18) โดยโครงสร้างทางเคมีของสารใหม่พิสูจน์ทราบด้วยเทคนิคทางสเปกโทรสโกปีและ single-crystal X-ray diffraction ในขณะที่สารที่เคยค้นพบแล้วได้ทำการพิสูจน์ทราบโดยการเปรียบเทียบกับข้อมูลจากงานวิจัยที่มีการรายงานมาก่อนหน้า จากนั้นได้นำสารบริสุทธิ์ที่แยกได้ทั้งหมดมาทดสอบฤทธิ์ในการต้านอนุมูลอิสระด้วยวิธี DPPH และ ABTS ซึ่งพบว่าสารบริสุทธิ์ใหม่ (-)-6*R*-signatone 4 มีแนวโน้มที่ดีมากในการต้านอนุมูล ABTS ด้วยค่า IC_{50} เท่ากับ $0.71 \pm 0.01 \mu M$ เมื่อเปรียบเทียบกับชุดควบคุมผลบวก Trolox[®] ซึ่งมีค่า IC_{50} เท่ากับ $27.26 \pm 0.33 \mu M$ นอกจากนี้สารกลุ่ม dimer bibenzyls กับสาร 3, 4, 8, 9, และ 17 ยังแสดงแนวโน้มในการยับยั้ง lipid peroxidation ในช่วง 53-70 % ในตัวอย่างสิ่งมีชีวิตที่ความเข้มข้น $5 \mu M$ สำหรับฤทธิ์ต้านการอักเสบ ผลการทดสอบแสดงให้เห็นว่าในบรรดาสารบริสุทธิ์ทั้งหมดที่ทดสอบฤทธิ์ยับยั้งการผลิตไนตริกออกไซด์ พบว่าสาร (-) kobusin 18 ในกลุ่มลิกันแนน เพิ่มการยับยั้งการผลิตไนตริกออกไซด์ได้เป็นอย่างดี ซึ่งมีค่า IC_{50} เท่ากับ $4.72 \pm 0.17 \mu M$ ในทำนองเดียวกับสาร *p*-hydroxyphenylethyl-*p*-coumarate 8 ในกลุ่มฟีนิลโพรพานอยด์ ที่แสดงการยับยั้งการผลิตไนตริกออกไซด์ได้สูงเช่นกัน ซึ่งมีค่า IC_{50} เท่ากับ $6.18 \pm 0.50 \mu M$ เมื่อเปรียบเทียบกับสารมาตรฐาน indomethacin (IC_{50} เท่ากับ $28.42 \pm 3.51 \mu M$)

สาขาวิชา เคมี
ปีการศึกษา 2563

ลายมือชื่อนิสิต
ลายมือชื่อ อ.ที่ปรึกษาหลัก

6172000623 : MAJOR CHEMISTRY

KEYWORD: ANTI-OXIDANT, ANTI-INFLAMMATORY, *Dendrobium signatum* Rchb.f., *Magnolia liliifera* (L.) Baill.

Prajak Khumploy : ANTI-OXIDANT AND ANTI-INFLAMMATORY COMPOUNDS FROM *Magnolia liliifera* (L.) Baill. FLOWER AND *Dendrobium signatum* Rchb.f.. Advisor: Prof. KHANITHA PUDHOM, Ph.D.

In this study, a purification of the EtOAc crude extract of *Dendrobium signatum* Rchb.f. aerial parts was performed fifteen compounds (1-15) and the hexane crude extracts of *Magnolia liliifera* (L.) Baill. were further isolated to accomplish three compounds (16-18). They yielded one new picrotoxane sesquiterpene, 7-hydroxydendroterpene B (2) and a new α -pyrone, (-)-6*R*-signatone (4), along with sixteen known compounds. These included dendroxine (1), crystallinin (3), dendrocandin B (5), dendrocandin I (6), 6''-de-*O*-methyl-dendrofindlaphenol A (7), *p*-hydroxyphenylethyl-*p*-coumarate (8), 3,4-dihydroxy-5,4'-dimethoxybibenzyl (9), 3-methoxy-5-[2-(4-methoxyphenyl) ethyl]phenol (10), 4,4'-dihydroxy-3,5-dimethoxybibenzyl (11), naringenin (12), (2*S*)-homoeridodictyol (13), (2*S*)-homohesperetin (14), (-)-syringaresinol (15), (+) sesamin (16), (+) fargesin (17) and (-) kobusin (18). Their structures of new compounds were elucidated through by analysis of spectroscopic data and single-crystal X-ray diffraction analysis, whereas those of the known ones were identified by comparison of their data in the literature. Afterward, all the extracted isolated compounds were evaluated for antioxidant activity using the DPPH and ABTS free radical scavenging assay. The results showed that the new (-)-6*R*-signatone 4 exhibited very promising ABTS scavenging activity with IC_{50} of $0.71 \pm 0.01 \mu M$ in comparison with a positive control Trolox[®] (IC_{50} of $27.26 \pm 0.33 \mu M$). Furthermore, the dimer bibenzyls (5-7) along with compounds 3, 4, 8, 9 and 17 were promising to inhibit the lipid peroxidation in range (53-70 %) in the vital model at concentration $5 \mu M$. For the anti-inflammatory activity, among all the compounds, it was found that lignans, (-) kobusin 18 (IC_{50} of $4.72 \pm 0.17 \mu M$) significantly enhanced the NO production inhibition activity. Similarly, phenylpropanoids, *p*-hydroxyphenylethyl-*p*-coumarate 8 also displayed the high potent inhibition with IC_{50} of $6.18 \pm 0.50 \mu M$ as compared to the standard indomethacin (IC_{50} of $28.42 \pm 3.51 \mu M$).

Field of Study: Chemistry

Student's Signature

Academic Year: 2020

Advisor's Signature

ACKNOWLEDGEMENTS

I wish to express my appreciation to my thesis advisor, Professor. Dr. Khanitha Pudhom, for the valuable guidance, endless support, and encouragement throughout this thesis. I would not have succeeded my thesis research without all the advice, kindness and helps that I have always received from her.

I would like to thank the Chairperson: Professor Dr. Vudhichai Parasuk, Department of Chemistry, Faculty of Science, Chulalongkorn University; the thesis examiners: Associate Professor Dr. Nattaya Ngamrojanavanich, Department of Chemistry, Faculty of Science, Chulalongkorn University, and Assistant Professor Dr. Wimonpan Rungprom, Faculty of Science and Technology, Department of Chemistry, Phranakhon Si Ayutthaya Rajabhat University for their invaluable discussion and suggestion.

I wish to thank the 90th Anniversary of Chulalongkorn University Fund (Ratchadaphiseksomphot Endowment Fund), the Research Assistantship Fund, Faculty of Science, Chulalongkorn University, and the Center of Excellence on Petrochemical and Materials Technology. I am grateful to the Ratchadapisek Sompoch Endowment Fund, Chulalongkorn University for the partial support of X-ray diffraction facility.

Special thanks to Dr. Siwattra Choodej for the anti-inflammatory test, Dr. Achara Raksat for the guidance of compounds elucidation and the member of KP Lab for their help and kind friendship.

Finally, I want to express my special gratitude to my family and friends for their love, support, and encouragement.

Prajak Khumploy

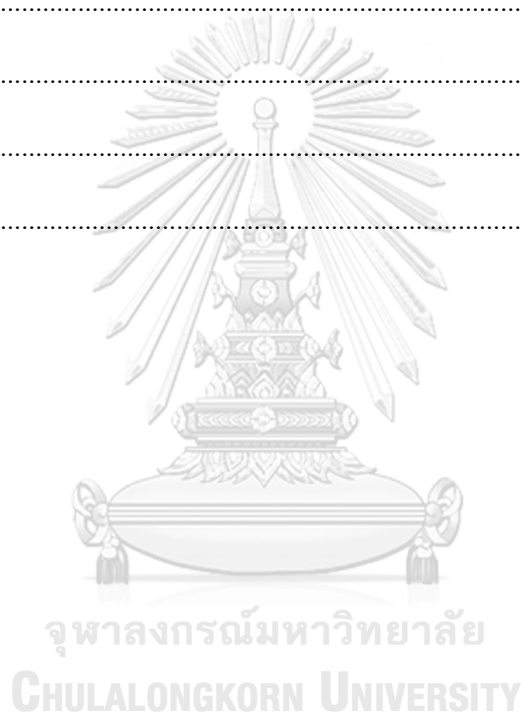
TABLE OF CONTENTS

	Page
ABSTRACT (THAI).....	iii
ABSTRACT (ENGLISH).....	iv
ACKNOWLEDGEMENTS	v
TABLE OF CONTENTS	vi
LIST OF FIGURES	x
LIST OF SCHEMES	xii
LIST OF TABLES	xiii
LIST OF ABBREVIATIONS	xv
CHAPTER I.....	1
1. Oxidative stress and free radicals	1
2. Oxidative stress-induced cellular damage	1
2.1 Protein	2
2.2 Lipids.....	3
2.3 DNA.....	3
3. Effects of oxidative stress on signal transduction.....	4
4. Oxidative Stress, Inflammatory and Diseases	5
5. Antioxidant.....	6
5.1 Mechanism of action of antioxidants.....	7
6. Secondary metabolites of plants.....	10
6.1 Chemical constituents of <i>Magnolia</i> and bioactivity	10
6.2 Chemical constituents of <i>Dendrobium</i> and biological activity	15

CHAPTER II.....	21
2.1 Plant Materials	21
2.2 General Experimental Procedures	21
2.2.1 Thin-layer chromatography (TLC).....	21
2.2.2 Column chromatography	21
2.2.3 Nuclear magnetic resonance spectroscopy (NMR).....	22
2.2.4 Mass spectrometry (MS)	22
2.2.5 Fourier transforms infrared spectrophotometry (FT-IR)	22
2.2.6 Optical Rotation	22
2.2.7 Melting Point.....	22
2.2.8 Ultraviolet-visible spectrophotometry (UV-vis).....	22
2.8.9 X-ray diffraction spectrometer	22
2.8.10 Microplate spectrophotometer	23
2.8.11 CO ₂ cell culture incubator.....	23
2.8.12 Biosafety cabinet	23
2.3 Chemicals.....	23
2.4 Extraction and isolation	23
2.4.1 Extraction of <i>D. signatum</i> aerial parts.....	23
2.4.2 Isolation of compounds from EtOAc crude extract.....	24
2.4.3 Extraction of <i>M. liliifera</i> flowers	30
2.4.4 Isolation of compounds from hexane crude extract	31
2.5 Biological activity evaluation	32
2.5.1 DPPH assay	32
2.5.2 ABTS assay.....	32

2.5.3 Lipid peroxidation inhibition assay	33
2.5.4 Nitric oxide inhibition assay	34
2.5.5 Cytotoxicity assay	35
CHAPTER III	36
3.1 Isolated compounds from <i>Dendrobium signatum</i> Rchb.f.	36
3.2 Structure elucidation of isolated compounds from <i>Dendrobium signatum</i> Rchb.f.	38
3.2.1 Structure elucidation of compound 1	38
3.2.2 Structure elucidation of compound 2	43
3.2.3 Structure elucidation of compound 3	48
3.2.4 Structure elucidation of compound 4	51
3.2.5 Structure elucidation of compound 5	54
3.2.6 Structure elucidation of compound 6	58
3.2.7 Structure elucidation of compound 7	62
3.2.8 Structure elucidation of compound 8	66
3.2.9 Structure elucidation of compound 9	68
3.2.10 Structure elucidation of compound 10	71
3.2.11 Structure elucidation of compound 11	74
3.2.12 Structure elucidation of compound 12	77
3.2.13 Structure elucidation of compound 13	80
3.2.14 Structure elucidation of compounds 14	83
3.2.15 Structure elucidation of compounds 15	86
3.3 Isolated compounds from <i>Magnolia liliifera</i> (L.) Baill.	89
3.4 Structure elucidation of isolated compounds from <i>Magnolia liliifera</i> (L.) Baill.	90

3.4.1 Structure elucidation of compound 16	90
3.4.2 Structure elucidation of compound 17	93
3.4.3 Structure elucidation of compounds 18.....	97
3.5 Free radical scavenging activity	100
3.6 Lipid peroxidation inhibition activity	105
3.7 Anti-inflammatory activity	107
CHAPTER IV	109
REFERENCES	111
APPENDIX.....	120
VITA.....	182



LIST OF FIGURES

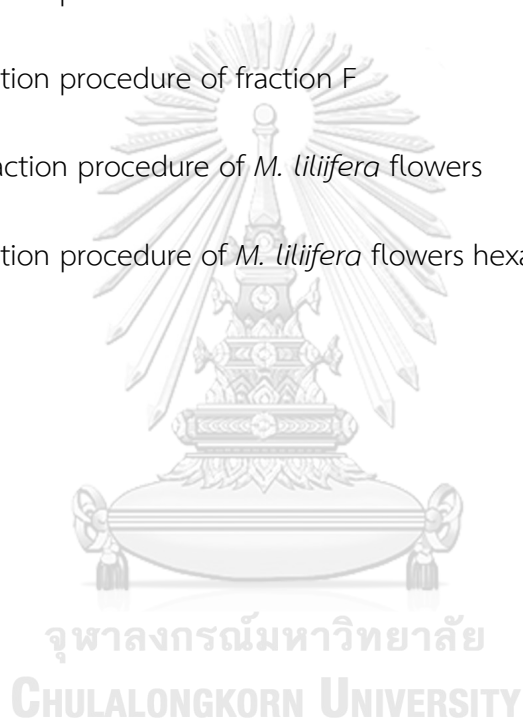
Figure 1.1 Oxidative stress and inflammation: imbalance of antioxidants and free radicals ¹	5
Figure 1.2 Reactions in the free radical chain oxidation mechanism ²	7
Figure 3.1 The chemical structures of isolated compounds from <i>D. signatum</i>	37
Figure 3.2 HMBC (a) and ¹ H- ¹ H COSY (b) correlations of compound 1	40
Figure 3.3 ¹ H- ¹ H NOESY correlations of compound 1	40
Figure 3.4 ORTEP diagram of compound 1	40
Figure 3.5 HMBC (a) and ¹ H- ¹ H COSY (b) correlations of compound 2	45
Figure 3.6 ¹ H- ¹ H NOESY correlations of compound 2	45
Figure 3.7 ORTEP diagram of compound 2	45
Figure 3.8 HMBC (a) and ¹ H- ¹ H COSY (b) correlations of compound 3	49
Figure 3.9 ¹ H- ¹ H NOESY correlations of compound 3	49
Figure 3.10 HMBC (a) and ¹ H- ¹ H COSY (b) correlations of compound 4	52
Figure 3.11 HMBC and ¹ H- ¹ H COSY correlations of compound 5	56
Figure 3.12 HMBC and ¹ H- ¹ H COSY correlations of compound 6	59
Figure 3.13 HMBC and ¹ H- ¹ H COSY correlations of compound 7	63
Figure 3.14 ¹ H- ¹ H NOESY correlations of compound 7	63
Figure 3.15 HMBC and ¹ H- ¹ H COSY correlations of compound 8	66
Figure 3.16 HMBC and ¹ H- ¹ H COSY correlations of compound 9	68
Figure 3.17 HMBC and ¹ H- ¹ H COSY correlations of compound 10	71
Figure 3.18 HMBC and ¹ H- ¹ H COSY correlations of compound 11	74
Figure 3.19 HMBC and ¹ H- ¹ H COSY correlations of compound 12	77
Figure 3.20 HMBC and ¹ H- ¹ H COSY correlations of compound 13	80
Figure 3.21 HMBC and ¹ H- ¹ H COSY correlations of compound 14	83
Figure 3.22 HMBC and ¹ H- ¹ H COSY correlations of compound 15	86
Figure 3.23 The chemical structures of isolated compounds from <i>M. lilifera</i>	88

Figure 3.24 HMBC and ^1H - ^1H COSY correlations of compound 16	90
Figure 3.25 HMBC and ^1H - ^1H COSY correlations of compound 17	93
Figure 3.26 HMBC and ^1H - ^1H COSY correlations of compound 18	97
Figure 3.27 The chemical structures (1-15) of isolated compounds from <i>D.signatum</i>	100
Figure 3.28 The chemical structures (16-18) of isolated compounds from <i>M. liliifera</i>	101
Figure 3.29 % Inhibition of lipid peroxidation of isolated compounds from <i>M. liliifera</i> and <i>D. signatum</i>	106



LIST OF SCHEMES

Scheme 2.1	Extraction of <i>D. signatum</i> stems	24
Scheme 2.2	Isolation procedure of fraction A	25
Scheme 2.3	Isolation procedure of fraction B	26
Scheme 2.4	Isolation procedure of fraction D	27
Scheme 2.5	Isolation procedure of fraction E	28
Scheme 2.6	Isolation procedure of fraction F	29
Scheme 2.7	Extraction procedure of <i>M. lilijfera</i> flowers	30
Scheme 2.8	Isolation procedure of <i>M. lilijfera</i> flowers hexane crude	31



LIST OF TABLES

Table 3.1 NMR data of compound 1 (CDCl ₃)	40
Table 3.2 Crystal data and structure refinement for compound 1	41
Table 3.3 NMR data of compound 2 (acetone- <i>d</i> ₆)	45
Table 3.4 Crystal data and structure refinement for compound 2	46
Table 3.5 NMR data of compound 3 (CDCl ₃) and crystallinin (acetone- <i>d</i> ₆)	49
Table 3.6 NMR data of compound 4 (CDCl ₃)	52
Table 3.7 NMR data of compound 5 and dendrocandin B (CDCl ₃)	55
Table 3.8 NMR data of compound 6 and dendrocandin I (CDCl ₃)	59
Table 3.9 NMR data of compound 7 (CDCl ₃) and 6"-de- <i>o</i> - methyldendrofindlaphenol A (methanol- <i>d</i> ₄)	63
Table 3.10 NMR data of compound 8 (acetone- <i>d</i> ₆) and <i>p</i> - hydroxyphenylethyl- <i>p</i> -coumarate (methanol- <i>d</i> ₄)	66
Table 3.11 NMR data of compound 9 and 3,4-dihydroxy-5,4'- dimethoxybibenzyl (CDCl ₃)	68
Table 3.12 NMR data of compound 10 and 3-methoxy-5-[2-(4- methoxyphenyl)ethyl]phenol (CDCl ₃)	71
Table 3.13 NMR data of compound 11 (CDCl ₃) and 4,4'-dihydroxy-3,5- dimethoxybibenzyl (acetone- <i>d</i> ₆)	75
Table 3.14 NMR data of compound 12 and naringenin (methanol- <i>d</i> ₄)	77
Table 3.15 NMR data of compound 13 (acetone- <i>d</i> ₆) and (2 <i>S</i>)- homoeridodictyol (methanol- <i>d</i> ₄)	80
Table 3.16 NMR data of compound 14 (methanol- <i>d</i> ₄) and (2 <i>S</i>)- homohesperetin (DMSO- <i>d</i> ₆)	83
Table 3.17 NMR data of compound 15 and (-) syringaresinol (CDCl ₃)	87
Table 3.18 NMR data of compound 16 and sesamin (CDCl ₃)	91

Table 3.19 NMR data of compound 17 and (+) fargesin (CDCl ₃)	94
Table 3.20 NMR data of compound 18 and (-) kobusin (CDCl ₃)	98
Table 3.21 Free radical scavenging activity of isolated compounds from <i>D. signatum</i> and <i>M. liliifera</i>	103
Table 3.22 Inhibitory effect of isolated compounds from <i>D. signatum</i> and <i>M. liliifera</i>	106



LIST OF ABBREVIATIONS

J	Coupling constant
δ	Chemical shift
δ_{H}	Chemical shift proton
δ_{C}	Chemical shift carbon
s	Singlet (for NMR spectra)
d	Doublet (for NMR spectra)
dd	Doublet of doublet (for NMR spectra)
t	Tripet (for NMR spectra)
m	Multiplet (for NMR spectra)
q	Quartet (for NMR spectra)
brs	Broad singlet (for NMR spectra)
qC	Quaternary carbon
calcd.	Calculated
^1H NMR	Proton nuclear magnetic resonance
^{13}C NMR	Carbon-13 nuclear magnetic resonance
2D NMR	Two-dimensional nuclear magnetic resonance
^1H - ^1H COSY	Homonuclear (proton-proton) correlation spectroscopy
HSQC	Heteronuclear single quantum coherence
HMBC	Heteronuclear multiple bond correlation
HRESIMS	High-resolution electrospray ionization mass spectrometry
CC	Column chromatography
RP-18	Reversed-phase C-18
TLC	Thin-layer chromatography
IC_{50}	Half maximal inhibitory concentration
CDCl_3	Deuterated chloroform
Acetone- d_6	Deuterated acetone

MeOH	Methanol
EtOH	Ethanol
CH ₂ Cl ₂	Dichloromethane
EtOAc	Ethyl acetate
DMSO	Dimethylsulfoxide
(NH ₄) ₆ Mo ₇ O ₂₄	Ammonium molybdate
H ₂ SO ₄	Sulfuric acid
SiO ₂	Silicon dioxide
g	Gram (s)
mg	Milligram (s)
mL	Milliliter (s)
μg	Microgram (s)
μL	Microliter (s)
μM	Micromolar
mM	Millimolar
L	Liter (s)
M	Molar
min	Minute
H	Hour
m	Meter (s)
mm	Millimeter (s)
cm	Centimeter (s)
nm	Nanometer
Hz	Hertz
MHz	Megahertz
cm ⁻¹	Reciprocal centimeter (unit of wavenumber)
ppm	Part per million

NMR	Nuclear magnetic resonance
MS	Mass spectrometry
IR	Infrared
UV	Ultraviolet
$[M+H]^+$	Protonated molecule
$[M+Na]^+$	Pseudomolecular ion
m.p.	Melting Point
α	Alpha
β	Beta
γ	Gamma
$[\alpha]_D^{24}$	Specific rotation at 24 °C and sodium D line (589 nm)
λ_{max}	The wavelength of maximum absorption
c	Concentration
ϵ	Molar extinction coefficient
°C	Degree Celcius
deg.	Degree
spp.	Species
No.	Number

CHAPTER I

INTRODUCTION

1. Oxidative stress and free radicals

Oxidative stress is defined as an imbalance between reactive species in cells and tissues and a biological system's ability to readily detoxify these reactive intermediates metabolites or to repair the resulting damage. Evidently, oxidative stress is caused by an overproduction of free radicals and/or decreased level of protective mechanisms, so-called antioxidants³. Free radicals are atom or molecules that contain singlet electrons, strongly reactive, highly short lived, and can either donate or receive electrons from other molecules⁴. In general, they can be divided into 2 types: (i) oxygen containing molecules, referred to as reactive oxygen species (ROS) (e.g., superoxide anion (O_2^-), hydroxyl radicals (OH^\cdot), hydrogen peroxide (H_2O_2), ozone (O_3), singlet oxygen (1O_2), peroxy radical (ROO^\cdot) and organic hydroperoxides ($ROOH$)), and (ii) nitrogen containing molecules, known as reactive nitrogen species (RNS) (e.g., nitric oxide (NO^\cdot), peroxynitrite ($ONOO^\cdot$), peroxy nitrous acid ($ONOOH$), nitrogen dioxide (NO_2), reactive aldehydes-malondialdehyde (MDA) and 4-hydroxynonenal (4-HNE))⁵. Both forms of free radical species are generated from endogenous and exogenous sources^{6, 7}. The former source involves electron transport chain in mitochondria, enzyme activities (e.g., NADPH oxidase, xanthine oxidase, and nitric oxidase synthase (NOS)), inflammatory response and oxidative stress⁸. Whereas the latter source is from environments such as air, water, foods, UV light, radiation and chemicals⁹.

2. Oxidative stress-induced cellular damage

Once the body is extremely under oxidative stress condition, the production of ROS/RNS has been found to play a pivotal role in disrupting biological functions. In fact, an excess production of free radical from both biological and environmental

sources is highly difficult to eliminate by endogenous antioxidants, which typically triggers various inflammatory-associated diseases¹. At the cellular level, oxidative stress can cause damage to proteins, leading to protein dysfunction. In addition, oxidative reactions result in oxysterol formation and lipid peroxidation, which destroy phospholipid functions and cell membrane integrity. Oxidative stress also stimulates oncogenes and/or inhibit tumor suppressor genes, ultimately leading to cellular mutations, epigenetic changes and genetic instability¹⁰. It is well known that free radicals are able to target almost all cellular components. The targets of ROS/RNS damage include all major biomolecular groups, as discussed below.

2.1 Protein

According to several studies¹¹⁻¹³, they found that some amino acids are able to react with free radicals, culminating in the change of protein structure and function ranging from less active to denatured proteins (i.e., non-functioning proteins)¹⁴. This is a result from an occurrence of small peptide chain fragment and aggregation of cross-linked reaction products upon free radical reactions. This has led to an electrical charge fluctuation of protein and increased delicacy to proteolysis. It should be noted that amino acids in a peptide differ in their delicacy to attack, likewise many forms of activated oxygen differ in their potential reactivity¹⁵. Specifically, methionine and cysteine residues are highly susceptible to oxidation reaction. For example, sulfhydryl group of methionine oxidized by free radicals probably affects conformational changes of protein secondary structure, protein unfolding, and eventually degradation^{16, 17}. In addition, metalloenzymes (i.e., enzymes containing metal ions) are more sensitive to metal-catalyzed oxidation reactions, which can inhibit their activities¹⁸.

2.2 Lipids

Lipid peroxidation is easily induced by oxidative stress, causing the disturbance of various organizations in lipid membrane architecture⁹. This results in an inactivation of the membrane-bound receptors and enzymes, and thereby raising tissue permeability and injury¹⁹. Moreover, the lipid peroxidation products (e.g., malondialdehyde and unsaturated aldehydes) further trigger inactivating many cellular proteins by their interactions with specific moiety of protein that leads to protein cross-linkages²⁰. This also affects the depletion of the intracellular antioxidant reduced glutathione (GSH), induces peroxide production²¹, activates epidermal growth factor receptor (EGFR)²² and elevates fibronectin production²³.

2.3 DNA

The long-term effects of oxidative stress are inflicted by modifications of DNA²⁴ within the cells. This relates to the degradation of nucleotide bases, single- or double-stranded DNA breaks, purine/pyrimidine or sugar-bound modifications, gene deletions and translocations, gene mutations, and cross-linking with proteins.

These DNA modifications induced by oxidative stress are highly interrelated to aging, carcinogenesis, neurodegenerative, cardiovascular and autoimmune diseases²⁵. For the classical damaging mechanism of free radicals to DNA, GC-rich sequences mostly located at the gene promoter are strongly susceptible to radical attacks that can convert the expression level of the related genes²⁶. Oxidation can also directly damage single-base, such as 8-oxoguanine and thymine glycol. More recently, the research focus has changed to some of the more complex defect, such as tandem DNA lesions, promoted at considerable frequency by metal-catalyzed H₂O₂ reactions and ionizing radiation²⁷.

3. Effects of oxidative stress on signal transduction

Oxidative stress commonly disturbs an imbalance of the ratio between reduced GSH and oxidized glutathione (GSSG), resulting in the stimulation of redox sensitive transcription factors, particularly the nuclear factor of activated T cells (NFAT) and hypoxia-inducible factor 1 (HIF-1). Owing to their entanglement in inflammatory responses, these factors can promote the transmission of information into the cells via a wide range of receptors. The targets involved in signal transduction of ROS/RNS include tyrosine kinase receptors, major of the growth factor receptors, such as EGFR, vascular endothelial growth factor receptor (VEGFR), and receptor for platelet-derived growth factor (PDGF) along with protein tyrosine phosphatases and serine/threonine kinases²⁸. Moreover, the produced reactive species are capable to adjust various of the extracellular signal regulated kinases, such as p38, which are the components of mitogen-activated protein kinase (MAPK) family. From this point of view, free radicals are linked to several processes in the cells including cell proliferation, differentiation and apoptosis²⁹. For example, phosphorylation of IκB protein at serine residues induced by ROS can activate the inducible transcription factor nuclear factor-κB (NF-κB), allowing the free NF-κB to enter the nucleus and control gene transcription³⁰. Note that NF-κB generally regulates angiogenesis, cell proliferation and differentiation³¹. Accordingly, NF-κB activation via oxidation, several antioxidant defenses involved in genes regarding immune response are provoked. These consist of the inflammatory mediators interleukin-1 β (IL-1 β), IL-6, IL-8, tumor necrosis factor- α (TNF- α) and several adhesion molecules. Note that several kinases mentioned above have also been shown to phosphorylate IκB; thus, they are considered as the major targets for oxidative signals³².

4. Oxidative Stress, Inflammatory and Diseases

In an inflammatory response, the immune cells particularly leukocytes and mast cells are recruited to the damaged area. This phenomenon is related to a “respiratory burst” as a result of an increased uptake of oxygen, thereby enhancing the production and release of ROS/RNS at the tissue lesion^{33, 34}. Additionally, the soluble inflammatory mediators were more generated by inflammatory cells, including cytokines, arachidonic acid and chemokines, triggering the release more reactive species. These mediators are essential markers that can stimulate various signaling pathways, mainly through NF- κ B, NFAT, signal transducer and activator of transcription 3 (STAT-3), activator protein-1 (AP-1), nuclear factor erythroid 2 (NF-E2)-related factor 2 (Nrf2) and hypoxia-inducible factor-1 α (HIF1- α), which are mediators in vital cellular stress reactions. The role of oxidative stress-induced inflammation^{35, 36} is also associated with the production of cyclooxygenase-2 (COX-2) and inducible nitric oxide synthase (iNOS), and high expression of inflammatory cytokines, including TNF- α , IL-1 β , IL-6 and chemokines (e.g., CXC chemokine receptor 4). The progression of immune response and oxidative stress promotes a repetitive injury, which could destroy healthy stromal cells and neighboring epithelial cells, and eventually induction of carcinogenesis after a long period of time^{35, 37}. Several studies have reported that ROS and RNS control the production of cytokines in macrophages through NF- κ B-dependent mechanisms³⁸. Overwhelming inflammatory responses have been known to cause cell death and tissue injury, leading to various diseases and their complications.

Cell damage is a result from the interaction between reactive species and cellular biological structure and DNA. The vital antioxidant substances are not enough to handle this condition and lead to unbalanced process and cell damage. This event results in several target organs diseases such as brain diseases (Parkinson’s disease, Alzheimer’s disease and stroke), cardiovascular diseases (hypertension,

ischemia, atherosclerosis and heart failure), lungs (asthma and chronic bronchitis), kidneys (chronic renal failure and glomerulonephritis), joints inflammation (arthritis and rheumatism), eyes (cataract and retinal disease) and multi-organs (cancers, diabetes, inflammations, aging and infections), as summarized in **Figure 1.1**

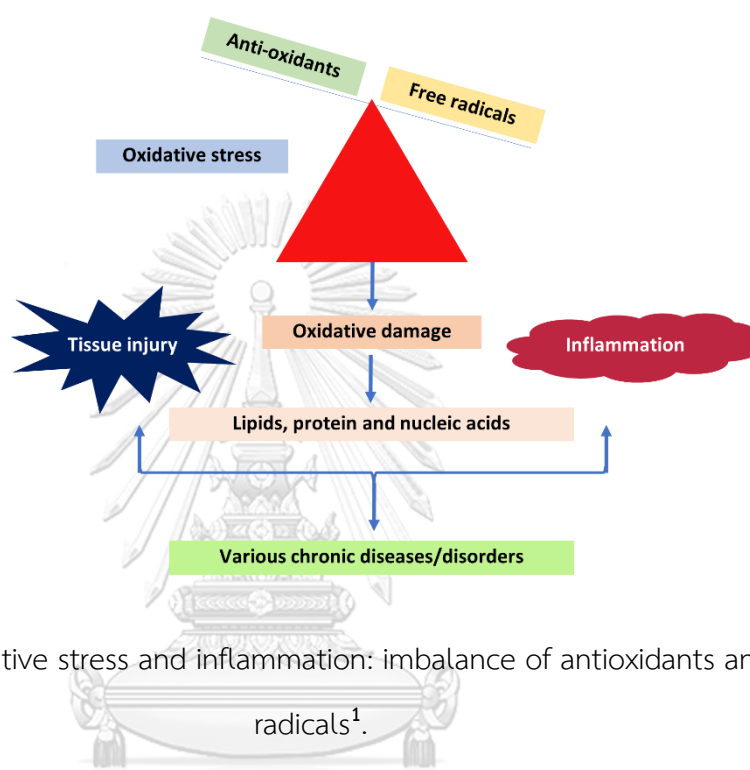


Figure 1.1 Oxidative stress and inflammation: imbalance of antioxidants and free radicals¹.

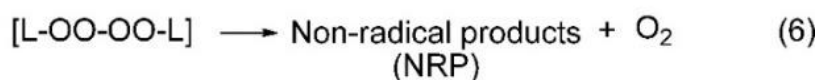
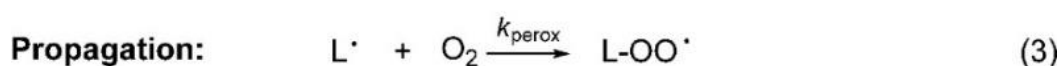
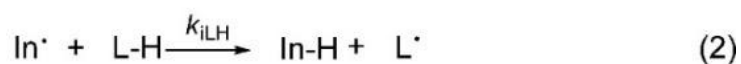
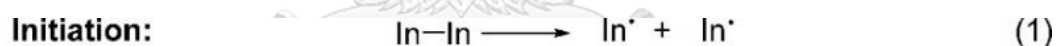
5. Antioxidant

Generally, humans have the system or substances, so-called antioxidants which protect many organs from oxidative damage or resist free radicals. Antioxidants are molecules which react with the generated free radicals before they interact with the target organs. Antioxidants can be divided into two groups: endogenous and exogenous antioxidants. Endogenous antioxidants, which are fundamental for maintaining cellular system, are enzymes such as superoxide dismutase (SOD), catalase (CAT), glutathione peroxidase (GPx), glutathione reductase (GR), glutathione-S-transferase (GST), thioredoxins (TRX), peroxiredoxins (PRX) or substances such as melatonin or coenzyme Q10³⁹. Meanwhile, exogenous antioxidants, which can obtain

from external sources, include the well-known ascorbic acid (vitamin C), α -tocopherol (vitamin E), selenium, β -carotene (carotenoids), omega-3 and omega-6 fatty acids and bioactive flavonoids³⁹. In addition, it has been found that these antioxidants could significantly enhance the activity of endogenous antioxidants^{40, 41}. The intake of exogenous antioxidants would decrease the severity of oxidative stress development through inhibiting the initiation or propagation of oxidative chain reaction (see below), served as free radical scavengers, quenchers of singlet oxygen and reducing agents⁴². An ideal antioxidant should be absolutely absorbed, should quench free radicals and chelate redox metals in cells.

5.1 Mechanism of action of antioxidants

Antioxidants can act at different steps of the oxidative radical reactions, and this can be commonly described by considering the lipid peroxidation in cell membranes indicating the sequent steps of initiation, propagation and chain termination², as shown in **Figure 2** below.



$$k_{iLH} = 6 \times 10^1 \text{ M}^{-1}\text{s}^{-1} \quad k_p = 6 \times 10^1 \text{ M}^{-1}\text{s}^{-1} \text{ for linoleate} \quad \text{In, Initiator; L, Lipid}$$

$$k_{\text{perox}} = 10^9 \text{ M}^{-1}\text{s}^{-1} \quad k_t = 1 \times 10^5 \text{ to } 10^7 \text{ M}^{-1}\text{s}^{-1}$$

Figure 1.2 Reactions in the free radical chain oxidation mechanism²

The part of the radical sequence steps, especially focused on initiation and propagation steps, represented that, for example, cell membranes can be promoted the lipid oxidation by chemical factors and exogenous physical, such as UV light, air pollution, ionization radiation and smoking, together with the electron transport chain in mitochondria and endogenous enzyme systems². Chemically, it was substantiated that the propagation step of peroxidation initiates by addition of oxygen to carbon-centered radicals, arising at, or near the diffusion-controlled rate. In the propagation, most oxidations following a radical sequent mechanism, begin at a normally slow rate, and the transfer of a hydrogen atom represents to the chain carrying peroxy radical. Carbon-carbon double bonds can be added by peroxy free radicals. Conjugated dienes perhaps especially subject to addition of peroxy. Moreover, radical cyclization reactions and substitution on peroxide by intramolecular radical may occur, increasing cyclic peroxides. Whereas polyunsaturated lipids associate with peroxidation reactions². Oxygen molecule can be reacted by depletion of antioxidants or decrease in its local concentration, eliminating prooxidative metal ions, capturing the extreme ROS such as hydrogen peroxide or superoxide anion radical, scavenging chain-initiating radicals like hydroxyl OH[•], alkoxy RO[•] or peroxy ROO[•]; as well as disrupting the radical sequence chain or quenching singlet oxygen (¹O₂)⁴³. Antioxidants breaking lipid peroxidation by quenching oxygen, decreasing its concentration, or capturing prooxidative transition metal ions, are called preventative antioxidants. Those able to deplete ROS by catalytic action are also preventative. Nonetheless, chain-breaking antioxidants, singlet oxygen quenchers and metal chelators are accrued, while performing their protective role. In many examples, the same antioxidant can attach more possible mechanisms of action: propyl gallate, a partially phenolic water-soluble food antioxidant, is a chain-breaking antioxidant, a radical scavenger, and its efficacy to bind iron has been reported^{43, 44}. It was defined that chain breaking antioxidants,

which are able to scavenge radical species, are called primary antioxidants. Whereas secondary antioxidants are peroxide decomposers, singlet oxygen quenchers that produce non-radical species, metal chelators, oxidative enzyme (e.g. lipooxygenase) inhibitors or UV radiation absorbers⁴⁵. Secondary antioxidants may display synergetic effects in combination with primary antioxidants, following various possible mechanisms as following⁴⁵:

1. stabilizing primary antioxidants by generating an acidic environment
2. procreating primary antioxidants by hydrogen donation
3. chelating pro-oxidative transition metal cations
4. quenching molecular oxygen

Moreover, it has been reported that antioxidant enzymes can catalyze the synthesis or the regeneration of non-enzymatic antioxidants⁴³. Antioxidant and anti-inflammatory agents are necessary to prevent the incompatibility effects of oxidative stress and inflammatory responses. Although various synthetic antioxidant and anti-inflammatory agents have been developed, they still have unsuspected danger such as low yield synthetic, side effects and high cost of production. Numerous studies have reported that various types of plant secondary metabolites such as carotenoids, curcuminoids, flavonoids and triterpenoids dominate antioxidant and anti-inflammatory activities⁴⁶. Besides having antioxidant activities, flavonoids and phenolic compounds have been shown to exert an effective role as anti-inflammatory factors. The anti-inflammatory activities of natural compounds have been reported in several preclinical studies⁴⁷. Their natural compounds have exerted their biological properties by blocking two major signaling pathways, NF- κ B and MAPKs, which play an essential role in the production of various proinflammatory mediators (see section 3)¹. Research of effective natural antioxidants and anti-

inflammatory compounds from botanical origins for pharmaceutical and nutritional purposes have acquired global attendance⁴⁸. To date, herbal bioactive compounds have inspired drug development.

Nowadays, trends in natural products containing cosmetics and supplements have an increasing interest, particularly plants displaying antioxidant and anti-inflammatory properties³⁹. Numerous researches in medicinal plant bioactive extracts and their identified/isolated active constituents have displayed all kinds of medicinal pharmacological properties against various acute and chronic diseases and disorders⁴⁹⁻⁵². The World Health Organization (WHO) has reported that around 80% world inhabitants utilized traditional medicine which requires the uses of herbal extracts and their active components due to natural antioxidant abundant in several plants, low side effects, less expensive costs and well-combined between modern medicine and traditional herbal medicine for treatment⁴⁷. There are many antioxidant compounds from plants that have been launched as a new drug, dietary supplement, and cosmetic ingredient³⁹.

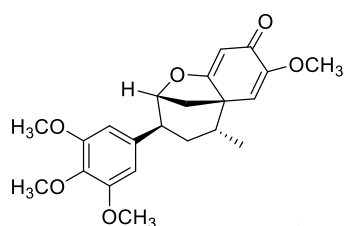
6. Secondary metabolites of plants

6.1 Chemical constituents of *Magnolia* and bioactivity

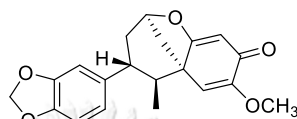
Many species of the genus *Magnolia* have been traditionally used for the treatment of allergic rhinitis, nasal empyema, nasal sinusitis and headaches⁵³. Plants belonging to this genus have been intensively investigated for their chemical constituents, which can be classified into seven categories, including alkaloids, coumarins, flavonoids, lignans, neolignans, phenylpropanoids, and terpenoids⁵⁴. Specifically, *Magnolia lilifera* (L.) Baill. commonly called in Thai as “Montha”, is a flowering tree native to the Indo-Malayan territory. It is appeared to have white to cream-colored flowers on terminal stems, where its height is ranged from 12 to 60 feet⁵⁵. However, the biological activities of the constituents have not fully

investigated yet. Some examples regarding the constituents from the relevant *Magnolia* species as well as their bioactivity are described as follows:

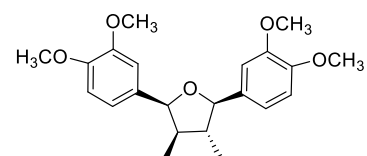
In 1982, Talapatra et al. reported four isolated compounds (**1-4**) from the leaves and twigs of *M. liliflora* Desr.⁵⁶



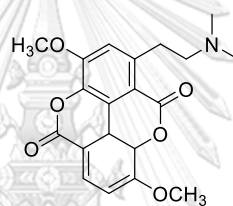
(1) (-)-maglifloenone



(2) futaenone

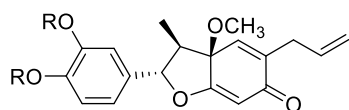


(3) veraguensin

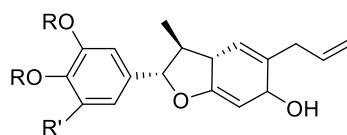


(4) taspine

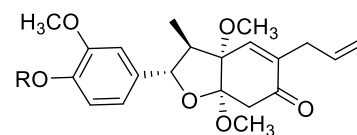
In 1983, Lida and colleagues completely elucidated the neolignans from fresh leaves of *M. liliflora* Desr., including dennudatin A (**5**) and B (**6**), liliflol A (**7**) and B (**8**), liliflone (**9**), liliflodione (**10**), burchellin (**11**), piperenone (**12**), (-)-maglifloenone (**1**), futaenone (**2**) and verraguensin (**23**)⁵⁷.



(5) R+R = CH₂



(7) R+R = CH₂, R' = H

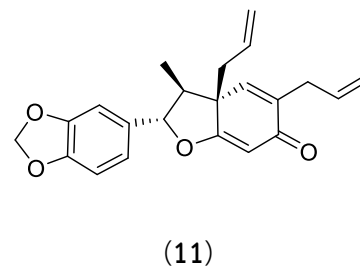
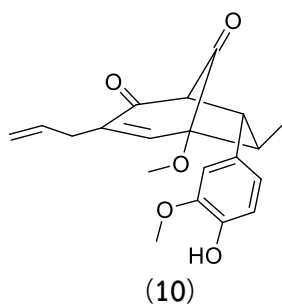


(9) R = H

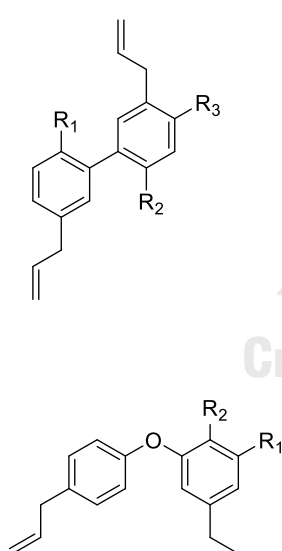
(6) R = CH₃

(8) R = CH₃, R' = H

(12) R = CH₃



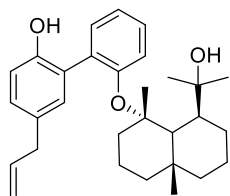
In 2001, Matsuda and co-workers reported isolated compounds (**13-32**) from the bark of *M. obovata* potential to inhibit nitric oxide (NO) production in lipopolysaccharide (LPS)-activated macrophages. Three active constituents (i.e., magnolol, honokiol and obovatol) showed weak inhibitory effect on iNOS activity, but potent inhibition of induction of iNOS and NF- κ B activation⁵⁸



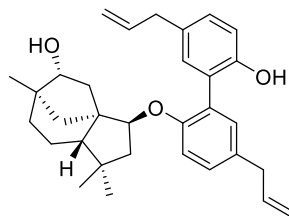
	R ₁	R ₂	R ₃
(13) magnolol	OH	OH	H
(14) honokiol	OH	H	OH
(15) 4- <i>o</i> -methylhonokiol	OCH ₃	H	OH
(16) 6- <i>o</i> -methylhonokiol	OH	H	OCH ₃

CHULALONGKORN UNIVERSITY

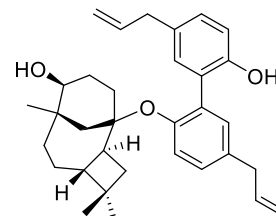
	R ₁	R ₂
(17) obovatol	OH	OH
(23) eudesobovatols A		OH
(24) eudesobovatols B	OH	



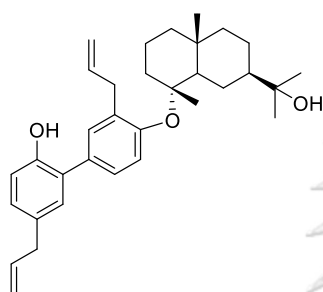
(18) eudesmagnolol



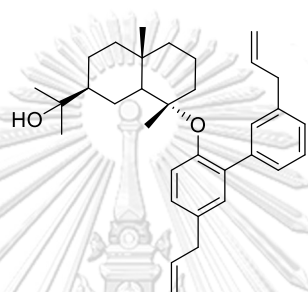
(19) clovanemagnotol



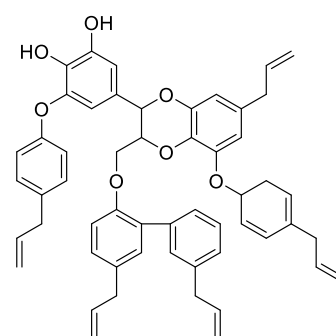
(20) caryolanemagnotol



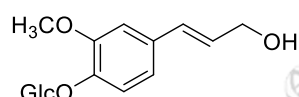
(21) eudeshonokiol A



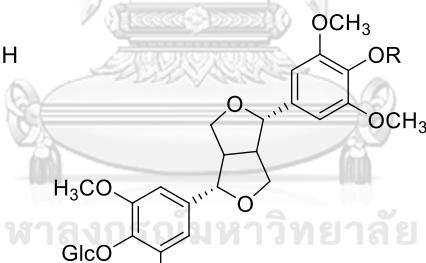
(22) eudeshonokiol B



(25) magnolianin



(26) syringin

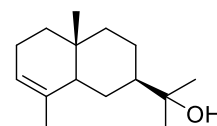
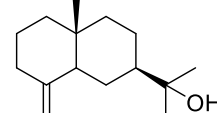
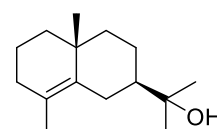


(27) liriodendrin ;

 β -D-glucopyranoside

(29) caryophyllene oxide

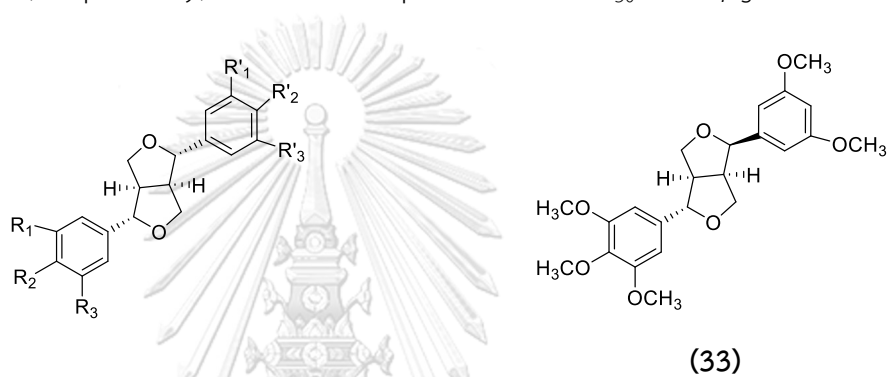
(28) (+)-syringaresinol ;

4'-o- β -D-glucopyranoside(30) α -eudesmol(31) β -eudesmol(32) γ -eudesmol

In 2009, Kim and co-workers reported the isolation and structural elucidation of a new lignan isolated from *M. fargesii*, namely epimagnolin B (33), along with three known derivatives, (+)-eudesmin (34), (+)-magnolin (35), (+)-yangambin (36), acting as

the inhibitors of NO production in LPS-activated microglia. The compound **33** showed good activity on inhibition of NO production with IC₅₀ value of 10.9 ± 1.6 μM. This compound was also proved to suppress I-κB-α degradation and nuclear translocation of p65 subunit of NF-κB⁵⁹.

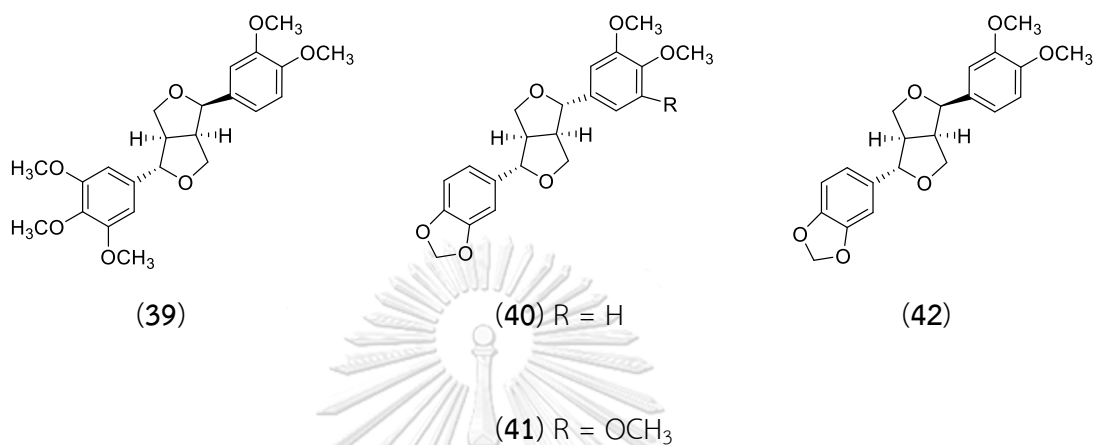
In 2009, Bajpai and colleagues reported the free radical scavenging activities of the oil and ethyl acetate extracted from *M. liliflora* Desr. with IC₅₀ values of 10.11 and 16.17 μg/mL, respectively, which were superior to BHA (IC₅₀ 18.27 μg/mL)⁶⁰.



	R ₁	R ₂	R ₃	R' ₁	R' ₂	R' ₃
(34)	OCH ₃	OCH ₃	H	OCH ₃	OCH ₃	H
(35)	OCH ₃	OCH ₃	OCH ₃	OCH ₃	OCH ₃	H
(36)	OCH ₃	OCH ₃	OCH ₃	OCH ₃	OCH ₃	OCH ₃
(37)	OCH ₃	OCH ₃	H	OCH ₃	OCH ₃	H
(38)	OCH ₃	OCH ₃	OCH ₃	OCH ₃	OCH ₃	OCH ₃

In 2018, Lee and colleagues identified biologically active compounds (+)-magnolol (**35**), dimethylpinoresinol (**37**), dimethyl-liroresinol (**38**), epimagnolol (**39**), dimethoxyaschantin (**40**), aschantin (**41**) and fargesin (**42**) from the CHCl₃ fraction of flower buds of *M. fargesii*. The suppression of the isolated compounds on infiltration of inflammatory cells (neutrophils and macrophages) and secretion of inflammatory mediators such as ROS, TNF-α, and IL-6 *in vivo* was performed. Notably, all lignans

significantly suppressed both extracellular signal-related kinase (ERK) and Akt phosphorylation levels in cancer stem cells (CSC-stimulated) human lung mucoepidermoid carcinoma (NCI-H292) cells⁶¹.



To our best knowledge, it can be seen that both chemical constituents and biological activity of *M. lilifera* (L.) Baill. is not fully determined, only those of other species in this genus were reported.

6.2 Chemical constituents of *Dendrobium* and biological activity

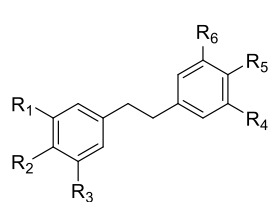
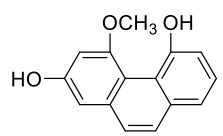
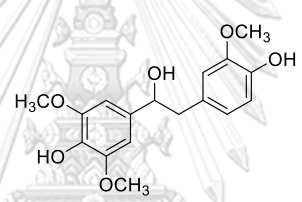
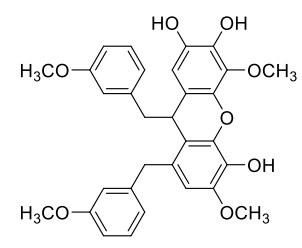
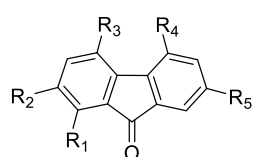
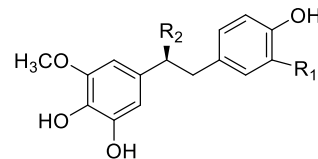
Dendrobium is one of the biggest genera in *Orchidaceae*, which has an approximately 1,100 species primarily found in Indo-Asian and Pacific regions^{1, 62}. Various series of isolated compounds, including bibenzyls, phenanthrenes, alkaloids, fluorenones, sesquiterpenes have been discovered and considered as the major secondary metabolites of this genus⁶³. Some of these compounds have been attracted great attention in many studies as they exhibited a wide range of pharmacological activities, such as antioxidant, anti-inflammatory, anti-metastatic, cytotoxic and immunoregulatory properties^{64,65, 66}. In Thailand, there are more than 100 species of *Dendrobium*, which have been reported and identified⁶⁷. Specifically,

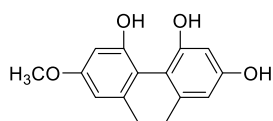
D. signatum Rchb.f., locally known in Thai as 'Ueang Khao Kiu', is extensively distributed in the North and upper Northeast of Thailand. It is an aerophytes orchid with thin or fleshy stems. It has white to cream color with twisted petals and sepals in the size 6-7 cm. The period of flowering is in February to April⁶⁸.

Various *Dendrobium* species have been used in traditional medicine. Their chemical constituents and pharmacology of *Dendrobium* species have been studied⁶⁹. Several studies have been accepted to provide specific evidence to rationalize medicinal uses for the treatment of various diseases including antioxidant, anti-inflammatory, antiplatelet aggregation, lymphocyte stimulation and α -glucosidase inhibitory activities⁶⁹.

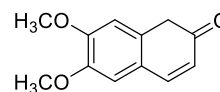
A number of studies on the antioxidant property of the bibenzyl and phenanthrene derivatives from *Dendrobium* genus signified that they were potent antioxidants. For instance, crepidatin (**43**), moscatilin (**44**), tristin (**45**) and moscatin (**46**) displayed strong antioxidant activity than that of BHA as determined by the method of ferric thiocyanate⁷⁰. Bibenzyl derivatives isolated from *D. nolile*, including crepidatin (**43**), chrysotoxin (**47**), nobilin D (**48**) and nobilin E (**49**) exhibited free radical scavenging activity stronger than or equivalent to vitamin C by means of the DPPH assay⁶⁵. In the ORAC assay, chrysotoxine (**47**), crepidatin (**43**), gigantol (**50**), moscatilin (**44**), nobilin D (**48**), dendroflorin (**51**) and nobilone (**52**) showed antioxidant activity stronger than vitamin C⁷¹. Moreover, the DPPH free radical scavenging assay was utilized to evaluate the antioxidant activities of dendrocandin C (**53**), D (**54**) and E (**55**) from *D. candidum*. The results indicated that dendrocandin E (**55**) had the most potent scavenging activity⁷². The phenanthrene derivative 7-methoxy-9,10-dihydrophenanthrene-2,4,5-triol (**56**) obtained from *D. draconis* displayed antioxidant potency similar to that of Trolox⁷³. The bibenzyl derivatives isolated from *D. densiflorum* such as gigantol (**50**) and moscatilin (**44**) and the coumarin scoparone (**57**) were preliminary investigated for their antiplatelet

aggregation activity on SD rat platelet *in vitro*⁷⁴. Further determination revealed that moscatilin (**44**) and moscatin (**46**) exhibited strong inhibitory effect on arachidonic acid and collagen induced platelet aggregation⁷⁵.

	R ₁	R ₂	R ₃	R ₄	R ₅	R ₆	
	(43)	OCH ₃	OCH ₃	OCH ₃	OCH ₃	OH	H
	(44)	OCH ₃	OH	OCH ₃	H	OH	OCH ₃
	(45)	OH	H	OH	H	OH	OCH ₃
	(47)	OCH ₃	OH	OCH ₃	OCH ₃	OCH ₃	H
	(50)	OCH ₃	H	H	H	OH	OCH ₃
	(46)						
	(48)						
	(49)						
	(51)	OH	H	OH	OCH ₃	OH	
	(52)	H	OH	H	OCH ₃	OH	
	(53)	H			OCH ₃		
	(54)	H			OCH ₂ CH ₃		
	(55)	OH			H		

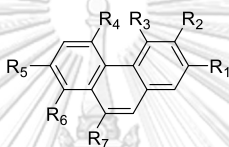


(56)

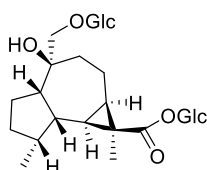


(57)

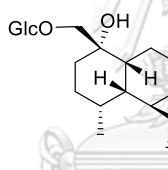
	R ₁	R ₂	R ₃	R ₄	R ₅	R ₆	R ₇
(58)	OH	H	OCH ₃	H	H	OH	H
(59)	OH	H	H	OH	OCH ₃	OCH ₃	OCH ₃
(60)	OH	OCH ₃	OCH ₃	H	H	OH	H



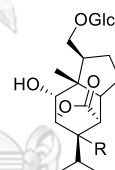
(61)



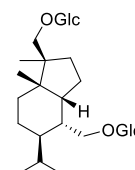
(62)



(63)



(64) R= H



(66)

(65) R= OH

จุฬาลงกรณ์มหาวิทยาลัย
CHULALONGKORN UNIVERSITY

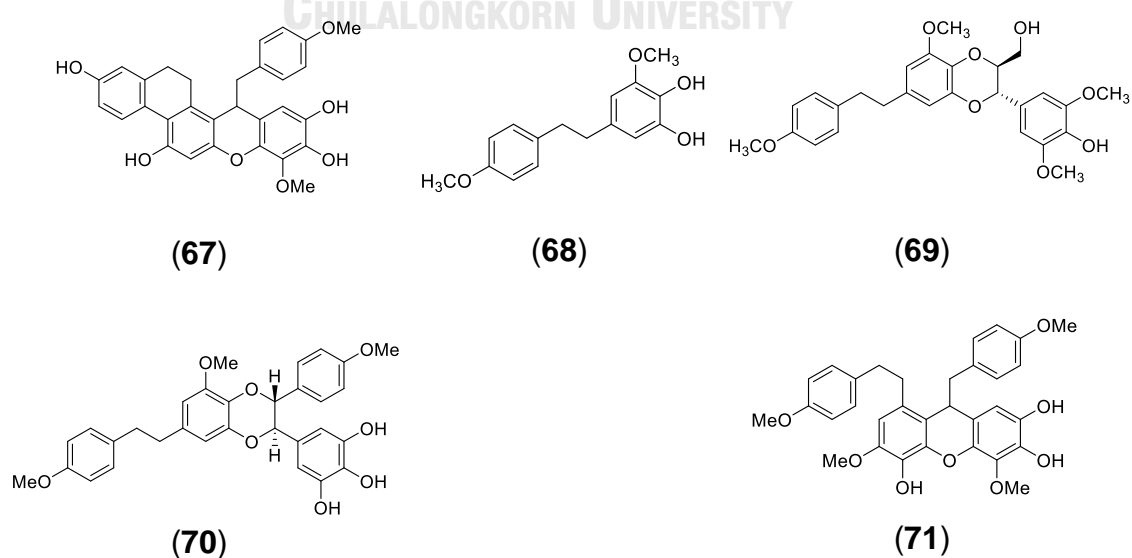
In the field of anti-inflammation research, several compounds from *D. nobile* were evaluated for inhibitory activities on LPS-induced NO generation in macrophage cells (RAW 264.7). The results demonstrated that 9,10-dihydrophenanthrene scaffold, such as coelonin (58), ephemeranthol A (59) and erianthridin (60) exerted more potent inhibitory activity than phenanthrenes and bibenzyls, including moscatilin (44) and fimbriol B (61)⁷⁶.

Regarding the inhibitory effects on NO production, strong activities were scrutinized for nobilin D (48), E (49) and dendroflorin (51)⁷⁷.

In a preliminary *in vitro* biological evaluation, dendrosides D-G (**62-56**), the sesquiterpene glycosides isolated from *D. nobile*, were able to stimulate the proliferation of murine T and/or B lymphocytes⁷⁸. Another subject described the stimulatory activity of dendronobiloside A (**60**) from *D. nobile* on the proliferation of B lymphocytes⁷⁹.

Toward α -glucosidase inhibitory activity, some compounds obtained from *Dendrobium* plants were found to possess this biological activity. For instance, the bibenzyl derivative gigantol (**50**) isolated from *D. denvonianum*, and the dimeric stibenenes Loddigesiinols extracted from *D. loddigesii* exhibited a significant α -glucosidase inhibitory activity⁸⁰.

In 2016, Mittraphab and co-workers first reported the chemical constituents from *D. signatum* and their cytotoxic activity against human cancer cell lines, including MDA-231, HepG2 and HT-29 cells. A new bibenzyl-dihydrophenanthrene derivative named dendrosignatol (**67**) was isolated, together with 3,4-dihydroxy-5,4'-dimethoxybibenzyl (**68**), dendrocandin B (**69**), dendrocandin I (**70**) and dendrofalconerol A (**71**). The results showed that all isolated compounds moderately exhibited the cytotoxicity⁸¹.



Recently, Chimsook and co-workers investigated antioxidant activity of the ethanol extract from *D. signatum*. The results showed that the extract had moderately radical scavenging ability as compared to vitamin C⁸².

From this point of view, the chemical constituents and biological activity of isolated compounds from *D. signatum* have not been investigated thoroughly yet, and only five bibenzyl derivatives **67-71** have been reported⁸¹. Therefore, the aims of this research were to discover more natural compounds with diverse structures from both *Magnolia liliifera*. (see section **6.1**) and *D. signatum*. The main objectives of this study are as follows:

1. To isolate chemical constituents from *M. liliifera* (L.) Baill. flower and *D. signatum* Rchb.f.
2. To characterize the chemical structures of the isolated compounds from *M. liliifera* (L.) Baill. flower and *D. signatum* Rchb.f. by spectroscopic techniques
3. To evaluate antioxidant and anti-inflammatory activities of isolated compounds and study on the action mechanism

CHAPTER II

EXPERIMENTS

2.1 Plant Materials

The aerial parts of *D. signatum* were collected from Mae Hong Son, Thailand (August 2018), and was identified by a Royal Forest Department staff, Mae Hong Son Province. A voucher specimen was assigned with the code CUCHEM2018-005. The flowers of *M. liliifera* were collected from Bangkok, Thailand (August 2018). A voucher specimen was assigned with the code CUCHEM2018-004. Plant samples are deposited at the Department of Chemistry, Faculty of Science, Chulalongkorn University

2.2 General Experimental Procedures

2.2.1 Thin-layer chromatography (TLC)

TLC analysis was performed on Silicycle's aluminum sheet coated with silica gel F-254, 20 × 20 cm, layer thickness 200 μm. The TLC reverse phase analysis was performed on Merck's aluminum sheets coated with silica gel 60 RP-18 F245s. The spot of metabolites was observed with UV light at 256 nm wavelength and dipped with ammonium molybdate ((NH₄)₆Mo₇O₂₄) in 5% H₂SO₄/EtOH then heating for 1-2 mins at 105-120°C on a hot plate.

2.2.2 Column chromatography

Column chromatography (CC) was performed using Silica gel 60H (Merck code No. 7734 and No. 9385) as packing materials. Reverse-phase C-18 (RP-18) chromatography was performed using Silica gel C-18 (Wako code No. 237-01555) as packing materials. Size exclusion chromatography was performed by Sephadex LH-20 (Pharmacia Code No. 17-0090-01) to separate metabolites according to their molecular weight.

2.2.3 Nuclear magnetic resonance spectroscopy (NMR)

The NMR spectra were recorded on a Bruker AV400 (400 MHz for ^1H -NMR, 100 MHz for ^{13}C -NMR) and JEOL (500 MHz for ^1H -NMR, 125 MHz for ^{13}C -NMR) using tetramethylsilane (TMS) as an internal standard.

2.2.4 Mass spectrometry (MS)

High-resolution electrospray ionization mass spectrometry (HRESIMS) spectra were obtained with a Bruker micrOTOF-Q II.

2.2.5 Fourier transforms infrared spectrophotometry (FT-IR)

FT-IR spectra were recorded on a Perkin-Elmer Model 1760X Fourier Transform Infrared Spectrophotometer. Solid samples were formally examined by incorporating the sample with potassium bromide (KBr) to form a pellet.

2.2.6 Optical Rotation

Optical rotation was measured on a Perkin-Elmer 341 polarimeter at 589 nm.

2.2.7 Melting Point

Melting points were recorded on a Fisher-Johns melting point apparatus.

2.2.8 Ultraviolet-visible spectrophotometry (UV-vis)

UV data were recorded on a CARY 50 Probe UV-visible spectrophotometer.

2.2.9 X-ray diffraction spectrometer

The crystal structure was solved by direct methods and using the SHELXS97 program. Crystallographic data, including structure factors, have been deposited at Cambridge Crystallographic Data Center.

2.8.10 Microplate spectrophotometer

The absorbance for biological assays was measured with a Biotek Power Wave XS2 microplate spectrophotometer.

2.8.11 CO₂ cell culture incubator

Cells using in present study were cultured in a Panasonic MCO-5AC CO₂ cell culture incubator.

2.8.12 Biosafety cabinet

All biological procedures including cell passage, biological assays were worked in a biosafety cabinet BIOHAZARD Class II MICROTECH Model V6-T.

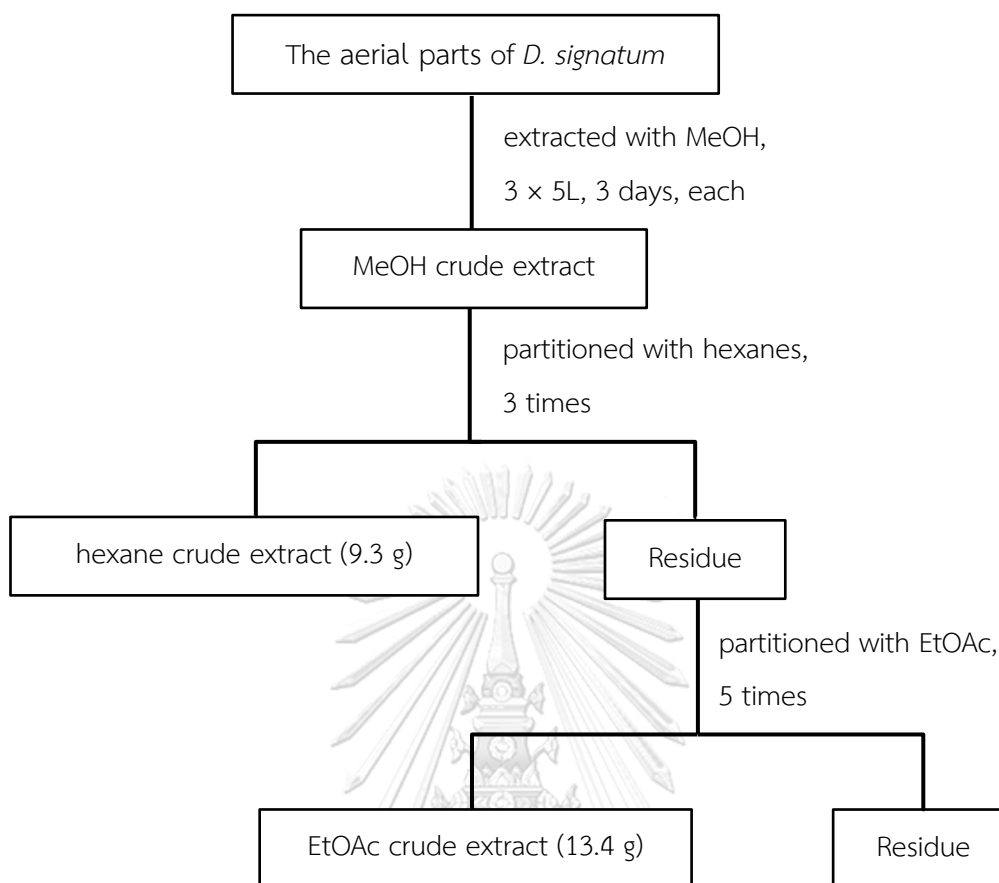
2.3 Chemicals

All commercial-grade solvents used in the present study, such as methanol (MeOH), acetone, ethyl acetate (EtOAc), dichloromethane (DCM) and n-hexane, were purified by distillation before use. The deuterated solvent for NMR experiments was chloroform-*d* (CDCl₃), methanol-*d*₄ and acetone-*d*₆. Cell culture grade DMSO was used for sample stock solution.

2.4 Extraction and isolation

2.4.1 Extraction of *D. signatum* aerial parts

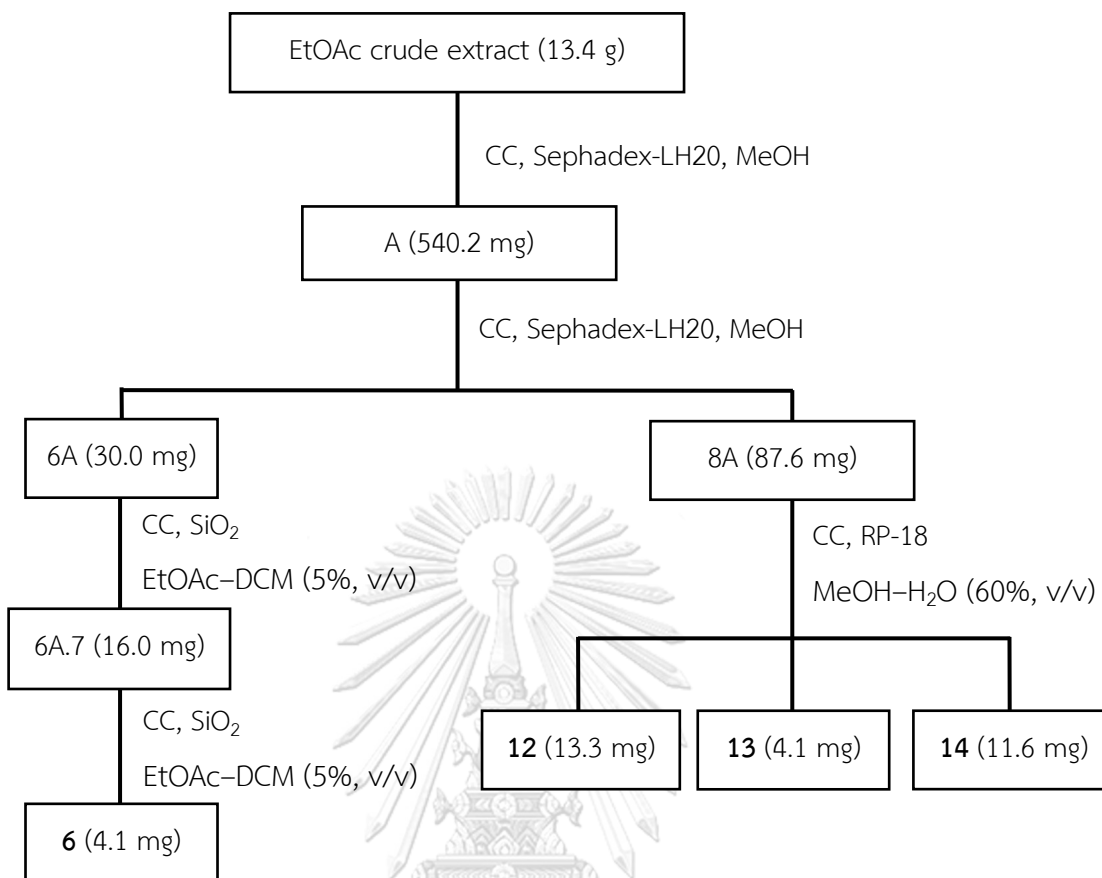
The air-dried and powdered aerial parts of *D. signatum* (934.0 g) were extracted with MeOH (3 × 5 L, for 3 days) at room temperature. Evaporation of the solvent under reduced pressure gave the MeOH extract (200 g), and the syrupy residue was suspended in water and partitioned in equal amounts for EtOAc (×5) and hexane (×3) and evaporated under reduced pressure to yield the EtOAc (13.4 g) and hexane (9.3 g) crude extracts, respectively. The extraction procedure is shown in **Scheme 2.1**.



Scheme 2.1 Extraction of *D. signatum* aerial parts

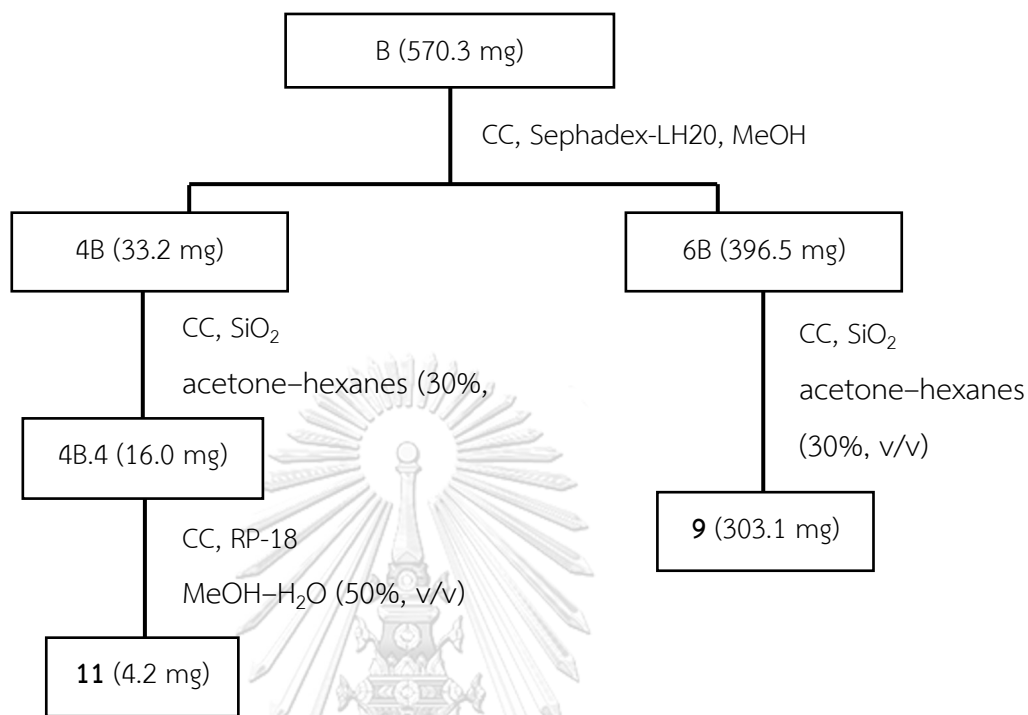
2.4.2 Isolation of compounds from EtOAc crude extract

The EtOAc crude extract (13.4 g) was subjected to CC on silica gel using a gradient of acetone-hexane (10→70 %) to provide seven fractions (A–G). Fraction A (540.2 mg) was further fractionated by Sephadex-LH20, eluted with MeOH to afford eight fractions (1A–8A). Subfraction 6A (30.0 mg) was purified by CC using EtOAc–DCM (5%, v/v), followed by CC using acetone-hexane (30%, v/v) to yield compound **6** (4.1 mg). Subfraction 8A (87.6 mg) was purified by RP-18 CC using MeOH–H₂O (60%, v/v) to yield compounds **12** (13.3 mg), **13** (4.1 mg) and **14** (11.6 mg). The isolation procedure is shown in **Scheme 2.2**.



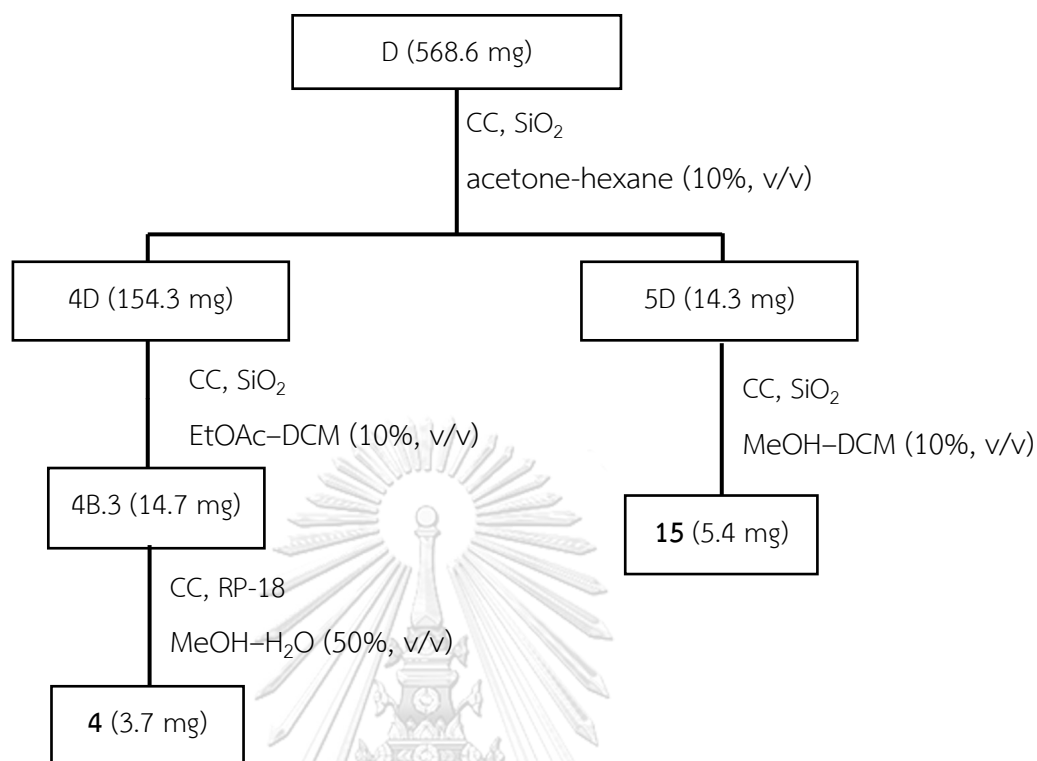
Scheme 2.2 Isolation procedure of fraction A

Fraction B (570.3 mg) was separated by Sephadex-LH20 CC with MeOH into six fractions (1B–6B). Subfraction 4B (33.2 mg) was purified by CC condition acetone–hexane (30%, v/v), followed by RP-18 CC using MeOH–H₂O (50%, v/v) to obtain compound **11** (4.2 mg). Subfraction 6B (366.5 mg) was purified by CC using acetone–hexane (30%, v/v) to yield **9** (303.1 mg). The isolation procedure is shown in **Scheme 2.3**.



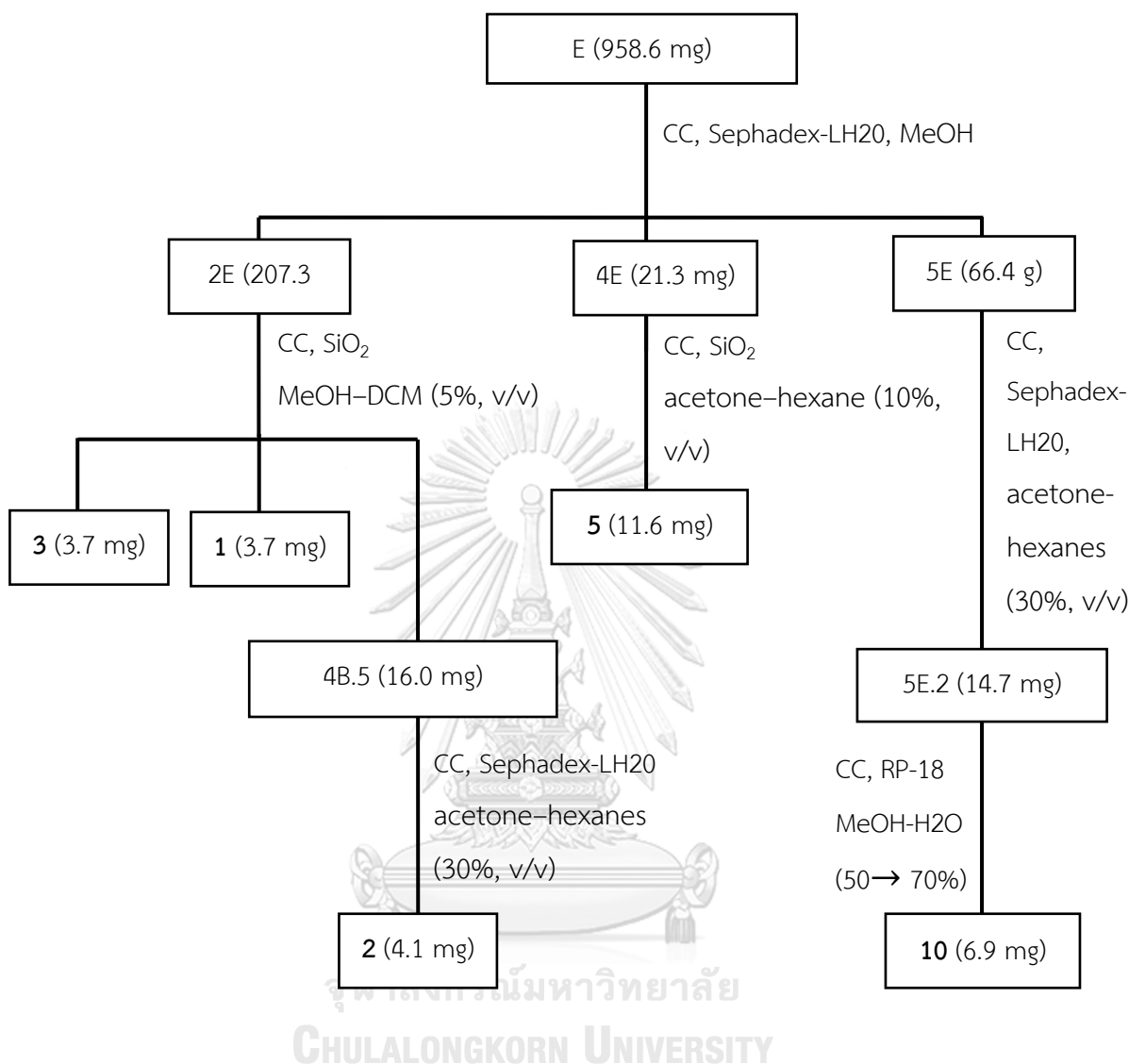
Scheme 2.3 Isolation procedure of fraction B

Compound **4** (3.7 mg) was isolated from fraction D (569.3 mg), which was separated by CC with condition acetone–hexane (10→30%, v/v) into six fractions (1D–6D). Afterward, subfraction 4D (154.3 mg) was purified by CC with EtOAc–DCM (10%, v/v), followed by RP-18 CC using MeOH–H₂O (50%, v/v) to yield compound **4**. And subfraction 5D (14.3 mg) was purified by CC with MeOH–DCM (10%, v/v) to yield compound **15** (5.4 mg) The isolation procedure is shown in **Scheme 2.4**.



Scheme 2.4 Isolation procedure of fraction D

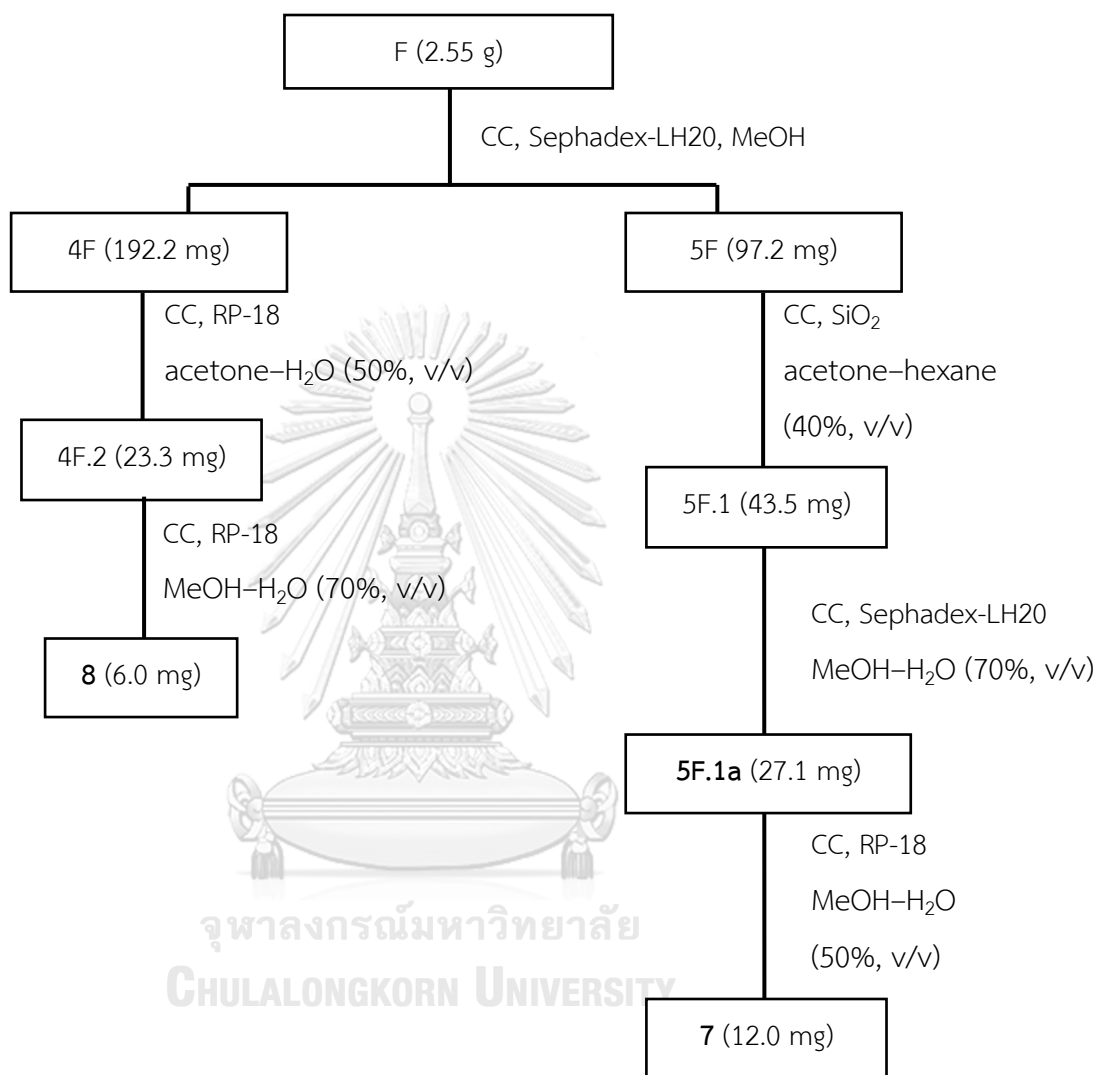
Fraction E (958.6 mg) was then separated into six fractions (1E–6E) by Sephadex-LH20 CC with MeOH. Subfraction 2E (207.3 mg) was purified by CC using MeOH–DCM (5%, v/v) to get compounds **3** (6.6mg) and **1** (4.0 mg), Then, 2E residue was separated by Sephadex-LH20 CC with acetone–hexane (30%, v/v) to yield compound **2** (4.1 mg). Subfraction 4E (211.3 mg) was purified by CC using acetone–hexane (40%, v/v) to obtain compound **5** (11.6 mg) together with compound **10** (6.9 mg), which was chromatographed from subfraction 5E (66.4 mg) on Sephadex LH-20 with acetone–hexane (30%, v/v), followed by RP-18 CC using MeOH–H₂O (50→70%, v/v). The isolation procedure is shown in **Scheme 2.5**.



Scheme 2.5 Isolation procedure of fraction E

Fraction F (2.55 g) was separated on a Sephadex-LH20 CC (MeOH) to give five fractions (1F–5F). Subfraction 4F (193.2 mg) was separated on a RP-18 CC using acetone–H₂O (50%, v/v) to yield three subfractions (4F.1–4F.3), the 4F.2 (23.3 mg) was then purified using MeOH–H₂O (70%, v/v) to afford compound **8** (6.0 mg). Subfraction 5F (97.2 mg) was separated on a CC by using acetone–hexane (40%, v/v) to yield two subfraction (5F.1–5F.2), then the 5F.1 (43.5 mg) was subjected to a

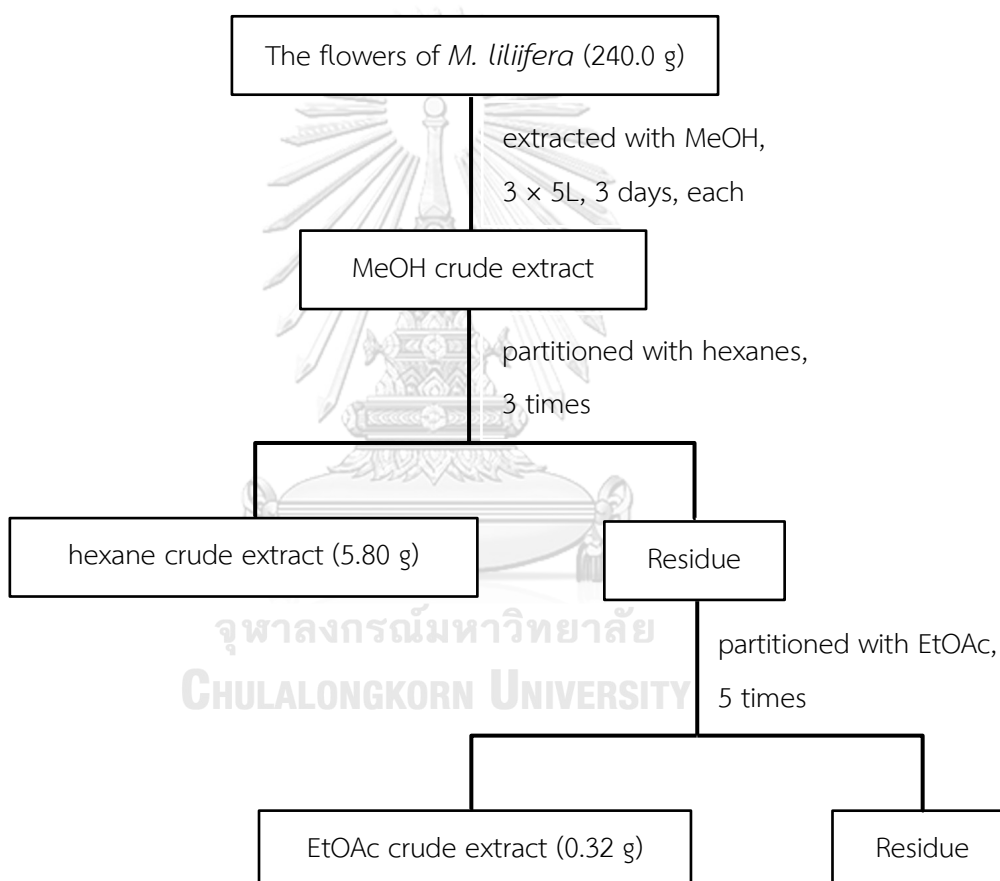
Sephadex-LH20 CC (MeOH), followed by RP-18 CC using MeOH–H₂O (50%, v/v) to yield compound **7** (12.0 mg). The isolation procedure is shown in **Scheme 2.6**.



Scheme 2.6 Isolation procedure of fraction F

2.4.3 Extraction of *M. liliifera* flowers

The air-dried flowers of *M. liliifera* (240.0 g) were extracted with MeOH (3 × 5 L, for 3 days) at room temperature. Evaporation of the solvent under reduced pressure gave the MeOH extract (167.0 g), and the syrupy residue was suspended in water and partitioned in equal amounts for EtOAc (×5) and hexanes (×3) and evaporated under reduced pressure to yield the EtOAc (0.33 g) and hexanes (5.80 g) crude extracts, respectively. The extraction procedure is shown in **Scheme 2.7**.

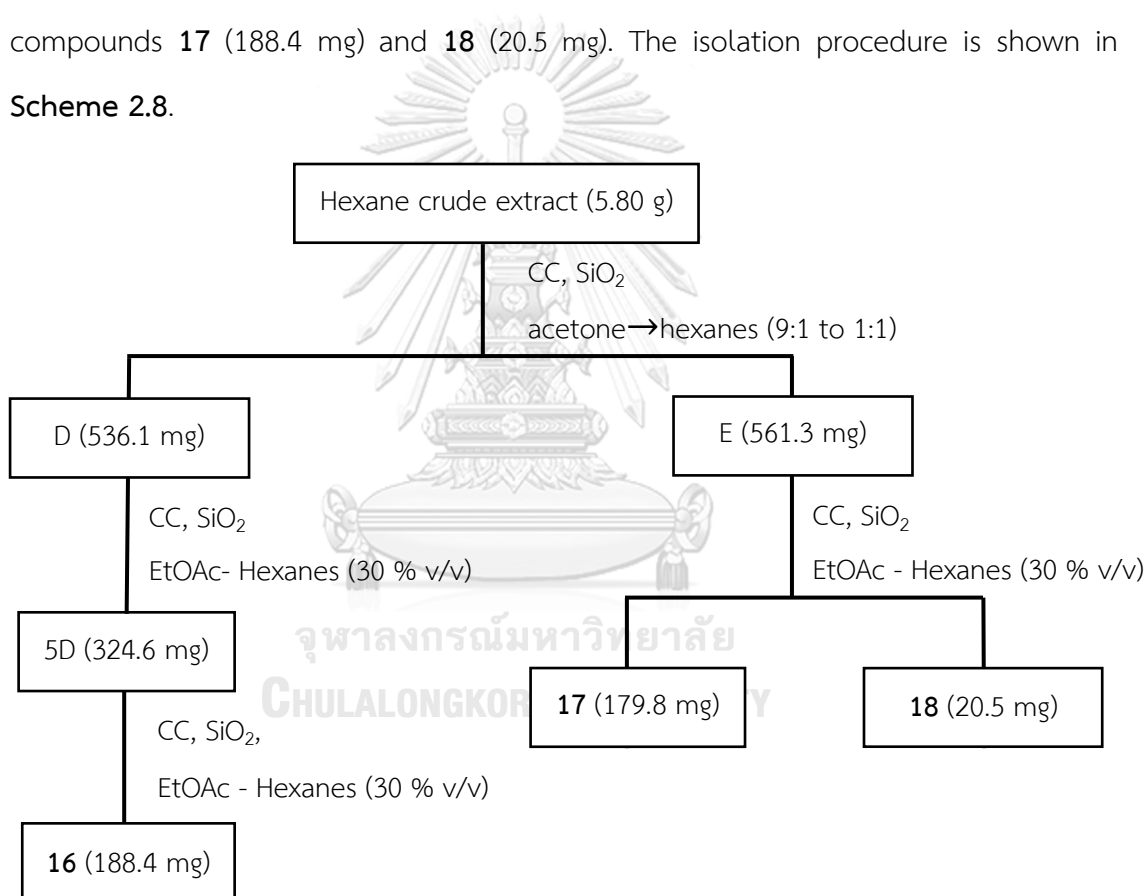


Scheme 2.7 Extraction procedure of *M. liliifera* flowers

2.4.4 Isolation of compounds from hexane crude extract

The hexane crude extract (5.80 g) was subjected to CC on silica gel using a gradient of acetone–hexane (10 → 70%) to provide eight fractions (A–H). Fraction D (536.1 mg) was further fractionated by SiO₂ CC, eluted with EtOAc–hexane (30%, v/v) to afford eight fractions (1D–8D). Subfraction 5D (324.6 mg) was purified by CC using EtOAc–hexane (30%, v/v) to yield compound **16** (188.4 mg). Fraction E (561.3 mg) was further fractionated by SiO₂ CC, eluted with EtOAc–hexane (30%, v/v) to afford compounds **17** (188.4 mg) and **18** (20.5 mg). The isolation procedure is shown in

Scheme 2.8.



Scheme 2.8 Isolation procedure of *M. liliifera* flowers hexane crude

2.5 Biological activity evaluation

2.5.1 DPPH assay

The 2,2-diphenyl-1-picryl-hydrazyl (DPPH) free radical scavenging activity assay is one of the popularly used assay for determination antioxidant capability of plant constituents. This method generates the stable free radical DPPH, which can observe a violet color. Sample that can donate a hydrogen atom to the DPPH radical will turn the color to yellow. The DPPH assay was carried out according to Lu et al⁸³. DPPH was dissolved in MeOH to give a concentration of 0.5 mM. Aliquots of samples dissolved in DMSO were plated out in triplicate in a 96-well microtiter plate at the concentration of 1-100 μ M. Quercetin were used as positive controls. The reaction of mixture consisted of 20 μ l of compound and 180 μ l of DPPH radical solution and was allowed to stay in the dark at room temperature for 30 min. The absorbance was then measured at 517 nm using a microplate reader (Biotek Power Wave XS2). The percentage of decolourisation was plotted against the concentration of the compound, and the IC₅₀ values were determined using Prism 5.00 software. The absorbance obtained was converted into free radical scavenging activity using the following formula;

$$\% \text{ DPPH free radical scavenging activity} = [(A_{\text{blank}} - A_{\text{sample}}) / A_{\text{blank}}] \times 100$$

Where A_{blank} and A_{sample} are the absorbance. The experiment was performed in triplicate and each experiment consisted of three repetitions. DMSO was used as a blank. Quercetin was used as positive control and treated under the same condition as the compounds.

2.5.2 ABTS assay

Measuring total antioxidant capacity of antioxidants are also based on electron transfer reaction. ABTS^{•+} radical scavenging is one of the frequent procedures used to measure an electron transfer-based potential. In the ABTS^{•+}

radical scavenging assay, the 2,2'-azino-bis(3-ethylbenzothiazoline-6-sulfonate) radical cation (ABTS^{•+}), which has a dark blue color, is reduced by an antioxidant into colorless ABTS, which can be measured spectrophotometrically. ABTS was dissolved in DI water to accomplish a concentration of 7 mmol/L and then ABTS solution was treated with potassium persulfate (K₂S₂O₈) concentration at 2.45 mM (ABTS : K₂S₂O₈, 1:0.5 mole/mole) to generate the radical cation ABTS^{•+} and allowing the mixture to stand in the dark at room temperature for 12–16 h to complete a dark blue solution produced. This solution was diluted with DI water (pH 7.4) until the absorbance was 0.7 ± 0.02 at 734 nm the diluted solution calls ABTS working solution⁸⁴. Then, aliquots of compounds dissolved in DMSO or Trolox[®] as positive control 50 µl were added in triplicate in a 96-well plate at the concentration of 1-100 µM and then 100 µl of ABTS working solution were added. After mixing with a sample solution with ABTS working solution, absorption is monitored for 30 min at 734 nm using the microplate reader (Biotek Power Wave XS2), and the IC₅₀ values were determined using Prism 5.00 software. The blank contained the same mixture without the compound or Trolox[®]. The percentage of ABTS^{•+} free radical scavenging activity of samples were calculated using the following formula;

$$\% \text{ ABTS}^{\bullet+} \text{ free radical scavenging activity} = [(A_{\text{blank}} - A_{\text{sample}}) / A_{\text{blank}}] \times 100$$

Where A_{blank} and A_{sample} are the absorbance. The experiment was performed in triplicate and each experiment consisted of three repetitions. They all were treated under the same condition.

2.5.3 Lipid peroxidation inhibition assay

The Thiobarbituric acid-reactive species (TBARS) assay described by Badmus⁸⁷ was used to evaluate the lipid peroxidation, using egg-yolk homogenates as lipid-rich media. Egg homogenate (100 µL, 10% in distilled water, v/v) and the 50 µL dissolved compounds in DMSO were mixed, 50 µL FeSO₄ (0.07 M) (prepared in

buffer pH 4) was added to the mixture in eppendorf and incubated for an hour, to induce lipid peroxidation. Thereafter, 150 μ L of 20% acetic acid (pH adjusted to 3.5 with NaOH) and 150 μ L of 0.8% TBA (w/v) and 0.05 mL 20% TCA were added (prepared in DI water), the eppendorf were vortexed and heated in a heating block for 60 min. After cooling, they were centrifuged at 3000 rpm for 10 min. The absorbance of the supernatant was measured at 532 nm using the microplate reader (Biotek Power Wave XS2). For the blank 50 μ L of DMSO was used in place of the tested compounds. The percentage of inhibition of lipid peroxide was calculated using the equation described in the following formula;

$$\% \text{ Lipid peroxidation inhibition} = [(A_{\text{blank}} - A_{\text{sample}}) / A_{\text{blank}}] \times 100$$

Where A_{blank} and A_{sample} are the absorbance. The experiment was performed in triplicate and each experiment consisted of three repetitions. They all were treated under the same condition.

2.5.4 Nitric oxide inhibition assay

The inhibitory ability of samples on NO production in the medium was measured using the Griess reaction according to a reported method⁸⁵. Murine macrophage J774.A1 cells (1×10^5) were seeded in 96-well plates in Dulbecco's Modified Eagle's Medium (DMEM) containing 10% fetal bovine serum (FBS). After incubation for 24 h at 37 °C in 5% CO₂, the cells were pretreated with various concentrations of the tested compounds or vehicle (DMSO) for 2 h and then stimulated with LPS (1 μ g/mL) for 20 h. The culture supernatant was collected and mixed with Griess reagent. Indomethacin (TCI, Tokyo, Japan) was used as a positive control. The absorbance of culture supernatant (50 μ L) of each well was measured at 540 nm with a microplate reader. All experiments were performed in triplicate and the data are presented as mean \pm SD.

2.5.5 Cytotoxicity assay

To determine the toxicity of the active compounds toward cells tested, the 3-(4,5-dimethyl-2-thiazolyl)-2,5-diphenyl-2*H*-tetrazolium bromide (MTT) colorimetric method was performed⁸⁶. The cells were seeds in 96-well plate with 1×10^4 cells/well and incubated for 24 h at 37° C in a humidified atmosphere containing 5% CO₂. After treatment with samples or vehicle (DMSO) for 24 h, MTT solution (10 μL, 5 mg-mL in phosphate buffer saline (PBS)) was then added to each well and incubated further for 4 h. The medium was removed and DMSO (100 μL/well) was added to dissolve the produced formazan crystals and the absorbance was measured at 540 nm using a microplate reader. Cells treated with only DMSO were used as a control.



CHAPTER III

RESULTS AND DISCUSSION

3.1 Isolated compounds from *Dendrobium signatum* Rchb.f.

The EtOAc crude extract of *D. signatum* aerial parts was subjected to chromatographic fractionation resulting in the isolation of 15 compounds. Their structures were elucidated by interpreting the spectroscopic data. The compounds include a new picrotoxane sesquiterpene, 7-hydroxydendroterpene B (**2**) and a new α -pyrone derivative, (-)-6*R*-signatone (**4**), along with thirteen known compounds classified as terpenoids, bibenzyls, flavonoids, lignans and coumarins. These included dendroxine (**1**), crystallinin (**3**), dendrocandin B (**5**), dendrocandin I (**6**), 6''-de-*O*-methyldendrofindlaphenol A (**7**), *p*-hydroxyphenylethyl-*p*-coumarate (**8**), 3,4-dihydroxy-5,4'-dimethoxybibenzyl (**9**), 3-methoxy-5-[2-(4-methoxyphenyl)ethyl]phenol (**10**), 4,4'-dihydroxy-3,5-dimethoxybibenzyl (**11**), naringenin (**12**), (2*S*)-homoeridodictyol (**13**), (2*S*)-homohesperetin (**14**) and (-)-syringaresinol (**15**). Chemical structures of isolated compounds are depicted in **Figure 3.1**.

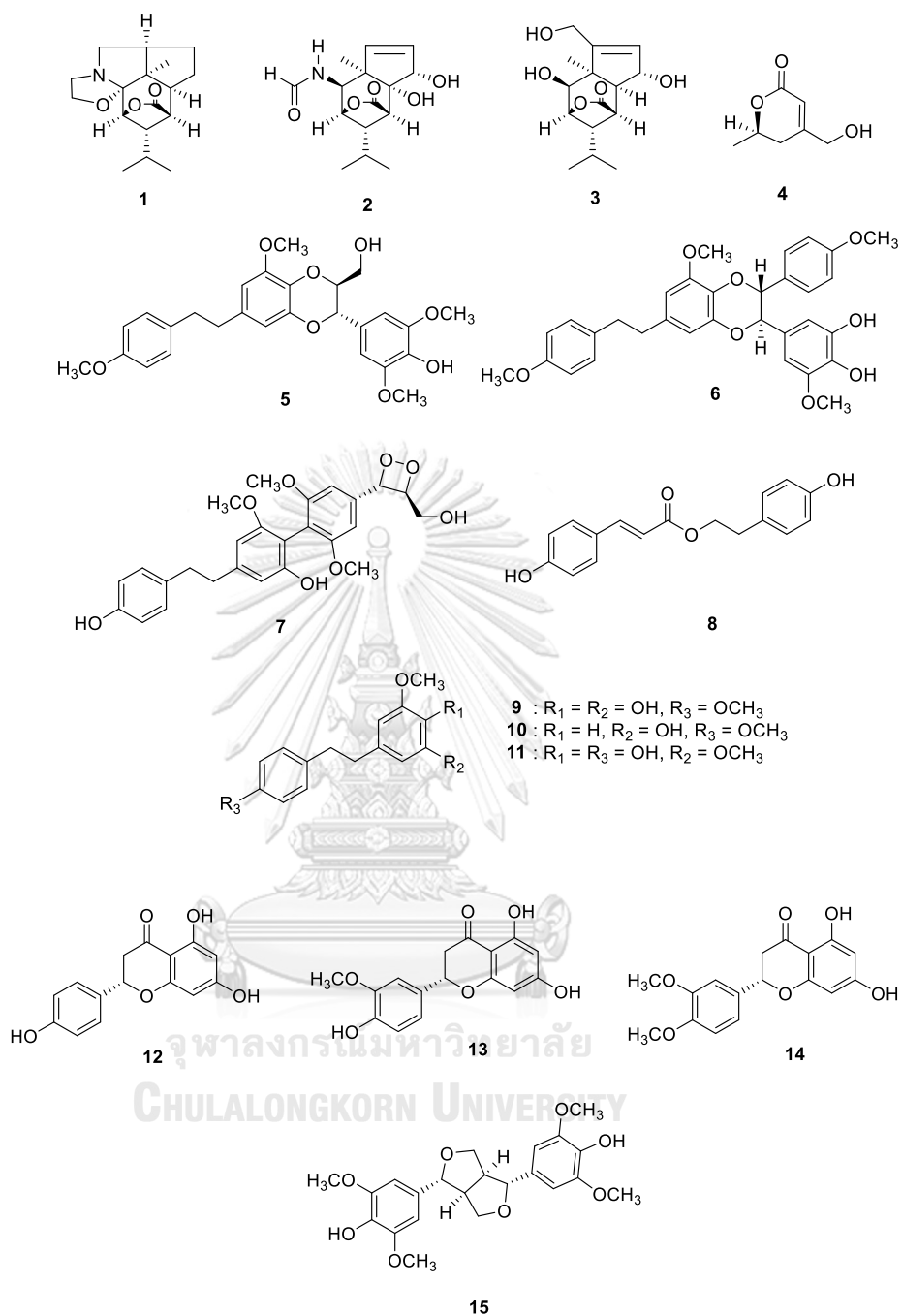
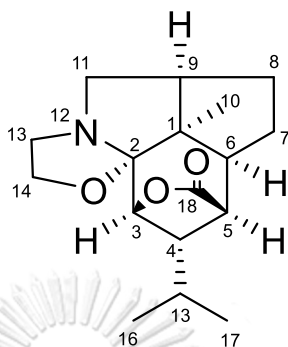


Figure 3.1 The chemical structures of isolated compounds from *D. signatum*

3.2 Structure elucidation of isolated compounds from *Dendrobium signatum*

Rchb.f.

3.2.1 Structure elucidation of compound 1



Molecular formula	$C_{17}H_{25}NO_3$
Appearance	colorless thin-plate crystal
Melting point	318-319 °C
$[\alpha]_D^{25}$ (c 0.1, MeOH)	+25.8
UV(MeOH) λ_{max} (log ϵ)	224 (+26.7)
IR (neat)	2964, 2860, 1775, 1466 cm^{-1}
1H and ^{13}C NMR ($CDCl_3$)	See Table 3.1

Compound **1** obtained as colorless thin-plate crystals, exhibited a molecular formula of $C_{17}H_{25}NO_3$ on the basis of the HR-TOFMS ion peak at m/z 292.1936 $[M+H]^+$ (calcd $C_{17}H_{26}NO_3$: 292.1913) and ^{13}C NMR data, corresponding to 6 indices of hydrogen deficiency. The major peak in the IR absorption indicated the characteristic band of a γ -lactone moiety at 1775 cm^{-1} . The 1H and ^{13}C NMR spectra of **1** (**Table 3.1**) displayed resonances attributable to an oxymethine proton [$\delta_{H/C}$ 4.27 (d, $J = 4.8$ Hz, H-3)/80.6], a set of non-equivalent oxymethylene protons [$\delta_{H/C}$ 3.89 (1H, ddd, $J = 7.8, 6.8, 3.6$ Hz, H-18b) and 3.80 (1H, td, $J = 8.6, 6.8$ Hz, H-18a)/64.7], three methyl protons [$\delta_{H/C}$ 1.26 (s, H₃-10)/27.9, 1.20 (d, $J = 6.2$ Hz, H₃-14)/21.4 and 0.94 (d, $J = 6.2$ Hz, H₃-15)/21.2] and several aliphatic methylenes and methines. The ^{13}C NMR (**Table**

3.1) and DEPT spectra displayed 17 signals, including one carbonyl (δ_C 178.5), one oxymethine (δ_C 80.6), five methines (δ_C 56.1, 51.9, 43.4, 42.3, 24.5), one oxymethylene (δ_C 64.7), four methylenes (δ_C 54.0, 51.8, 31.7, 30.9) and two quaternary carbons (δ_C 103.4, 53.6). The above ^1H and ^{13}C NMR data showed a signal pattern similar to that of a dendrobine-type alkaloid framework⁸⁸. The HMBC correlations (**Figure 3.2**) from H-4 to C-3, C-14, C-15, C-5, and C-16 and from H-3 to C-1, C-2, and C-16, along with the sequential COSY correlations (**Figure 3.2**) from H-4 to H₃-14 and H₃-15 through H-13 suggested that the isopropyl moiety attached at C-4 and the units are linked through C-3/C-16 bond, constructing a γ -lactone ring. In the HMBC spectrum, the correlations from H₃-10 to C-1, C-2, C-6 and C-9 confirmed the H₃-10 at C-1. The functionalities accounting for 4 out of 6 indices of hydrogen deficiency required the presence of two additional ring. Furthermore, a 5/5 fused bicyclic core was deduced by the HMBC correlations from H₂-11 to C-1, C-2 and C-17, from H₂-17 to C-11 and from H₂-18 to C-2, constructing the C(2)-N and C(2)-O-C(18) bonds. The relative configuration of C-3 was defined by the coupling constant observed for H-3 ($J = 4.8$ Hz) which indicated that H-3 were in a pseudo-equatorial position. This was confirmed from the NOESY experiments observed for the correlations of H-3/H-4, H-4/H-5, and H-5/H-6. The NOESY correlations (**Figure 3.3**) between H-6/H-10 and H-9/H-10 observed were in agreement with an α -orientation. The ECD spectrum (**Figure S1**) of compound **1** exhibited a positive Cotton effect at 230 ($\Delta\epsilon +26.7$) nm. Refinement of the Cu K α data of **1** resulted in a Flack parameter of $-0.01(16)$ allowing the unambiguous assignment of the absolute configuration as 1*S*, 2*R*, 3*R*, 4*S*, 5*R*, 6*S*, 9*R* (**Figure 3.4**). Thus, the structure of **1** was established as picrotoxane sesquiterpenes, namely dendroxine⁸⁹, as shown in Figure **3.3**. To the best of our knowledge, this is the first report for the full NMR assignment and the crystal data of the compound.

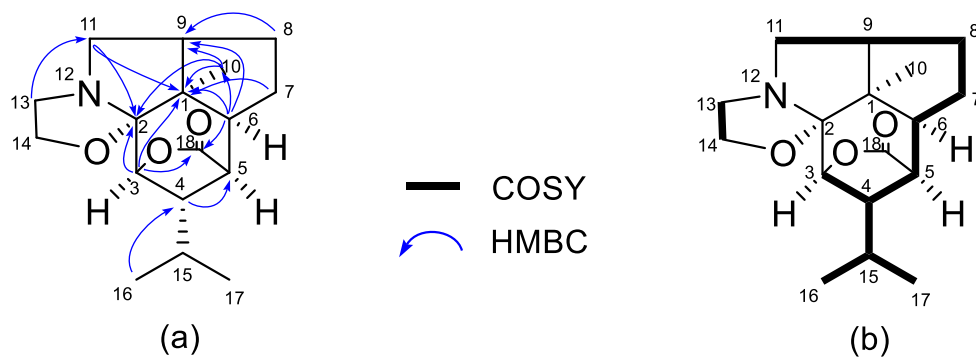


Figure 3.2 HMBC (a) and ^1H - ^1H COSY (b) correlations of compound 1

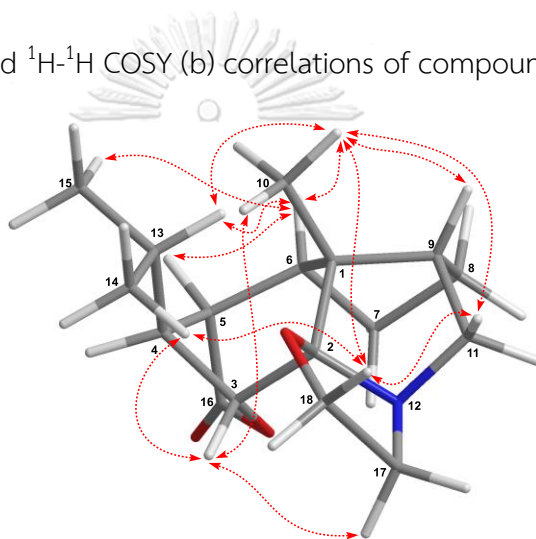


Figure 3.3 ^1H - ^1H NOESY correlations of compound 1

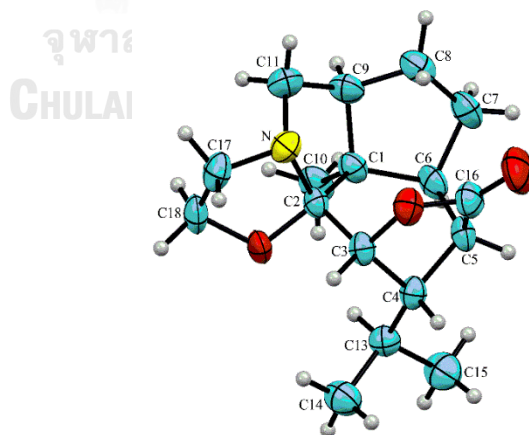


Figure 3.4 ORTEP diagram of compound 1

Table 3.1 NMR data of compound **1** (CDCl₃)

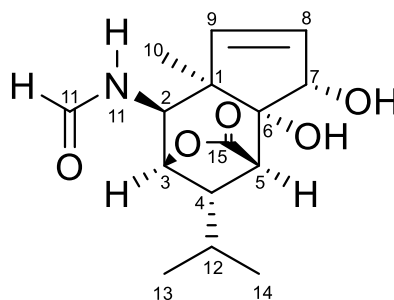
no.	compound 1	
	δ_c^a	δ_H [mult, J in Hz] ^b
1	53.6	
2	103.4	
3	80.6	4.27 (d, J = 4.8 Hz, 1H)
4	51.9	2.13 (m)
5	43.4	2.48 (dd, J = 6.3, 4.4 Hz, 1H)
6	42.3	2.10 (dd, J = 4.4 Hz, 1H)
7	31.7	1.89 (tdd, J = 13.3, 8.9, 6.3 Hz, 1H); 2.00 (dd, J = 13.3, 6.3 Hz, 1H)
8	30.9	1.56 (m); 1.73 (dt, J = 13.3, 7.3 Hz, 1H)
9	56.1	2.22 (dtd, J = 12.0, 7.3, 2.0 Hz, 1H)
10	27.9	1.26, s
11	54.0	2.81 (dd, J = 9.9, 7.3 Hz, 1H); 3.03 (dd, J = 9.9, 2.0 Hz, 1H)
12		
13	24.5	2.03 (q, J = 6.2 Hz, 1H)
14	21.4	1.20 (d, J = 6.2 Hz, 3H)
15	21.2	0.94 (d, J = 6.2 Hz, 3H)
16	178.5	
17	51.9	3.02 (ddd, J = 12.0, 8.6, 6.8 Hz, 1H); 3.20 (ddd, J = 12.0, 8.6, 6.8 Hz, 1H)
18	64.7	3.80 (td, J = 8.6, 6.8 Hz, 1H); 3.89 (ddd, J = 7.8, 6.8, 3.6 Hz, 1H)

^a Spectra were recorded at 125, ^b 500 MHz.,

Table 3.2 Crystal data and structure refinement for compound **1**

Formula	C ₁₇ H ₂₅ NO ₃
Molecular weight	291.39
Crystal size (mm)	0.06×0.40×0.48
Crystal system	orthorhombic
Space group	<i>P</i> 2 ₁ 2 ₁ 2 ₁
<i>a</i> (Å)	9.2548(1)
<i>b</i> (Å)	10.1196(1)
<i>c</i> (Å)	16.1677(2)
<i>V</i> [Å ³]	1514.18(3)
<i>Z</i>	4
ρ_{calcd} [Mg m ⁻³]	1.278
μ (mm ⁻¹)	0.695
<i>F</i> (000)	632
Reflns collected / unique / > 2 σ (<i>I</i>)	11868, 2755, 2508
<i>R</i> _{int}	0.0763
<i>R</i> ₁	0.0969
<i>wR</i> ₂ ^b [<i>I</i> > 2 σ (<i>I</i>)]	0.2092

3.2.2 Structure elucidation of compound 2



Molecular formula	$C_{15}H_{21}NO_5$
Appearance	colorless triangular crystal
Melting point	285-286 °C
$[\alpha]_D^{25}$ (c 0.1, MeOH)	+2.0
UV(MeOH) λ_{max} (log ϵ)	228 nm (+9.0)
IR (neat)	3260, 2964, 2851, 1757, 1662 cm^{-1}
1H and ^{13}C NMR ($CDCl_3$)	See Table 3.3

Compound **2** was isolated as colorless crystals and had a molecular formula $C_{15}H_{21}NO_5$ as determined by the HR-TOFMS ion at m/z 318.1331 $[M + Na]^+$ (calcd $C_{15}H_{21}NNaO_5$, 318.1317) and ^{13}C NMR data, corresponding to 6 indices of hydrogen deficiency. The IR spectrum indicated the presence of hydroxy (3260 cm^{-1}), lactone carbonyl (1757), and α,β -unsaturated carbonyl (1662 cm^{-1}) groups. The 1H NMR spectrum of **2** (**Table 3.3**) displayed resonances attributed to three methyl protons [δ_H 1.00 (d, $J = 6.2$ Hz, H_3 -14), 1.11 (d, $J = 6.2$ Hz, H_3 -15), 1.12 (s, H_3 -10)], six methine protons [δ_H 2.12 (dt, $J = 11.0, 4.8$ Hz, H-4), 2.40 (m, H-2), 2.53 (d, $J = 4.2$ Hz, H-5), 4.40 (d, $J = 5.6$ Hz, H-3), 4.45 (d, $J = 9.8$ Hz, H-7), 4.48 (dd, $J = 6.1, 2.8$ Hz, H-2)], two olefinic protons [δ_H 5.72 (dd, $J = 6.4, 2.8$ Hz, H-8), 6.14 (d, $J = 6.4$ Hz, H-9)], and one shielded aldehyde proton (δ_H 8.27, s). The ^{13}C NMR (**Table 3.3**), DEPT and HSQC data revealed a total of 15 carbon signals, consisting of one aldehyde carbonyl (δ_C 161.8),

one ester carbonyl (δ_C 176.5), six methines (δ_C 27.5, 51.1, 53.0, 79.3, 79.4, 83.9), one carbon-carbon double bond (δ_C 130.8, 142.5), two quaternary carbons (δ_C 53.6, 78.0), and three methyls (δ_C 20.4, 22.3, 25.6). The ^1H - ^1H COSY spectrum and key HMBC correlations of H₃-10 to C-1, C-2, C-6 and C-9, H-2 to C-1 and C-9, H-5 to C-6, and H-8 to C-6 (**Figure 3.5**) suggested that **1** was a picrotoxane-type sesquiterpene^{90, 91}. From the HMBC spectrum, the cross-peaks of H-3 and H-6 to a carbonyl carbon (C-16) at δ_C 176.5 revealed the presence of closed a γ -lactone ring between C-3 and C-5. The formamide moiety at C-2 was deduced by the appearance of highly shielded chemical shifts of the aldehyde group at δ_H 8.27/ δ_C 161.8, along with the HMBC correlation from H-2 to the aldehyde carbonyl were observed, along with the HMBC correlations (**Figure 3.5**) from H-7 to C-1, C-5, C-6, C-8 and C-9 and from H-9 to C-1, C-6 and C-10 suggested that the $\Delta^{8(9)}$ bond and hydroxy group located at C-8(9) and C-7, respectively. Certainly, the NMR data of **2** is in agreement with the dendroterpene B⁹¹. Comparing their NMR data one oxygenated methine appeared in **2**, replacing one of the methylene in dendroterpene B was surely indicated by the 2D NMR data (**Figure 3.5**). In addition, the relative configuration was determined by NOESY experiment (**Figure 3.6**), the cross-peaks of H-2/H₃-10, H-2/H-13, H-3/H-5 and H-3/H₃-14 revealed that these protons were co-facial and assigned as α -oriented. Whereas the lack of the correlations of them with H-4 and H-7 indicated that these protons were related to β -oriented. Furthermore, the electronic circular dichroism (ECD) was measured, and the spectrum exhibited a positive Cotton effect at 228 ($\Delta\epsilon$ +9.0) nm (**Fig. S1**). The (1*R*, 2*S*, 3*S*, 4*R*, 5*R*, 6*R*, 7*S*) absolute configuration of **2** was confirmed by single-crystal X-ray diffraction data (**Figure 3.7**) with the estimated Flack parameter 0.06(6). From the above data, compound **2** was proposed to be the new structure, named as 7- hydroxydendroterpene B.

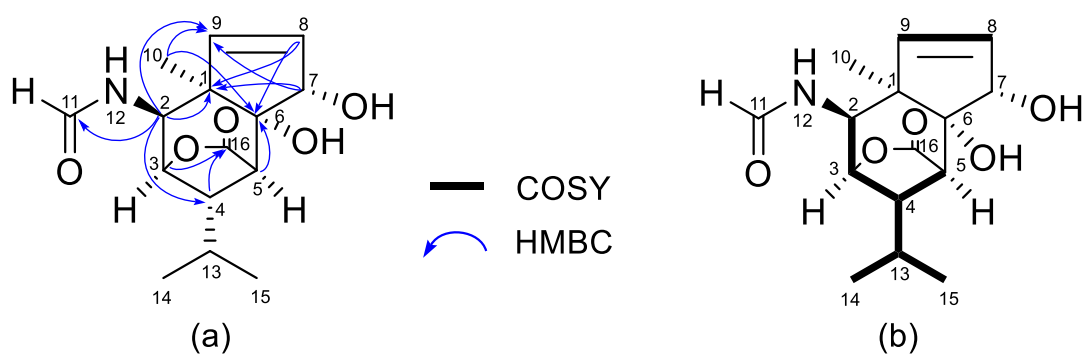


Figure 3.5 HMBC (a) and ^1H - ^1H COSY (b) correlations of compound 2

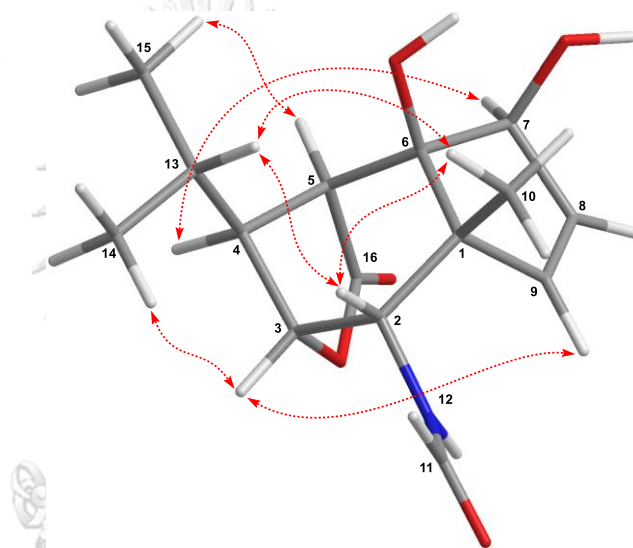


Figure 3.6 ^1H - ^1H NOESY correlations of compound 2

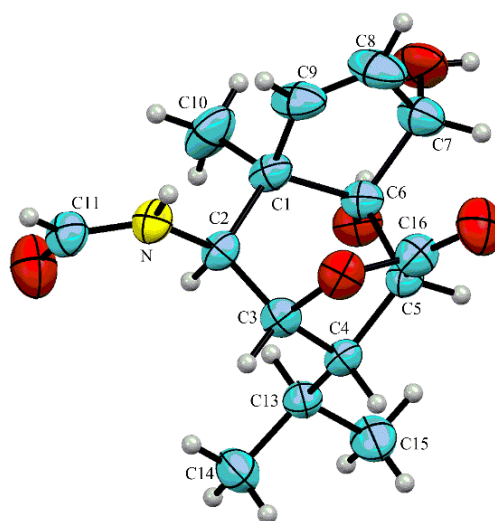


Figure 3.7 ORTEP diagram of compound 2

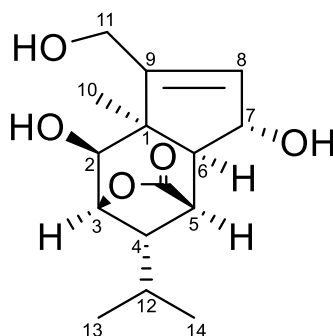
Table 3.3 NMR data of compound **2** (acetone- d_6)

no.	δ_c^a	δ_H [mult, J in Hz] ^b
1	53.6	
2	79.3	4.48 (dd, $J = 6.1, 2.8$ Hz, 1H)
3	83.9	4.40 (<i>br d</i> , $J = 5.6$ Hz, 1H)
4	53.0	2.12 (dt, $J = 11.0, 4.8$ Hz, 1H)
5	51.1	2.53 (<i>br d</i> , $J = 4.2$ Hz, 1H)
6	78.0	
7	79.4	4.45 (<i>br d</i> , $J = 9.8$ Hz, 1H)
8	130.8	5.72 (dd, $J = 6.4, 2.8$ Hz, 1H)
9	142.5	6.14 (d, $J = 6.4$ Hz, 1H)
10	25.6	1.12 (s, 3H)
11	161.8	8.27 (s, 1H)
12		
13	27.5	2.41-2.38 (m, 1H)
14	20.4	1.00 (d, $J = 6.2$ Hz, 3H)
15	22.3	1.11 (d, $J = 6.2$ Hz, 3H)
16	176.5	

^a Spectra were recorded at 125, 500 MHz ^b

Table 3.4 Crystal data and structure refinement for compound **2**

Formula	C ₁₅ H ₂₁ NO ₅
Molecular weight	295.33
Crystal size (mm)	0.40×0.42×0.52
Crystal system	Tetragonal
Space group	<i>P</i> 4 ₃ 2 ₁ 2
<i>a</i> (Å)	9.7813(2)
<i>b</i> (Å)	9.7813(2)
<i>c</i> (Å)	30.8333(8)
<i>V</i> [Å ³]	2949.94(14)
<i>Z</i>	8
ρ_{calcd} [Mg m ⁻³]	1.330
μ (mm ⁻¹)	0.829
<i>F</i> (000)	1264
Reflns collected / unique / > 2 σ (<i>I</i>)	15848, 2685, 2553
<i>R</i> _{int}	0.0319
<i>R</i> ₁	0.0292
<i>wR</i> ₂ ^b [<i>I</i> > 2 σ (<i>I</i>)]	0.0728

3.2.3 Structure elucidation of compound **3**

Molecular formula	$C_{15}H_{22}O_5$
Appearance	white needles crystal
$[\alpha]_D^{25}$ (c 0.1, MeOH)	+95.6
IR (neat)	3387, 2764, 2847, 1746, 1676 cm^{-1}
1H and ^{13}C NMR ($CDCl_3$)	See Table 3.3

Compound **3** was obtained as white needles, and the molecular formula was identified as $C_{15}H_{22}O_5$ using the HR-TOFMS ion at m/z 305.1376 $[M + Na]^+$ (calcd $C_{15}H_{22}NaO_5$, 305.1365). In the IR spectrum, absorption bands at 3387 and 1746 cm^{-1} suggested the presence of hydroxyl and γ -lactone groups, respectively. The ^{13}C and DEPT-135 NMR spectrum of **3** revealed 15 carbon signals including three methyl, one methylene, eight methine, and three quaternary carbons. The 1H NMR spectrum exhibited the presence of three methyl groups at δ_H 1.53, 1.01, and 1.01, two oxygenated methylene protons at δ_H 4.30 and 4.12, and three oxygenated methine protons at δ_H 3.71, 4.60, and 4.71. The ^{13}C NMR spectral data and the presence of five degrees of unsaturation in compound **3** suggested that it was a sesquiterpene with a $\Delta^{8(9)}$ bond possessing a picrotoxane-type scaffold. As compared to the known compound crystallinin⁶³, their NMR spectral data were very similar (**Table 3.5**). Analysis of the NOESY spectra showed the correlations between H-2/H-3, H-2/H₃-13, H-2/H₃-14 and H-3/H₃-13, H-3/H₃-14 and H-6/H₃-10, suggesting that the

methyl group at C-1, two methine protons at H-2, H-6 and the isopropyl group at C-4 were all in the same orientation. Likewise, the correlation between H-5/H-7 confirmed that the hydroxy at C-7 was in the same orientation. Accordingly, **3** was confirmed to be a known picrotoxinin-type sesquiterpene, namely crystallinin that was first isolated from *D. crystallinum*⁶³.

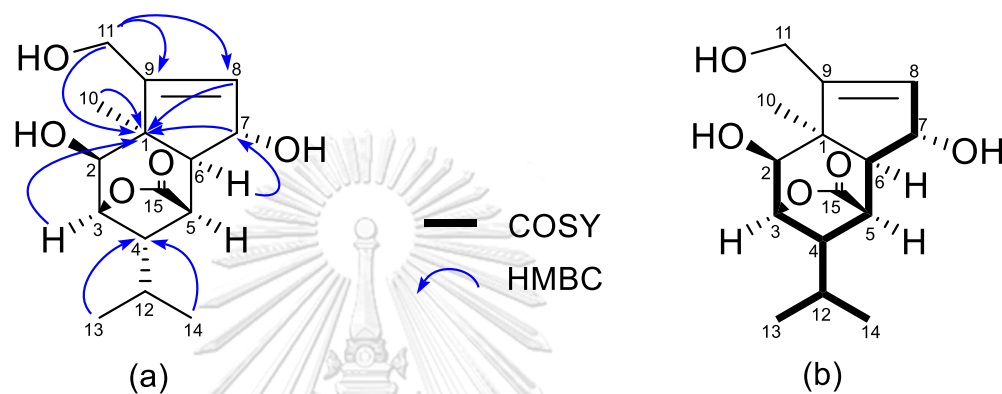


Figure 3.8 HMBC (a) and ^1H - ^1H COSY (b) correlations of compound **3**

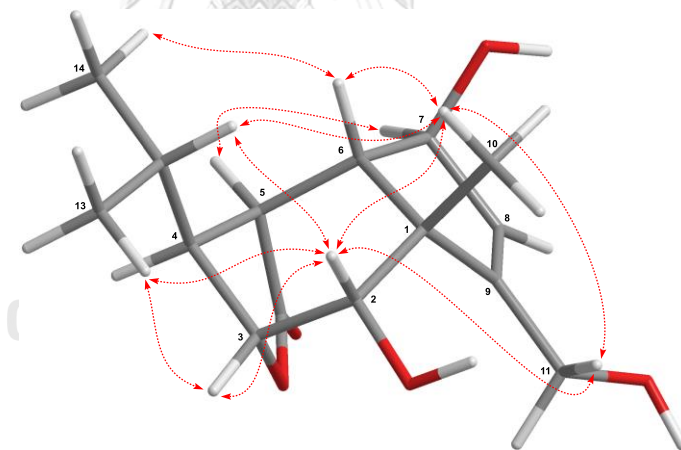


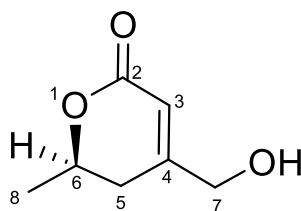
Figure 3.9 ^1H - ^1H NOESY correlations of compound **3**

Table 3.5 NMR data of compound **3** (CDCl₃) and crystallinin (acetone-d₆)

no.	crystallinin		compound 3	
	δ_C^c	δ_H [mult, <i>J</i> in Hz] ^d	δ_C^a	δ_H [mult, <i>J</i> in Hz] ^b
1	54.1		53.3	
2	75.5	3.81 (s, 1H)	74.3	3.71 (d, 5.4 Hz, 1H)
3	85.3	4.45 (d, <i>J</i> = 5.5 Hz, 1H)	85.4	4.60 (dd, 5.4, 1.1 Hz, 1H)
4	52.9	2.08 (m, 1H)	51.6	2.12 (dt, 10.6, 5.0 Hz, 1H)
5	52.3	2.11 (d, <i>J</i> = 3.7 Hz, 1H)	50.1	2.24 (d, 3.6 Hz, 1H)
6	45.9	2.48 (m, 1H)	44.8	2.55 (dd, 3.6 Hz, 1H)
7	78.5	4.59 (d, <i>J</i> = 2.6 Hz, 1H)	77.6	4.71 (d, 2.6 Hz, 1H)
8	130.7	5.59 (d, <i>J</i> = 1.8 Hz, 1H)	132.8	5.75 (d, 2.6 Hz, 1H)
9	155.5		153.2	
10	31.4	1.53, s, 1H	30.5	1.53, s Hz, 1H
11	61.3	4.12 (s, 1H); 4.30 (s, 1H)	59.5	4.12 (d, 12.4 Hz, 1H); 4.30 (d, 12.4 Hz, 1H)
12	26.7	1.76-1.78 (m Hz, 1H)	25.5	1.69-1.79 (m Hz, 1H)
13	21.7	1.01 (d, <i>J</i> = 6.7 Hz, 1H)	21.1	1.01 (d, 6.6 Hz, 1H)
14	20.5	1.01 (d, <i>J</i> = 6.7 Hz, 1H)	19.5	1.01 (d, 6.6 Hz, 1H)
15	178.3		178.9	

^a Spectra were recorded at 125, ^b 500, ^c 75, ^d 300 MHz.

3.2.4 Structure elucidation of compound 4



Molecular formula	$C_7H_{10}O_3$
Appearance	pale-yellow oil
$[\alpha]_D^{25}$ (c 0.1, MeOH)	-13.06
UV(MeOH) λ_{max} (log ϵ)	220 nm (-9.0), 250 nm (-10.0)
IR (neat)	3365, 2962, 2913, 1752, 1467 cm^{-1}
1H and ^{13}C NMR ($CDCl_3$)	See Table 3.6

Compound **4** was obtained as a pale-yellow oil. The HR-TOFMS ion at m/z 165.0527 $[M+Na]^+$ (calcd $C_7H_{10}NaO_3$: 165.0528) gave a molecular formula of $C_7H_{10}O_3$. The presence of carbonyl and hydroxy functionalities was established from the IR absorptions at the respective 1752 and 3365 cm^{-1} . Interpretation of ^{13}C NMR, DEPT and HSQC spectra of compound **4** (**Table 3.6**) showed 7 signals including a methyl (δ_C 20.9), an oxygenated methylene (δ_C 64.0), a methylene (δ_C 31.8), an oxygenated methine (δ_C 74.1), an olefinic methine (δ_C 114.2), a quaternary olefinic carbon (δ_C 159.5), and a carbonyl carbon (δ_C 165.4). The 1H NMR spectrum showed the presence of an olefinic signal [δ_H 6.08 (dd, J = 1.4, 2.0 Hz, H-3)], an oxymethine proton [δ_H 4.56 (dq, J = 8.6, 6.4 Hz, H-6)], one methyl protons [δ_H 1.45 (d, J = 6.4 Hz, H₃-8)], one methylene signal [δ_H 2.27 (d, J = 7.1 Hz, H₂-5)], and hydroxy methylene unit [δ_H 4.29 (s Hz, H₂-7)]. The correlations of H-5/H-6/H₃-8 in the COSY spectrum along with their HMBC correlations observed for H-5 to C-2, C-3 and C-6 and H-6 to C-2, C-4 and C-8 accounted for confirmation of an α -pyrone structure. The HMBC

correlation from H₃-8 to C-5 and C-6 confirmed the location of the methyl group at C-6, while a hydroxymethyl group was connected to C-4 due to the correlation of H-3 to C-4, C-5 and C-7. From the above data, the structure of compound **4** was implicitly related to 4-(hydroxymethyl)-5,6-dihydro-pyran-2-one⁹², with only differences in methyl substituted group. The C-6 methyl group was pseudo-equatorially oriented in the most stable conformation of side chain that can be inferred from consideration of steric factors by Snatzke's rules^{93,94}. In addition, the ECD spectrum (Figure S1) of compound **4** exhibited a negative Cotton effect at 220 nm ($\Delta\epsilon$ -9.0) and at 250 nm ($\Delta\epsilon$ -10.0) resulting the absolute configuration for 6*R* by comparison of its ORD curve with that of parasorbic acid⁹⁵. Hence, the structure of **4** was determined as a new 6-methyl-5,6-dihydro- α -pyrones, named as (-)-6*R*-signatone.

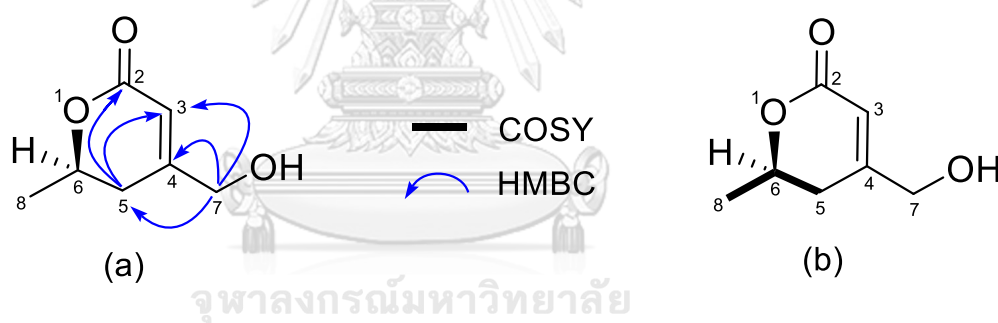


Figure 3.10 HMBC (a) and ¹H-¹H COSY (b) correlations of compound **4**

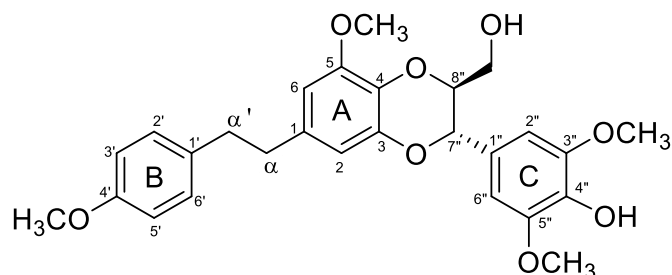
Table 3.6 NMR data of compound **4** (CDCl₃)

no.	δ_C^a	δ_H [mult, <i>J</i> in Hz] ^b
2	165.4	
3	114.2	6.08 (dd, <i>J</i> = 1.4, 2.0 Hz, 1H)
4	159.5	
5	31.8	2.27 (d, <i>J</i> = 7.1 Hz, 2H)
6	74.1	4.56 (dq, <i>J</i> = 8.6, 6.4 Hz, 1H)
7	64.0	4.45 (s, 2H)
8	20.9	1.45 (d, <i>J</i> = 6.4, 3H)

^a Spectra were recorded at 125, ^b 500 MHz



3.2.5 Structure elucidation of compound 5



Molecular formula	$C_{27}H_{30}O_8$
Appearance	white powder
$[\alpha]_D^{25}$ (c 0.1, MeOH)	-3.2
1H and ^{13}C NMR ($CDCl_3$)	See Table 3.7

Compound **5** was obtained as a white powder. Its specific optical rotation $[\alpha]_D^{25}$ (c 0.1, MeOH) was recorded to be -3.2. Analysis of 1H and ^{13}C NMR spectroscopic data revealed the molecular formula of $C_{27}H_{30}O_8$. The structure of **5** was deduced from its 1D and 2D NMR data. The ^{13}C NMR spectrum (**Table 3.7**) displayed twenty-four carbon signals that corresponded the presence of three methoxy groups at (δ_C 55.4, 56.3 and 56.6), two methylene carbons at (δ_C 37.1, 38.1), one oxygenated methylene carbons at (δ_C 61.8), two oxygenated methine carbons at (δ_C 76.7 and 78.5), seven oxygenated quaternary carbons at (δ_C 144.3, 131.9, 148.6, 158.1, 147.5, 135.5, and 147.5), three olefinic quaternary carbons (δ_C 133.4, 134.8 and 127.5). together with, six aromatic methine carbons at (δ_C 109.7, 104.4, 129.5, 113.9, 127.5 and 105.1).

According to 1H -NMR data (**Table 3.7**), the signals of six aromatic protons were distributed to three aromatic rings on the basis of the coupling constants. The two pair signals of methylene protons at δ_H 2.79 (m, H- α') and δ_H 2.85 (m, H- α) and

four singlet methoxy groups at δ_{H} 3.79 (5-OCH₃ and 4'-OCH₃), δ_{H} 3.91 (3''-OCH₃) and δ_{H} 3.85 (5''-OCH₃) were observed.

Besides, the coupling constants in the ¹H-NMR spectrum, *o*-coupled signals appeared at δ_{H} 7.10 (d, *J* = 8.5 Hz, H-2', H-6') and δ_{H} 6.83 (d, *J* = 8.5 Hz, H-3', H-5'), illustrating the presence of a 1,4-disubstituted aromatic ring B. Two *m*-coupled signals appeared at δ_{H} 6.51 (d, *J* = 1.5 Hz, H-2) and δ_{H} 6.67 (d, *J* = 1.5 Hz, H-6), indicating the presence of a 1,3,4,5-tetrasubstituted aromatic ring A, along with two protons singlet appeared at δ_{H} 6.32 (s, H-2'', H-6''), revealing a symmetrically 1,3,4,5-tetrasubstituted aromatic ring C.

In addition, the HMBC (**Figure 3.11**) demonstrated that correlation peaks from H₂- α to C-1, C-2, C-6 and C- α' , from H-2 to C-3, C-4, C-6 and C- α , from H-6 to C-1, C-2, C-4, C-5 and C- α , from H₂- α' to C-1', C-2', C-6' and C- α , from H-2' to C-3', C-4', C-6' and C- α' and from H-3' to C-1', C-4' and C-5' were observed, which suggested the presence of a bibenzyl unit. The HMBC correlation peaks from H-2'' to C-1'', C-3'', C-4'' and C-7'' and from H-7'' to C-1'', C-2'', C-6'', C-8'' and C-9'' deduced the presence of a phenylpropane unit. The deshielded doublet at δ_{H} 4.95 (d, *J* = 8.2 Hz, H-7''), characteristic of a benzylic methine substituted by an oxygen, and the multiplet at δ_{H} 3.91 (m, H-8''), which were coupled to oxygenated methylene at δ_{H} 3.56 (m, H_a-9'') and δ_{H} 3.88 (m, H_b-9''), indicated the presence of a 1,4-dioxane ring between a bibenzyl moiety and a phenyl ring^{96, 97}.

Based on the aforementioned spectroscopic data, compound **5** was determined as dendrocandin B⁹⁸, which was first isolated from *D. candidum*⁹⁸.

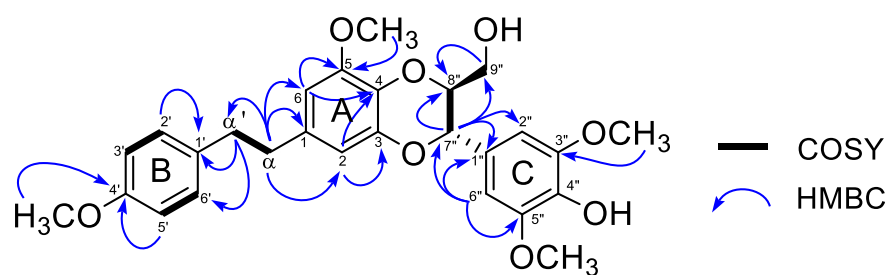


Figure 3.11 HMBC and ^1H - ^1H COSY correlations of compound **5**

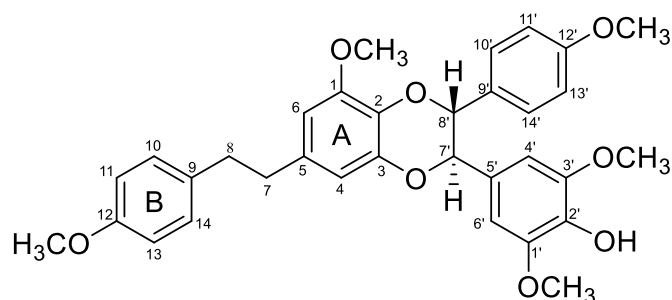
Table 3.7 NMR data of compound **5** and dendrocandin B (CDCl_3)

no.	dendrocandin B		compound 5	
	δ_{C}^a	δ_{H} [mult, J in Hz] ^b	δ_{C}^a	δ_{H} [mult, J in Hz] ^b
1	134.5		133.4	
2	109.5	6.52 (d, $J = 1.0$ Hz, 1H)	109.7	6.51 (d, $J = 1.5$ Hz, 1H)
3	144.1		144.3	
4	131.0		131.9	
5	148.4		148.6	
6	104.8	6.32 (d, $J = 1.5$ Hz, 1H)	104.4	6.67 (d, $J = 1.5$ Hz, 1H)
1'	133.7		134.8	
2'	129.4	7.10 (d, $J = 8.0$ Hz, 1H)	129.5	7.10 (d, $J = 8.5$ Hz, 1H)
3'	113.7	6.83 (d, $J = 8.0$ Hz, 1H)	113.9	6.83 (d, $J = 8.5$ Hz, 1H)
4'	160.1		158.1	
5'	113.7	6.83 (d, $J = 8.0$ Hz, 1H)	113.9	6.83 (d, $J = 8.5$ Hz, 1H)
6'	129.4	7.10 (d, $J = 8.0$ Hz, 1H)	127.5	7.10 (d, $J = 8.5$ Hz, 1H)
α	38.0	2.82 (m, 2H)	37.1	2.85 (m, 2H)
α'	37.0	2.82 (m, 2H)	38.1	2.79 (m, 2H)
5-OCH ₃	56.0	3.85 (s, 3H)	55.4	3.79 (s, 3H)
4'-OCH ₃	55.3	3.79 (s, 3H)	55.4	3.79 (s, 3H)

1"	127.3		127.5	
2"	104.0	6.68 (s, 1H)	105.1	6.32 (s, 1H)
3"	147.2		147.5	
4"	135.2		135.5	
5"	147.2		147.5	
6"	104.0	6.68 (s, 1H)	105.1	6.32 (s, 1H)
7"	76.4	4.96 (d, $J = 8.2$ Hz, 1H)	76.7	4.95 (d, $J = 8.2$ Hz, 1H)
8"	78.2	3.98 (m, 1H)	78.5	3.91 (m, 1H)
9"	61.5	3.55 (dd, $J = 12.0, 3.0$ Hz, 2H)	61.8	3.56 (m, 1H); 3.88 (m, 1H)
3"-OCH ₃	56.4	3.92 (s, 3H)	56.6	3.91 (s, 3H)
5"-OCH ₃	56.4	3.92 (s, 3H)	56.3	3.85 (s, 3H)

^a Spectra were recorded at 125, ^b 500 MHz.

3.2.6 Structure elucidation of compound 6



Molecular formula	$C_{32}H_{32}O_8$
Appearance	brown amorphous solid
$[\alpha]_D^{25}$ (c 0.1, MeOH)	+ 2.78°
1H and ^{13}C NMR ($CDCl_3$)	See Table 3.8

Compound **6** was obtained as a brown amorphous solid, and its molecular formula was $C_{32}H_{32}O_8$ as determined by the HR-TOFMS ion at m/z 567.2000 $[M+Na]^+$ (calcd $C_{32}H_{32}NaO_8$: 567.1995). Its specific optical rotation $[\alpha]_D^{25}$ (c 0.1, MeOH) was recorded to be +2.78. The ^{13}C -NMR (**Table 3.8**) data revealed the presence of four methoxy groups, two methylenes, two oxygenated methines, 12 aromatic methines, and 12 aromatic quaternary carbons. The 1H NMR spectrum of compound **6** (**Table 3.8**) represented resonances for four singlet methoxy groups at δ_H 3.69 (1-OCH₃, 1'-OCH₃), δ_H 3.77 (12'-OCH₃) and δ_H 3.80 (12-OCH₃), two methylene groups at δ_H 2.83 (m, H-7) and 2.86 (m, H-8), two oxygenated methine groups at δ_H 4.73 (d, $J = 8.0$ Hz, H-7') and δ_H 4.82 (d, $J = 8.0$ Hz, H-7') and 12 aromatic protons, including as two pairs of *m*-coupled signals at δ_H 6.54 (d, $J = 2.0$ Hz, H-4), 6.34 (d, $J = 2.0$ Hz, H-6), 6.45 (d, $J = 2.0$ Hz, H-4') and 6.10 (d, $J = 2.0$ Hz, H-6'), on the basis of the coupling constants implied that the presence of two 1,3,4,5-tetrasubstituted aromatic rings. The two pairs of *o*-coupled doublets at δ_H 6.84 (2H, d, $J = 8.6$ Hz, H-11, H-13), 7.12 (2H, d, $J = 8.6$ Hz, H-10, H-14), 7.04 (2H, d, $J = 8.9$ Hz, H-10', 14') and 6.78 (2H, d, $J =$

8.6 Hz, H-11', 13'), which indicated the presence of two 1,4-disubstituted aromatic rings. Based on the ^1H - and ^{13}C -NMR data and molecular formula, the scaffold of compound **6** was identified as a bisbibenzyl derivative with two hydroxy and four methoxy groups.

In accordance with the HMBC correlations (**Figure 3.12**), two bibenzyl units were deduced by correlations from H-4 to C-2, C-3, C-6 and C-7, from H-8 to C-7, 9 and 10, from H-4' to C-2', 3', 5', 6' and 7' and from H-8 to C-7, 9 and 10. Based on the molecular formula and its degree of unsaturation, compound **6** was supposed to contain a 1,4-dioxane ring. The ring linked at C-2 with C-8' *via* an oxygen atom and at C-3 with C-7' *via* another oxygen atom, which was confirmed by HMBC correlations from H-7' to C-3 and from H-8' to C-2. The relative configurations of the chiral centers of dioxane ring were deduced as *trans* from the coupling constant between H-7' and H-8' ($J_{7',8'} = 8.0\text{ Hz}$)^{96, 97}. According to the spectroscopic data, compound **6** was elucidated as dendrocandin I⁹⁹. This compound was firstly discovered from *D. candidum*⁹⁹.

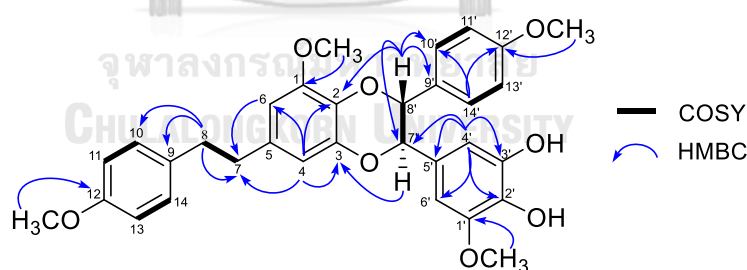


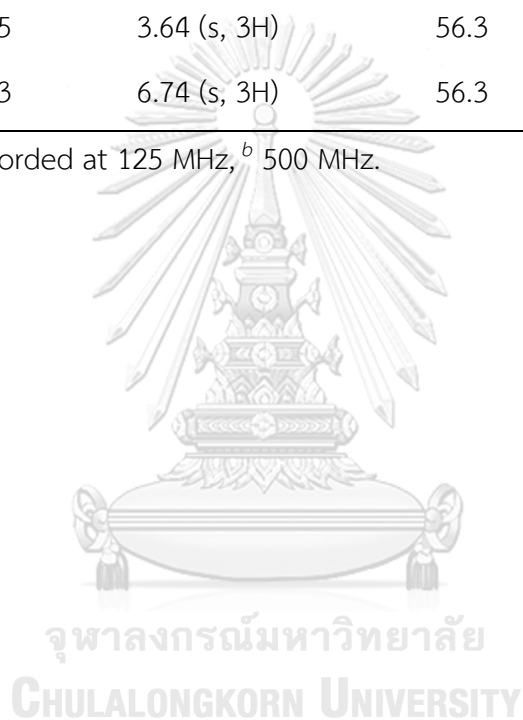
Figure 3.12 HMBC and ^1H - ^1H COSY correlations of compound **6**

Table 3.8 NMR data of compound **6** and dendrocandin I (CDCl₃)

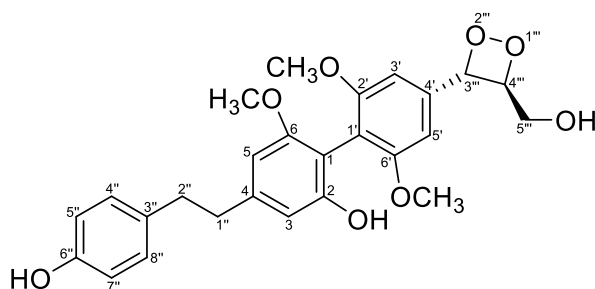
no.	dendrocandin I		compound 6	
	δ_C^a	δ_H [mult, J in Hz] ^b	δ_C^a	δ_H [mult, J in Hz] ^b
1	149.9		148.6	
2	133.3		131.8	
3	145.7		144.4	
4	110.7	6.45 (<i>br s</i> , 1H)	109.5	6.54 (d, $J = 2.0$ Hz, 1H)
5	135.6		130.6	
6	106.5	6.36 (<i>br s</i> , 1H)	105.0	6.34 (d, $J = 2.0$ Hz, 1H)
7	39.1	2.79, (m, 2H)	38.2	2.83, (m, 2H)
8	38.2	2.82, (m, 2H)	37.2	2.86, (m, 2H)
9	135.1		134.1	
10	130.5	7.08 (d, $J = 8.5$ Hz, 1H)	129.5	7.12 (d, $J = 8.6$ Hz, 1H)
11	114.7	6.81 (d, $J = 8.5$ Hz, 1H)	113.9	6.84 (d, $J = 8.6$ Hz, 1H)
12	159.4		158.0	
13	114.7	6.81 (d, $J = 8.5$ Hz, 1H)	113.8	6.84 (d, $J = 8.6$ Hz, 1H)
14	130.5	7.08 (d, $J = 8.5$ Hz, 1H)	129.5	7.12 (d, $J = 8.6$ Hz, 1H)
1'	149.2		146.6	
2'	135.3		132.5	
3'	146.3		143.8	
4'	109.4	6.30 (d, $J = 1.5$ Hz, 1H)	108.6	6.45 (d, $J = 2.0$ Hz, 1H)
5'	128.7		132.5	
6'	104.5	6.13 (<i>br s</i> , 1H)	103.2	6.10 (d, $J = 2.0$ Hz, 1H)
7'	82.0	4.70 (d, $J = 8.0$ Hz, 1H)	80.7	4.73 (d, $J = 8.0$ Hz, 1H)
8'	81.7	4.70 (d, $J = 8.0$ Hz, 1H)	80.4	4.82 (d, $J = 8.0$ Hz, 1H)
9'	130.3		128.3	

10'	130.2	7.04 (d, $J = 8.5$ Hz, 1H)	129.0	7.04 (d, $J = 8.9$ Hz, 1H)
11'	114.5	6.79 (d, $J = 8.5$ Hz, 1H)	113.9	6.78 (d, $J = 8.6$ Hz, 1H)
12'	161.2		159.8	
13'	114.5	6.79 (d, $J = 8.5$ Hz, 1H)	113.8	6.78 (d, $J = 8.6$ Hz, 1H)
14'	130.2	7.04 (d, $J = 8.5$ Hz, 1H)	129.0	7.04 (d, $J = 8.9$ Hz, 1H)
1-OCH ₃	55.7	3.75 (s, 3H)	56.3	3.69 (s, 3H)
12-OCH ₃	54.5	3.75 (s, 3H)	55.4	3.80 (s, 3H)
1'-OCH ₃	55.5	3.64 (s, 3H)	56.3	3.69 (s, 3H)
12'-OCH ₃	55.3	6.74 (s, 3H)	56.3	6.77 (s, 3H)

^a Spectra were recorded at 125 MHz, ^b 500 MHz.



3.2.7 Structure elucidation of compound 7



Molecular formula	$C_{26}H_{28}O_8$
Appearance	white amorphous powder
$[\alpha]_D^{25}$ (c 0.1, MeOH)	-3.40°
1H and ^{13}C NMR ($CDCl_3$)	See Table 3.9

Compound **7**, a white amorphous powder, had a molecular formula of $C_{26}H_{28}O_8$, with 13 indices of hydrogen deficiency. Its specific optical rotation $[\alpha]_D^{25}$ (c 0.1, MeOH) was determined at -3.40. The ^{13}C NMR (**Table 3.9**) inferred the presence of three methoxy, three methylene (one oxygenated), two oxygenated methine, and 18 aromatic carbons. Its 1H -NMR spectrum revealed the presence of two pair of *m*-coupled aromatic signals at δ_H 6.40 (d, $J = 1.9$ Hz, H-3), 6.33 (d, $J = 1.9$ Hz, H-5), and 6.71 (*br s*, H-3', H-5') that indicated the presence of two 1,2,3,5-tetrasubstituted benzene rings, along with *m*-coupled aromatic signals at δ_H 6.96 (d, $J = 8.5$ Hz, H-4'', 8''), and 6.67 (d, $J = 8.5$ Hz, H-5'', 7'') that indicated the presence of one 1,4-disubstituted benzene unit. The combining skeleton accounted for the 12 of 13 unsaturated degrees. Analysis of the 1H - 1H COSY data resulted in the deduction of the fragments CH_2CH_2 and $CH(-O)-CH(-O)-$, therefore, the another fragment with the remaining unsaturation degree, the presence of a 1,2-dioxetane ring was suggested. The constitution of **7** was established on the basis of HMBC cross-peaks (**Figure 3.13**) from H-4'' to C-2'' and C-6'', from H-5 to C-1'', C-1, C-3 and C-6, from H-3 to C-1'', C-2 and C-5, from H-3' and H-5' to C-1', from H-3''' to C-4', C-5', C-4''' and C-5'''.

relative configuration of the 1,2-dioxetane ring was established on the basis of its NOESY spectrum, in which this correlation (**Figure 3.14**) was observed between H-3^{'''}/H-3'. The correlation of NOESY between H-5/6-OCH₃ displayed that the methoxy group δ_{H} 3.78 (6-OCH₃) was connected to δ_{C} 149.7 (C-6) along with, between H-3'/5-OCH₃, confirming the connection of another methoxy group δ_{H} 3.85 (2'-OCH₃) at δ_{C} 149.4 (C-2'). According to the spectroscopic data, compound **7** was elucidated as 6''-de-*o*-methyldendrofindlaphenol A¹⁰⁰. This compound was firstly discovered from *D. findlayanum*¹⁰⁰.

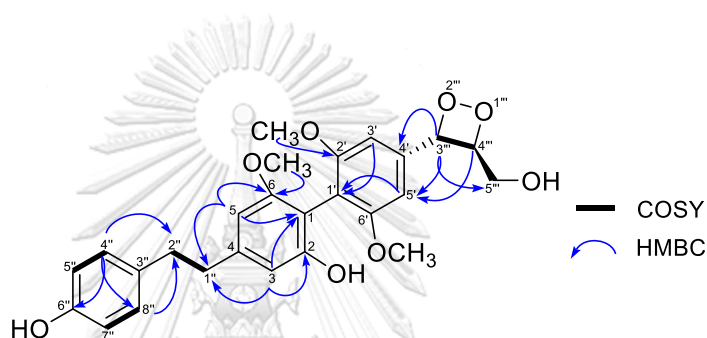


Figure 3.13 HMBC and ¹H-¹H COSY correlations of compound **7**

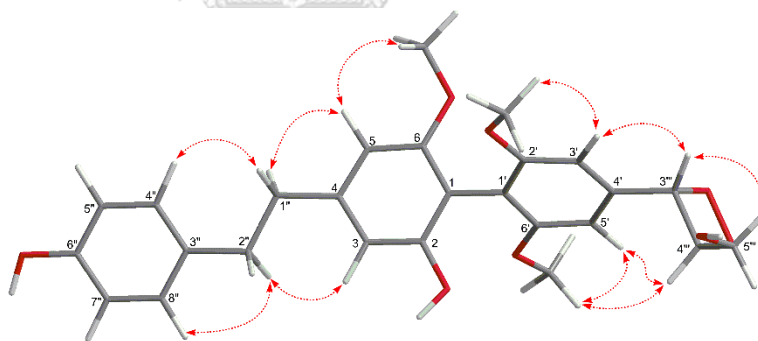


Figure 3.14 ¹H-¹H NOESY correlations of compound **7**

Table 3.9 NMR data of compound **7** (CDCl₃) and 6''-de-o-methyldendrofindlaphenol A (methanol-d₄)

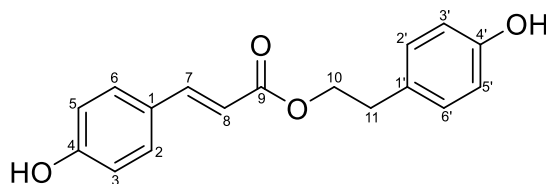
no.	6''-de-o-methyldendrofindlaphenol		compound 6	
	δ_C^c	δ_H [mult, <i>J</i> in Hz] ^d	δ_C^a	δ_H [mult, <i>J</i> in Hz] ^b
1	132.5		132.5	
2	145.5		145.5	
3	110.6	6.39 (d, <i>J</i> = 1.6 Hz, 1H)	110.7	6.40 (d, <i>J</i> = 1.9 Hz, 1H)
4	133.9		135.7	
5	106.3	6.33 (d, <i>J</i> = 1.6 Hz, 1H)	106.4	6.33 (d, <i>J</i> = 1.9 Hz, 1H)
6	149.7		149.7	
1'	137.1		137.2	
2'	149.4		149.4	
3'	105.8	6.70 (<i>br s</i> , 1H)	105.9	6.71 (<i>br s</i> , 1H)
4'	128.7		128.7	
5'	105.8	6.70 (<i>br s</i> , 1H)	105.9	6.71 (<i>br s</i> , 1H)
6'	149.4		149.4	
1''	39.2	2.74, (m, 2H)	39.2	2.75, (m, 2H)
2''	38.3	2.74, (m, 2H)	38.3	2.75, (m, 2H)
3''	135.6		133.9	
4''	130.5	6.94 (d, <i>J</i> = 8.4 Hz, 1H)	130.5	6.96 (d, <i>J</i> = 8.5 Hz, 1H)
5''	116.0	6.65 (d, <i>J</i> = 8.4 Hz, 1H)	116.0	6.67 (d, <i>J</i> = 8.5 Hz, 1H)
6''	156.4		156.5	
7''	116.0	6.65 (d, <i>J</i> = 8.5 Hz, 1H)	116.0	6.67 (d, <i>J</i> = 8.5 Hz, 1H)
8''	130.5	6.94 (d, <i>J</i> = 8.5 Hz, 1H)	130.5	6.96 (d, <i>J</i> = 8.5 Hz, 1H)
3'''	77.8	4.82 (d, <i>J</i> = 8.0 Hz, 1H)	77.8	4.83 (d, <i>J</i> = 8.0 Hz, 1H)

4 ^{'''}	79.8	4.00-3.97 (m, 1H)	79.9	3.98 (ddd, $J = 2.5, 4.5, 7.5$ Hz, 1H)
5 ^{'''}	62.1	3.70 (dd, $J = 3.6, 12.4$ Hz, 1H)	62.2	3.69 (dd, $J = 2.5, 12.4$ Hz, 1H)
		3.45 (dd, $J = 3.6, 12.4$ Hz, 1H)		3.48 (dd, $J = 4.5, 12.4$ Hz, 1H)
6-OCH ₃	56.6	3.77 (s, 3H)	56.6	3.78 (s, 3H)
2'-OCH ₃	56.8	3.84 (s, 3H)	56.8	3.85 (s, 3H)
6'-OCH ₃	56.8	3.84 (s, 3H)	56.8	3.85 (s, 3H)

^a Spectra were recorded at 125, ^b 500, ^c 100, ^d 400 MHz.



3.2.8 Structure elucidation of compound 8



Molecular formula	$C_{17}H_{16}O_4$
Appearance	white powder
1H and ^{13}C NMR ($CDCl_3$)	See Table 3.10

Compound **8**, a white powder, had a molecular formula of $C_{17}H_{16}O_4$. Based on the ^{13}C NMR spectrum (**Table 3.10**), ten methine carbons, two methylene group carbons, four quaternary carbons and one carbonyl carbon were identified. Two *p*-disubstituted benzene rings were determined from the characteristic splitting patterns of two doublet pairs for ring A at δ_H 6.85 (d, $J = 8.6$ Hz, H-3, H-5) and δ_H 7.42 (d, $J = 8.6$ Hz, H-2, H-6), and for ring B at δ_H 6.76 (d, $J = 8.4$ Hz, H-3', H-5') and δ_H 7.06 (d, $J = 8.4$ Hz, H-6', H-6'). A *trans* double bond was identified using the 1H NMR spectrum (**Table 3.10**) due to two doublet peaks at δ_H 7.46 (H-7) with δ_H 6.47 (H-8), which had a coupling constant of 15.5 Hz. The two methylene protons at δ_H 3.48 (t, $J = 7.4$ Hz, H₂-10) correlate with δ_H 2.74 (t, $J = 7.4$ Hz, H₂-11) in the HMBC spectrum. Additionally, the H-11 resonance was appeared to relate to the C-2' and C-6' in the HMBC spectrum (**Figure 3.15**). The C-9 ester carbonyl resonance (δ_H 166.4) was relevant to the δ_H 7.46 (H-7), δ_H 6.47 (H-8) and δ_H 3.48 (H-10) proton resonances. Since no other groups were identified using the proton or ^{13}C NMR spectra, the two *p*-position substituents were identified as hydroxy groups. Based on the above spectral data, the compound **8** was elucidated as *p*-hydroxyphenylethyl-*p*-coumarate¹⁰¹, which has been isolated from *D. falconeri*¹⁰².

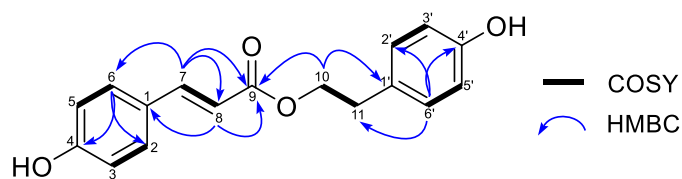


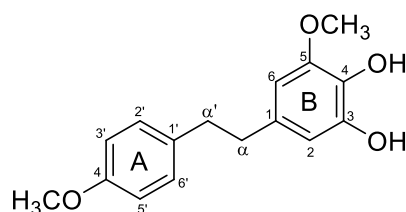
Figure 3.15 HMBC and ^1H - ^1H COSY correlations of compound **8**

Table 3.10 NMR data of compound **8** (acetone- d_6) and *p*-hydroxyphenylethyl-*p*-coumarate (methanol- d_4)

no.	<i>p</i> -hydroxyphenylethyl- <i>p</i> -coumarate		compound 8	
	δ_{C}^c	δ_{H} [mult, J in Hz] ^d	δ_{C}^a	δ_{H} [mult, J in Hz] ^b
1	128.7		127.8	
2	130.7	7.42 (d, $J = 8.5$ Hz, 1H)	130.1	7.42 (d, $J = 8.6$ Hz, 1H)
3	116.9	6.81 (d, $J = 8.5$ Hz, 1H)	116.6	6.85 (d, $J = 8.6$ Hz, 1H)
4	160.6		159.7	
5	116.9	6.81 (d, $J = 8.5$ Hz, 1H)	116.6	6.85 (d, $J = 8.6$ Hz, 1H)
6	130.7	7.42 (d, $J = 8.5$ Hz, 1H)	130.1	7.42 (d, $J = 8.6$ Hz, 1H)
7	142.0	7.46 (d, $J = 15.5$ Hz, 1H)	140.1	7.46 (d, $J = 15.6$ Hz, 1H)
8	118.6	6.40 (d, $J = 15.5$ Hz, 1H)	119.8	6.47 (d, $J = 15.6$ Hz, 1H)
9	184.7		166.4	
10	42.7	3.48 (t, $J = 7.5$ Hz, 1H)	41.9	3.48 (t, $J = 7.4$ Hz, 1H)
11	36.0	2.77 (t, $J = 7.5$ Hz, 1H)	35.8	2.74 (t, $J = 7.4$ Hz, 1H)
1'	128.1		131.2	
2'	130.9	7.08 (d, $J = 8.4$ Hz, 1H)	130.5	7.06 (d, $J = 8.4$ Hz, 1H)
3'	116.4	6.74 (d, $J = 8.4$ Hz, 1H)	116.1	6.76 (d, $J = 8.4$ Hz, 1H)
4'	157.1		156.73	
5'	116.4	6.74 (d, $J = 8.4$ Hz, 1H)	116.1	6.76 (d, $J = 8.4$ Hz, 1H)
6'	130.9	7.08 (d, $J = 8.4$ Hz, 1H)	130.5	7.06 (d, $J = 8.4$ Hz, 1H)

^a Spectra were recorded at 125, ^b 500, ^c 100, ^d 400 MHz.

3.2.9 Structure elucidation of compound 9



Molecular formula	$C_{16}H_{18}O_4$
Appearance	red amorphous solid
1H and ^{13}C NMR ($CDCl_3$)	See Table 3.11

Compound **9** was obtained as a red amorphous solid. The ^{13}C NMR spectrum (**Table 3.11**) showed sixteen carbon signals, including two methoxy groups at δ_c 55.3 and 56.2. The remaining fourteen carbon signals could be differentiated into two methylene carbon at δ_c 37.1 (C- α') and 38.1 (C- α), six methine carbon signals at δ_c 103.7 (C-2), 108.8 (C-6), 113.8 (C-3'), 113.8 (C-5'), 129.4 (C-2') and 129.4 (C-6') and six quaternary carbon signals at δ_c 132.5 (C-1), 133.6 (C-1'), 134.6 (C-4), 143.8 (C-5), 146.7 (C-3) and 157.9 (C-4').

The 1H NMR spectrum (**Table 3.11**) represented signals for two pairs of methylene protons at δ_H 2.85 (m $H_{2-\alpha}$, $H_{2-\alpha'}$) and two methoxy singlets at δ_H 3.84 (3-OCH₃) and 3.85 (4'-OCH₃). The *m*-coupled signals at δ_H 6.28 (d, $J = 1.2$ Hz, H-2) with δ_H 6.49 (d, $J = 1.2$ Hz, H-6) suggested the 1,3,4,5 tetrasubstituted in aromatic ring A. Two groups of *o*-coupled signals of another aromatic ring were appeared at δ_H 7.12 (d, $J = 8.5$ Hz, H-2', H-6') and δ_H 6.87 (d, $J = 8.5$ Hz, H-3', H-5'), as suggestive of the presence of a 1,4-disubstituted aromatic ring. The HMBC (**Figure 3.16**) correlations of 3-OCH₃ to C-4' and 4'-OCH₃ to C-5 helped to connect the methoxy group to C-4' and C-5, respectively. Through analysis of their spectroscopic data and comparison with previously reports, compound **9** was identified as 3,4-dihydroxy-5,4'-

dimethoxybibenzyl¹⁰³. This compound in *Dendrobium* species has been previously reported in *D. candidum*⁹⁸, *D. moniliforme*¹⁰³, and *D. officinale*¹⁰⁴.

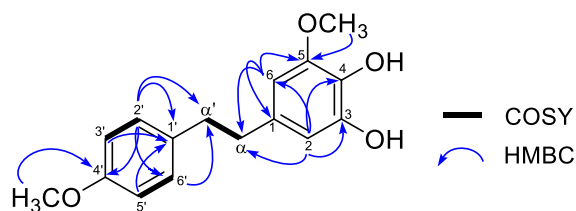


Figure 3.16 HMBC and ¹H-¹H COSY correlations of compound **9**

Table 3.11 NMR data of compound **9** and 3,4-dihydroxy-5,4'-dimethoxybibenzyl (CDCl₃)

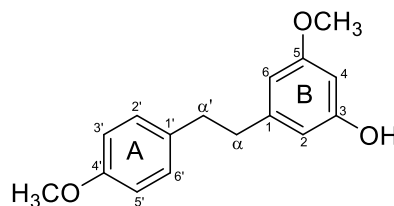
no.	3,4-dihydroxy-5,4'- dimethoxybibenzyl		compound 9	
	δ_C^c	δ_H [mult, <i>J</i> in Hz] ^d	δ_C^a	δ_H [mult, <i>J</i> in Hz] ^b
1	133.4		132.5	
2	108.7	6.20 (d, <i>J</i> = 1.3 Hz, 1H)	103.7	6.28 (d, <i>J</i> = 1.2 Hz, 1H)
3	143.7		146.7	
4	130.5		134.6	
5	146.9		143.8	
6	103.6	6.44 (d, <i>J</i> = 1.3 Hz, 1H)	108.8	6.49 (d, <i>J</i> = 1.2 Hz, 1H)
α	37.6	2.71 (m, 2H)	38.1	2.81 (m, 2H)
α'	36.7	2.71 (m, 2H)	37.1	2.85 (m, 2H)
1'	133.7		133.6	
2'	129.3	7.01 (d, <i>J</i> = 8.2 Hz, 1H)	129.4	7.12 (d, <i>J</i> = 8.5 Hz, 1H)
3'	113.4	6.78 (d, <i>J</i> = 8.2 Hz, 1H)	113.8	6.87 (d, <i>J</i> = 8.5 Hz, 1H)
4'	157.3		157.9	
5'	113.4	6.78 (d, <i>J</i> = 8.2 Hz, 1H)	113.8	6.87 (d, <i>J</i> = 8.5 Hz, 1H)

6'	129.3	7.01 (d, $J = 8.5$ Hz, 1H)	129.4	7.12 (d, $J = 8.5$ Hz, 1H)
3-OCH ₃	55.7	3.66 (s, 3H)	56.2	3.85 (s, 3H)
4'-OCH ₃	54.6	3.69 (s, 3H)	55.3	3.84 (s, 3H)

^a Spectra were recorded at 125, ^b 500, ^c 75, ^d 300 MHz.



3.2.10 Structure elucidation of compound 10



Molecular formula	C ₁₆ H ₁₈ O ₃
Appearance	Light-yellow oil
¹ H and ¹³ C NMR (CDCl ₃)	See Table 3.12

Compound **10** was obtained as a light-yellow oil. The ¹³C NMR spectrum (**Table 3.12**) displayed sixteen carbon signals, including two methoxy signals at δ_c 55.5 (3-OCH₃, 4'-OCH₃), two methylene carbons at δ_c 36.3 (C- α') and 38.2 (C- α), six methine carbon at δ_c 107.9 (C-2, C-6), 129.5 (C-2', C-6'), and 113.7 (C-3', C-5'), three oxygenated quaternary carbons at δ_c 156.5 (C-3), 157.8 (C-4'), and 160.8 (C-5), along with two quaternary carbon at δ_c 144.6 (C-1) and 133.8 (C-1').

Two signals for pairs of methylene protons at δ_H 2.82 (m H₂- α , H₂- α') and two singlets methoxy at δ_H 3.75 (5-OCH₃) and 3.79 (4'-OCH₃) in ¹H NMR spectrum (**Table 3.12**) were represented. The *m*-coupled signals at δ_H 6.25 (d, *J* = 1.8 Hz, H-2, H-6) with δ_H 6.32 (d, *J* = 1.2 Hz, H-4) suggested the 1,3,5 trisubstituted in aromatic ring A. Two groups of *o*-coupled signals aromatic ring appeared at δ_H 7.09 (d, *J* = 8.6 Hz, H-2', H-6') and δ_H 6.83 (d, *J* = 8.6 Hz, H-3', H-5'), which was characteristic of the presence of a 1,4-disubstituted aromatic ring B. The HMBC correlations (**Figure 3.17**) of 5-OCH₃ to C-5 and 4'-OCH₃ to C-4' which revealed the methoxy groups were connected at C-5 and C-4', respectively, together with correlation of H-4 to C-2 and C-6 supporting the H-4 position, and other HMBC correlations, as shown in **Figure 3.17**. By comparing ¹H,¹³C-NMR data of this compound with the previous report

regarding 1,2-diphenylethanes derivatives synthesis data¹⁰⁵, compound **10** was identified as 3-methoxy-5-[2-(4-methoxyphenyl)ethyl]phenol¹⁰⁵. This compound in *Dendrobium* species has been previously reported in *D. wardianum*¹⁰⁶ and *D. devonianum*¹⁰⁷.

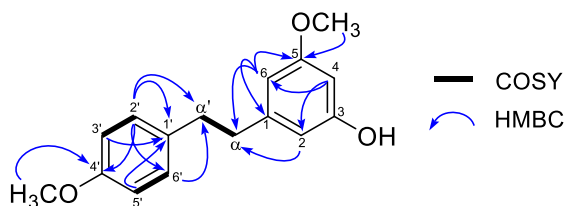


Figure 3.17 HMBC and ^1H - ^1H COSY correlations of compound **10**

Table 3.12 NMR data of compound **10** and 3-methoxy-5-[2-(4-methoxyphenyl)ethyl]phenol (CDCl_3)

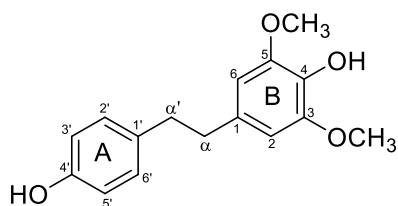
no.	3-methoxy-5-[2-(4-methoxyphenyl)ethyl]phenol		compound 10 ^a	
	δ_{C} ^c	δ_{H} [mult, J in Hz] ^d	δ_{C} ^a	δ_{H} [mult, J in Hz] ^b
1	144.8		144.8	
2	107.0	6.25 (d, $J = 1.8$ Hz, 1H)	107.9	6.25 (d, $J = 1.8$ Hz, 1H)
3	161.1		160.8	
4	99.2	6.32 (t, $J = 1.8$ Hz, 1H)	99.0	6.32 (t, $J = 1.8$ Hz, 1H)
5	158.1		157.8	
6	108.0	6.25 (d, $J = 1.8$ Hz, 1H)	107.9	6.25 (d, $J = 1.8$ Hz, 1H)
α	38.4	2.75-2.85 (m, 2H)	38.2	2.82 (m, 2H)
α'	36.8	2.75-2.85 (m, 2H)	36.3	2.82 (m, 2H)
1'	133.9		133.8	
2'	129.5	7.11 (d, $J = 8.8$ Hz, 1H)	129.5	7.09 (d, $J = 8.6$ Hz, 1H)
3'	113.9	6.82 (d, $J = 8.8$ Hz, 1H)	113.9	6.83 (d, $J = 8.6$ Hz, 1H)
4'	156.8		156.5	

5'	113.9	6.82 (d, $J = 8.8$ Hz, 1H)	113.7	6.83 (d, $J = 8.6$ Hz, 1H)
6'	129.5	7.11 (d, $J = 8.8$ Hz, 1H)	129.3	7.09 (d, $J = 8.6$ Hz, 1H)
5-OCH ₃	55.5	3.75 (s, 3H)	55.4	3.75 (s, 3H)
4'-OCH ₃	55.2	3.79 (s, 3H)	55.4	3.79 (s, 3H)

^a Spectra were recorded at 125, ^b 500, ^c 100, ^d 400 MHz.



3.2.11 Structure elucidation of compound 11



Molecular formula	C ₁₆ H ₁₈ O ₄
Appearance	Brown amorphous solid
¹ H and ¹³ C NMR (CDCl ₃)	See Table 3.13

Compound **11** was obtained as a brown amorphous solid. The ¹³C NMR spectrum (**Table 3.13**) represent sixteen carbon signals, corresponding to two methoxy carbons at δ_C 56.3 (5-OCH₃, 3'-OCH₃), two methylene carbons at δ_C 37.7 (C- α') and 38.5 (C- α), six aromatic methine carbons at δ_C 105.2 (C-2, C-6), 129.7 (C-2', C-6') and 115.2 (C-3', C-5'), two quaternary carbons at δ_C 132.9 (C-1), 134.1 (C-1') and four oxygenated quaternary carbons at δ_C 146.9 (C-3, C-5), 134.0 (C-4) and 154.0 (C-4')

The ¹H NMR spectrum represented two signals for pairs of methylene protons at δ_H 2.81-2.85 (m H₂- α , H₂- α') and two methoxy singlets at δ_H 3.84 (5-OCH₃, 3'-OCH₃). Characteristic of the presence of a 1,4-disubstituted aromatic in the ring A was assigned from the *o*-coupled signals of the aromatic proton, which were appeared at δ_H 7.12 (d, *J* = 8.3 Hz, H-2', H-6') and δ_H 6.74 (d, *J* = 8.3 Hz, H-3', H-5'). The aromatic ring B of compound **11** showed a two-protons singlet at δ_H 6.34 (H-2, H-6), instead of three *m*-coupled triplets (of H-2, H-4 and H-6) as observed in compound **10**, making ring B symmetrically substituted. The HMBC correlations (**Figure 3.18**) that displayed coupled peak of two protons H-2 and H-6 to C-3, C-4 and C- α . They confirmed the ring B as symmetrical 1,3,4,5 tetrasubstituted aromatic ring. The positions of methoxy groups were deduced from the HMBC correlations, as shown in **Figure 3.18**.

On the basis of the above ^1H and ^{13}C NMR evidence, compound **11** was determined to be 4,4'-dihydroxy-3,5-dimethoxybiphenyl¹⁰⁸. It has been elucidated previously from several *Dendrobium* species, including *D. candidum*⁹⁸, *D. findlayanum*¹⁰⁹, *D. ellipsophyllum*¹⁰⁸, *D. officinale*¹¹⁰, *D. williamsonii*¹¹¹ and *D. crystallinum*¹¹².

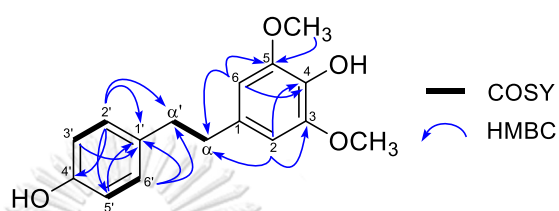


Figure 3.18 HMBC and ^1H - ^1H COSY correlations of compound **11**

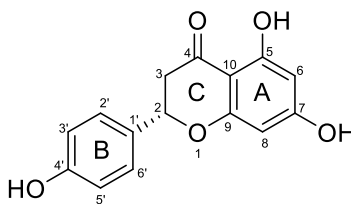


Table 3.13 NMR data of compound **11** (CDCl₃) and 4,4'-dihydroxy-3,5-dimethoxybibenzyl (acetone-*d*₆)

no.	4,4'-dihydroxy-3,5-dimethoxybibenzyl		compound 11	
	δ_C^a	δ_H [mult, <i>J</i> in Hz] ^b	δ_C^a	δ_H [mult, <i>J</i> in Hz] ^b
1	133.1		132.9	
2	106.7	6.46 (s, 1H)	105.2	6.34 (s, 1H)
3	148.4		146.9	
4	134.9		134.0	
5	148.4		146.9	
6	106.7	6.46 (s, 1H)	105.2	6.34 (s, 1H)
α	39.0	2.76 (m, 2H)	38.5	2.81-2.85 (m, 2H)
α'	38.0	2.76 (m, 2H)	37.7	2.85-2.85 (m, 2H)
1'	133.5		134.1	
2'	130.1	7.00 (d, <i>J</i> = 8.5 Hz, 1H)	129.7	7.12 (d, <i>J</i> = 8.3 Hz, 1H)
3'	115.8	6.72 (d, <i>J</i> = 8.5 Hz, 1H)	115.2	6.74 (d, <i>J</i> = 8.3 Hz, 1H)
4'	156.3		154.0	
5'	115.8	6.72 (d, <i>J</i> = 8.5 Hz, 1H)	115.2	6.74 (d, <i>J</i> = 8.3 Hz, 1H)
6'	130.1	7.00 (d, <i>J</i> = 8.56 Hz, 1H)	129.7	7.12 (d, <i>J</i> = 8.3 Hz, 1H)
5-OCH ₃	56.4	3.76 (s, 3H)	56.3	3.84 (s, 3H)
4'-OCH ₃	56.4	3.76 (s, 3H)	56.3	3.84 (s, 3H)

^a Spectra were recorded at 125, ^b 500 MHz.

3.2.12 Structure elucidation of compound 12



Molecular formula	C ₁₅ H ₁₂ O ₅
Appearance	white amorphous solid
¹ H and ¹³ C NMR (CDCl ₃)	See Table 3.14

Compound **12** was obtained as a white powder. Its specific optical rotation $[\alpha]_D^{25}$ (c 0.1, MeOH) was determined at -23.4. The ¹³C NMR spectrum (**Table 3.14**) represented fifteen carbon signals, consisting of a signal of carbonyl carbon at δ_C 197.3, six quaternary carbons at δ_C 164.8 (C-5), 165.5 (C-7), 169.9 (C-9), 102.9 (C-10), 131.2 (C-1') and 159.0 (C-4'). The seven methine carbons were found at δ_C 116.2 (C-3', C-5'), 129.0 (C-2', C-6'), 80.4 (C-2), 97.4 (C-6), and 96.6 (C-8), along with one methylene carbon at δ_C 44.0 (C-3).

The ¹H NMR spectrum (**Table 3.14**) exhibited two *m*-coupled signals at δ_H 5.82 (d, *J* = 2.4, H-6) and δ_H 5.84 (d, 2.4, H-8), displaying the presence of a 5,7-disubstituted A benzene ring system in the flavone skeleton. The four aromatic protons at δ_H 7.29 (d, *J* = 8.5 Hz, H-2', 6') and δ_H 6.79 (d, *J* = 8.5 Hz, H-3', 5') suggested the presence of 1',4'-disubstituted aromatic ring B. Additionally, the protons at position 3 resonated as two signals δ_H 2.65 (dd, *J* = 17.2, 3.0 Hz, H_a-3) and δ_H 3.70 (dd, *J* = 17.2, 13.0 Hz, H_b-3) and oxygenated methine protons δ_H 5.30 (dd, *J* = 13.0, 3.0 Hz, H-2) in ring C were observed. The HMBC correlations (**Figure 3.19**) of H_a-3 to C-4, H-6 to C-10 and H-8 to C-9 proved the positions of protons of A ring. The COSY and HSQC experiments were fully supported this as a flavonoids scaffold¹¹³.

Based on the above evidence, the structure of compound **12** was elucidated as the well-known naringenin¹¹³

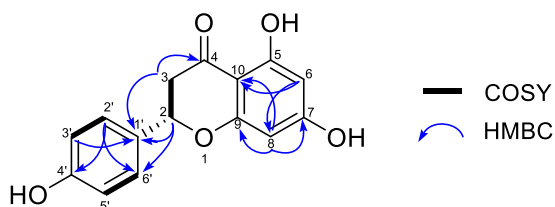


Figure 3.19 HMBC and ^1H - ^1H COSY correlations of compound **12**

Table 3.14 NMR data of compound **12** and naringenin (methanol- d_4)

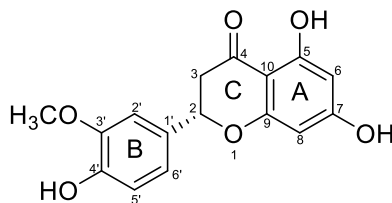
no	naringenin		compound 12	
	$\delta_{\text{C}}^{\text{c}}$	δ_{H} [mult, J in Hz] ^d	$\delta_{\text{C}}^{\text{a}}$	δ_{H} [mult, J in Hz] ^b
1				
2	79.5	5.34 (dd, $J = 12.9, 3.0$ Hz, 1H)	80.4	5.30 (dd, $J = 13.0, 3.0$ Hz, 1H)
3	43.0	3.12 (dd, $J = 17.1, 12.9$ Hz, 1H); 2.70 (dd, $J = 17.1, 3.0$ Hz, 1H)	44.0	3.07 (dd, $J = 17.2, 13.0$ Hz, 1H); 2.65 (dd, $J = 17.2, 3.0$ Hz, 1H)
4	196.8		197.3	
5	164.4		164.8	
6	96.1	5.89 (d, $J = 2.1$ Hz, 1H)	97.4	5.82 (d, $J = 2.4$ Hz, 1H)
7	167.3		165.5	
8	95.2	5.91 (d, $J = 2.1$ Hz, 1H)	96.6	5.84 (d, $J = 2.4$ Hz, 1H)
9	163.9		169.9	
10	102.4		102.9	
1'	130.1		131.2	
2'	128.0	7.33 (d, $J = 8.4$ Hz, 1H)	129.0	7.29 (d, $J = 8.2$ Hz, 1H)
3'	115.3	6.83 (d, $J = 8.4$ Hz, 1H)	116.2	6.79 (d, $J = 8.2$ Hz, 1H)

4'	158.0		159.0	
5'	115.3	6.83 (d, $J = 8.4$ Hz, 1H)	116.2	6.79 (d, $J = 8.2$ Hz, 1H)
6'	128.0	7.31 (d, $J = 8.2$ Hz, 1H)	129.0	7.29 (d, $J = 8.2$ Hz, 1H)

^a Spectra were recorded at 125, ^b 500, ^c 75, ^d 300 MHz.



3.2.13 Structure elucidation of compound 13



Molecular formula	$C_{16}H_{14}O_6$
Appearance	Light yellow needles
$[\alpha]_D^{25}$ (c 0.1, MeOH)	- 17.6
1H and ^{13}C NMR ($CDCl_3$)	See Table 3.15

Compound **13** was obtained as a white powder, and its specific optical rotation $[\alpha]_D^{25}$ (c 0.1, MeOH) was determined at -17.6. The ^{13}C NMR spectrum (**Table 3.15**) established sixteen carbon signals, comprising a signal of keto group at δ_C 197.2, one methoxy carbon at δ_C 56.3, seven quaternary carbons at δ_C 165.4 (C-5), 167.4 (C-7), 164.4 (C-9), 103.9 (C-10), 131.4 (C-1'), 148.6 (C-3'), 148.1 (C-4') and one methylene carbon at δ_C 43.7 (C-3). The six methine carbons were observed at δ_C 129.0 (C-2'), 115.8 (C-5'), 120.6 (C-6'), 96.9 (C-6), 96.6 (C-8), 80.4 (C-2).

The 1H NMR spectrum (**Table 3.15**) revealed two *m*-coupled signals at δ_H 5.94 (d, $J = 2.1$, H-6) and δ_H 5.97 (d, $J = 2.1$, H-8), displaying the presence of a 5,7-disubstituted aromatic ring A of the flavone skeleton. The three aromatic protons coupling at δ_H 6.87 (d, $J = 8.1$ Hz, H-5'), 7.00 (dd, $J = 8.1, 2.0$ Hz, H-6') and 7.19 (d, $J = 2.0$ Hz, H-2') suggested the presence of 1',3',4'-trisubstituted aromatic ring B. Additionally, position 3 resonated as two signals δ_H 2.73 (dd, $J = 17.0, 13.0$ Hz, H_a -3) and δ_H 3.22 (dd, $J = 17.0, 13.0$ Hz, H_b -3) with oxygenated methine protons δ_H 5.44 (dd, $J = 13.0, 3.0$ Hz, H-2) in ring C, and one hydroxy proton at δ_H 12.19 (5-OH) proved that compound **13** was a flavone as similar to **12**. The HMBC correlations (**Figure 3.24**) of 3'-OCH₃ to C-3' allowed the presence of methoxy substituted at C-3'

position. From the above data and through comparison with previously elucidated compounds, compound **13** was determined as (2*S*)-homoeridodictyol¹¹³.

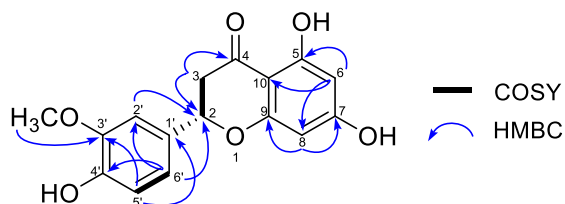


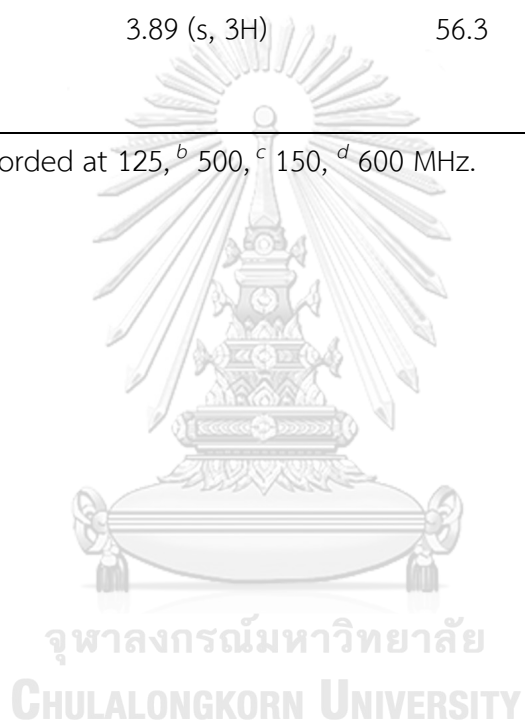
Figure 3.20 HMBC and ¹H-¹H COSY correlations of compound **13**

Table 3.15 NMR data of compound **13** (acetone-d₆) and (2*S*)-homoeridodictyol (methanol-d₄)

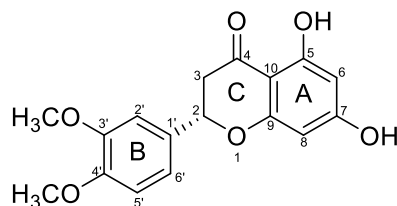
no.	(2 <i>S</i>)-homoeridodictyol		compound 13	
	δ_C^c	δ_H [mult, <i>J</i> in Hz] ^d	δ_C^a	δ_H [mult, <i>J</i> in Hz] ^b
1				
2	80.3	5.44 (dd, <i>J</i> = 13.2, 3.0 Hz, 1H)	80.2	5.44 (dd, <i>J</i> = 13.0, 3.0 Hz, 1H)
3	43.7	3.25 (dd, <i>J</i> = 17.4, 13.2 Hz, 1H); 2.73 (dd, <i>J</i> = 17.4, 13.0 Hz, 1H)	43.6	3.22 (dd, <i>J</i> = 17.0, 13.0 Hz, 1H); 2.73 (dd, <i>J</i> = 17.0, 13.0 Hz, 1H)
4	197.2		197.2	
5	165.4		164.4	
6	96.9	5.96 (d, <i>J</i> = 2.4 Hz, 1H)	96.9	5.94 (d, <i>J</i> = 2.1 Hz, 1H)
7	167.4		167.6	
8	96.0	5.97 (d, <i>J</i> = 1.8 Hz, 1H)	95.9	5.97 (d, <i>J</i> = 2.1 Hz, 1H)
9	164.4		165.3	
10	103.9		103.1	

1'	131.4		131.3	
2'	111.4	7.21 (d, $J = 1.8$ Hz, 1H)	111.1	7.19 (d, $J = 2.0$ Hz, 1H)
3'	148.6		148.5	
4'	148.1		147.9	
5'	115.8	6.89 (d, $J = 7.8$ Hz, 1H)	115.7	6.87 (d, $J = 8.1$ Hz, 1H)
6'	120.6	7.01 (dd, $J = 8.4, 2.4$ Hz, 1H)	120.5	7.00 (dd, $J = 8.1, 2.0$ Hz, 1H)
3'-OCH ₃	56.5	3.89 (s, 3H)	56.3	3.88 (s, 3H)
5-OH				12.19 (s, 1H)

^a Spectra were recorded at 125, ^b 500, ^c 150, ^d 600 MHz.



3.2.14 Structure elucidation of compounds 14



Molecular formula	$C_{17}H_{16}O_6$
Appearance	White amorphous powder
$[\alpha]_D^{25}$ (c 0.1, MeOH)	- 13.7
1H and ^{13}C NMR ($CDCl_3$)	See Table 3.16

Compound **14** was obtained as a white amorphous powder, and its specific optical rotation $[\alpha]_D^{25}$ (c 0.1, MeOH) was determined at -13.7. The ^{13}C NMR spectrum (**Table 3.16**) displayed seventeen carbon signals, including a signal of keto group at δ_C 197.7 (C-4), two methoxy carbon at δ_C 56.5 (3'-OCH₃, 4'-OCH₃), seven quaternary carbons at δ_C 164.9 (C-5), 165.5 (C-7), 168.7 (C-9), 103.3 (C-10), 131.8 (C-1'), 149.1 (C-3'), 148.1 (C-4') and one methylene carbon at δ_C 44.2 (C-3). The six methine carbons were found at δ_C 111.3 (C-2'), 116.1 (C-5'), 120.5 (C-6'), 97.2 (C-6), 96.3 (C-8) and 80.7 (C-2).

The two *m*-coupled signals at δ_H 5.88 (d, $J = 2.1$, H-6) and δ_H 5.90 (d, $J = 2.1$, H-8) in 1H NMR spectrum (**Table 3.16**) implied the presence of a 5,7-disubstituted aromatic ring A of the flavone skeleton. The three aromatic protons coupling at δ_H 6.82 (dd, $J = 8.1, 1.8$ Hz, H-5'), 6.92 (dd, $J = 8.1, 1.8$ Hz, H-6') and 7.07 (br s, H-2') suggested the presence of 1',3',4'-trisubstituted aromatic ring B. Besides, the position 3 resonated as two signals δ_H 2.70 (dt, $J = 17.1, 2.5$ Hz, H_a-3) and δ_H 3.14 (ddd, $J = 17.1, 13.0, 2.5$ Hz, H_b-3) with oxygenated methine protons δ_H 5.34 (dd, $J = 13.0, 2.5$ Hz, H-2) in ring C proved that compound **14** was a flavone as similar to

13 different the presence of methoxy at C-4'. The HMBC correlations (**Figure 3.21**) of the methoxy proton of 3'-OCH₃ to C-3' and 4'-OCH₃ to C-4' allowed the presence of methoxy substituted at C-3' and C-4' position, respectively. From the above data and through comparison with previously elucidated report, compound **14** was determined as (2*S*)-homohesperetin^{115, 116}.

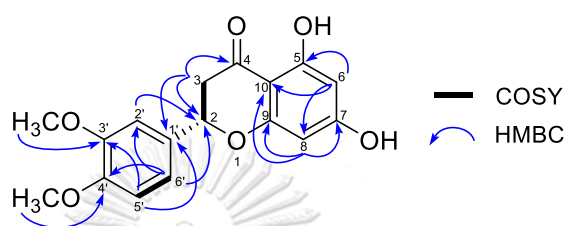


Figure 3.21 HMBC and ¹H-¹H COSY correlations of compound **14**

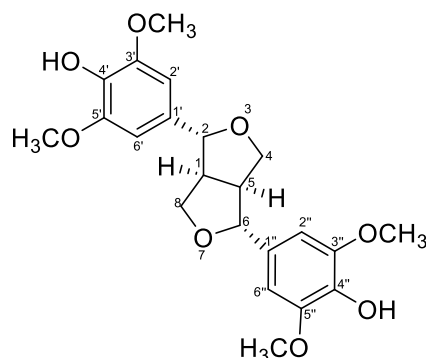
Table 3.16 NMR data of compound **14** (methanol-*d*₄) and (2*S*)-homohesperetin (DMSO-*d*₆)

no.	(2 <i>S</i>)-homohesperetin		compound 14	
	δ_C^c	δ_H [mult, <i>J</i> in Hz] ^d	δ_C^a	δ_H [mult, <i>J</i> in Hz] ^b
1				
2	78.5	5.46 (dd, <i>J</i> = 12.7, 3.1 Hz, 1H)	80.7	5.34 (dt, <i>J</i> = 13.0, 2.5 Hz, 1H)
3	42.1	3.30 (m, 1H); 2.70 (dd, <i>J</i> = 17.2, 3.1 Hz, 1H)	44.2	3.14 (ddd, <i>J</i> = 17.1, 13.0, 1.8 Hz, 1H); 2.70 (dt, <i>J</i> = 17.1, 2.5 Hz, 1H)
4	196.1		197.7	
5	163.5		164.9	
6	95.9	5.86 (d, <i>J</i> = 1.9 Hz, 1H)	97.2	5.88 (d, <i>J</i> = 2.1 Hz, 1H)
7	166.9		165.5	
8	95.1	5.88 (d, <i>J</i> = 1.9 Hz, 1H)	92.2	5.90 (d, <i>J</i> = 2.1 Hz, 1H)

9	162.8		168.7	
10	101.7		103.3	
1'	131.0		131.8	
2'	110.6	7.11 (d, $J = 1.8$ Hz, 1H)	111.3	7.07 (br s, 1H)
3'	148.7		149.1	
4'	149.0		148.1	
5'	111.6	6.96 (d, $J = 8.2$, Hz, 1H)	116.1	6.82 (dd, $J = 8.1, 1.8$ Hz, 1H)
6'	119.2	7.01 (dd, $J = 8.2, 1.8$ Hz, 1H)	120.5	6.92 (dd, $J = 8.1, 1.8$ Hz, 1H)
3'-OCH ₃	55.6	3.76 (s, 3H)	56.5	3.88 (s, 3H)
4'-OCH ₃	55.6	3.75 (s, 3H)	56.5	3.87 (s, 3H)

^a Spectra were recorded at 125, ^b 500, ^c 150, ^d 600 MHz.

3.2.15 Structure elucidation of compounds 15



Molecular formula	$C_{22}H_{16}O_8$
Appearance	White amorphous powder
$[\alpha]_D^{25}$ (c 0.1, MeOH)	- 7.3
1H and ^{13}C NMR ($CDCl_3$)	See Table 3.17

Compound **15** was obtained as a white amorphous powder. Its specific optical rotation $[\alpha]_D^{25}$ (c 0.1, MeOH) was determined at -7.3. The ^{13}C NMR spectrum (**Table 3.17**) displayed twenty-two carbon signals, including four methoxy carbons at δ_C 56.7 (3'-OCH₃, 5'-OCH₃, 3''-OCH₃, 5''-OCH₃), eight quaternary carbons at δ_C 150.1 (C-3', C-5', C-3'', C-5''), 130.9 (C-1', C-1''), 139.4 (C-4', C-4'') and two oxygenated methylene carbons at δ_C 72.7 (C-4, C-8). The six methine carbons were at δ_C 104.8 (C-2', C-6', C-2'', C-6''), 130.9 (C-1, C-5) and two oxygenated methines at δ_C 88.0 (C-2, C-6).

1H NMR spectrum (**Table 3.17**) revealed symmetrical characteristic of methine protons at δ_H 3.14 (*br s*, H-1, H-5) an oxygenated methylene protons at δ_H 4.23 (*ddd*, $J = 9.5, 6.4, 2.6$ Hz H_a-4, H_a-8), δ_H 3.83 (*dd*, $J = 5.5, 2.2$ Hz H_b-4, H_b-8), along with oxygenated methine signals at δ_H 4.67 (*br s*, H-2, H-3) that indicated the presence of a bis-tetrahydrofuran ring of 2,6-diaryl-3,7-dioxabicyclic[3,3,0]-octane type lignans¹¹⁷. The (C-1)-(C-5) bond of naturally occurring bis-tetrahydrofuran lignans was characterized in the *cis* configuration, and the 1H NMR at δ_H 3.14 (*br s*, H-1, H-5) and

δ_{H} 4.67 (*br s*, H-2, H-6), confirming that the configuration of position 2 and 6 were pointed into the same face, but in the opposite direction to position 1 and 5⁷⁵. The aromatic methines at δ_{H} 6.60 (*d*, $J = 2.6$ Hz H-2', H-6', H-2'', H-6'') were deduced the two of 1,3,4,5 tetra-substituted aromatic ring. Additionally, HMBC correlations (**Figure 3.22**) of the methoxy proton of 3'-OCH₃ to C-3', 3''-OCH₃ to C-3'', 5'-OCH₃ to C-5' and 5''-OCH₃ to C-5'' allowed the presence of methoxy substituted at C-3', C-3'', C-5' and C-5'', respectively. From the above data and through comparison with previously elucidated report, compound **15** was determined as (-) syringaresinol¹¹⁸.

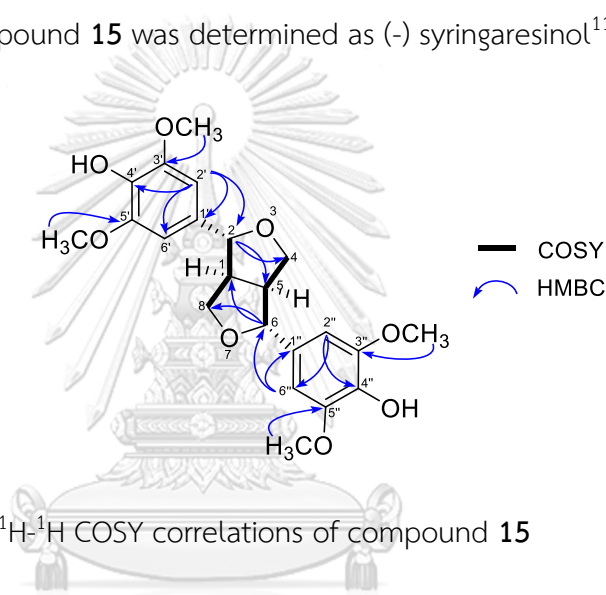


Figure 3.22 HMBC and ¹H-¹H COSY correlations of compound **15**

Table 3.17 NMR data of compound **15** and (-) syringaresinol (CDCl₃)

no.	(-) syringaresinol		compound 15	
	δ_C^c	δ_H [mult, J in Hz] ^d	δ_C^a	δ_H [mult, J in Hz] ^b
1/5	54.3	3.11 (m, 2H)	55.4	3.14 (m, 2H)
2/6	86.1	4.74 (d, $J = 4.3$ Hz, 2H)	88.0	4.67 (d, $J = 4.2$ Hz, 2H)
4/8	71.8	4.29 (d, $J = 9.6, 6.8$ Hz, 2H); 3.91 (dd, $J = 9.6, 3.6$ Hz, 2H)	72.7	4.23 (ddd, $J = 9.5, 6.4, 2.6$ Hz, 2H); 3.83 (dd, $J = 9.5, 2.6$ Hz, 2H)
1'/1"	132.1		130.9	
2'/2"	102.8	6.59 (s, 2H)	104.8	6.60 (d, $J = 2.6$ Hz, 2H)
3'/3"	147.2		150.1	
4'/4"	134.4		139.4	
5'/5"	147.2		150.1	
6'/6"	102.8	6.59 (s, 2H)	104.8	6.60 (d, $J = 2.6$ Hz, 2H)
3'/3"-	56.4	3.91 (s, 6H)	56.8	3.81 (s, 6H)
OCH ₃				
5'/5"-	56.4	3.91 (s, 6H)	56.8	3.83 (s, 6H)
OCH ₃				

^a Spectra were recorded at 125, ^b 500, ^c 100, ^d 400 MHz

3.3 Isolated compounds from *Magnolia liliifera* (L.) Baill.

The hexane crude extracts of *M. liliifera* were separated to accomplish three known compounds. The structures of these compounds were confirmed by comparing their physical characteristics and spectroscopic data with the previously reported data that were classified as lignans, including (+) sesamin (**16**), (+) fargesin (**17**) and (-) kobusin (**18**). They are presented in **Figure 3.23**.

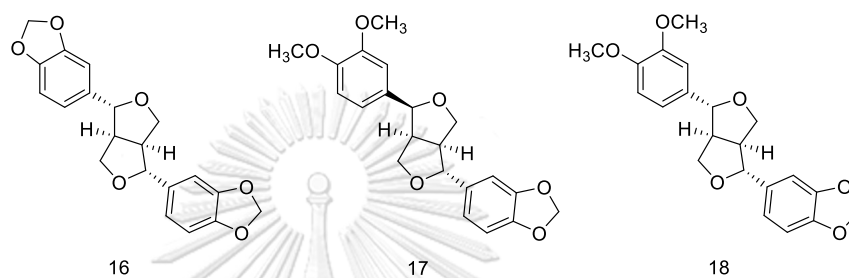
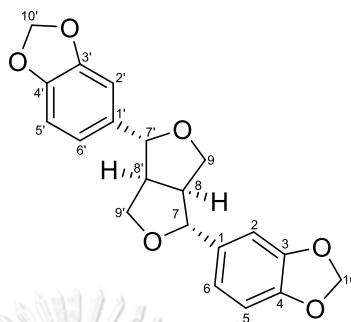


Figure 3.23 The chemical structures of isolated compounds from *M. liliifera*

3.4 Structure elucidation of isolated compounds from *Magnolia liliifera* (L.)

Baill.

3.4.1 Structure elucidation of compound 16



Molecular formula	$C_{20}H_{18}O_6$
Appearance	Colorless crystal
$[\alpha]_D^{25}$ (c 0.1, MeOH)	+59.2
1H and ^{13}C NMR ($CDCl_3$)	See Table 3.18

Compound **16** was obtained as colorless crystals, its specific optical rotation $[\alpha]_D^{25}$ (c 0.1, MeOH) was determined at +59.2. The ^{13}C NMR spectrum (**Table 3.18**) established twenty-two carbon signals, consisting of six quaternary carbons at δ_C 135.1 (C-1, C-1'), 148.2 (C-3, C-3'), 147.3 (C-4, C-4'). The six aromatic methine carbons were observed at δ_C 106.6 (C-2, C-2'), 108.4 (C-5, C-5'), 119.5 (C-6, C-6'), two methine at δ_C 54.6 (C-8, C-8'), four oxygenated methine at δ_C 85.9 (C-7, C-7') and δ_C 88.0 (C-2, C-6) along with, four oxygenated methylene carbon at δ_C 71.9 (C-9, C-9') and δ_C 101.2 (C-10, C-10').

1H NMR spectrum (**Table 3.18**) showed symmetrical characteristic of methine protons at δ_H 3.05 (m, H-8, H-8') an oxygenated methine protons at δ_H 4.71 (d, $J = 4.5$, H-7, H-7') and oxygenated methylene protons at δ_H 4.23 (dd, $J = 9.0, 6.8$ Hz, H_a -9, H_a -9') and 4.23 (dd, $J = 9.0, 3.4$ Hz, H_b -9, H_b -9') that indicated the presence of a bis-tetrahydrofuran ring of 2,6-diaryl-3,7-dioxabicyclic[3,3,0]-octane type lignans¹¹⁷. Nevertheless, the aromatic methine at δ_H 6.85 (d, $J = 1.4$ Hz, H-2, H-2'), δ_H 6.78 (d, J

= 8.0 Hz, H-5, H-5') and δ_{H} 6.79 (dd, J = 8.0, 1.7 Hz, H-6, H-6') were deduced the two of 1,3,4 tetra-substituted aromatic ring. Additionally, HMBC correlations (**Figure 3.24**) of the oxygenated methylene protons H-10 to C-3, C-4 and H-10' to C-3', C-4' allowed the presence of 1,3 benzodioxole ring. From the above data and through comparison with previously elucidated report, compound **16** was determined as (+) sesamin^{119, 120}. It has been first elucidated in *Magnolia* genus from *Magnolia kobus* DC¹²¹.

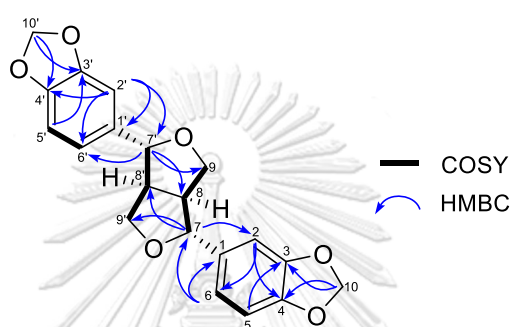


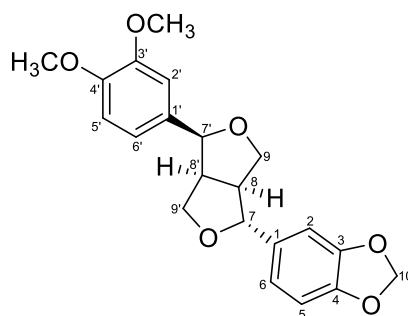
Figure 3.24 HMBC and ^1H - ^1H COSY correlations of compound **16**

Table 3.18 NMR data of compound **16** and sesamin (CDCl₃)

no.	(+) sesamin		compound 16	
	δ_C^c	δ_H [mult, J in Hz] ^d	δ_C^a	δ_H [mult, J in Hz] ^b
1/1'	135.0		135.1	
2/2'	106.6	6.85 (s, 2H)	106.6	6.85 (d, $J = 1.4$ Hz, 2H)
3/3'	148.1		148.2	
4/4'	147.2		147.3	
5/5'	108.4	6.78 (d, $J = 8.0$ Hz, 2H)	108.4	6.78 (d, $J = 8.0$ Hz, 2H)
6/6'	119.5	6.80 (dd, $J = 8.0, 1.7$ Hz, 2H)	119.5	6.79 (dd, $J = 8.0, 1.7$ Hz, 2H)
7/7'	85.9	4.71 (d, $J = 4.0$ Hz, 2H)	85.9	4.71 (d, $J = 4.5$ Hz, 2H)
8/8'	54.5	3.05 (m, 2H)	54.6	3.05 (m, 2H)
9/9'	71.8	4.20 (dd, $J = 9.2, 6.9$ Hz, 2H); 3.90 (dd, $J = 9.2, 3.9$ Hz, 2H)	71.9	4.23 (dd, $J = 9.0, 6.8$ Hz, 2H); 3.89 (dd, $J = 9.0, 3.4$ Hz, 2H)
10/10'	101.2	5.95 (s, 4H)	101.2	5.95 (s, 4H)

^a Spectra were recorded at 125 MHz, ^b 500 MHz, ^c 100, ^d 400 MHz.

3.4.2 Structure elucidation of compound 17



Molecular formula	C ₂₁ H ₂₂ O ₆
Appearance	White powder
$[\alpha]_D^{25}$ (c 0.1, MeOH)	+72.7
¹ H and ¹³ C NMR (CDCl ₃)	See Table 3.18

Compound **17** was obtained as a white powder, its specific optical rotation $[\alpha]_D^{25}$ (c 0.1, MeOH) was determined at +72.7. The ¹³C NMR spectrum (**Table 3.19**) established twenty-one carbon signals, comprising two methoxy groups at δ_C 56.1 (3'-OCH₃, 4'-OCH₃), two quaternary carbons at δ_C 135.1 (C-1), 131.7 (C-1'), four oxygenated quaternary carbons at δ_C 149.1 (C-3'), 147.4 (C-4'), 148.3 (C-3), 147.5 (C-4), two methine at δ_C 54.9 (C-8), 50.4 (C-8') and two oxygenated methine at δ_C 87.8 (C-7), 82.2 (C-7'). The six aromatic methine carbons were at δ_C 106.7 (C-2), 108.3 (C-5), 109.3 (C-2'), 111.3 (C-5'), 119.5 (C-6), 117.9 (C-6'), three oxygenated methylene carbon at δ_C 69.9 (C-9), δ_C 101.2 (C-10) and δ_C 71.2 (C-9').

¹H NMR spectrum (**Table 3.19**) showed symmetrical characteristic of methine protons at δ_H 2.88 (m, H-8), 3.84-3.86 (m, H-8'), an oxygenated methine protons at δ_H 4.42 (d, *J* = 7.0, H-7), 4.87 (d, *J* = 5.3, H-7'), an oxygenated methylene protons at δ_H 3.91-3.82 (m, H_a-9), 3.37-3.28 (m, H_b-9), 3.86 (m, H_a-9') and 4.12 (d, *J* = 9.4 Hz, H_b-9') that assumed the presence of a bis-tetrahydrofuran ring of 2,6-diaryl-3,7-dioxabicyclic[3,3,0]-octane type lignans¹¹⁷. The splitting pattern of structure **17**

showed similar proton signals at H-2, H-5, H-6, H-7, H-8, H-9, H-2', H-5', H-6', H-7', H-8' and H-9' in compound **16**. Contrariwise, the appearance of two methoxy groups at δ_{H} 3.91 (3'-OCH₃) and 3.88 (4'-OCH₃) were observed in compound **17**.

Additionally, HMBC correlations (Figure 3.25) of methoxy protons at 3'-OCH₃ to C-3' and 4'-OCH₃ to C-4' allowed the presence of two methoxies substituted at C-3' and C-4', respectively. From the above data and through comparison with previously elucidated report, compound **17** was indicated the neolignan types¹²², named as (+) fargesin¹²³, which was first reported from *M. kobus* DC¹²¹.

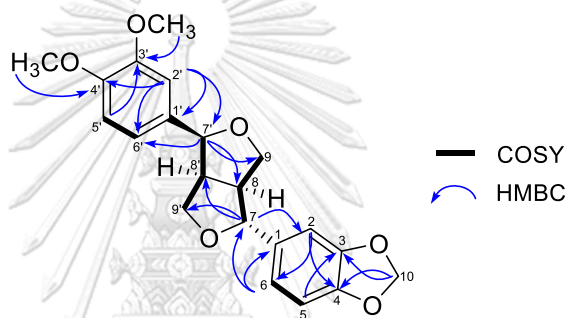


Figure 3.25 HMBC and ¹H-¹H COSY correlations of compound **17**

Table 3.19 NMR data of compound **17** and (+) fargesin (CDCl₃)

no.	(+ fargesin		compound 17	
	δ_C^c	δ_H [mult, J in Hz] ^d	δ_C^a	δ_H [mult, J in Hz] ^b
1	135.1		135.5	
2	106.5	6.91-6.79 (m, 1H)*	106.7	6.86 (s, 1H)
3	147.9		148.3	
4	147.2		147.5	
5	108.1	6.91-6.79 (m, 1H)*	108.3	6.86 (d, $J = 8.0$ Hz, 1H)
6	119.5	6.91-6.79 (m, 1H)*	119.5	6.78 (dd, $J = 8.0, 1.7$ Hz, 1H)
7	87.6	4.40 (d, $J = 7.0$ Hz, 1H)	87.8	4.42 (d, $J = 7.0$ Hz, 1H)
8	54.6	2.85 (m, 1H)	54.9	2.88 (m, 1H)
9	69.7	3.85-3.72 (m, 1H); 3.35-3.24 (m, 1H)	69.9	3.91-3.82 (m, 1H); 3.37-3.28 (m, 1H)
10	101.0	5.93 (s, 2H)	101.2	5.95 (s, 2H)
1'	130.9		131.7	
2'	108.9	6.91-6.79 (m, 1H)*	109.3	6.93 (s, 1H)
3'	148.8		149.1	
4'	147.9		147.4	
5'	110.9	6.91-6.79 (m, 1H)*	111.3	6.93 (s, 1H)
6'	117.6	6.91-6.79 (m, 1H)*	117.9	6.93 (s, 1H)
7'	82.0	4.85 (d, $J = 5.3$ Hz, 1H)	82.2	4.87 (d, $J = 5.3$ Hz, 1H)
8'	50.1	3.35-3.24 (m, 1H)	50.4	3.84-3.86 (m, 1H)
9'	71.0	4.10 (<i>br</i> d, $J = 10.0$, 1H); 3.85-3.72 (m, 1H)	71.2	4.12 (<i>br</i> d, $J = 9.4$, 1H); 3.86 (m, 1H)
3'-OCH ₃	55.9	3.89 (s, 3H)	56.0	3.91 (s, 3H)

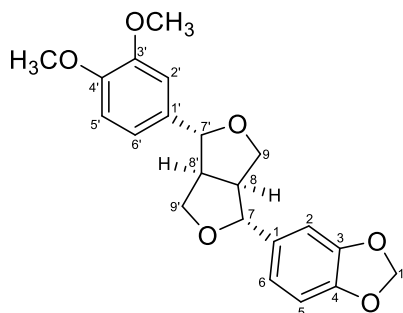
4'-OCH ₃	55.9	3.86 (s, 3H)	56.1	3.88 (s, 3H)
---------------------	------	--------------	------	--------------

* Report the same chemical shift at aromatic ring,

^a Spectra were recorded at 125 MHz, ^b 500 MHz, ^c 63, ^d 250 MHz.



3.4.3 Structure elucidation of compounds 18



Molecular formula	$C_{21}H_{22}O_6$
Appearance	Colorless oil
$[\alpha]_D^{25}$ (c 0.1, MeOH)	-32.3
1H and ^{13}C NMR ($CDCl_3$)	See Table 3.19

Compound **18** was obtained as a colorless oil, its specific optical rotation $[\alpha]_D^{25}$ (c 0.1, MeOH) was determined at -32.3. The ^{13}C NMR spectrum (**Table 3.20**) established twenty-one carbon signals, composing of two methoxy groups at δ_C 56.0 (3'-OCH₃), 56.1 (4'-OCH₃), two quaternary carbons at δ_C 133.2 (C-1), 135.2 (C-1'), four oxygenated quaternary carbons at δ_C 149.5 (C-3'), 148.7 (C-4'), 148.5 (C-3), 147.3 (C-4), two methine at δ_C 54.5 (C-8), 54.3 (C-8') and two oxygenated methine at δ_C 86.0 (C-7) and 85.9 (C-7'). The six aromatic methine carbons were at δ_C 106.7 (C-2), 108.4 (C-5), 109.5 (C-2'), 111.3 (C-5'), 119.5 (C-6), 118.4 (C-6') and two oxygenated methylene carbon at δ_C 71.9 (C-9, C-9') and 101.2 (C-10).

1H NMR spectrum (**Table 3.20**) showed the characteristic of methine protons at δ_H 3.11-3.06 (m, H-8, H-8') an oxygenated methine protons at δ_H 4.42 (t, $J = 4.5$, H-7, H-7') with oxygenated methylene protons at δ_H 3.88 (m, H_a-9, H_a-9'), 4.25 (m, H_b-9, H_b-9') that assumed the presence of a bis-tetrahydrofuran ring of 2,6-diaryl-3,7-dioxabicyclic[3,3,0]-octane type lignans¹¹⁷. The small differences in chemical shifts between H-7/H-7', H-8/H-8', and H-9/H-9', indicated that the furofuran moiety is

symmetrical and coupling constant between H-7/H-8 and between H-7'/H-8' are both $J \sim 4.5$ Hz, which is in agreement with a *trans* relationship between these two protons. By considering the NMR data of a number of furofuran lignans, it was proposed that the relative configuration of these compounds could be derived by considering the chemical shift differences between the two diastereotopic protons on C-9 and C-9'¹²⁴. Finally, the difference in chemical shift between the two diastereotopic C-9 protons was $\Delta\delta_{\text{H}} = 4.25 - 3.88 = 0.39$, which was characteristic of a H-7/ H-8 *trans*, and also H-7'/H-8' *trans* isomer¹²⁴. The splitting pattern and J coupling constant of aromatic methine proton were deduced as the two 1,3,4 tetra-substituted aromatic ring in this structure. The HMBC correlations (**Figure 3.26**) of 3'-OCH₃ to C-3' and 4'-OCH₃ to C-4' confirmed the presence of methoxy substituted at C-3' and C-4'.

Based on the NMR data discussed above, the structure of compound **18** was identified as (-) kobusin, a lignan that was first isolated from *M. kobus* DC¹²¹. The NMR data was in good agreement with the published data^{57, 125}.

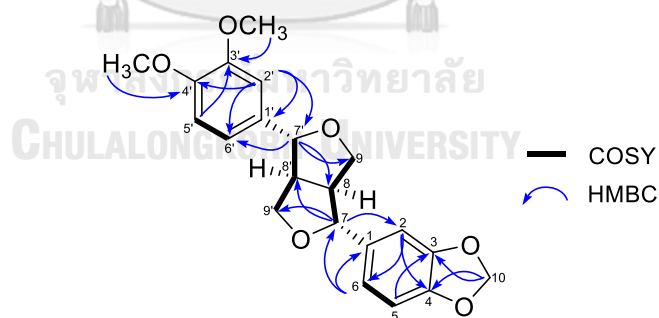


Figure 3.26 HMBC and ¹H-¹H COSY correlations of compound **18**

Table 3.20 NMR data of compound **18** and (-) kobusin (CDCl₃)

no.	(-) kobusin		compound 17	
	δ_C^a	δ_H [mult, J in Hz] ^b	δ_C^a	δ_H [mult, J in Hz] ^b
1	135.3		133.2	
2	106.7	6.92-6.79 (m, 1H)*	106.7	6.86 (d, J = 1.9 Hz, 1H)
3	148.2		148.5	
4	147.3		147.3	
5	108.4	6.92-6.79 (m, 1H)*	108.4	6.78 (d, J = 8.0 Hz, 1H)
6	119.6	6.92-6.79 (m, 1H)*	119.5	6.78 (dd, J = 8.0, 1.4 Hz, 1H)
7	86.0	4.76 (dd, J = 10.5, 5.0 Hz, 1H)	86.0	4.74 (t, J = 4.5 Hz, 1H)
8	54.6	3.10 (m, 1H)	54.5	3.11-3.06 (m, 1H)
9	72.0	4.27 (dd, J = 9.0, 4.0, 1H); 3.91 (m, 1H)	71.9	4.25 (d, J = 9.4 Hz, 1H); 3.88-3.86 (m, 1H)
10	101.3	5.97 (s, 2H)	101.2	5.95 (s, 2H)
1'	133.8		135.2	
2'	109.5	6.92-6.79 (m, 1H)*	109.5	6.90 (d, J = 1.9 Hz, 1H)
3'	149.4		149.5	
4'	148.9		148.7	
5'	111.3	6.92-6.79 (m, 1H)*	111.3	6.85 (d, J = 8.3 Hz, 1H)
6'	118.5	6.92-6.79 (m, 1H)*	118.4	6.88 (dd, J = 9.9, 1.9 Hz, 1H)
7'	86.1	4.76 (dd, J = 10.5, 5.0 Hz, 1H)	85.9	4.74 (t, J = 4.5 Hz, 1H)
8'	54.4	3.10 (m, 1H)	54.3	3.11-3.06 (m, 1H)

9'	71.9	4.27 (dd, $J = 9.0, 4.0$, 1H); 3.91 (m, 1H)	71.9	4.25 (d, $J = 9.4$ Hz, 1H); 3.88-3.85 (m, 1H)
3'-OCH ₃	56.1	3.88 (s, 3H)	56.0	3.88 (s, 3H)
4'-OCH ₃	56.2	3.89 (s, 3H)	56.1	3.90 (s, 3H)

* Report the same chemical shift at aromatic ring

^a Spectra were recorded at 125, ^b 500 MHz.

3.5 Free radical scavenging activity

The fifteen compounds (**1-15**) from *D. signatum* (**Figure 3.27**) and three compounds (**16-18**) from *M. lilifera* (**Figure 3.28**) were evaluated for free radical scavenging activity using two *in vitro* assays, including DPPH and ABTS tests. Results from both methods (**Table 3.21**) are reported as IC₅₀ value (if the compound showed more than 50% inhibition). Note that quercetin and Trolox[®] were used as positive controls.

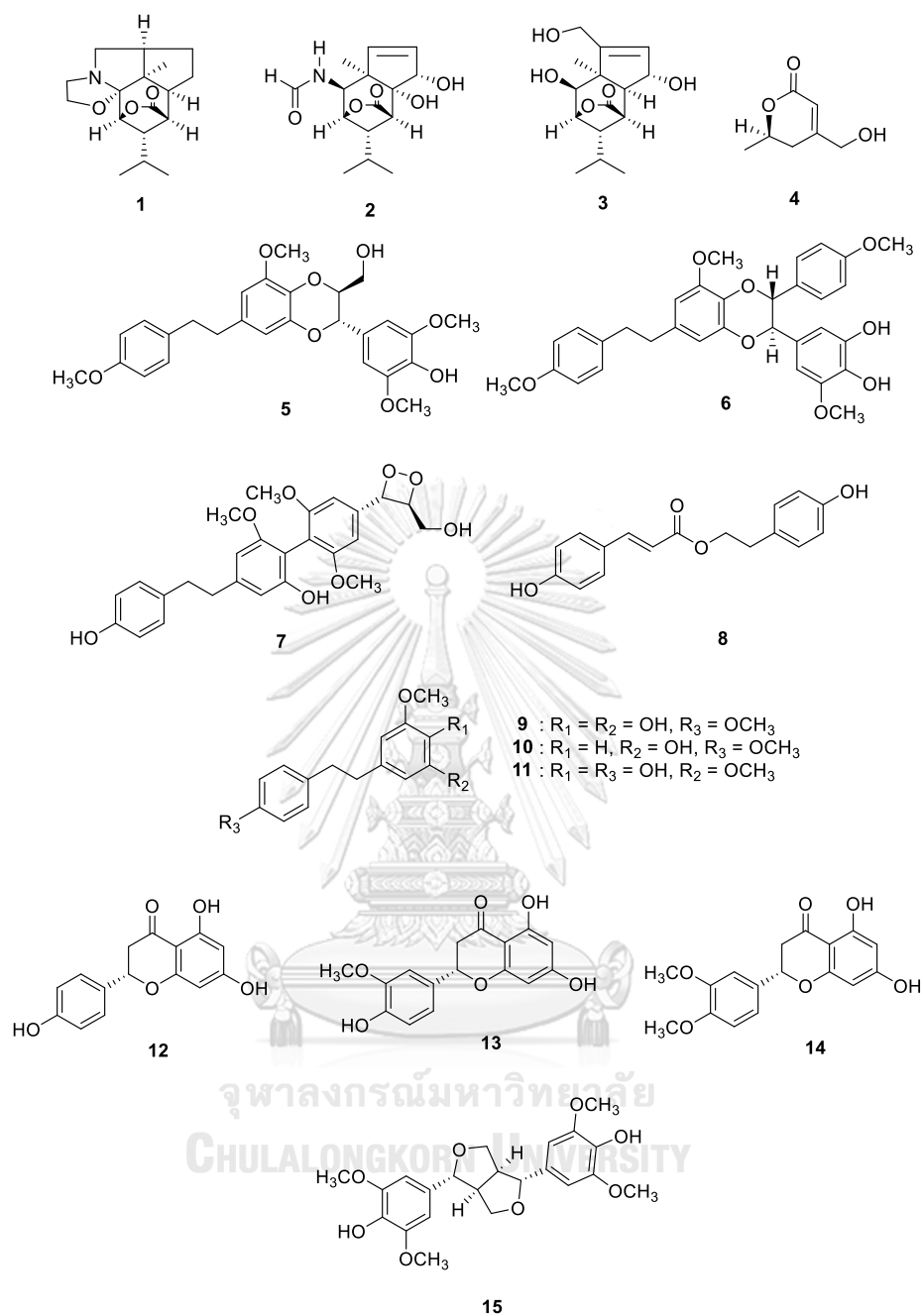


Figure 3.27 The chemical structures (1-15) of isolated compounds from *D. signatum*

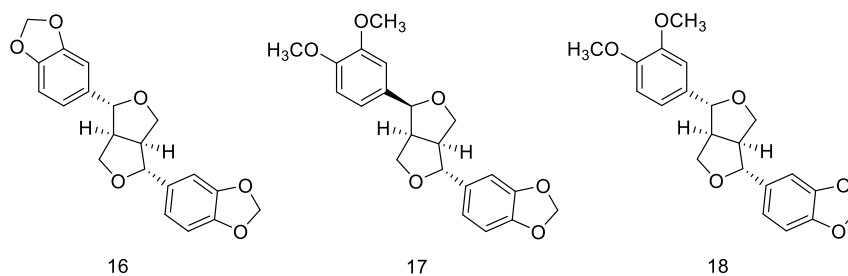


Figure 3.28 The chemical structures (**16-18**) of isolated compounds from *M. liliifera*

The results in **Table 3.21** highlighted that the new compound (-)-6*R*-signatone (**4**) exhibited the potent ABTS scavenging activity with IC_{50} value of $0.71 \pm 0.01 \mu\text{M}$, which was obviously greater than a positive control Trolox[®] (IC_{50} of $27.26 \pm 0.33 \mu\text{M}$). However, this compound showed less DPPH scavenging activity than that of a positive control quercetin with IC_{50} of $21.81 \pm 0.04 \mu\text{M}$. Likewise, the other sesquiterpenes dendroxine (**1**) and crystallinin (**3**) also exhibited less potent free radical scavenging activity in the DPPH assay, with IC_{50} of $16.39 \pm 0.05 \mu\text{M}$ and $15.40 \pm 0.03 \mu\text{M}$, respectively as compared to the control. On the other hand, similar to compound **4**, both compounds displayed a prominent effect in the ABTS assay, with IC_{50} of $8.87 \pm 0.01 \mu\text{M}$ for **1** and $6.93 \pm 0.02 \mu\text{M}$ for **3**, which were evidently stronger than a positive control Trolox[®]. Based on these findings, it suggested that these compounds could significantly reduce the free radical through neutralization of the radical cation $\text{ABTS}^{+\cdot}$ by either direct reduction *via* electron donation or by radical quenching *via* hydrogen atom donation¹²⁶.

Moreover, the bibenzyls dendrocandin B (**5**), dendrocandin I (**6**), and 6''-de-*O*-methyl dendrofindlaphenol A (**7**) possessed moderate radical scavenging activity in the DPPH assay (IC_{50} value 8.95 ± 0.11 , 15.64 ± 0.22 and $10.23 \pm 0.07 \mu\text{M}$) and in the ABTS assay (IC_{50} value 17.95 ± 0.10 , 8.11 ± 0.04 and $23.97 \pm 0.18 \mu\text{M}$). It can be implied from the ABTS assay that compound **6** containing an 1,4 disubstituted aromatic ring at C-9'' of 1,4-dioxane ring displayed a better $\text{ABTS}^{+\cdot}$ radical-scavenging

activity than that of **5**. The presence of this moiety turned out to be important for the antioxidant activity *via* electron donation or by radical quenching *via* hydrogen atom to ABTS^{•+} radical. Nonetheless, it should be noted that the result was in contrast to the DPPH assay among these two compounds. This might be due to the fact that the complexity of compound, polarity and chemical properties could lead to varying bioactivity results depending on the method adopted⁸⁷.

The three bibenzyls 3,4-dihydroxy-5,4'-dimethoxybibenzyl (**9**), 3-methoxy-5-[2-(4-methoxyphenyl) ethyl]phenol (**10**), and 4,4'-dihydroxy-3,5-dimethoxybibenzyl (**11**) also showed moderate to weak scavenging activity in the DPPH assay (IC_{50} of 9.11 ± 0.26 , 7.18 ± 0.05 and $13.97 \pm 0.12 \mu M$) and in the ABTS assay (IC_{50} of 12.00 ± 0.32 , 25.51 ± 0.14 , $18.48 \pm 0.18 \mu M$). The results revealed that compound **10** established the similar radical scavenging potency as positive control in both assays. While compounds **9** and **11** displayed the significantly higher antioxidant activity in ABTS^{•+} scavenging assay but showed the weaker scavenging capability with DPPH radical in comparison with compound **10**.

The phenylpropanoids derivatives, *p*-hydroxyphenylethyl-*p*-coumarate (**8**) showed the moderate scavenging ability in the DPPH and ABTS assays with IC_{50} of $5.45 \pm 0.03 \mu M$ and $25.76 \pm 0.19 \mu M$, respectively.

Three flavonoids naringenin (**12**), (2*S*)-homoeriodictyol (**13**), (2*S*)-homohesperetin (**14**) can be considered as weak radical scavenger based on the DPPH method with IC_{50} of 20.95 ± 0.09 , 20.06 ± 0.05 , $18.01 \pm 0.05 \mu M$, respectively. Likewise, compounds **13** and **14** also exerted the weak radical scavenging activity in the ABTS assay with the respective IC_{50} of 17.44 ± 0.06 and $17.34 \pm 0.02 \mu M$, in which compound **12** had no antioxidant activity ($IC_{50} > 50 \mu M$).

Table 3.21 Free radical scavenging activity of isolated compounds from *D. signatum* and *M. liliifera*

Compounds	IC ₅₀ (μ M)		Compounds	IC ₅₀ (μ M)	
	DPPH	ABTS		DPPH	ABTS
1	16.39 \pm 0.05	8.87 \pm 0.01	11	13.97 \pm 0.12	18.48 \pm 0.18
2	nd	nd	12	20.95 \pm 0.09	>50
3	15.40 \pm 0.03	6.93 \pm 0.02	13	20.06 \pm 0.05	17.44 \pm 0.06
4	21.81 \pm 0.04	0.71 \pm 0.01	14	18.01 \pm 0.05	17.34 \pm 0.02
5	8.95 \pm 0.11	17.95 \pm 0.10	15	8.72 \pm 0.09	16.22 \pm 0.11
6	15.64 \pm 0.22	8.11 \pm 0.04	16	22.42 \pm 0.06	>50
7	10.23 \pm 0.07	23.97 \pm 0.18	17	29.55 \pm 0.03	7.71 \pm 0.01
8	5.45 \pm 0.03	25.76 \pm 0.19	18	7.16 \pm 0.26	15.85 \pm 0.01
9	9.11 \pm 0.26	12.00 \pm 0.32	Quercetin	7.29 \pm 0.18	nd
10	7.18 \pm 0.05	25.51 \pm 0.14	Trolox [®]	nd	27.26 \pm 0.33

nd = not determined

Four lignan derivatives including (-)-syringaresinol (**15**), (+) sesamin (**16**), (+) fargesin (**17**) and (-) kobusin (**18**) displayed moderate to weak radical scavenging activity on the two studied assays. Among these derivatives, compounds **15** and **18** established quite similar magnitude of the scavenging ability on the DPPH assay (IC₅₀ of 8.72 \pm 0.09 μ M for **15** and 7.16 \pm 0.26 μ M for **18**) and on the ABTS assay (IC₅₀ of

16.22 ± 0.11 μM for **15** and 15.85 ± 0.01 μM for **18**). This can be implied that the presence of substituents at aromatic ring played the role in radical-scavenging activity. In addition, it was found that compound **17** (IC₅₀ value 29.55 ± 0.03 μM) showed less scavenging ability than compound **18** (IC₅₀ value 7.16 ± 0.26 μM), but exhibited the stronger antioxidant activity on the ABTS assay. Hence, the different *R* or *S* configuration of **17** and **18** might differently affect the free radical scavenging¹²⁷. Besides, lignan **17** showed strong antioxidant (7.71 ± 0.01 μM) for scavenging ABTS^{•+} radical. For lignan **15** (16.22 ± 0.11 μM) and **18** (15.85 ± 0.01 μM) were observed as moderate ABTS^{•+} radical scavenger. Compound **16** containing an aromatic dioxane ring established inactive or weak antioxidant capacity (IC₅₀ > 50 μM) in the ABTS assay, and IC₅₀ of 22.42 ± 0.06 μM in the DPPH assay.

3.6 Lipid peroxidation inhibition activity

Lipid peroxidation is a chain reaction initiated by the hydrogen abstraction or addition of an oxygen radical. Polyunsaturated fatty acids are more sensitive than saturated ones, its activated methylene (RH) bridge represents a critical target site. The presence of a double bond adjacent to a methylene group makes the methylene C-H bond weaker and hence the hydrogen is more receptive to abstraction. This leaves an unpaired electron on the carbon, forming a carbon-centered radical, which is stabilized by a molecular rearrangement of the double bonds to form a conjugated diene which then combines with oxygen to form a peroxy radical. The peroxy radical is itself capable of abstracting a hydrogen atom from another polyunsaturated fatty acid and so of starting a chain reaction¹²⁸. Reduced iron complexes (Fe²⁺) react with lipid peroxides (ROOH) to give alkoxy radicals, whereas oxidized iron complexes (Fe³⁺) react more slowly to produce peroxy radicals. Both radicals can take part in the propagation of the chain reaction. The end products of these complex metal ion-catalyzed breakdowns of lipid

hydroperoxides include the cytotoxic aldehydes such as major malonaldehyde (MDA), 4-hydroxynonenal (HNE) and ethane gases ¹²⁹.

In the present study, the lipid peroxidation inhibition of isolated compounds from *D. signatum* and *M. liliifera* at 5 μ M was measured by monitoring the inhibition of malonaldehyde (MDA) production in Fe²⁺-activated egg yolk using TBARS method. The results expressed as % lipid peroxidation inhibition are summarized in **Figure 3.29**

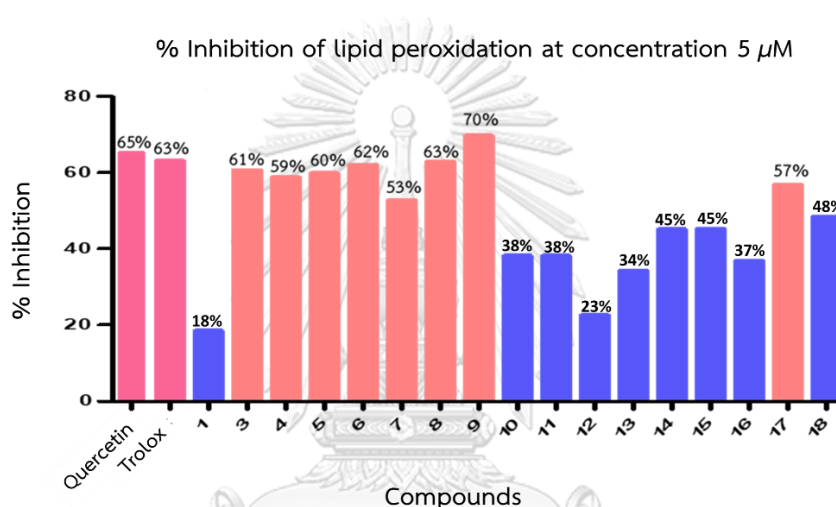


Figure 3.29 % Inhibition of lipid peroxidation of isolated compounds from *M. liliifera* and *D. signatum*

Among all the tested compounds, the results showed that crystallinin (**3**), (-)-6*R*-signatone (**4**), dendrocandine B (**5**), dendrocandine I (**6**), 6''-de-*O*-methyl dendrofindlaphenol A (**7**), *p*-hydroxyphenylethyl-*p*-coumarate (**8**), 3,4-dihydroxy-5,4'-dimethoxybibenzyl (**9**) and (+) fargesin (**17**) established the lipid peroxidation inhibition in range 53 - 70 %, which was similar to or better than the standard quercetin (65 %) and Trolox (63%). It evidently revealed that one monomer bibenzyl (**9**) showed the highest inhibition at 70%. Likewise, all the dimer bibenzyls (**5-7**) along with compounds **3**, **4**, **8** and **17** were promising to inhibit the lipid peroxidation in the vital model. Also, these eight compounds exerted good free

radical scavenging activity based on DPPH and ABTS assay and were very interesting to further study in cell-based assay.

3.7 Anti-inflammatory activity

The inflammatory processes are normal immune responses. Macrophages play a crucial role in the regulation of inflammation by producing nitric oxide (NO), prostaglandin E₂ (PGE₂), and other pro-inflammatory cytokines¹³⁰. The secretion of NO and PGE₂ relies on the expression of the two key enzymes, namely inducible nitric oxide synthase (iNOS) and cyclooxygenase-2 (COX-2), which are induced by pro-inflammatory cytokines and lipopolysaccharide (LPS)¹³¹. Several studies have suggested that ROS can control the production of cytokines in macrophages through NF-κB dependent mechanisms. Excessive inflammatory responses are known to cause cell death and tissue damage, thereby leading to various diseases and their complications¹³².

In the present study, the anti-inflammatory activity of isolated compounds from *D. signatum* and *M. lilifera* was thus evaluated by monitoring the inhibition of nitric oxide (NO) production in LPS-activated murine macrophage J774.A1 cells. The results expressed as IC₅₀ ± SD are summarized in **Table 3.22**. Among the tested compounds, (-) kobusin **18** possessed the highest anti-inflammatory activity with IC₅₀ value of 4.72 ± 0.17 μM, whereas the different stereoisomer (+) fargesin **17** showed moderate activity with IC₅₀ value of 12.87 ± 1.02 μM. Hence, it can be suggested here that the (*R*)-configuration of 3,4-dimethoxy aromatic ring at C-7' may significantly enhance the NO production inhibition activity of this type of lignan. Furthermore, the *p*-hydroxyphenylethyl-*p*-coumarate (**8**) presented the high potent inhibition with IC₅₀ value of 6.18 ± 0.50 μM.

Although the bibenzyl derivatives showed quite weak inhibitory activity levels, this was except for compound **7**, 6''-de-O-methyldendrofindlaphenol A, which displayed the moderate NO production inhibition with IC_{50} of $12.96 \pm 0.97 \mu M$. Therefore, the presence of aromatic ring substituent at C-1 and 1,2-dioxetane ring may encourage the role of inhibition of NO production. Nevertheless, the sesquiterpenes and flavonoids were appeared to be inactive or weak inhibition ability as compared to the standard indomethacin ($28.42 \pm 3.51 \mu M$).

Table 3.22 Inhibitory effect of isolated compounds from *D. signatum* and *M. liliifera*

Compounds	IC_{50} (μM)	Compounds	IC_{50} (μM)
1	>50	10	32.79 ± 1.39
2	nd	11	25.26 ± 1.32
3	>50	12	>50
4	>50	13	>50
5	49.9 ± 1.65	14	24.94 ± 1.26
6	39.32 ± 0.82	15	22.19 ± 1.26
7	12.96 ± 0.97	16	26.8 ± 1.33
8	6.18 ± 0.50	17	12.87 ± 1.02
9	23.28 ± 1.33	18	4.72 ± 0.17
Indomethacin	28.42 ± 3.51		

CHAPTER IV

CONCLUSION

In this study, a purification of the EtOAc crude extract of *D. signatum* aerial parts was performed. It yielded one new picrotoxane sesquiterpene, 7-hydroxydendroterpene B (**2**) and a new α -pyrone, (-)-6*R*-signatone (**4**), along with thirteen known compounds. These included dendroxine (**1**), crystallinin (**3**), dendrocandin B (**5**), dendrocandin I (**6**), 6''-de-*O*-methyl dendrofindlaphenol A (**7**), *p*-hydroxyphenylethyl-*p*-coumarate (**8**), 3,4-dihydroxy-5,4'-dimethoxybibenzyl (**9**), 3-methoxy-5-[2-(4-methoxyphenyl) ethyl]phenol (**10**), 4,4'-dihydroxy-3,5-dimethoxybibenzyl (**11**), naringenin (**12**), (2*S*)-homoeridodictyol (**13**), (2*S*)-homohesperetin (**14**) and (-)-syringaresinol (**15**). Moreover, the hexane crude extracts of *M. liliifera* were further separated to accomplish three known compounds, (+) sesamin (**16**), (+) fargesin (**17**) and (-) kobusin (**18**). Afterward, all the isolated compounds were evaluated for free radical scavenging activity by means of the DPPH and ABTS assays and anti-inflammatory activity.

The new α -pyrone derivative, (-)-6*R*-signatone **4**, exhibited very promising ABTS scavenging activity with IC_{50} of $0.71 \pm 0.01 \mu M$ in comparison with a positive control Trolox[®]. Likewise, sesquiterpenes **1** and **3** also displayed a prominent antioxidant effect on the ABTS assay, with IC_{50} of $8.87 \pm 0.01 \mu M$ and $6.93 \pm 0.02 \mu M$, respectively. Based on these observations, it suggested that these compounds could significantly reduce the free radical through neutralization of the radical cation ABTS^{•+} by either direct reduction *via* electron donation or by radical quenching *via* hydrogen atom donation.

In addition, it can be seen from the ABTS assay that compound **6** (IC_{50} of $8.11 \pm 0.04 \mu M$) containing an 1,4 disubstituted aromatic ring at C-9'' of 1,4-dioxane ring

displayed a better ABTS^{•+} radical-scavenging activity than that of compound **5** (IC₅₀ of 17.95 ± 0.10 μM). This indicated that the presence of this moiety played a pivotal role for the antioxidant activity. Nonetheless, it was of note that the result contrasted with the DPPH assay among these two compounds. This might be owing to the fact that the complexity of compound, polarity and chemical properties could lead to varying bioactivity results depending on the method used.

Based on the structure comparison between compounds **9** and **11**, it demonstrated that the presence of the respective hydroxy and methoxy group substituent at C-3 and C-4' in **9** possessed the predominant role for antioxidant activity in both free radical scavenging assays.

The vital model study, lipid peroxidation inhibition revealed that monomer bibenzyl (**9**), all dimer bibenzyls (**5-7**) along with compounds **3**, **4**, **8**, and **17** exhibited the promising inhibition as compared to the standard quercetin and Trolox. Together with good free radical scavenging based on DPPH and ABTS assay of these compounds, it was interesting to further investigation by cell-based assay.

For the anti-inflammatory activity, among all the tested compounds, it was found that (*R*)-configuration of 3,4-dimethoxy aromatic ring at C-7' in (-) kobusin considerably enhance the NO production inhibition activity of this type of lignan. Noticeable, (-) kobusin **18** (IC₅₀ of 4.72 ± 0.17 μM) exerted the higher activity than that of the different configuration (+) fargesin **17** (IC₅₀ of 12.87 ± 1.02 μM) by ~3 fold. Similarly, phenylpropanoids, the *p*-hydroxyphenylethyl-*p*-coumarate **8** also displayed the high potent inhibition with IC₅₀ of 6.18 ± 0.50 μM.

In conclusion, this study is the second report of natural constituents and biological activities of *D. signatum*. Promisingly, the free radical scavenging and anti-inflammatory activities observed in this thesis indicated that *D. signatum* and *M. liliferra* should be of interest to the natural product research community

REFERENCES



จุฬาลงกรณ์มหาวิทยาลัย
CHULALONGKORN UNIVERSITY

References

1. Arulseivan, P.; Fard, M. T.; Tan, W. S.; Gothai, S.; Fakurazi, S.; Norhaizan, M. E.; Kumar, S. S., Role of Antioxidants and Natural Products in Inflammation. *Oxid. Med. Cell. Longev.* **2016**.
2. Yin, H.; Xu, L.; Porter, N. A., Free Radical Lipid Peroxidation: Mechanisms and Analysis. *Chem. Rev.* **2011**, *111* (10), 5944-5972.
3. Conti, V.; Izzo, V.; Corbi, G.; Russomanno, G.; Manzo, V.; De Lise, F.; Di Donato, A.; Filippelli, A., Antioxidant Supplementation in the Treatment of Aging-Associated Diseases. *Front Pharmacol* **2016**, *7* (24), 24.
4. Mohammed, M.; Kadhim, S.; Mohammed noori jassim; Abdulkadir; Isam, S., Free radicals and human health. *IJISR* **2015**, *4*, 218-223.
5. Phaniendra, A.; Jestadi, D. B.; Periyasamy, L., Free Radicals: Properties, Sources, Targets, and Their Implication in Various Diseases. *Indian J Clin Biochem* **2015**, *30* (1), 11-26.
6. Lobo, V.; Patil, A.; Phatak, A.; Chandra, N., Free radicals, antioxidants and functional foods: Impact on human health. *Pharmacogn. Rev.* **2010**, *4* (8), 118-126.
7. Pham-Huy, L. A.; He, H.; Pham-Huy, C., Free radicals, antioxidants in disease and health. *Int J Biomed Sci* **2008**, *4* (2), 89-96.
8. Di Meo, S.; Reed, T. T.; Venditti, P.; Victor, V. M., Role of ROS and RNS Sources in Physiological and Pathological Conditions. *Oxid. Med. Cell. Longev.* **2016**, *2016*, 1245049.
9. Shahidi, F.; Zhong, Y., Lipid Oxidation and Improving the Oxidative Stability. *Chem. Soc. Rev* **2010**, *39*, 4067-79.
10. Thanan, R.; Oikawa, S.; Hiraku, Y.; Ohnishi, S.; Ma, N.; Pinlaor, S.; Yongvanit, P.; Kawanishi, S.; Murata, M., Oxidative stress and its significant roles in neurodegenerative diseases and cancer. *Int. J. Mol. Sci.* **2014**, *16* (1), 193-217.
11. Pacher, P.; Beckman, J. S.; Liaudet, L., Nitric oxide and peroxynitrite in health and disease. *Physiol. Rev* **2007**, *87* (1), 315-424.
12. Schulz, J. B.; Matthews, R. T.; Beal, M. F., Role of nitric oxide in neurodegenerative diseases. *Curr. Opin. Neurol.* **1995**, *8* (6).
13. Miquel, J.; Fleming, J. E., A two-step hypothesis on the mechanisms of in vitro cell aging: Cell differentiation followed by intrinsic mitochondrial mutagenesis. *Exp. Gerontol.* **1984**, *19* (1), 31-36.
14. Butterfield, D. A.; Koppal, T.; Howard, B.; Subramaniam, R.; Hall, N.; Hensley, K.; Yatin, S.; Allen, K.; Aksenov, M.; Aksenova, M.; Carney, J., Structural and functional changes in proteins induced by free radical-mediated oxidative stress and protective action of the antioxidants N-tert-butyl- α -phenylnitron and vitamin E. In *Ann N Y Acad Sci.*, 1998; Vol. 854, pp 448-462.
15. Dean, R. T.; Roberts, C. R.; Jessup, W., Fragmentation of extracellular and intracellular polypeptides by free radicals. *Prog. Clin. Biol. Res.* **1985**, *180*, 341-350.
16. Keck, R. G., The use of t-butyl hydroperoxide as a probe for methionine oxidation in proteins. *Anal. Biochem.* **1996**, *236* (1), 56-62.
17. Lyras, L.; Cairns, N. J.; Jenner, A.; Jenner, P.; Halliwell, B., An assessment of oxidative damage to proteins, lipids, and DNA in brain from patients with Alzheimer's disease. *J. Neurochem.* **1997**, *68* (5), 2061-2069.
18. Stadtman, E. R., Metal ion-catalyzed oxidation of proteins: Biochemical mechanism and biological consequences. *Free Radic. Biol. Med.* **1990**, *9* (4), 315-325.
19. Giugliano, D.; Ceriello, A.; Paolisso, G., Oxidative stress and diabetic vascular complications. *Diabetes Care* **1996**, *19* (3), 257-267.

20. Esterbauer, H.; Koller, E.; Slezacek, R. G.; Kostner, J. F., Possible involvement of the lipid-oxidation product 4-hydroxynonenal in the formation of fluorescent chromolipids. *Biochem. J.* **1986**, *239* (2), 405-409.
21. Uchida, K.; Shiraishi, M.; Naito, Y.; Torii, Y.; Nakamura, Y.; Osawa, T., Activation of stress signaling pathways by the end product of lipid peroxidation: 4-Hydroxy-2-nonenal is a potential inducer of intracellular peroxide production. *J. Biol. Chem.* **1999**, *274* (4), 2234-2242.
22. Suc, I.; Meilhac, O.; Lajoie-Mazenc, I.; Vandaele, J.; Jürgens, G.; Salvayre, R.; Nègre-Salvayre, A., Activation of EGF receptor by oxidized LDL. *FASEB J.* **1998**, *12* (9), 665-671.
23. Tsukagoshi, H.; Kawata, T.; Shimizu, Y.; Ishizuka, T.; Dobashi, K.; Mori, M., 4-Hydroxy-2-Nonenal Enhances Fibronectin Production by IMR-90 Human Lung Fibroblasts Partly via Activation of Epidermal Growth Factor Receptor-Linked Extracellular Signal-Regulated Kinase p44/42 Pathway. *Appl. Pharmacol.* **2002**, *184* (3), 127-135.
24. Sies, H., "Oxidative stress: introductory remarks". In *Oxidative Stress*, In H. Sies, E., Ed. Academic Press: London, 1985.
25. Singh, A.; Kukreti, R.; Saso, L.; Kukreti, S., Oxidative Stress: A Key Modulator in Neurodegenerative Diseases. *Molecules* **2019**, *24* (8).
26. Ghosh, R.; Mitchell, D. L., Effect of oxidative DNA damage in promoter elements on transcription factor binding. *Nucleic Acids Res.* **1999**, *27* (15), 3213-3218.
27. Lee, D.-H., Oxidative DNA damage induced by copper and hydrogen peroxide promotes CG->TT tandem mutations at methylated CpG dinucleotides in nucleotide excision repair-deficient cells. *Nucleic Acids Res* **2002**, *30*, 3566-3573.
28. Sun, Y.; Oberley, L. W., Redox regulation of transcriptional activators. *Free Radic. Biol. Med.* **1996**, *21* (3), 335-348.
29. Redza-Dutordoir, M.; Averill-Bates, D. A., Activation of apoptosis signalling pathways by reactive oxygen species. *Biophys. Acta, Mol. Cell Res.* **2016**, *1863* (12), 2977-2992.
30. Perkins, N. D., Integrating cell-signalling pathways with NF-kappaB and IKK function. *Nat. Rev. Mol. Cell Biol.* **2007**, *8* (1), 49-62.
31. Akira, S.; Kishimoto, T., NF-IL6 and NF-kappa B in cytokine gene regulation. *Adv Immunol* **1997**, *65*, 1-46.
32. Gilmore, T. D., Introduction to NF-kB: players, pathways, perspectives. *Oncogene* **2006**, *25* (51), 6680-6684.
33. Coussens, L. M.; Werb, Z., Inflammation and cancer. *Nature* **2002**, *420* (6917), 860-867.
34. Hussain, S. P.; Hofseth Lj Fau - Harris, C. C.; Harris, C. C., Radical causes of cancer. *Nat Rev Cancer* **2003**, *3*(4), 276-85.
35. Federico, A.; Morgillo, F.; Tuccillo, C.; Ciardiello, F.; Loguercio, C., Chronic inflammation and oxidative stress in human carcinogenesis. *Int. J. Cancer Res.* **2007**, *121* (11), 2381-2386.
36. Hussain, S. P.; Harris, C. C., Inflammation and cancer: An ancient link with novel potentials. *Int. J. Cancer Res.* **2007**, *121* (11), 2373-2380.
37. Reuter, S.; Gupta Sc Fau - Chaturvedi, M. M.; Chaturvedi Mm Fau - Aggarwal, B. B.; Aggarwal, B. B., Oxidative stress, inflammation, and cancer: how are they linked? *Free Radic Biol Med* **2010**, *49*(11), 1603-1616.
38. Gloire, G.; Legrand-Poels, S.; Piette, J., NF-kB activation by reactive oxygen species: Fifteen years later. *Biochem. Pharmacol* **2006**, *72* (11), 1493-1505.

39. Barbulova, A.; Colucci, M. G.; Apone, F., New Trends in Cosmetics: By-Products of Plant Origin and Their Potential Use as Cosmetic Active Ingredients. *Cosmetics* **2015**, *2*, 82-92.
40. Fraunberger, E.; Scola, G.; Laliberté, V.; Duong, A.; Andrezza, A., Redox Modulations, Antioxidants, and Neuropsychiatric Disorders. *Oxid. Med. Cell. Longev.* **2016**, *2016*, 1-14.
41. Nimse, S. B.; Pal, D., Free radicals, natural antioxidants, and their reaction mechanisms. *RSC Adv.* **2015**, *5* (35), 27986-28006.
42. Baiano, A.; Del Nobile, M. A., Antioxidant Compounds from Vegetable Matrices: Biosynthesis, Occurrence, and Extraction Systems. *Crit Rev Food Sci Nutr* **2016**, *56* (12), 2053-2068.
43. Martysiak-Żurowska, D.; Wenta, W., A comparison of ABTS and DPPH methods for assessing the total antioxidant capacity of human milk. *Acta Sci Pol Technol Aliment.* **2012**, *11* (1), 83-9.
44. Gutteridge, J. M. C., Biological origin of free radicals, and mechanisms of antioxidant protection. *Chem.-Biol. Interact.* **1994**, *91* (2), 133-140.
45. Ferreira, C. A.; Ni, D.; Rosenkrans, Z. T.; Cai, W., Scavenging of reactive oxygen and nitrogen species with nanomaterials. *Nano Res* **2018**, *11* (10), 4955-4984.
46. Ravipati, A. S.; Zhang, L.; Koyyalamudi, S. R.; Jeong, S. C.; Reddy, N.; Bartlett, J.; Smith, P. T.; Shanmugam, K.; Münch, G.; Wu, M. J.; Satyanarayanan, M.; Vysetti, B., Antioxidant and anti-inflammatory activities of selected Chinese medicinal plants and their relation with antioxidant content. *BMC Compl Alternative Med* **2012**, *12* (1), 173.
47. Cai, Y.; Luo, Q.; Sun, M.; Corke, H., Antioxidant activity and phenolic compounds of 112 traditional Chinese medicinal plants associated with anticancer. *Life Sci.* **2004**, *74* (17), 2157-2184.
48. Raghavendra, M.; Madhusudhana Reddy, A.; Raghuvveer Yadav, P.; Sudharshan Raju, A.; Siva Kumar, L., Comparative studies on the in vitro antioxidant properties of methanolic leafy extracts from six edible leafy vegetables of India. *Asian J. Pharm. Sci.* **2013**, *6* (3), 96-99.
49. Gothai, S.; Arulselvan, P.; Tan, W. S.; Fakurazi, S., Wound healing properties of ethyl acetate fraction of *Moringa oleifera* in normal human dermal fibroblasts. *J. Intercult. Ethnopharmacol* **2016**, *5* (1), 1-6.
50. Tan, W. S.; Arulselvan, P.; Karthivashan, G.; Fakurazi, S., *Moringa oleifera* Flower Extract Suppresses the Activation of Inflammatory Mediators in Lipopolysaccharide-Stimulated RAW 264.7 Macrophages via NF- κ B Pathway. *Mediators Inflamm* **2015**, *2015*, 720171-720171.
51. Arulselvan, P.; Ghofar, H. A. A.; Karthivashan, G.; Halim, M. F. A.; Ghafar, M. S. A.; Fakurazi, S., Antidiabetic therapeutics from natural source: A systematic review. *Biomed. Prev. Nutr.* **2014**, *4* (4), 607-617.
52. Fürst, R.; Zündorf, I., Plant-Derived Anti-Inflammatory Compounds: Hopes and Disappointments regarding the Translation of Preclinical Knowledge into Clinical Progress. *Mediators Inflamm* **2014**, *2014*, 146832.
53. Liu Y.H.; Luo X.R.; Wu Y.F., *Menispermaceae, Magnoliaceae*. Beijing: Science Press, **1996**; Vol. 30.
54. Park, C. H.; Park, S.-Y.; Lee, S. Y.; Kim, J. K.; Park, S. U., Analysis of Metabolites in White Flowers of *Magnolia Denudata* Desr. and Violet Flowers of *Magnolia Liliiflora* Desr. *Molecules* **2018**, *23* (7).
55. Nooteboom, H. P.; P. Chalermglin, *The Magnoliaceae of Thailand*. Thai Forest Bulletin (Botany): **2009**; Vol. 37.

56. Talapatra, B.; Chaudhuri, P. K.; Talapatra, S. K., (-)-Maglifloenone, a novel spirocyclohexadienone neolignan and other constituents from *Magnolia liliflora*. *Phytochemistry* **1982**, *21* (3), 747-750.
57. Iida, T.; Ito, K., Four phenolic neolignans from *Magnolia liliflora*. *Phytochemistry* **1983**, *22* (3), 763-766.
58. Matsuda, H.; Kageura, T.; Oda, M.; Morikawa, T.; Sakamoto, Y.; Yoshikawa, M., Effects of Constituents from the Bark of *Magnolia obovata* on Nitric Oxide Production in Lipopolysaccharide-Activated Macrophages. *Chem. Pharm. Bull.* **2001**, *49* (6), 716-720.
59. Kim, J. Y.; Lim, H. J.; Lee, D. Y.; Kim, J. S.; Kim, D. H.; Lee, H. J.; Kim, H. D.; Jeon, R.; Ryu, J.-H., In vitro anti-inflammatory activity of lignans isolated from *Magnolia fargesii*. *Bioorganic Med. Chem. Lett.* **2009**, *19* (3), 937-940.
60. Bajpai, V. K.; Yoon, J. I.; Kang, S. C., Antioxidant and antidermatophytic activities of essential oil and extracts of *Magnolia liliflora* Desr. *Food Chem Toxicol* **2009**, *47* (10), 2606-2612.
61. Lee, S.-U.; Ryu, H. W.; Lee, S.; Shin, I.-S.; Choi, J.-H.; Lee, J.-W.; Lee, J.; Kim, M. O.; Lee, H.-J.; Ahn, K.-S.; Hong, S.-T.; Oh, S.-R., Lignans Isolated From Flower Buds of *Magnolia fargesii* Attenuate Airway Inflammation Induced by Cigarette Smoke in vitro and in vivo. *Front Pharmacol* **2018**, *9*, 970-970.
62. Cameron, K. M.; Chase, M. W.; Whitten, W. M.; Kores, P. J.; Jarrell, D. C.; Albert, V. A.; Yukawa, T.; Hills, H. G.; Goldman, D. H., A phylogenetic analysis of the Orchidaceae: evidence from rbcL nucleotide. *Am J Bot* **1999**, *86* (2), 208-24.
63. Wang, L.; Zhang, C. F.; Wang, Z. T.; Zhang, M.; Xu, L. S., Five new compounds from *Dendrobium crystallinum*. *J. Asian Nat. Prod. Res.* **2009**, *11* (11), 903-911.
64. Zhang, G. N.; Zhong, L. Y.; Bligh, S. W. A.; Guo, Y. L.; Zhang, C. F.; Zhang, M.; Wang, Z. T.; Xu, L. S., Bi-bicyclic and bi-tricyclic compounds from *Dendrobium thyrsiflorum*. *Phytochemistry* **2005**, *66* (10), 1113-1120.
65. Chanvorachote, P.; Kowitdamrong, A.; Ruanghirun, T.; Sritularak, B.; Mungmee, C.; Likhitwitayawuid, K., Anti-metastatic activities of bibenzyls from *Dendrobium pulchellum*. *Nat. Prod. Commun.* **2013**, *8* (1), 115-118.
66. Liu, X. F.; Zhu, J.; Ge, S. Y.; Xia, L. J.; Yang, H. Y.; Qian, Y. T.; Ren, F. Z., Orally administered *Dendrobium officinale* and its polysaccharides enhance immune functions in BALB/c mice. *Nat. Prod. Commun.* **2011**, *6* (6), 867-870.
67. Smitinand, T., *Thai plant names (Botanical names-vernacular names)*. Revised edition ed.; Royal forest department: Bangkok, 2001.
68. Vaddhanaphuti N., *A field guide to the wild orchids of Thailand fourth and expanded edition*. Silkworm Books: Chiang Mai, **2005**.
69. Gutierrez, R., Orchids: A review of uses in traditional medicine, its phytochemistry and pharmacology. *J. Med. Plant Res.* **2010**, *4*, 592-638.
70. Ono, M.; Ito, Y.; Masuoka, C.; Koga, H.; Nohara, T., Antioxidative Constituents from *Dendrobium* Herba (Stems of *Dendrobium* spp.). *Food Sci Technol Int* **1995**, *1* (2), 115-120.
71. Zhang, C. F.; Wang, M.; Wang, L.; Linuma, M.; Zhang, M.; Xu, L. S.; Wang, Z. T., ChemInform Abstract: Chemical Constituents of *Dendrobium gratiosissimum* and Their Cytotoxic Activities. *Indian J. Chem.* **2008**, *39*, 952-956.
72. Li, Y.; Wang, C.-L.; Wang, Y.-J.; Guo, S.-X.; Yang, J.-S.; Chen, X.-M.; Xiao, P.-G., Three New Bibenzyl Derivatives from *Dendrobium candidum*. *Chem. Pharm. Bull.* **2009**, *57* (2), 218-219.
73. Sritularak, B.; Anuwat, M.; Likhitwitayawuid, K., A new phenanthrenequinone from *Dendrobium draconis*. *J. Asian Nat. Prod. Res.* **2011**, *13*, 251-255.

74. Fan, C.; Wang, W.; Wang, Y.; Qin, G.; Zhao, W., Chemical constituents from *Dendrobium densiflorum*. *Phytochemistry* **2001**, *57* (8), 1255-1258.
75. Chen, C.-C.; Wu, L.-G.; Ko, F.-N.; Teng, C.-M., Antiplatelet Aggregation Principles of *Dendrobium loddigesii*. *J. Nat. Prod.* **1994**, *57* (9), 1271-1274.
76. Hwang, J. S.; Lee, S. A.; Hong, S. S.; Han, X. H.; Lee, C.; Kang, S. J.; Lee, D.; Kim, Y.; Hong, J. T.; Lee, M. K.; Hwang, B. Y., Phenanthrenes from *Dendrobium nobile* and their inhibition of the LPS-induced production of nitric oxide in macrophage RAW 264.7 cells. *Bioorganic Med. Chem. Lett.* **2010**, *20* (12), 3785-3787.
77. Zhang, X.; Xu, J.-K.; Wang, J.; Wang, N.-L.; Kurihara, H.; Kitanaka, S.; Yao, X.-S., Bioactive Bibenzyl Derivatives and Fluorenones from *Dendrobium nobile*. *J. Nat. Prod.* **2007**, *70* (1), 24-28.
78. Ye, Q.; Qin, G.; Zhao, W., Immunomodulatory sesquiterpene glycosides from *Dendrobium nobile*. *Phytochemistry* **2003**, *61*, 885-90.
79. Zhao, W.; Ye, Q.; Tan, X.; Jiang, H.; Li, X.; Chen, K.; Kinghorn, A. D., Three New Sesquiterpene Glycosides from *Dendrobium nobile* with Immunomodulatory Activity. *J. Nat. Prod.* **2001**, *64* (9), 1196-1200.
80. Lu, Y.; Kuang, M.; Hu, G.-P.; Wu, R.-B.; Wang, J.; Liu, L.; Lin, Y.-C., Loddigesiinols G–J: α -Glucosidase Inhibitors from *Dendrobium loddigesii*. *Molecules* **2014**, *19*, 8544-8555.
81. Mittraphab, A.; Muangnoi, C.; Likhitwitayawuid, K.; Rojsitthisak, P.; Sritularak, B., A New Bibenzyl-phenanthrene Derivative from *Dendrobium signatum* and its Cytotoxic Activity. *Nat. Prod. Commun.* **2016**, *11* (5), 1934578X1601100526.
82. Chimsook, T., Phytochemical Screening, Total Phenolic Content, Antioxidant Activities and Cytotoxicity of *Dendrobium signatum* Leaves. *MATEC Web Conf.* **2016**, *62*.
83. Lu, Y.; Shipton, F.; Khoo, T.-J.; Wiart, C., Antioxidant Activity Determination of Citronellal and Crude Extracts of *Cymbopogon citratus* by 3 Different Methods. *Pharmacol Pharm* **2014**, *05*, 395-400.
84. Erel, O., A novel automated direct measurement method for total antioxidant capacity using a new generation, more stable ABTS radical cation. *Clin. Biochem.* **2004**, *37* (4), 277-285.
85. Sarigaputi, C.; Sommit, D.; Teerawatananond, T.; Pudhom, K., Weakly Anti-inflammatory Limonoids from the Seeds of *Xylocarpus rumphii*. *J. Nat. Prod.* **2014**, *77* (9), 2037-2043.
86. Khan, S.; Shin, E.; Choi, R.; Jung, Y.; Kim, J.; Tosun, A.; Kim, Y., Suppression of LPS-induced inflammatory and NF- κ B responses by anomalin in RAW 264.7 macrophages. *J. Cell. Biochem.* **2011**, *112*, 2179-88.
87. Okoh, S. O.; Asekun, O. T.; Familoni, O. B.; Afolayan, A. J., Antioxidant and Free Radical Scavenging Capacity of Seed and Shell Essential Oils Extracted from *Abrus precatorius* (L). *Antioxidants (Basel)* **2014**, *3* (2), 278-287.
88. Fau, G. I.; Leander, K.; Fau, L. K.; Lüning, B.; Lüning, B., Studies on orchidaceae alkaloids. XVI. A new alkaloid, 2-hydroxydendrobine, from *Dendrobium findlayanum* par. et Rchb. f. *Acta Chem. Scand.* **1970**, *24*, 1209-1212.
89. Okamoto, T.; Natsume, M.; Onaka, T.; Uchimarui, F.; Shimizu, M., The Structure of Dendroxine The Third Alkaloid from *Dendrobium nobile*. *Chem. Pharm. Bull.* **1966**, *14* (6), 672-675.
90. Zhao, W. M.; Ye, Q. H.; Dai, J. Q.; Martin, M. T.; Zhu, J. P., allo-aromadendrane- and picrotoxane-type sesquiterpenes from *Dendrobium moniliforme*. *Planta Med.* **2003**, *69* (12), 1136-1140.

91. Wang, P.; Chen, X.; Wang, H.; Huang, S. Z.; Cai, C. H.; Yuan, J. Z.; Zhu, G. L.; Xu, X. L.; Mei, W. L.; Dai, H. F., Four New Picrotoxane-Type Sesquiterpenes From *Dendrobium nobile* Lindl. *Front. Chem.* **2019**, *7*.
92. Punya, J.; Tachaleat, A.; Wattanachaisaereekul, S.; Haritakun, R.; Boonlarpradab, C.; Cheevadhanarak, S., Functional expression of a foreign gene in *Aspergillus oryzae* producing new pyrone compounds. *Fungal Genet. Biol.* **2013**, *50* (1), 55-62.
93. Snatzke, G., Circular Dichroism and Optical Rotatory Dispersion — Principles and Application to the Investigation of the Stereochemistry of Natural Products. *Angew. Chem. Int. Ed.* **1968**, *7* (1), 14-25.
94. Elvidge, J. A.; Ralph, P. D., Polyene acids. Part X. The conformation of hexenolactone and the configuration of the derived sorbic acid as indicated by proton magnetic resonance spectroscopy. *J. Chem. Soc. B* **1966**, (0), 243-244.
95. Mori, K., Absolute Configuration of (-)-Massoilactone as Confirmed by a Synthesis of Its (S)-(+)-Isomer. *Agric. Biol. Chem.* **1976**, *40* (8), 1617-1619.
96. Ma; Zhang, H. J.; Tan, G. T.; Hung, N. V.; Cuong, N. M.; Soejarto, D. D.; Fong, H. H. S., Antimalarial Compounds from *Grewia bilamellata*. *J. Nat. Prod.* **2006**, *69* (3), 346-350.
97. Kim, T. H.; Ito, H.; Hayashi, K.; Hasegawa, T.; Machiguchi, T.; Yoshida, T., Aromatic Constituents from the Heartwood of *Santalum album* L. *Chem. Pharm. Bull.* **2005**, *53* (6), 641-644.
98. Li, Y.; Wang, C. L.; Guo, S. X.; Yang, J. S.; Xiao, P. G., Two new compounds from *Dendrobium candidum*. *Chem Pharm Bull.* **2008**, *56* (10), 1477-1479.
99. Li, Y.; Wang, C. L.; Wang, Y. J.; Wang, F. F.; Guo, S. X.; Yang, J. S.; Xiao, P. G., Four new bibenzyl derivatives from *Dendrobium candidum*. *Chem. Pharm. Bull.* **2009**, *57* (9), 997-999.
100. Yang, D.; Cheng, Z. Q.; Yang, L.; Hou, B.; Yang, J.; Li, X. N.; Zi, C. T.; Dong, F. W.; Liu, Z. H.; Zhou, J.; Ding, Z. T.; Hu, J. M., Seco-Dendrobine-Type Alkaloids and Bioactive Phenolics from *Dendrobium findlayanum*. *J. Nat. Prod.* **2018**, *81* (2), 227-235.
101. Kaewamatawong, R.; Ruangrunsi, N.; Likhitwitayawuid, K., Chemical constituents of *Polyalthia parviflora* stem. *J. Nat. Med* **2007**, *61* (3), 349-350.
102. Sritularak, B.; Likhitwitayawuid, K., New Bisbibenzyls from *Dendrobium falconeri*. *Helv. Chim. Acta* **2009**, *92*, 740-744.
103. Bi, Z.; Wang, Z.; Xu, L., Chemical constituents of *Dendrobium moniliforme*. *Acta Bot. Sin.* **2004**, *46* (1), 124-126.
104. Chen, X.; Wang, F.; Wang, Y.; Li, X.; Wang, A.; Wang, C.; Guo, S., Discrimination of the rare medicinal plant *Dendrobium officinale* based on naringenin, bibenzyl, and polysaccharides. *Sci. China Life Sci.* **2012**, *55* (12), 1092-1099.
105. Reyes-Ramirez, A.; Leyte-Lugo, M.; Figueroa, M.; Serrano-Alba, T.; Gonzalez-Andrade, M.; Mata, R., Synthesis, biological evaluation, and docking studies of gigantol analogs as calmodulin inhibitors. *Eur. J. Med. Chem.* **2011**, *46* (7), 2699-2708.
106. Zhang, C.; Liu, S.-J.; Yang, L.; Yuan, M.-Y.; Li, J.-Y.; Hou, B.; Li, H.-M.; Yang, X.-Z.; Ding, C.-C.; Hu, J.-M., Sesquiterpene amino ether and cytotoxic phenols from *Dendrobium wardianum* Warner. *Fitoterapia* **2017**, *122*, 76-79.
107. Meng, Z. X.; Dong, H. L.; Wang, C. L.; Guo, S.-X., Chemical constituents of *Dendrobium devonianum*. *Chin. Pharm. J.* **2013**, *48*, 855-859.
108. Tanagornmeatar, K.; Chaotham, C.; Sritularak, B.; Likhitwitayawuid, K.; Chanvorachote, P., Cytotoxic and Anti-metastatic Activities of Phenolic Compounds from *Dendrobium ellipsophyllum*. *Anticancer Res.* **2014**, *34* (11), 6573.

109. Liu, G.-Y.; Tan, L.; Cheng, L.; Ding, L.-S.; Zhou, Y.; Deng, Y.; He, Y.-Q.; Guo, D.-L.; Xiao, S.-J., Dendrobine-type alkaloids and bibenzyl derivatives from *Dendrobium findlayanum*. *Fitoterapia* **2020**, *142*, 104497.
110. Ren, G.; Deng, W.-Z.; Xie, Y.-F.; Wu, C.-H.; Li, W.-Y.; Xiao, C.-Y.; Chen, Y.-L., Bibenzyl Derivatives From Leaves of *Dendrobium officinale*. *Nat. Prod. Commun.* **2020**, *15* (2), 1934578X2090867.
111. Yang, M.; Zhang, Y.; Chen, L.; Chen, Y., A new (propylphenyl)bibenzyl derivative from *Dendrobium williamsonii*. *Nat. Prod. Res* **2018**, *32* (14), 1699-1705.
112. Chu, C.; Li, T.; Pedersen, H. A.; Kongstad, K. T.; Yan, J.; Staerk, D., Antidiabetic constituents of *Dendrobium officinale* as determined by high-resolution profiling of radical scavenging and α -glucosidase and α -amylase inhibition combined with HPLC-PDA-HRMS-SPE-NMR analysis. *Phytochem. Lett* **2019**, *31*, 47-52.
113. Zhang, X.; Hung, T. M.; Phuong, P. T.; Ngoc, T. M.; Min, B.-S.; Song, K.-S.; Seong, Y. H.; Bae, K., Anti-inflammatory activity of flavonoids from *Populus davidiana*. *Arch. Pharm. Res.* **2006**, *29* (12), 1102-1108.
114. Wang, X.-g.; Wei, X.-y.; Tian, Y.-q.; Shen, L.-t.; Xu, H.-h., Antifungal Flavonoids from *Ficus sarmentosa* var. *henryi* (King) Corner. *AGR SCI CHINA* **2010**, *9* (5), 690-694.
115. Carvalho, M.; da, C.; Abreu, H., Flavanones from *Vernonia diffusa*. *J BRAZIL CHEM SOC* **1999**, *10*.
116. Miyashita, T.; Adhikari-Devkota, A.; Hori, K.; Watanabe, M.; Watanabe, T.; Devkota, H. P., Flavonoids from the Flowers of Citrus 'Hebesu'. *Nat. Prod. Commun.* **2018**, *13* (7), 1934578X1801300714.
117. Li, N.; Wu, J.-l.; Hasegawa, T.; Sakai, J.-i.; Bai, L.-m.; Wang, L.-y.; Kakuta, S.; Furuya, Y.; Ogura, H.; Kataoka, T.; Tomida, A.; Tsuruo, T.; Ando, M., Bioactive Lignans from *Peperomia duclouxii*. *J. Nat. Prod.* **2007**, *70* (4), 544-548.
118. Chen, C.-Y.; Wu, T.-Y.; Chang, F.-R.; Wu, Y.-C., Lignans and Kauranes from the Stems of *Annona cherimola*. *J Chin Chem Soc* **1998**, *45* (5), 629-634.
119. Lee, C.-K.; Chang, M. H., The Chemical Constituents from the Heartwood of *Eucalyptus Citriodora*. *J Chin Chem Soc* **2000**, *47*.
120. Kuo, P.-C.; Lin, M.-C.; Chen, G.-F.; Yiu, T.-J.; Tzen, J. T. C., Identification of Methanol-Soluble Compounds in Sesame and Evaluation of Antioxidant Potential of Its Lignans. *J. Agric. Food Chem.* **2011**, *59* (7), 3214-3219.
121. Kamikado, T.; Chang, C.-F.; Murakoshi, S.; Sakurai, A.; Tamura, S., Isolation and Structure Elucidation of Growth Inhibitors on Silkworm Larvae from *Magnolia kobus* DC. *Agric. Biol. Chem.* **1975**, *39* (4), 833-836.
122. Zálezák, F.; Bon, D. J.-Y. D.; Pospíšil, J., Lignans and Neolignans: Plant secondary metabolites as a reservoir of biologically active substances. *Pharmacol. Res.* **2019**, *146*, 104284.
123. Hua, X. G.; Ah, K. J.; Hee, P. S.; Ryang, S. A.; Soo, C. T.; Wook, C. H.; Ryun, C. S.; Ho, L. S., Isolation of melanin biosynthesis inhibitory compounds from the flowers of *Magnolia denudata*. *Saengyak Hakhoe Chi* **2004**, *35*, 152-156.
124. Xu, W.-H.; Zhao, P.; Wang, M.; Liang, Q., Naturally occurring furofuran lignans: structural diversity and biological activities. *Nat. Prod. Res.* **2019**, *33* (9), 1357-1373.
125. Chang, S.; Kim, K. H.; Lee, I.; Choi, S.; Lee, K., Phytochemical Constituents of *Geranium eriostemon*. *Nat. Prod. Sci.* **2009**, *15*.
126. Duc Hung, N.; Le, D. A. T.; Bingtian, Z.; Ma, E.; Min, B.; Woo, M., Antioxidant Compounds Isolated from the Roots of *Phlomis umbrosa* Turcz. *Nat. Prod. Sci.* **2018**, *24*, 119.

127. Yang, H.; Xue, X.; Li, H.; Apandi, S. N.; Tay-Chan, S. C.; Ong, S. P.; Tian, E. F., The relative antioxidant activity and steric structure of green tea catechins – A kinetic approach. *Food Chem.* **2018**, *257*, 399-405.
128. Halliwell, B.; Gutteridge, J. M., Oxygen toxicity, oxygen radicals, transition metals and disease. *Biochem. J.* **1984**, *219* (1), 1-14.
129. Fridovich, S. E.; Porter, N. A., Oxidation of arachidonic acid in micelles by superoxide and hydrogen peroxide. *J. Biol. Chem* **1981**, *256* (1), 260-265.
130. Surh, Y.-J.; Chun, K.-S.; Cha, H.-H.; Han, S. S.; Keum, Y.-S.; Park, K.-K.; Lee, S. S., Molecular mechanisms underlying chemopreventive activities of anti-inflammatory phytochemicals: down-regulation of COX-2 and iNOS through suppression of NF-κB activation. *Mutat. Res.* **2001**, *480-481*, 243-268.
131. Jung, H.; Kwak, H. K.; Hwang, K. T., Antioxidant and antiinflammatory activities of cyanidin-3-glucoside and cyanidin-3-rutinoside in hydrogen peroxide and lipopolysaccharide-treated RAW264.7 cells. *Food Sci. Biotechnol.* **2014**, *23* (6), 2053-2062.
132. Gloire, G.; Legrand-Poels, S.; Piette, J., NF-κB activation by reactive oxygen species: Fifteen years later. *Biochem. Pharmacol.* **2006**, *72* (11), 1493-1505.



APPENDIX

Table S1. X-ray crystallographic data for compound 1

Compound	Compound 1
Crystal habit	Thin plate, colorless
Crystal size [mm ³]	0.06×0.40×0.48
Empirical formula	C ₁₇ H ₂₅ NO ₃
Formula weight	291.38
Crystal system	Orthorhombic
Space group	<i>P</i> 2 ₁ 2 ₁ 2 ₁ (No. 19)
<i>a</i> [Å]	9.2548(1)
<i>b</i> [Å]	10.1196(1)
<i>c</i> [Å]	16.1677(2)
α [°]	90
β [°]	90
γ [°]	90
<i>V</i> [Å ³]	1514.18(3)
<i>Z</i>	4
ρ_{calcd} [Mg m ⁻³]	1.278
μ [mm ⁻¹]	0.695
<i>F</i> (000)	632
<i>T</i> [K]	296(2)
Radiation [Å]	CuK α , 1.54178
θ_{max} [°]	68.28
Completeness to $\theta = 67.68$ [%]	99.6
Reflns collected / unique / $> 2\sigma(I)$	11868, 2755, 2508
<i>R</i> _{int}	0.0763
Data / parameters	2755 / 194
Goodness on fit	1.116
<i>R</i> ₁ , ^a <i>wR</i> ₂ ^b [<i>I</i> $> 2\sigma(I)$]	0.0969, 0.2092
<i>R</i> ₁ , <i>wR</i> ₂ [all data]	0.0997, 0.2135
$\Delta\rho$ [e Å ⁻³]	-0.64, 0.62
Absolute structure parameter	-0.01(16)
CCDC	2078877

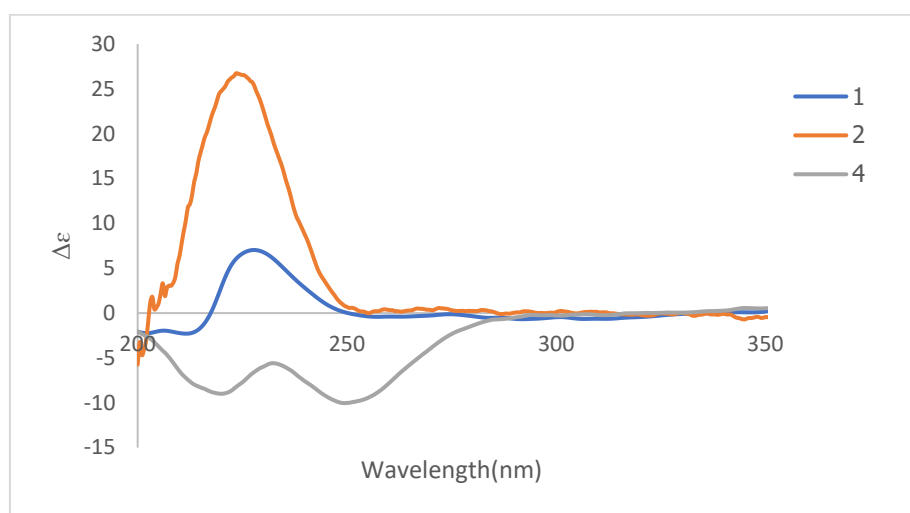
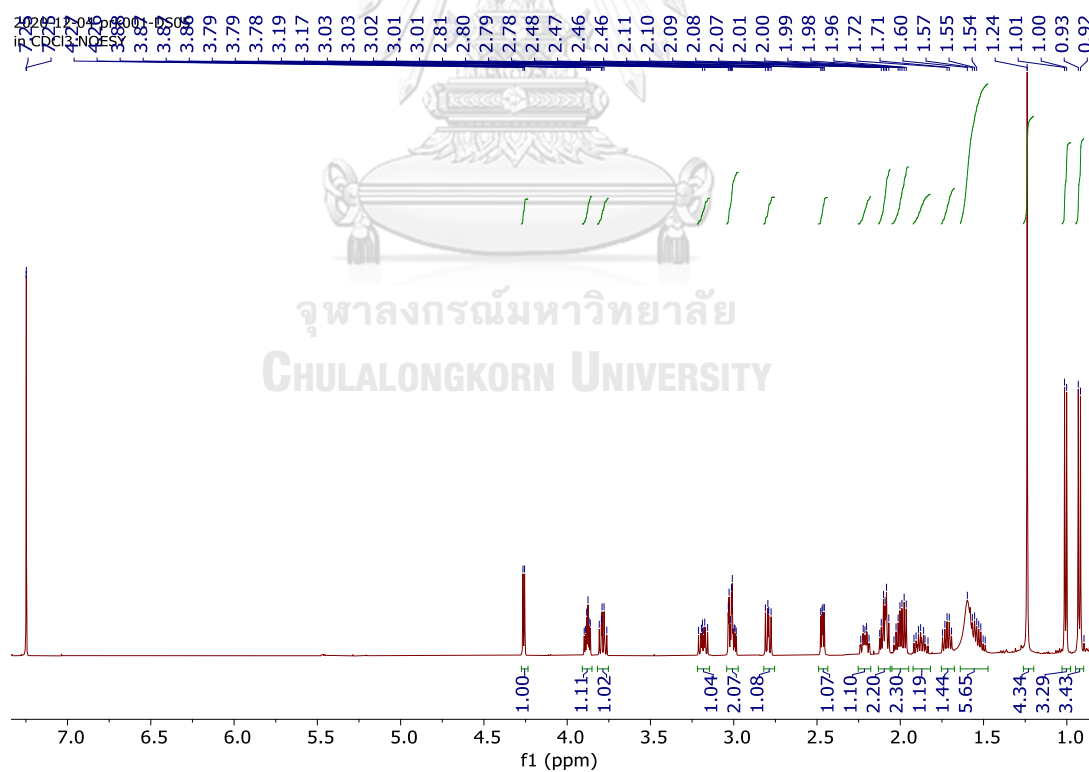
Figure S1. Analysis ECD spectra of **1**, **2** and **4**.**Figure S2.** ^1H NMR spectrum (500 MHz, CDCl_3) of compound **1**

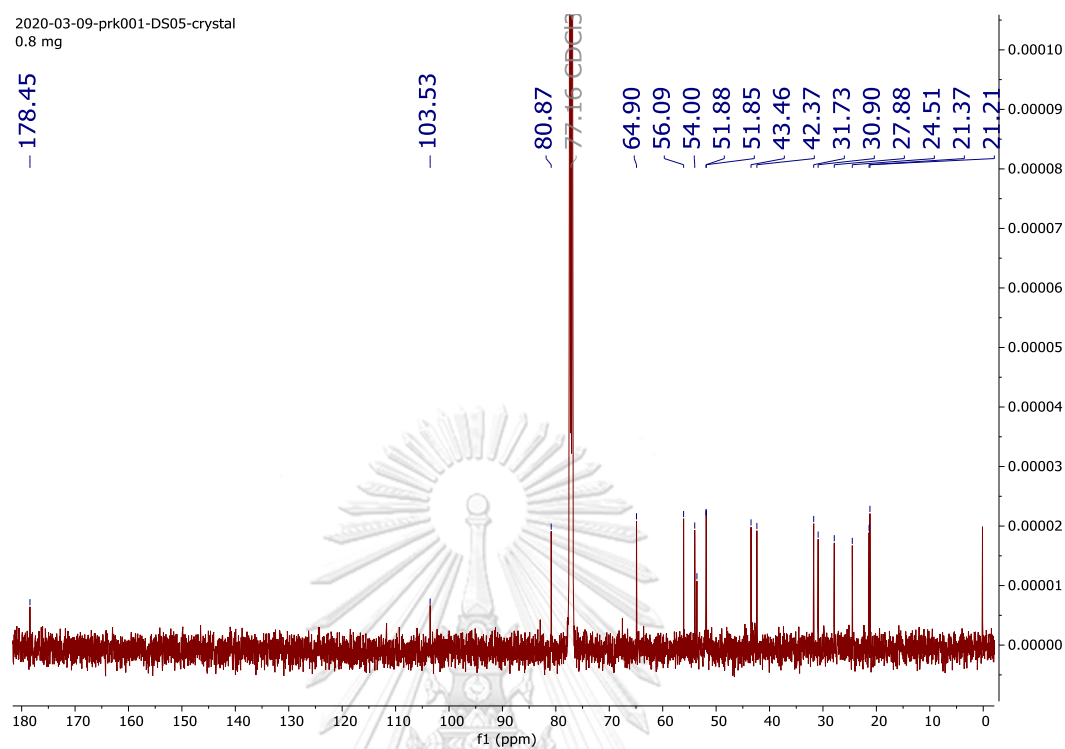
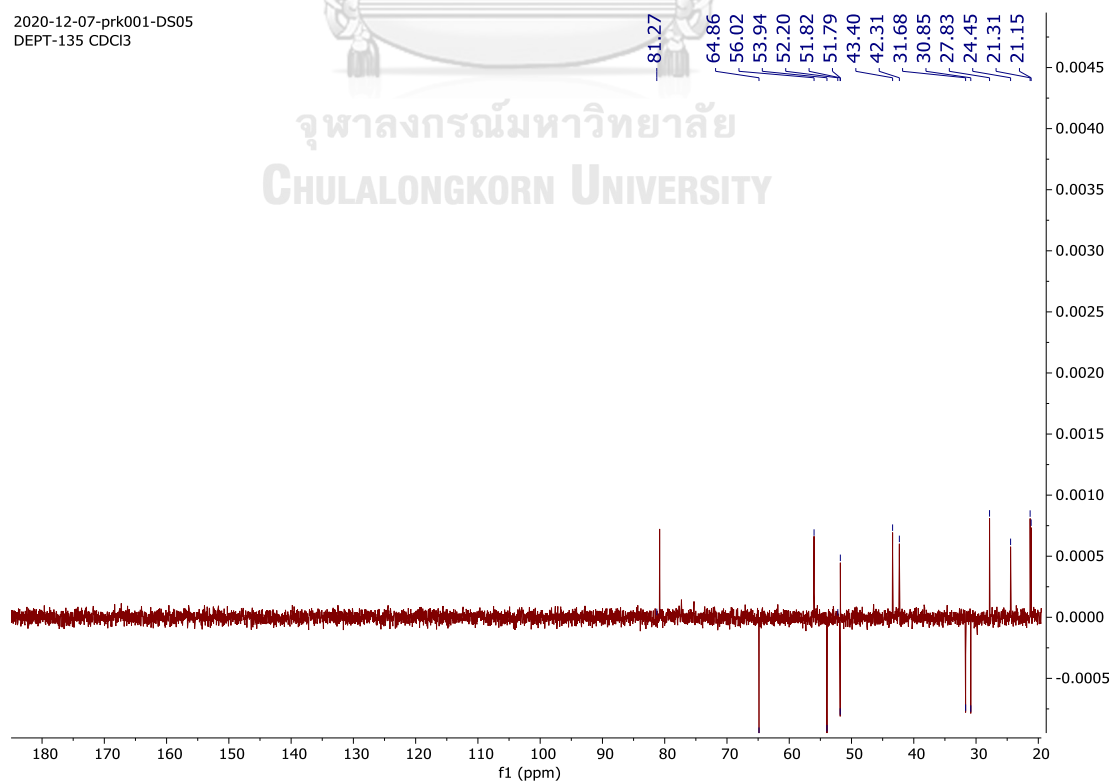
Figure S3. ^{13}C NMR spectrum (125 MHz, CDCl_3) of compound **1****Figure S4.** ^{13}C -DEPT-135 NMR spectrum (125 MHz, CDCl_3) of compound **1**

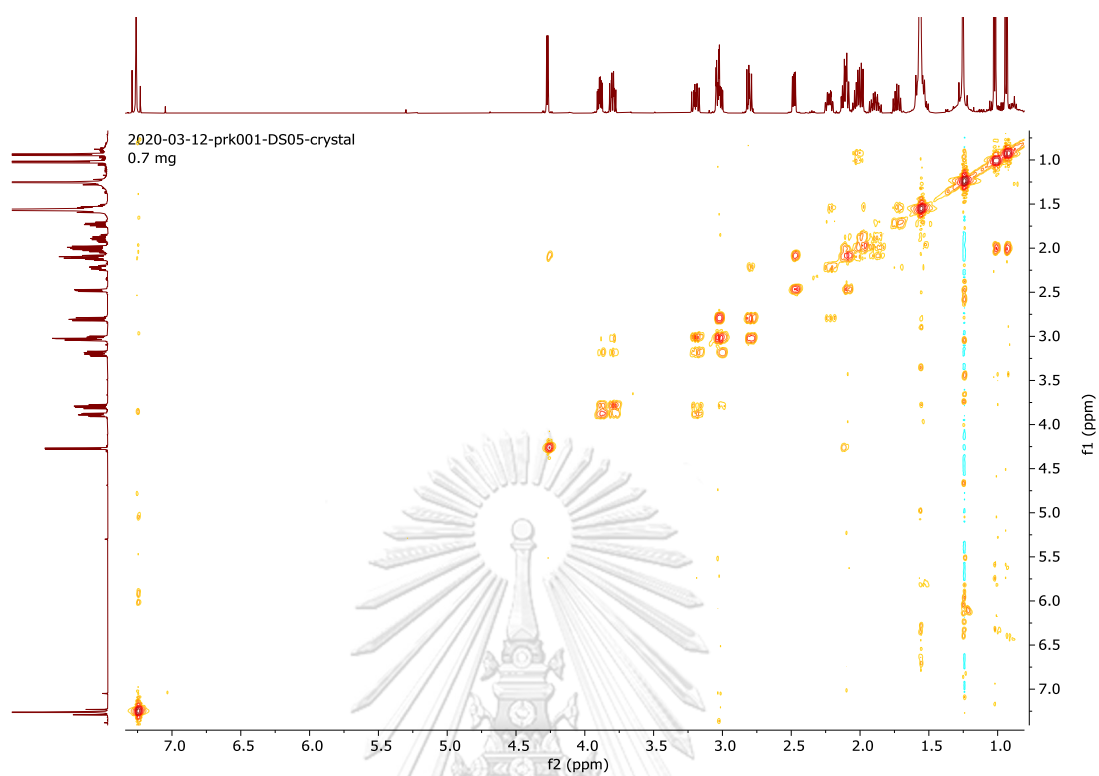
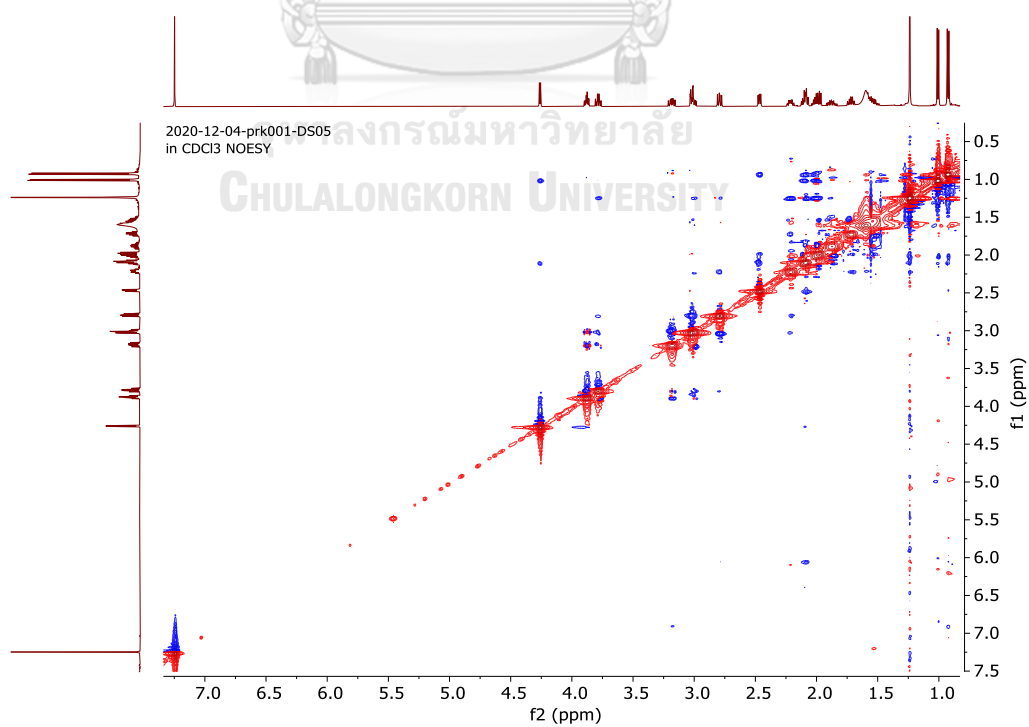
Figure S5. COSY spectrum of compound 1**Figure S6. NOESY spectrum of compound 1**

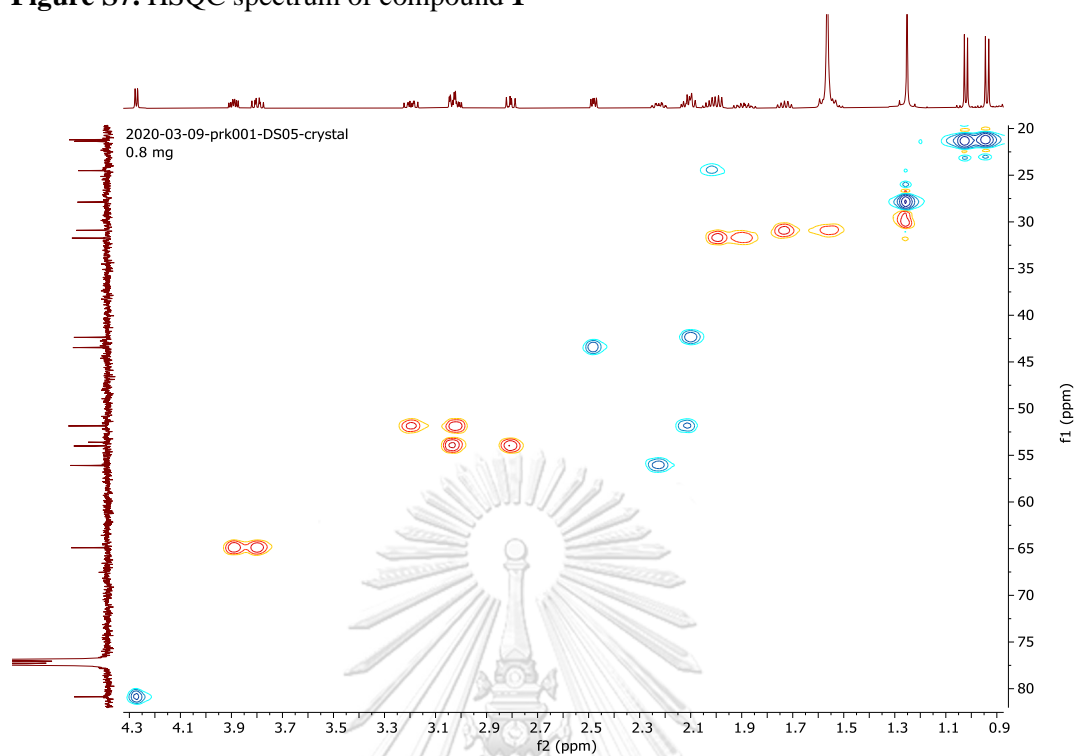
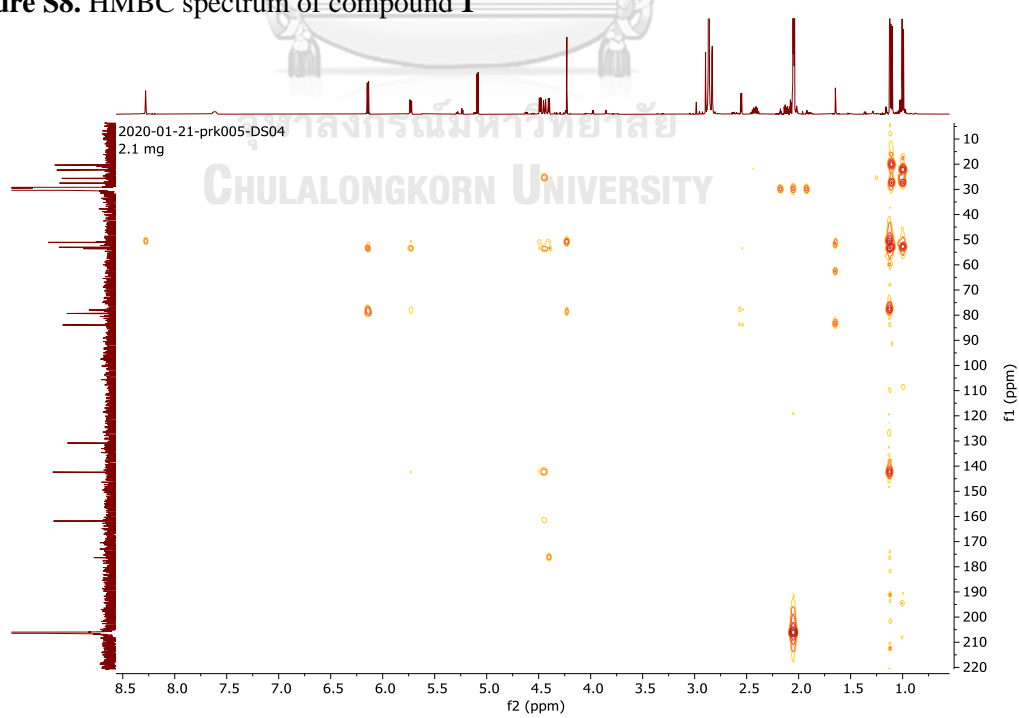
Figure S7. HSQC spectrum of compound 1**Figure S8. HMBC spectrum of compound 1**

Figure S9. HRTOFMS spectrum of compound 1

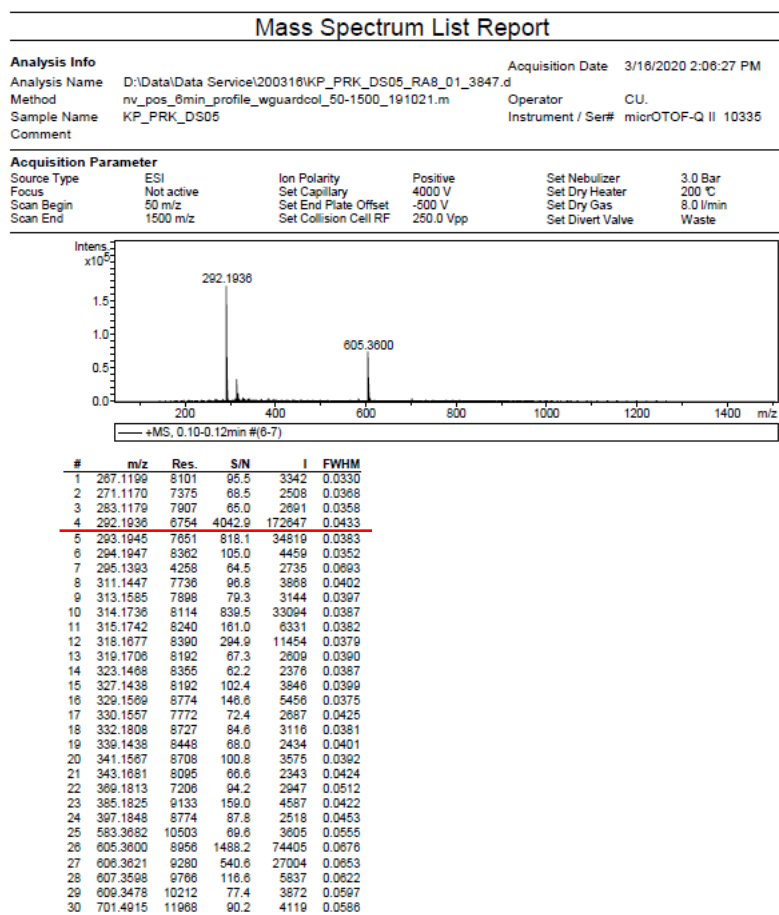


Table S2. X-ray crystallographic data for compound **2**

Compound	Compound 2
Crystal habit	Triangular, colorless
Crystal size [mm ³]	0.40×0.42×0.52
Empirical formula	C ₁₅ H ₂₁ NO ₅
Formula weight	295.33
Crystal system	Tetragonal
Space group	<i>P</i> 4 ₃ 2 ₁ 2 (No. 96)
<i>a</i> [Å]	9.7813(2)
<i>b</i> [Å]	9.7813(2)
<i>c</i> [Å]	30.8333(8)
α [°]	90
β [°]	90
γ [°]	90
<i>V</i> [Å ³]	2949.94(14)
<i>Z</i>	8
ρ_{calcd} [Mg m ⁻³]	1.330
μ [mm ⁻¹]	0.829
<i>F</i> (000)	1264
<i>T</i> [K]	296(2)
Radiation [Å]	CuK α , 1.54178
θ_{max} [°]	68.29
Completeness to $\theta = 67.68$ [%]	99.6
Reflns collected / unique / $> 2\sigma(I)$	15848, 2685, 2553
<i>R</i> _{int}	0.0319
Data / parameters	2685 / 196
Goodness on fit	1.040
<i>R</i> ₁ , ^a <i>wR</i> ₂ ^b [<i>I</i> $> 2\sigma(I)$]	0.0292, 0.0728
<i>R</i> ₁ , <i>wR</i> ₂ [all data]	0.0309, 0.0737
$\Delta\rho$ [e Å ⁻³]	-0.10, 0.14
Absolute structure parameter	0.06(6)
CCDC	2078878

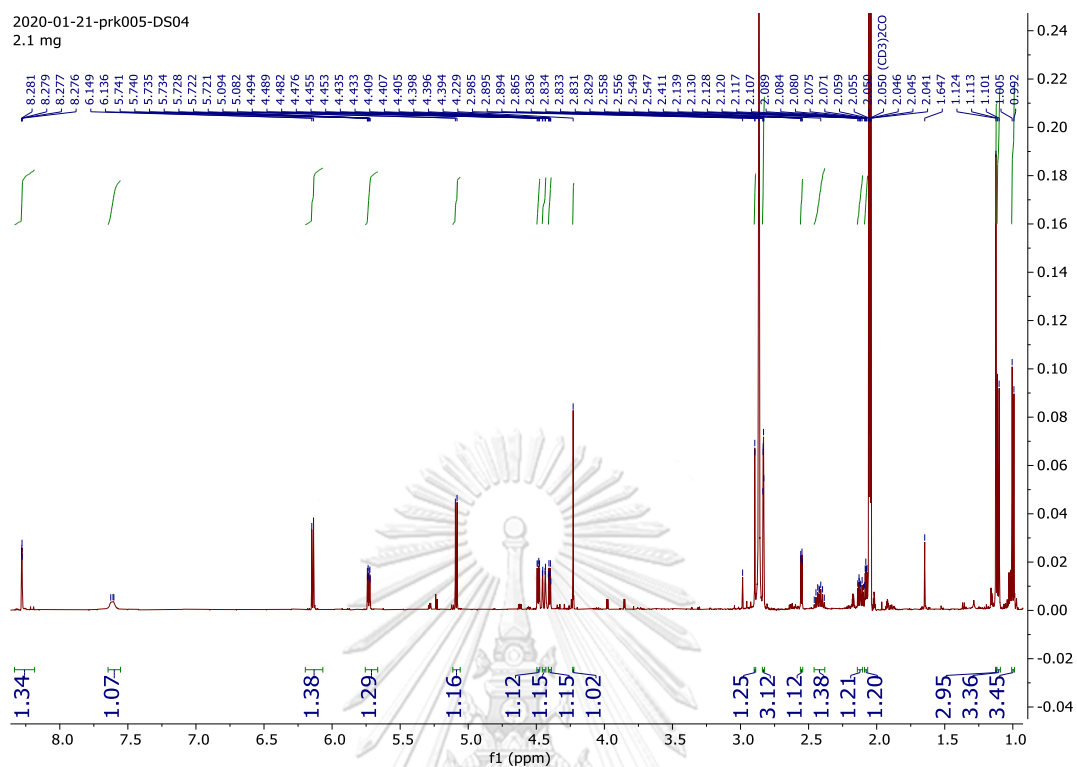
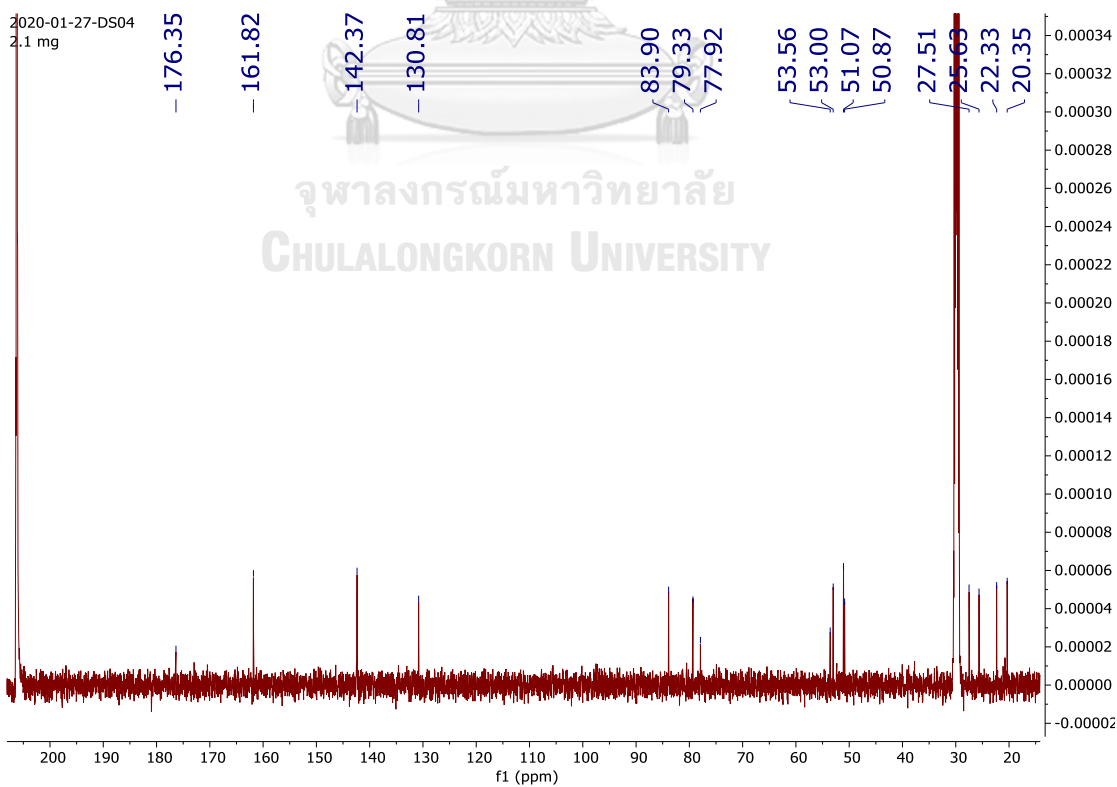
Figure S10. ^1H NMR spectrum (500 MHz, Acetone- d_6) of compound **2****Figure S11.** ^{13}C NMR spectrum (125 MHz, Acetone- d_6) of compound **2**

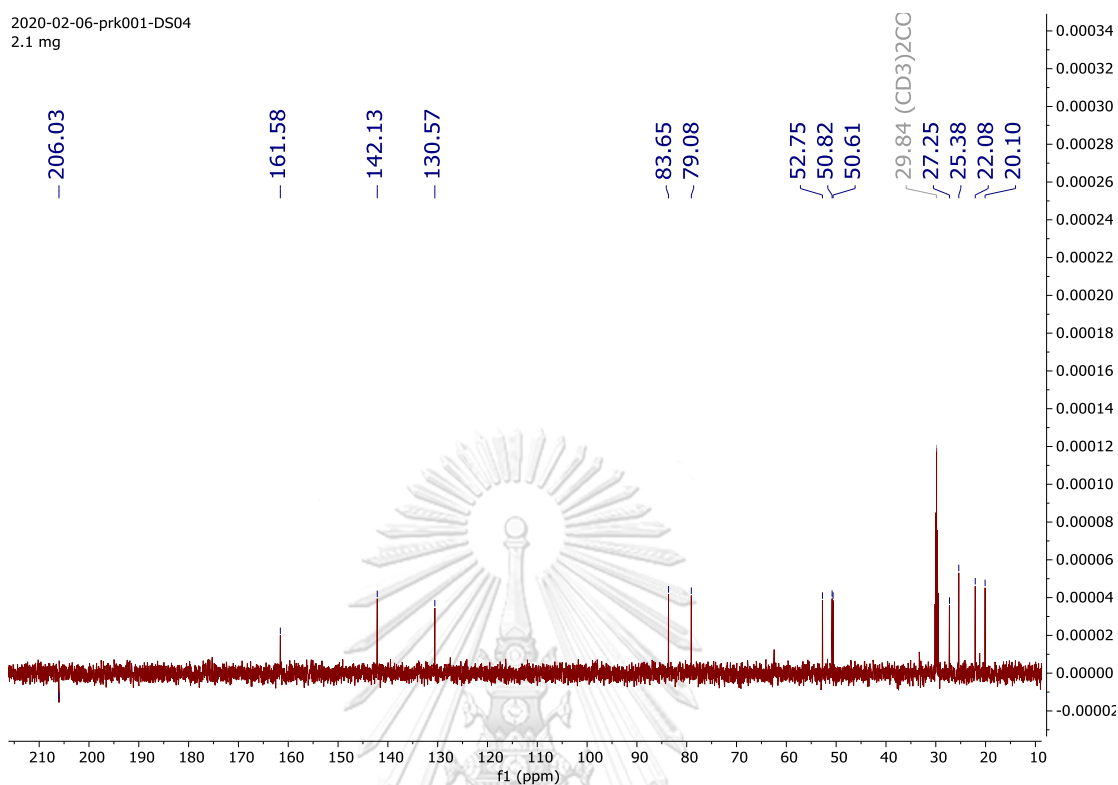
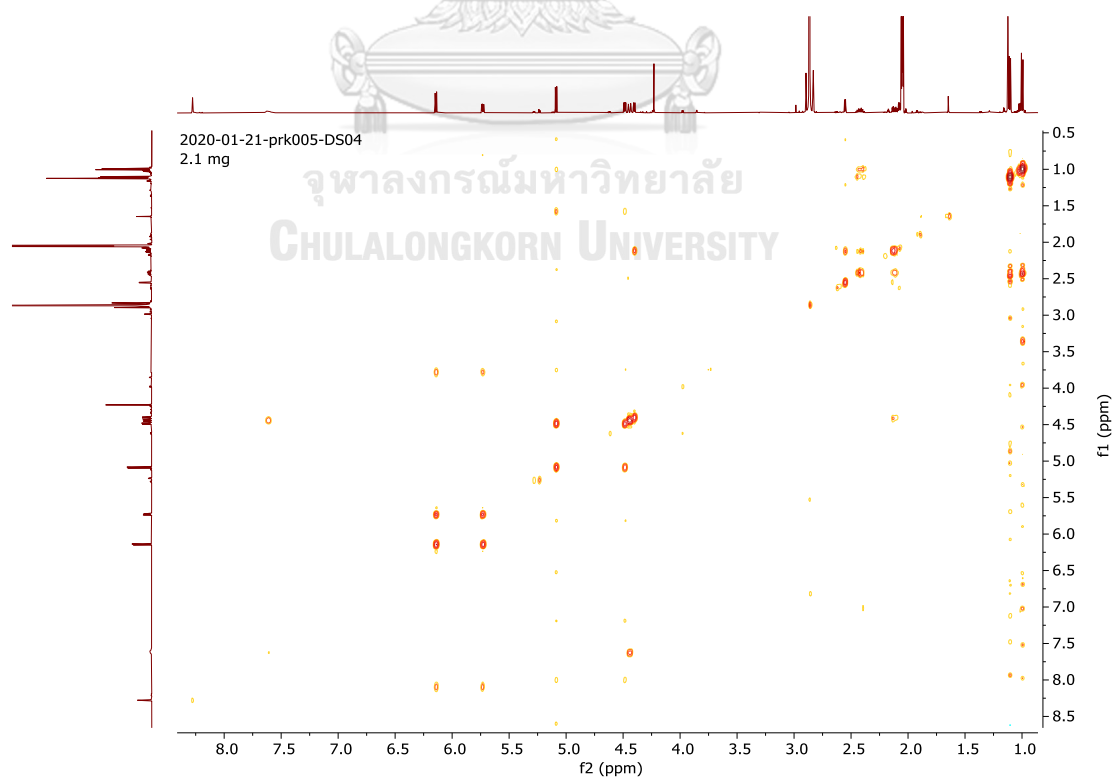
Figure S12. ^{13}C -DEPT-135 NMR spectrum (125 MHz, Acetone- d_6) of compound **2****Figure S13.** COSY spectrum of compound **2**

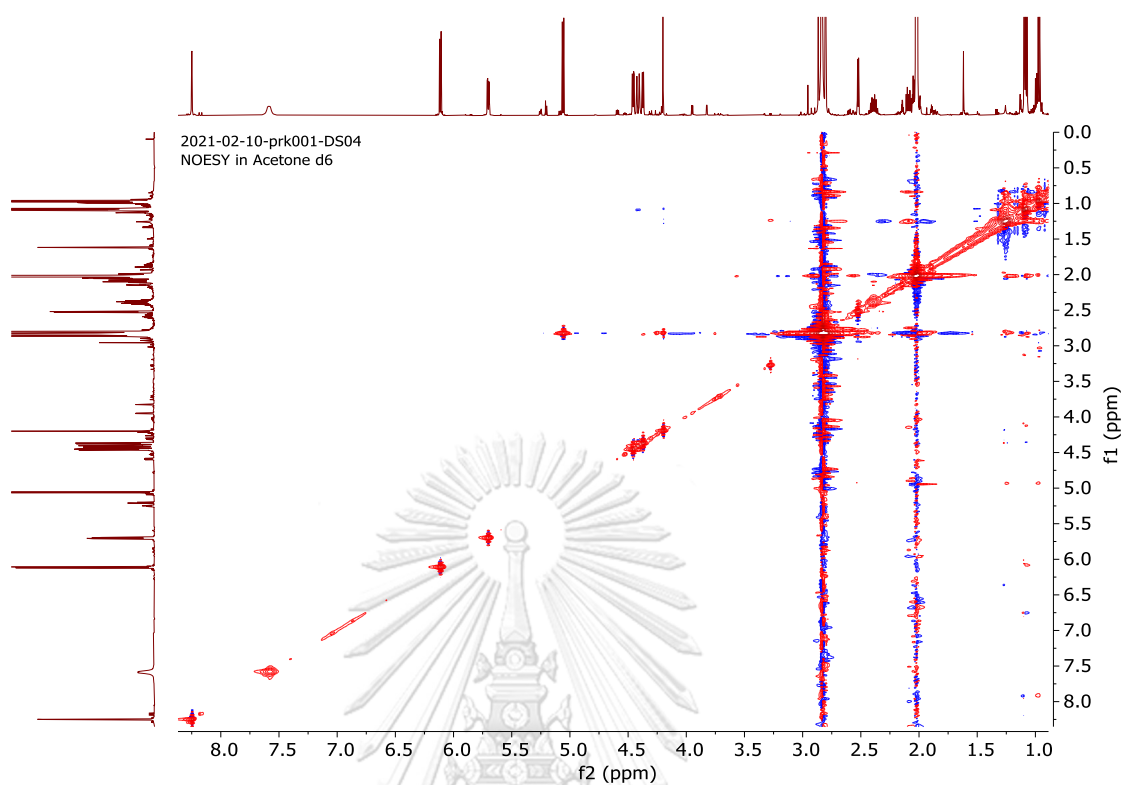
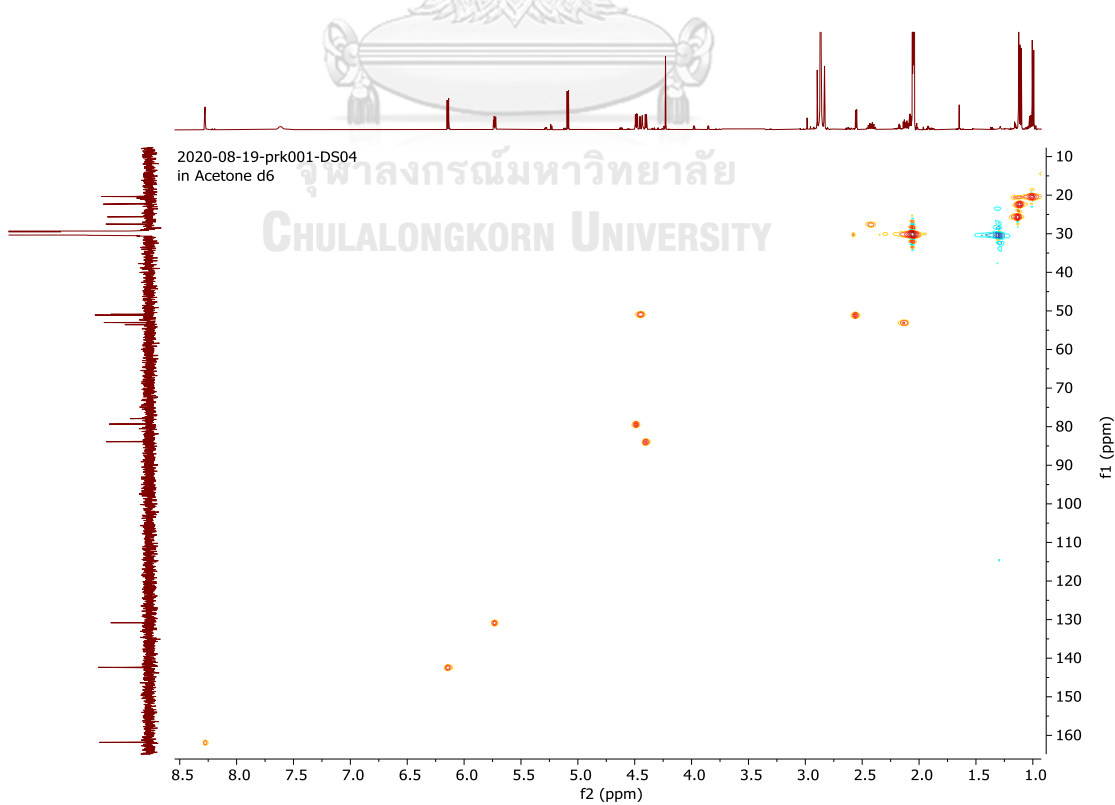
Figure S14. NOESY spectrum of compound **2****Figure S15.** HSQC spectrum of compound **2**

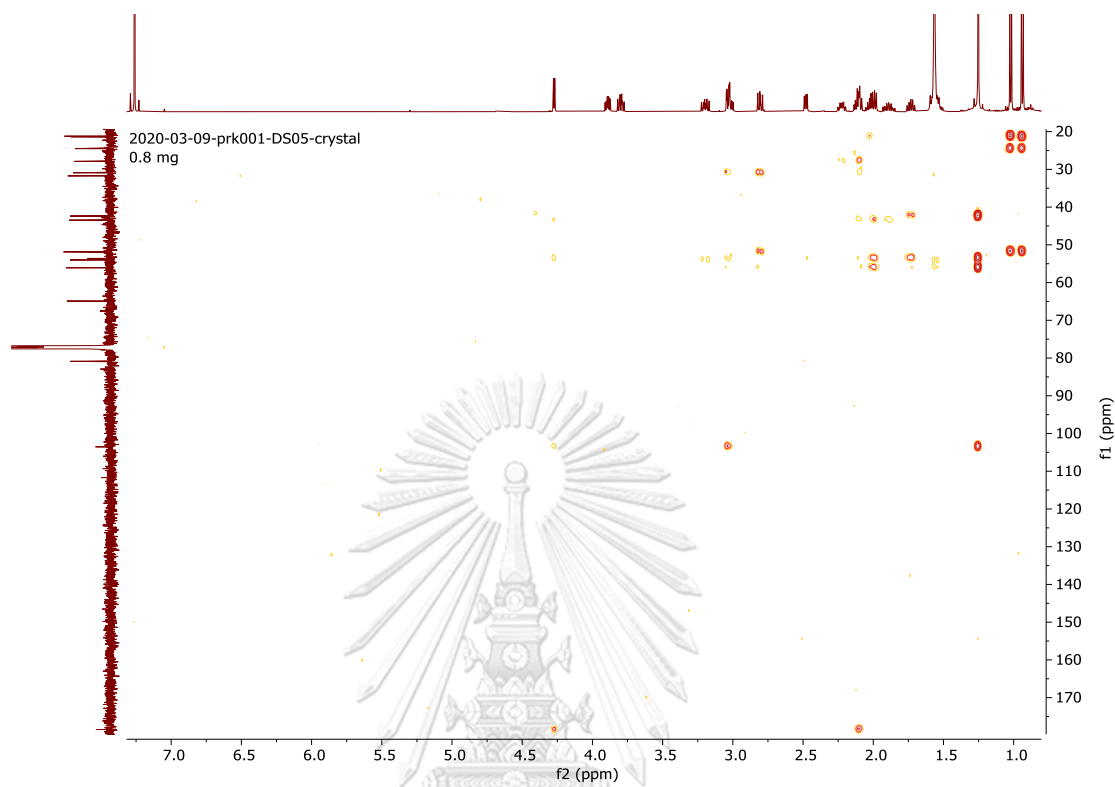
Figure S16. HMBC spectrum of compound **2**

Figure S17. HRTOFMS spectrum of compound 2

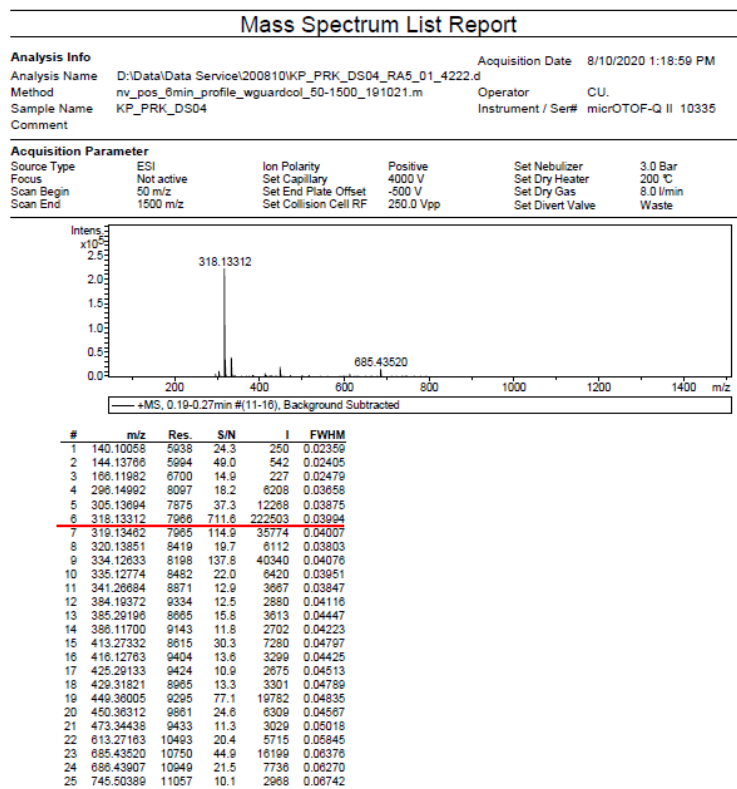


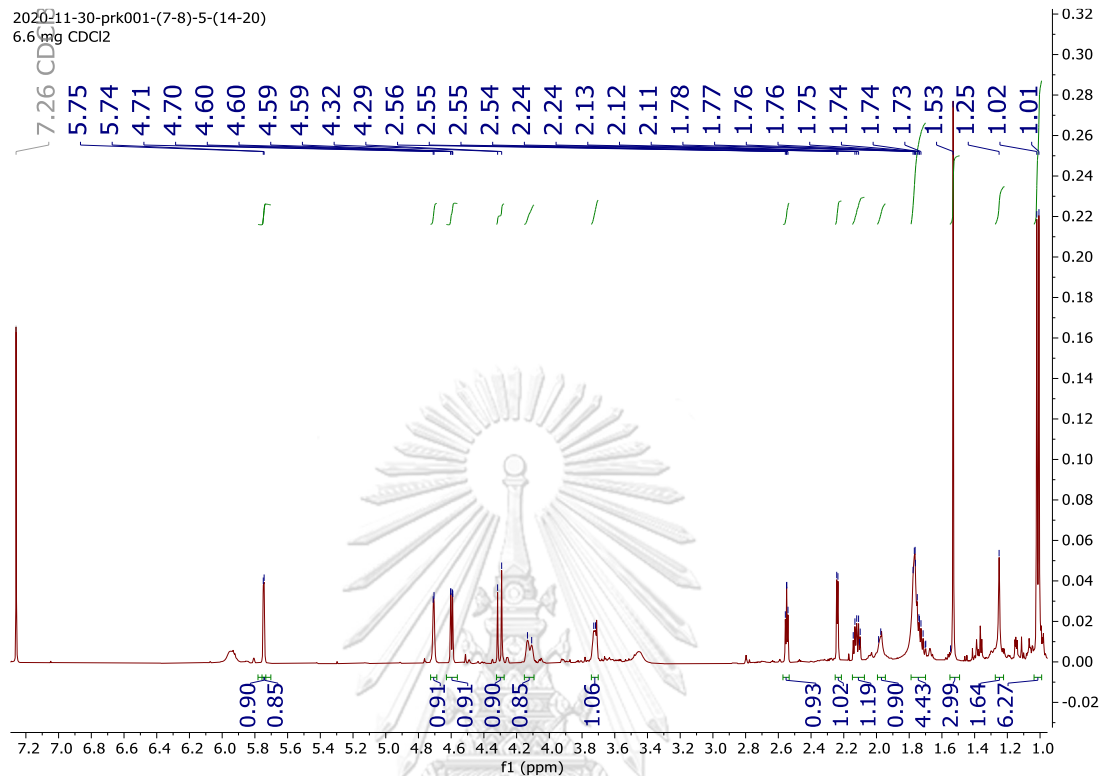
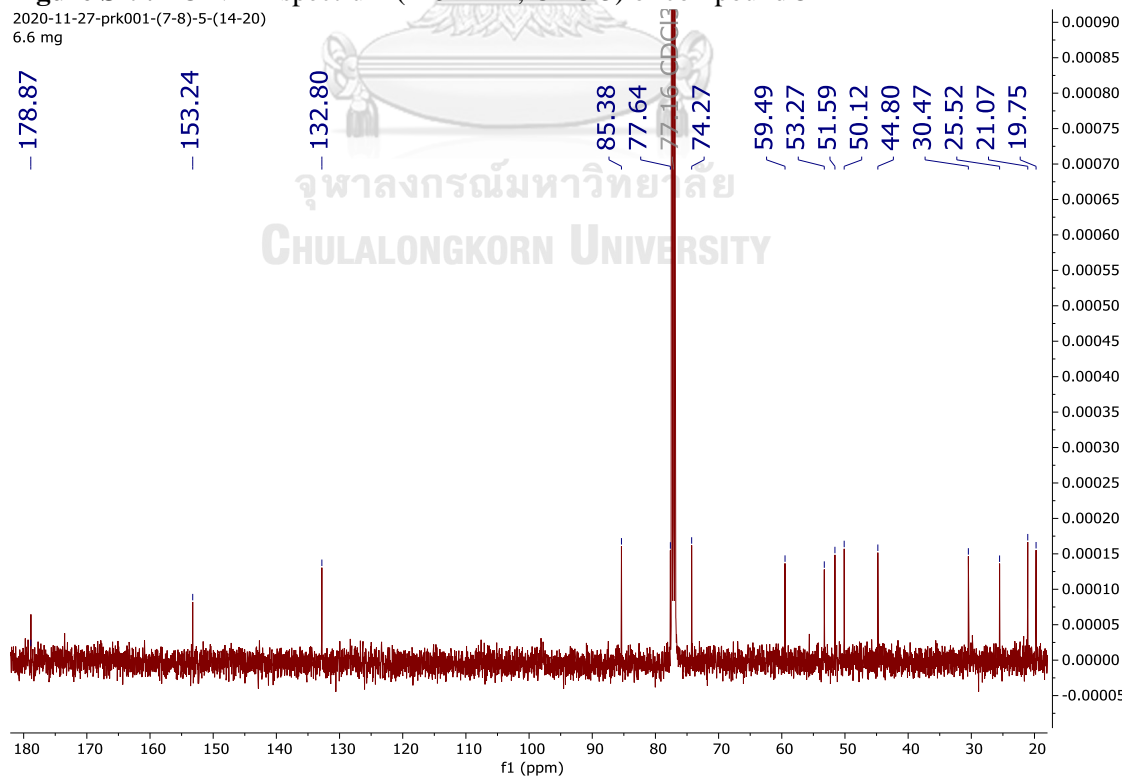
Figure S18. ^1H NMR spectrum (500 MHz, CDCl_3) of compound **3****Figure S19.** ^{13}C NMR spectrum (125 MHz, CDCl_3) of compound **3**

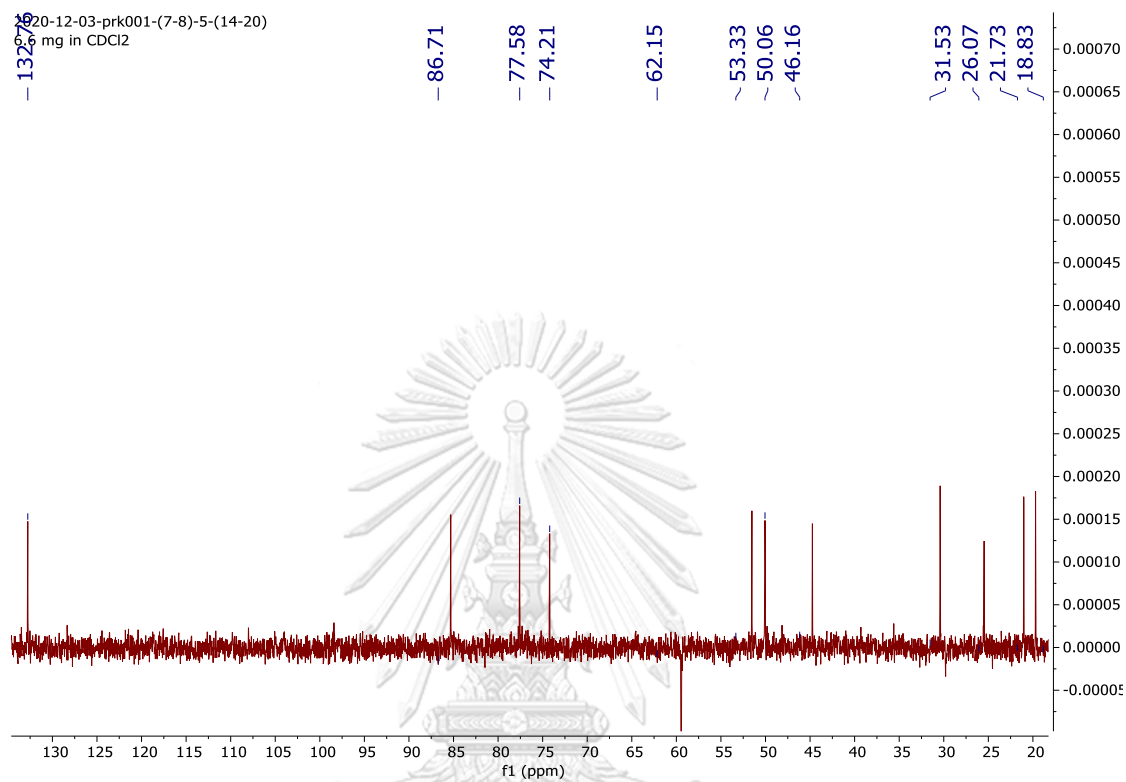
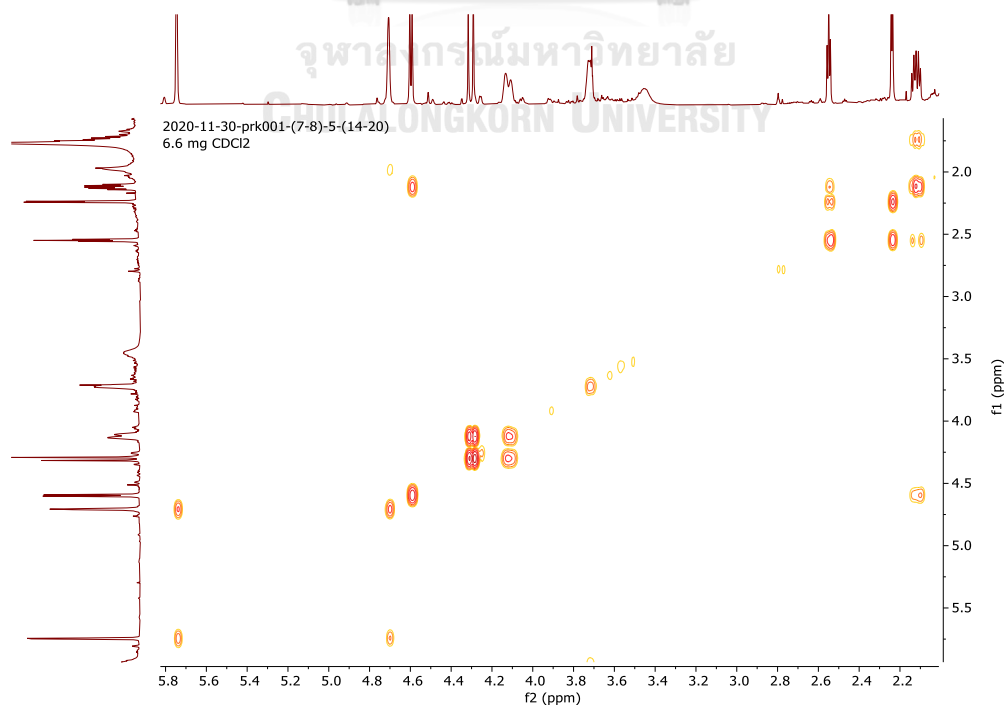
Figure S20. ^{13}C -DEPT-135 NMR spectrum (125 MHz, CDCl_3) of compound **3****Figure S21.** COSY spectrum of compound **3**

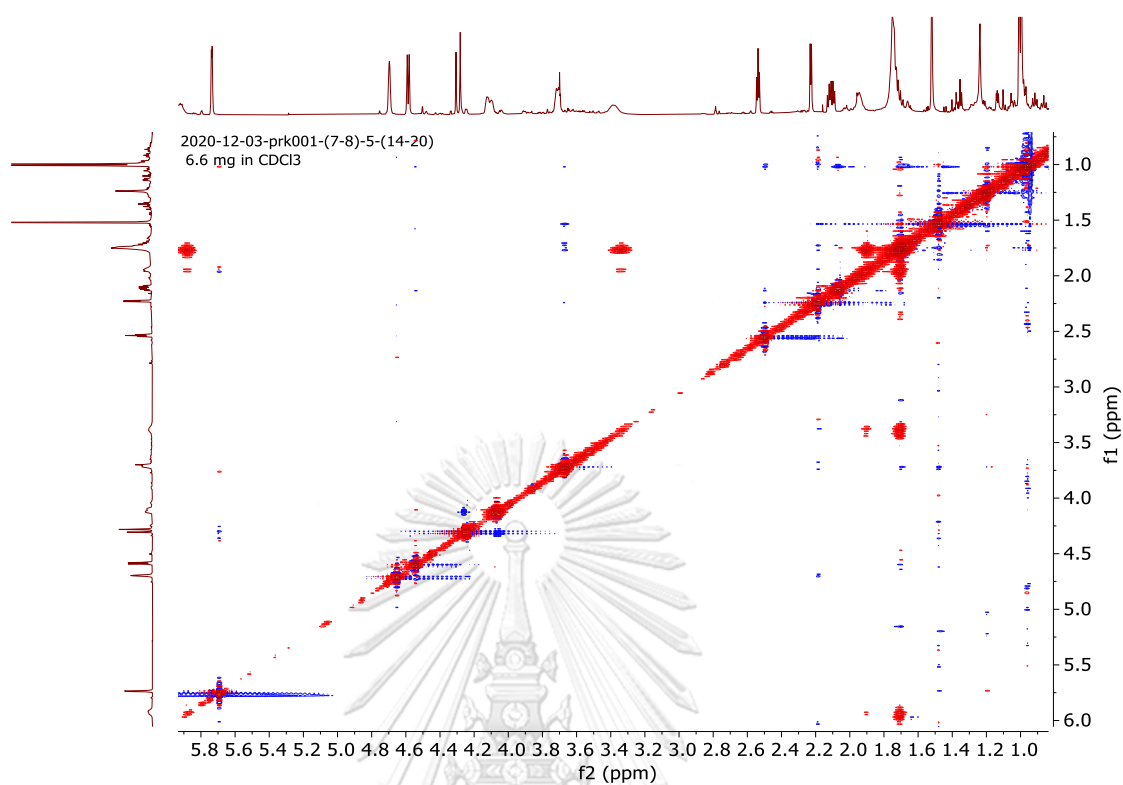
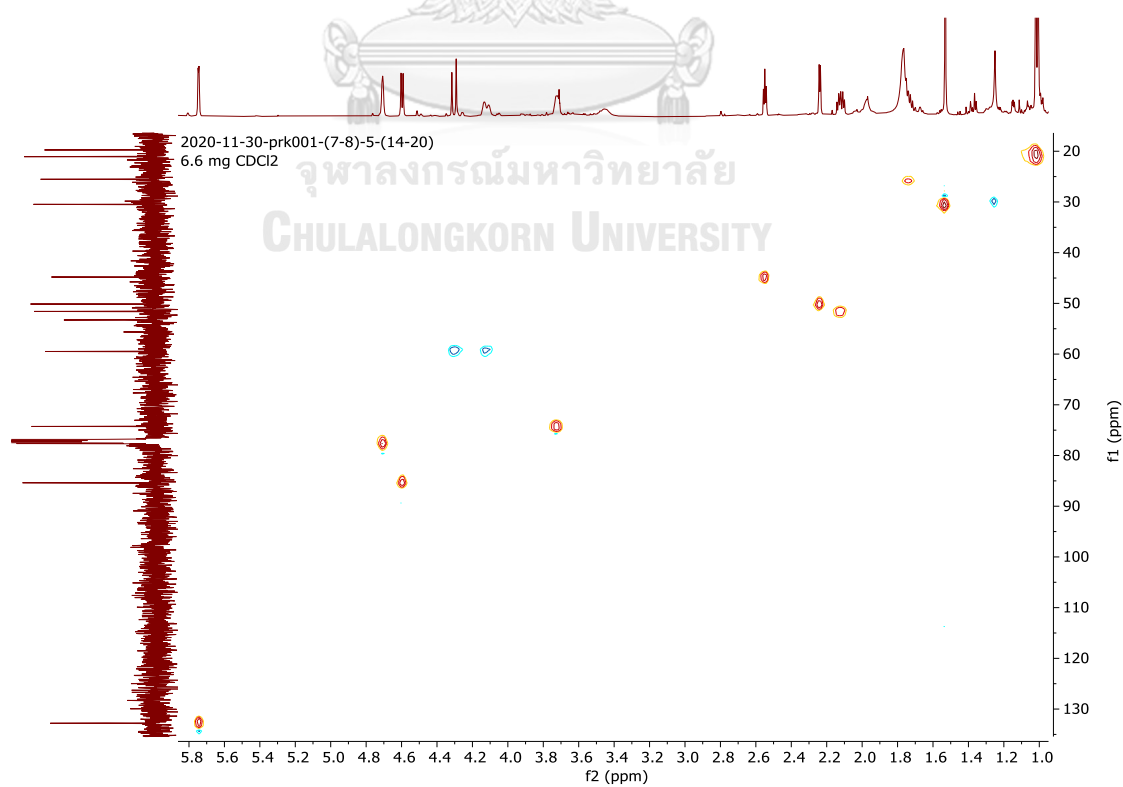
Figure S22. NOESY spectrum of compound **3****Figure S23.** HSQC spectrum of compound **3**

Figure S24. HMBC spectrum of compound 3

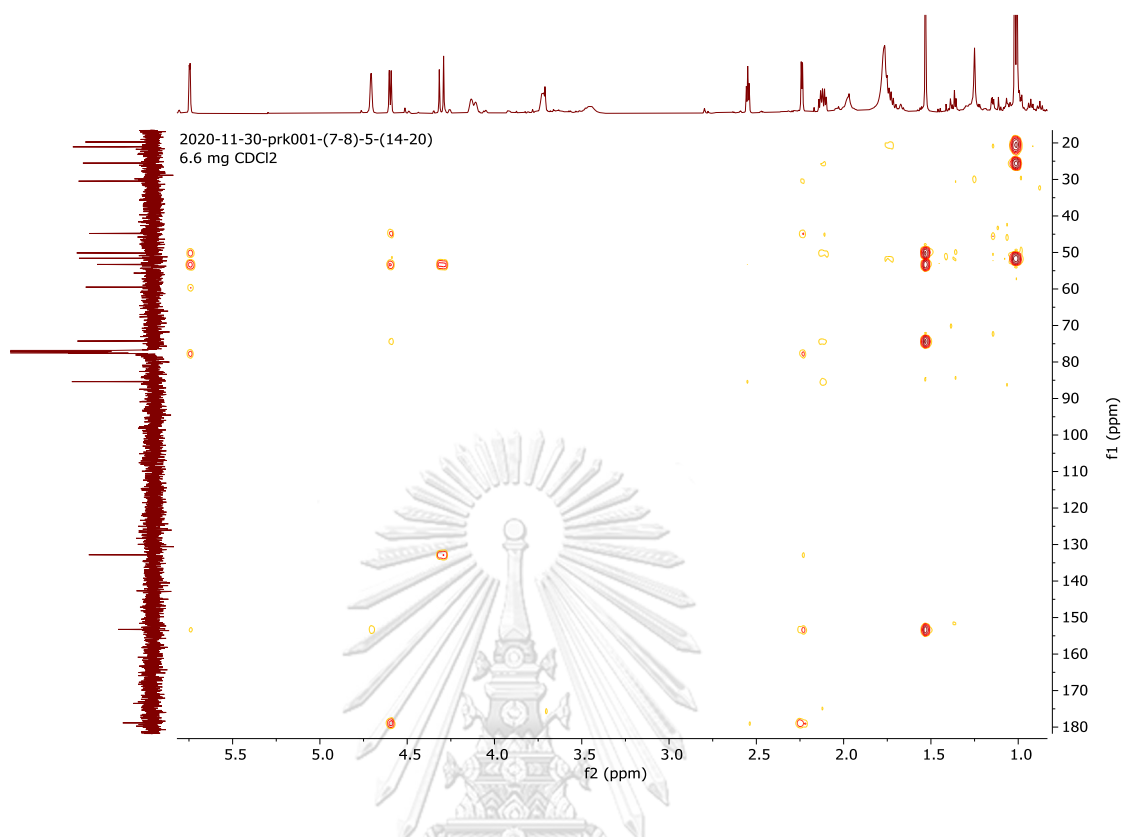


Figure S25. HRTOFMS spectrum of compound 3

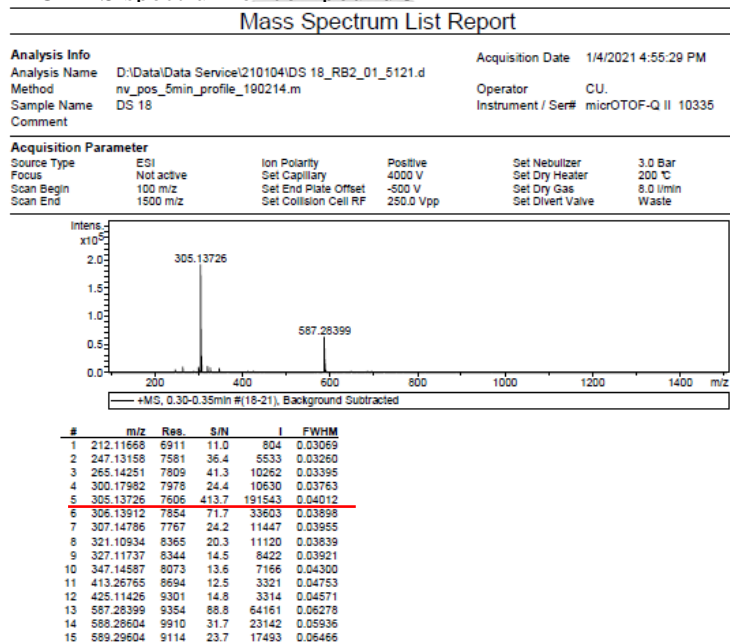


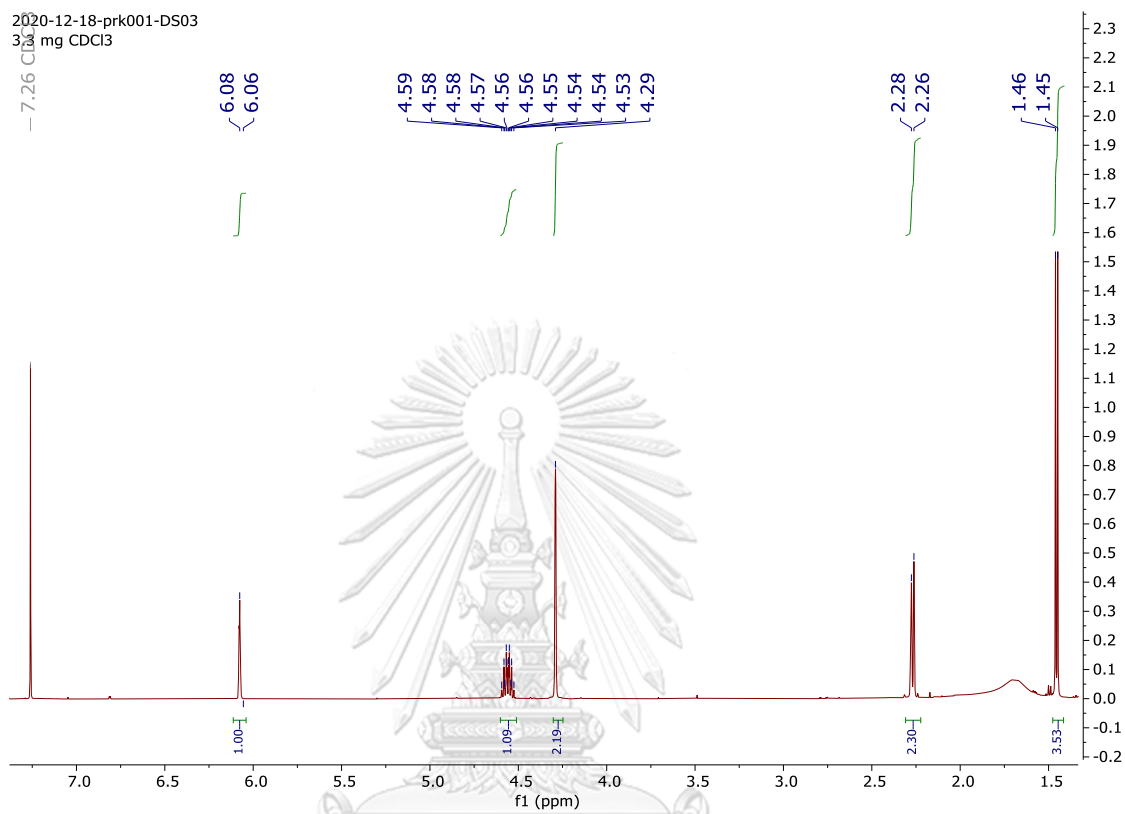
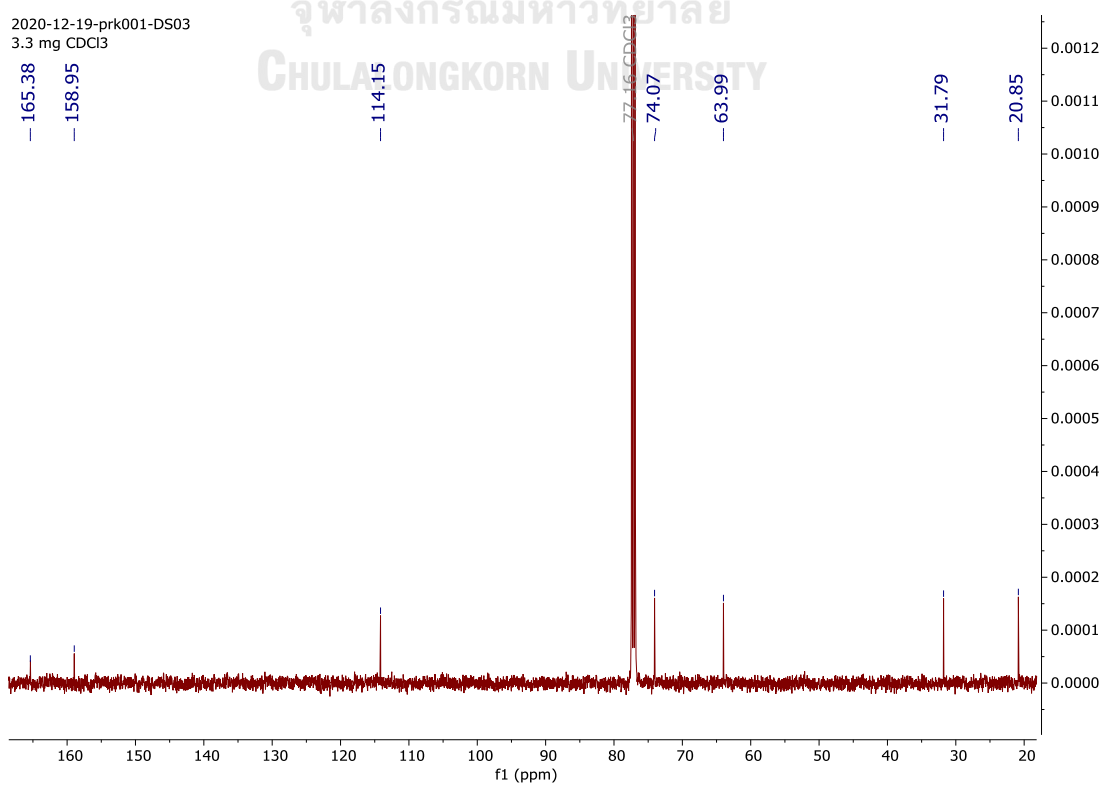
Figure S26. ^1H NMR spectrum (500 MHz, CDCl_3) of compound **4****Figure S27.** ^{13}C NMR spectrum (125 MHz, CDCl_3) of compound **4**

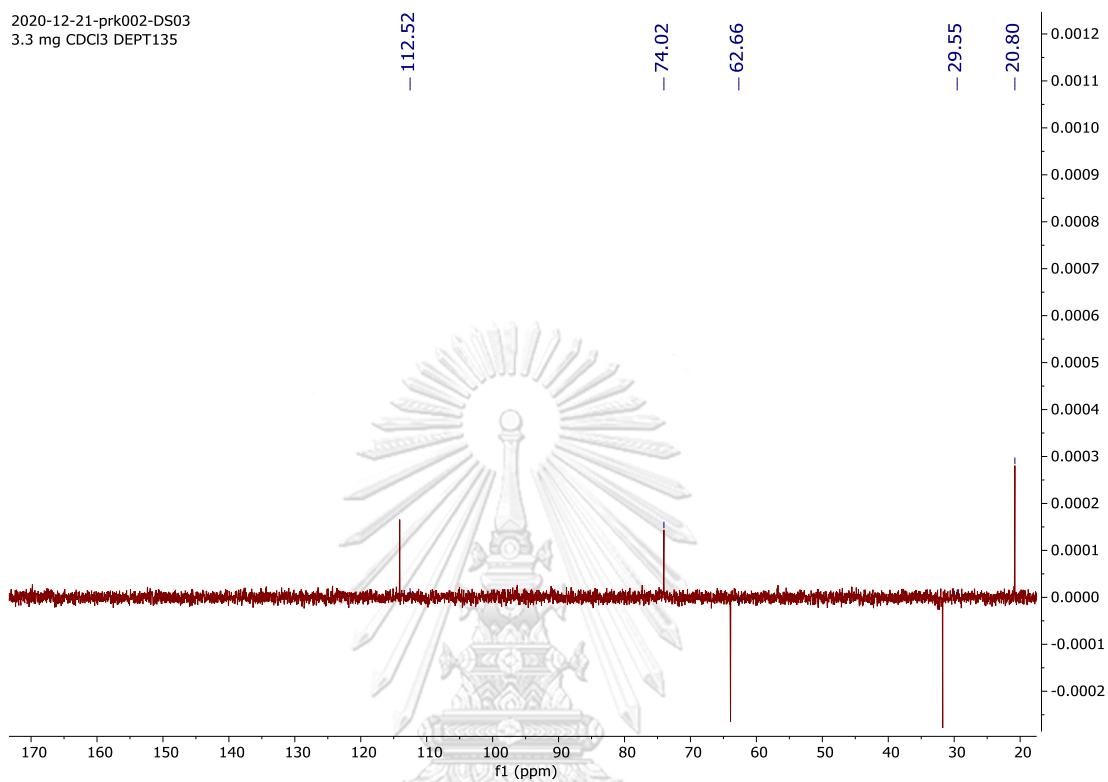
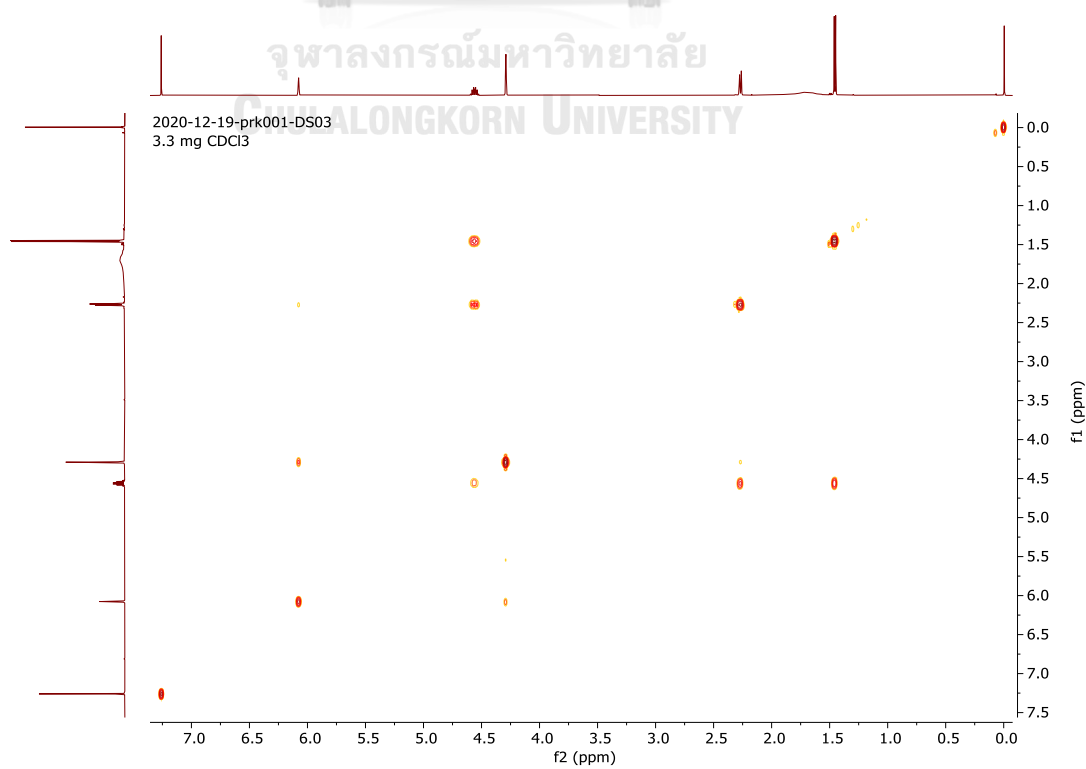
Figure S28. ^{13}C -DEPT-135 NMR spectrum (125 MHz, CDCl_3) of compound **4****Figure S29.** COSY spectrum of compound **4**

Figure S30. HSQC spectrum of compound 4

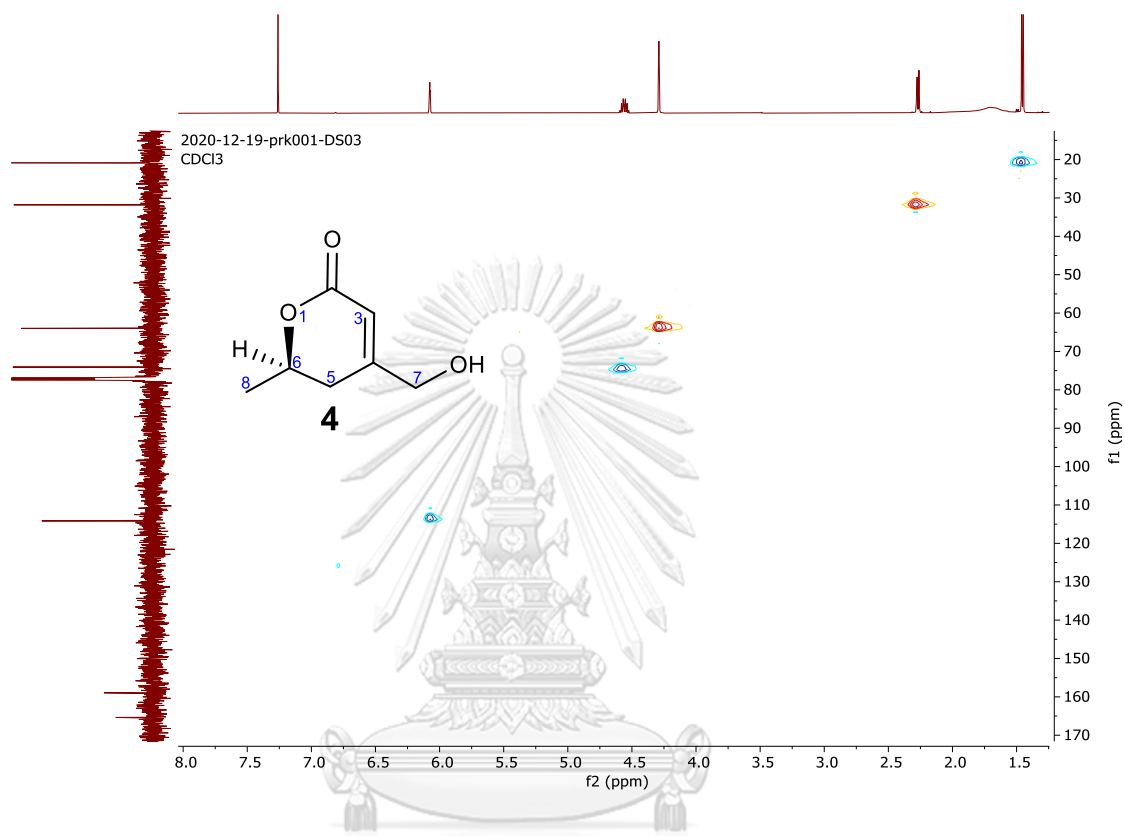


Figure S31. HMBC spectrum of compound 4

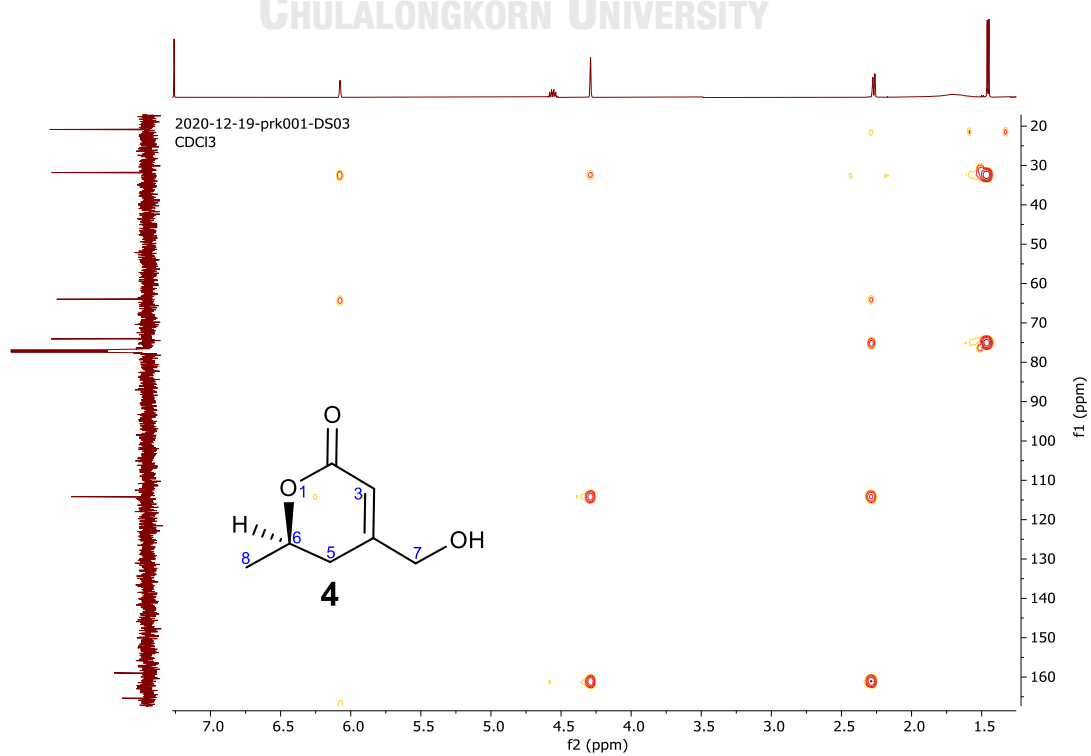


Figure S32. HRTOFMS spectrum of compound 4

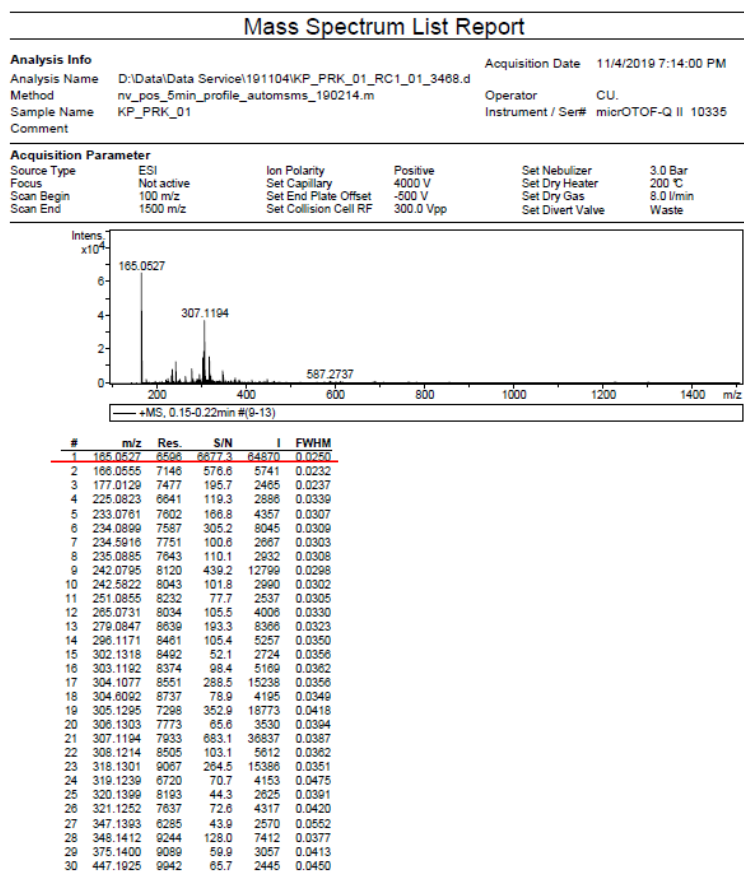


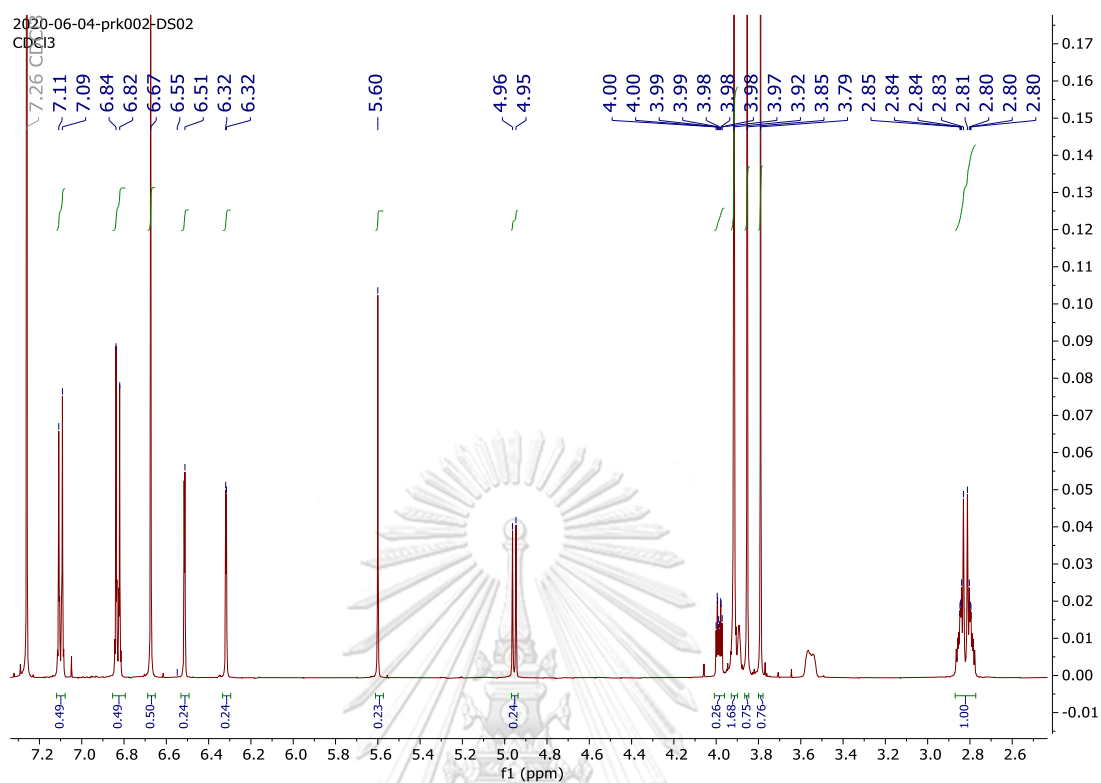
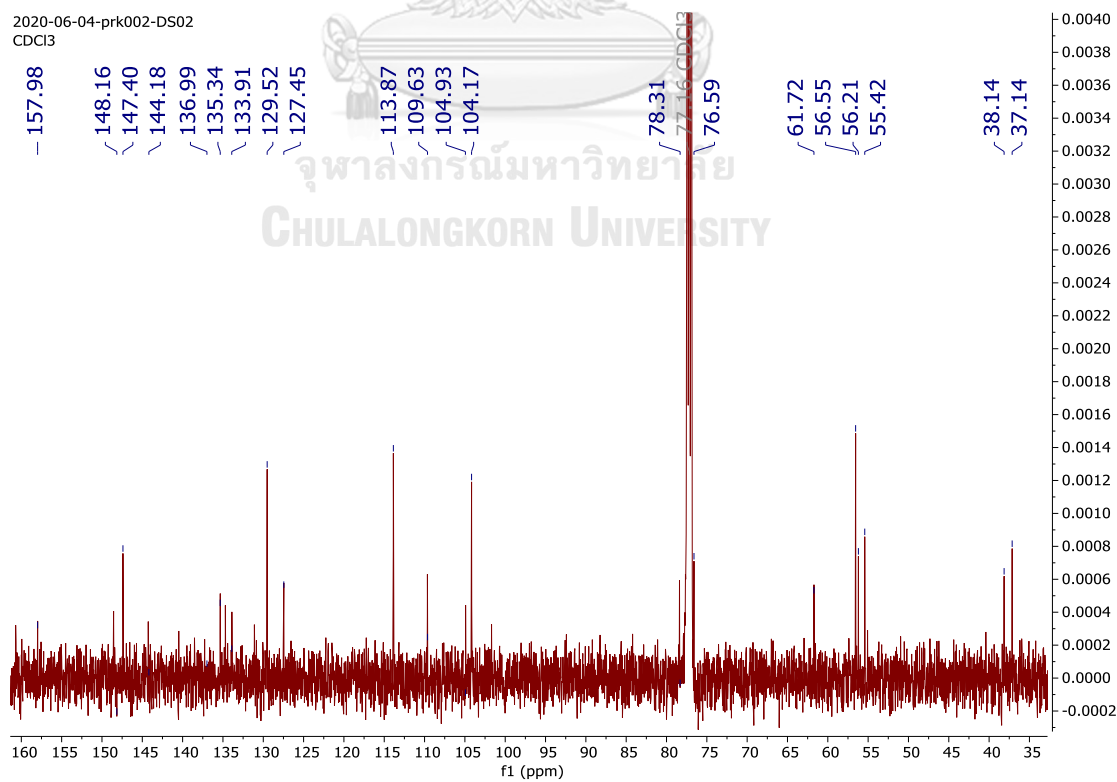
Figure S33. ^1H NMR spectrum (500 MHz, CDCl_3) of compound **5****Figure S34.** ^{13}C NMR spectrum (125 MHz, CDCl_3) of compound **5**

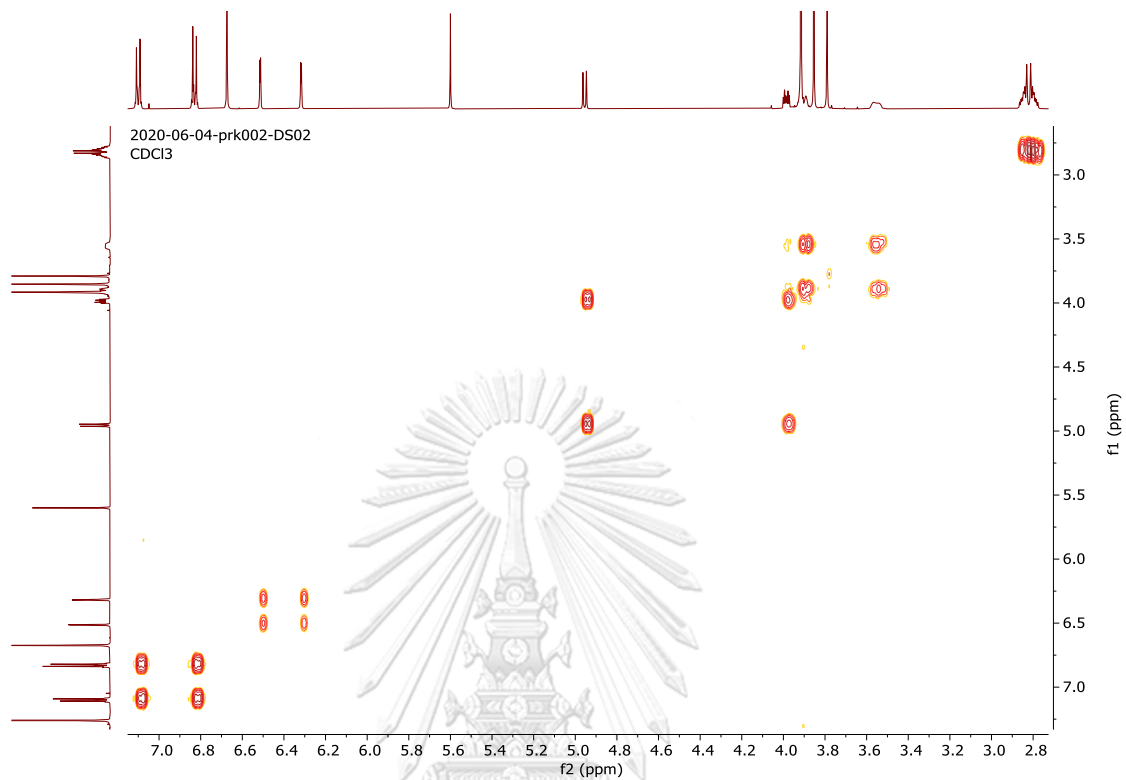
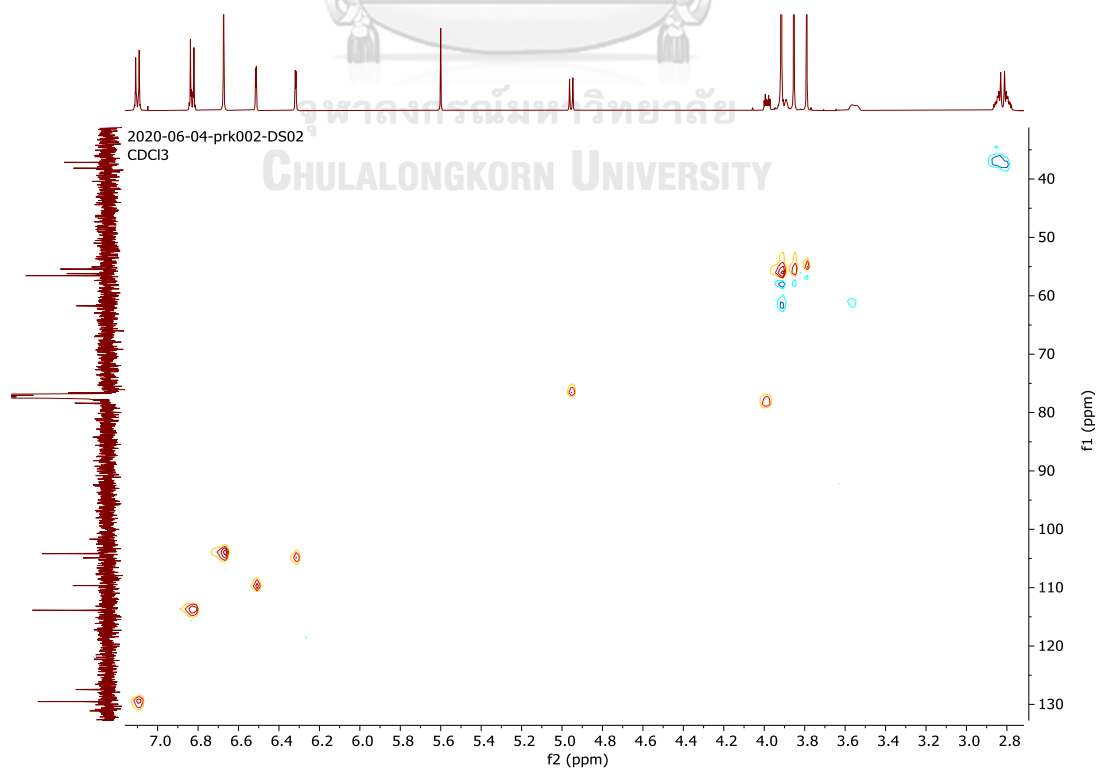
Figure S35. COSY spectrum of compound **5****Figure S36.** HSQCC spectrum of compound **5**

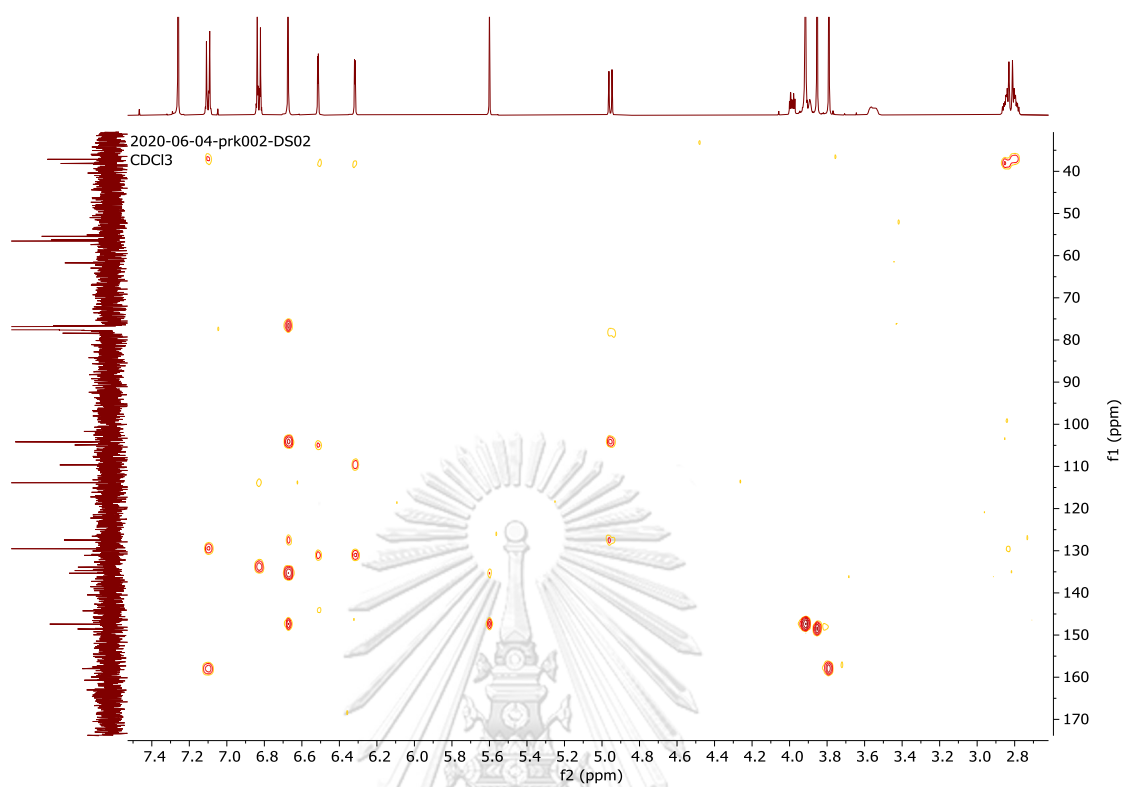
Figure S37. HMBC spectrum of compound **5**

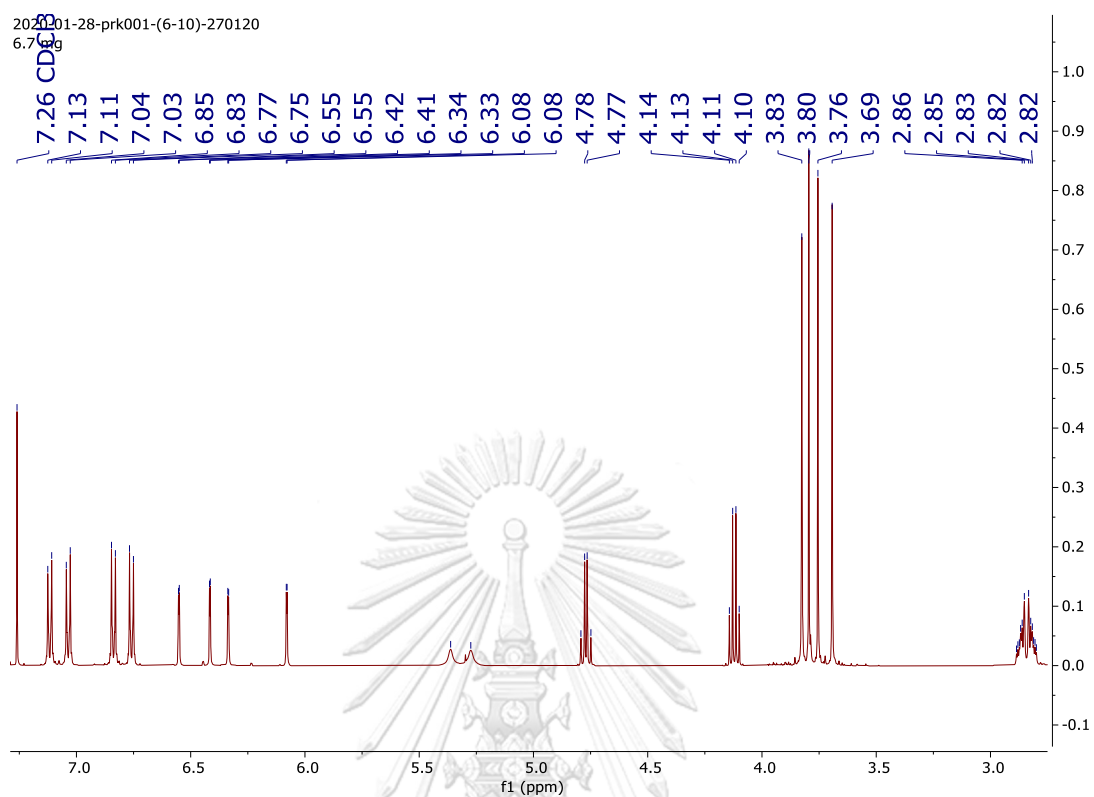
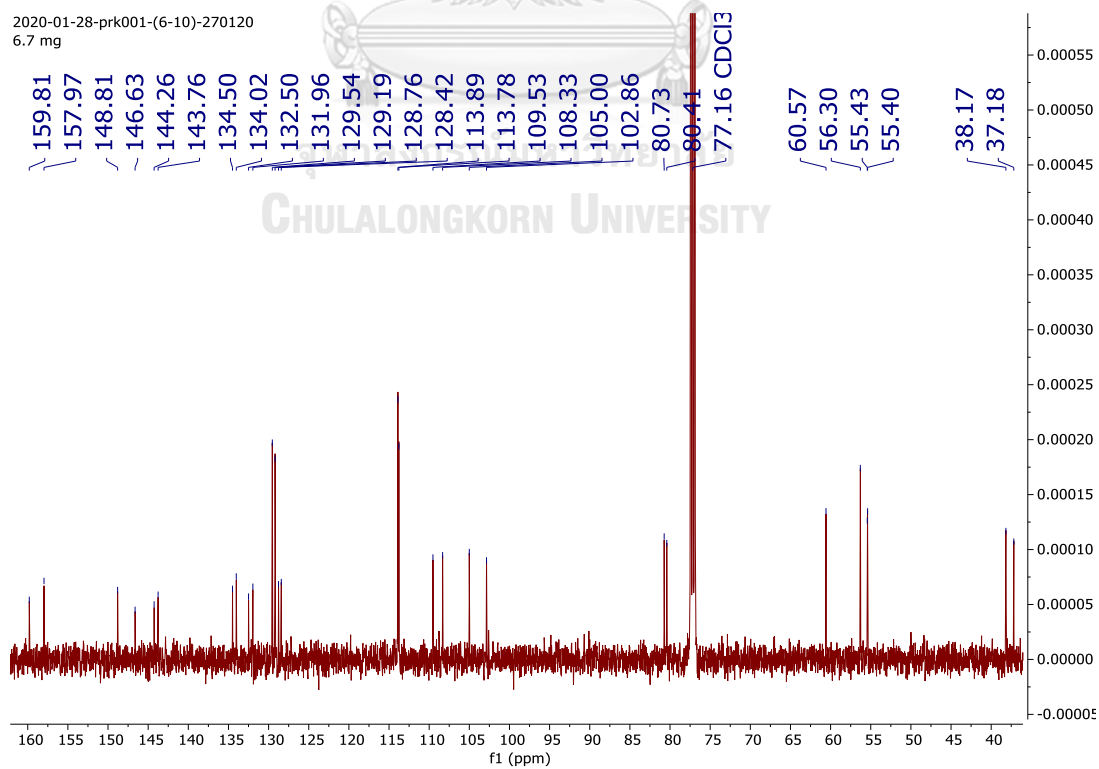
Figure S38. ^1H NMR spectrum (500 MHz, CDCl_3) of compound **6****Figure S39.** ^{13}C NMR spectrum (125 MHz, CDCl_3) of compound **6**

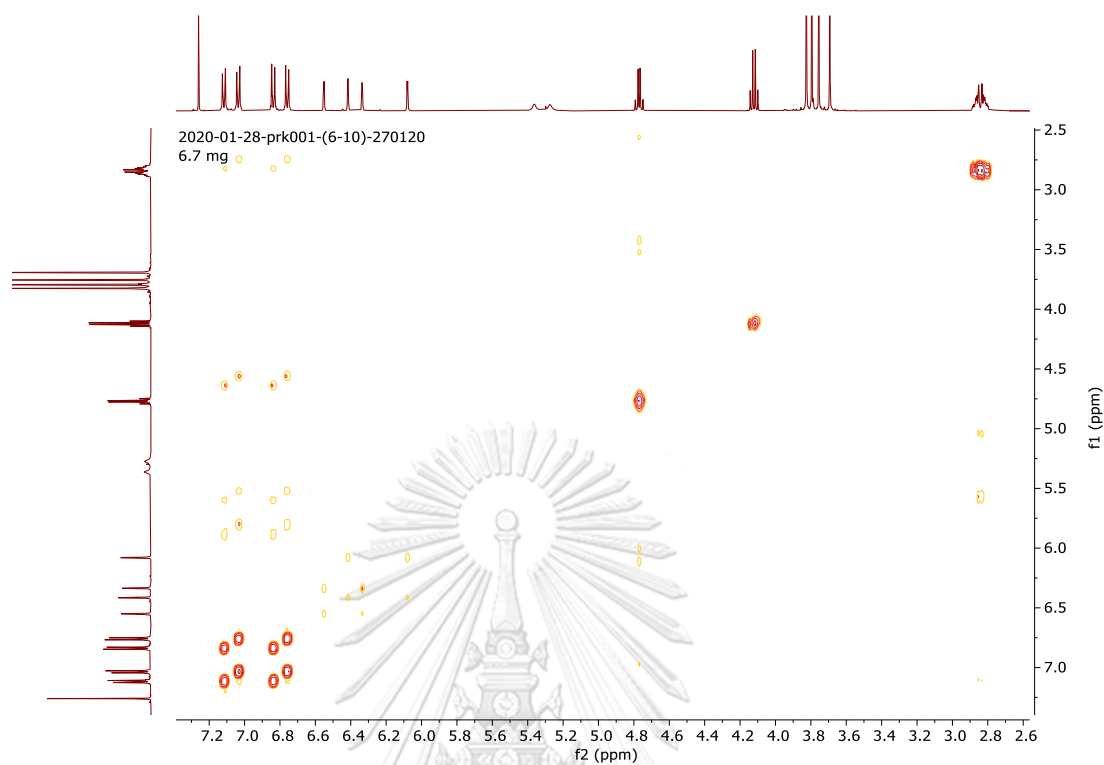
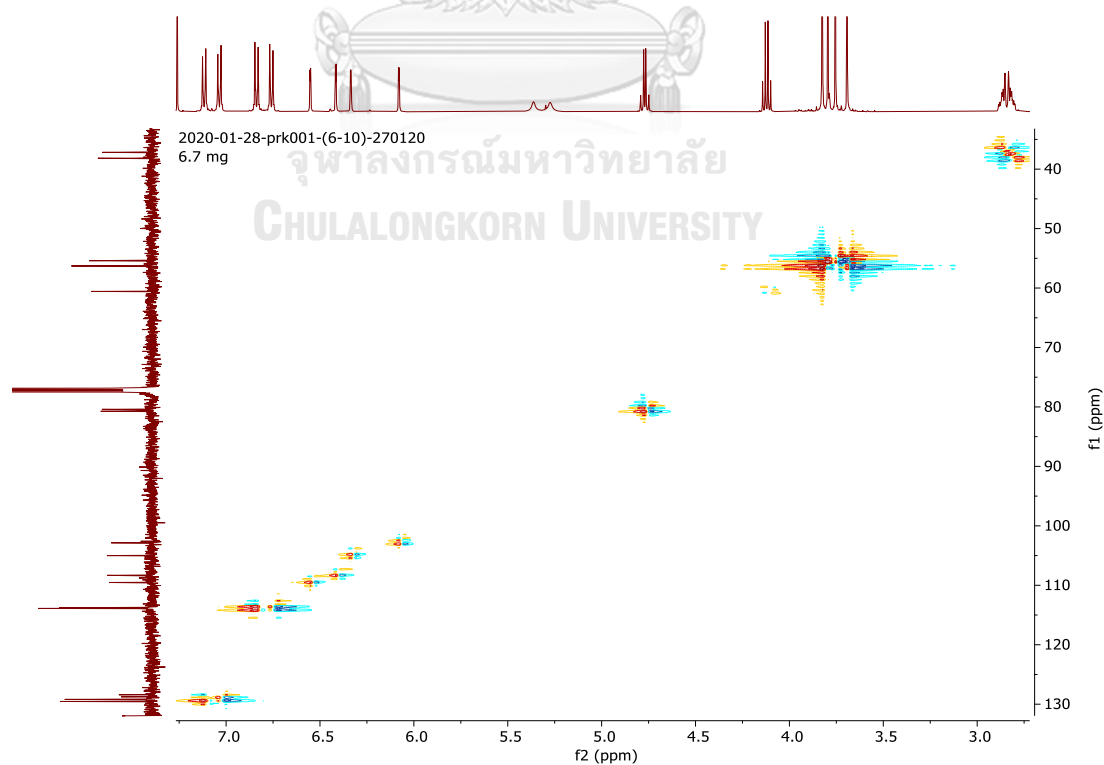
Figure S40. COSY spectrum of compound **6****Figure S41.** HSQC spectrum of compound **6**

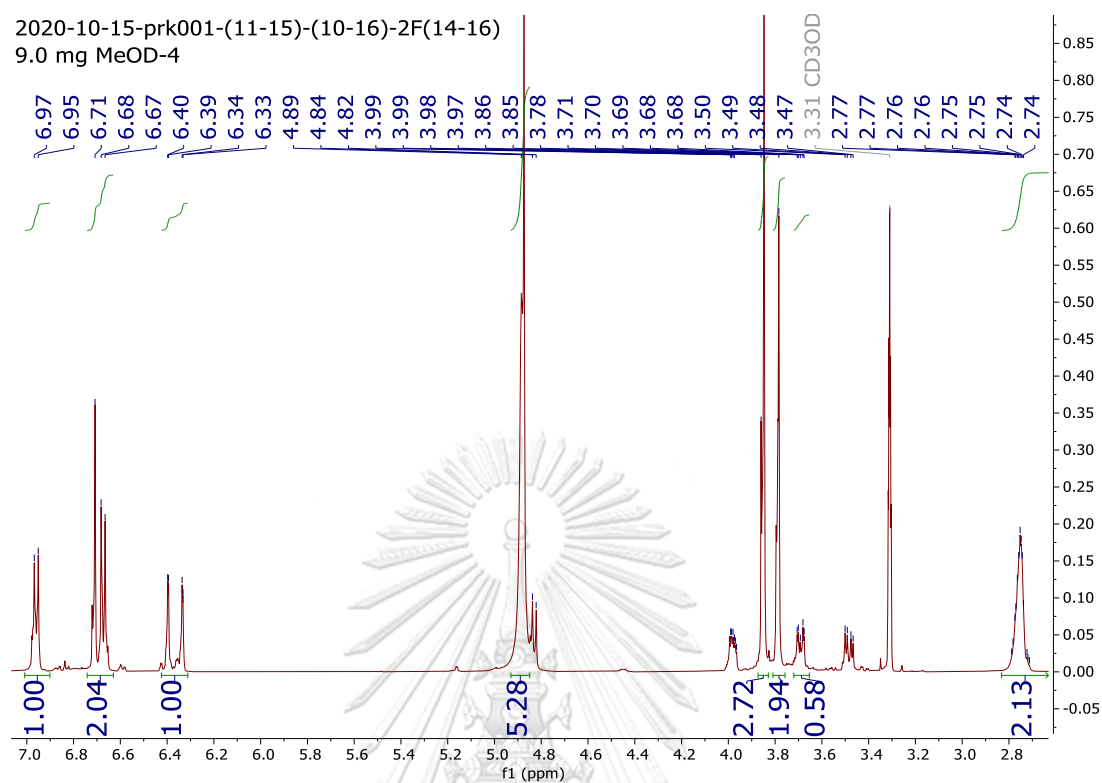
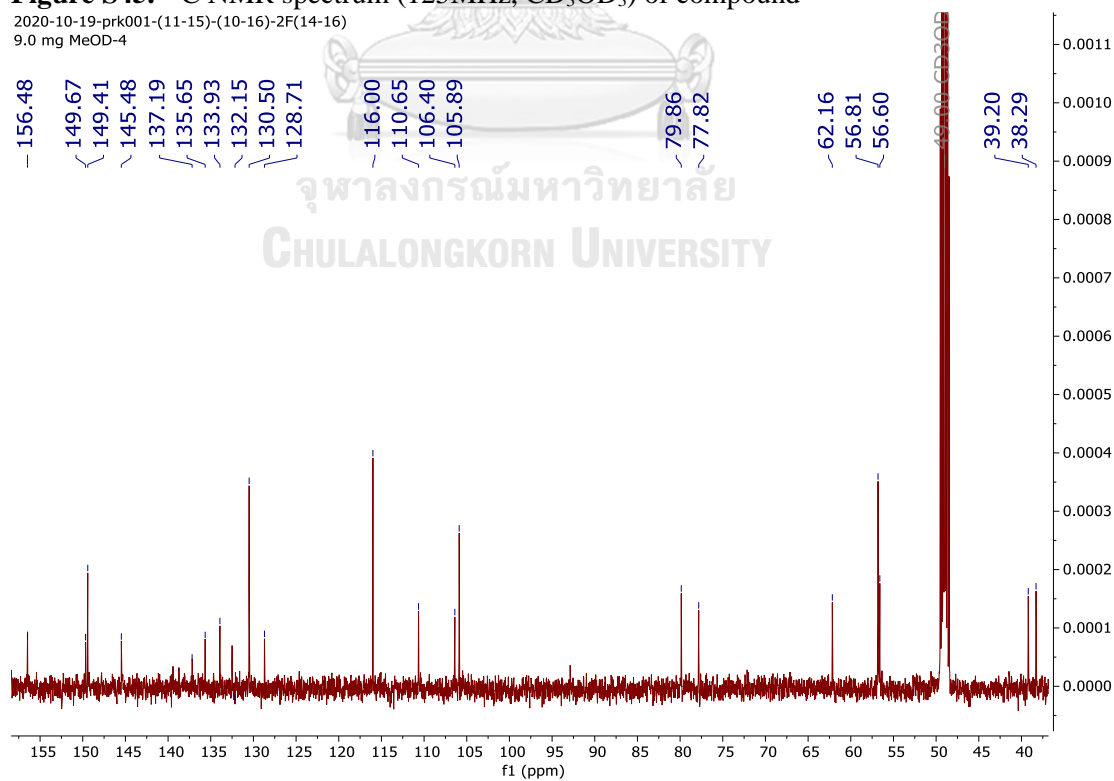
Figure S44. ^1H NMR spectrum (500 MHz, CD_3OD_3) of compound **7****Figure S45.** ^{13}C NMR spectrum (125MHz, CD_3OD_3) of compound **7**

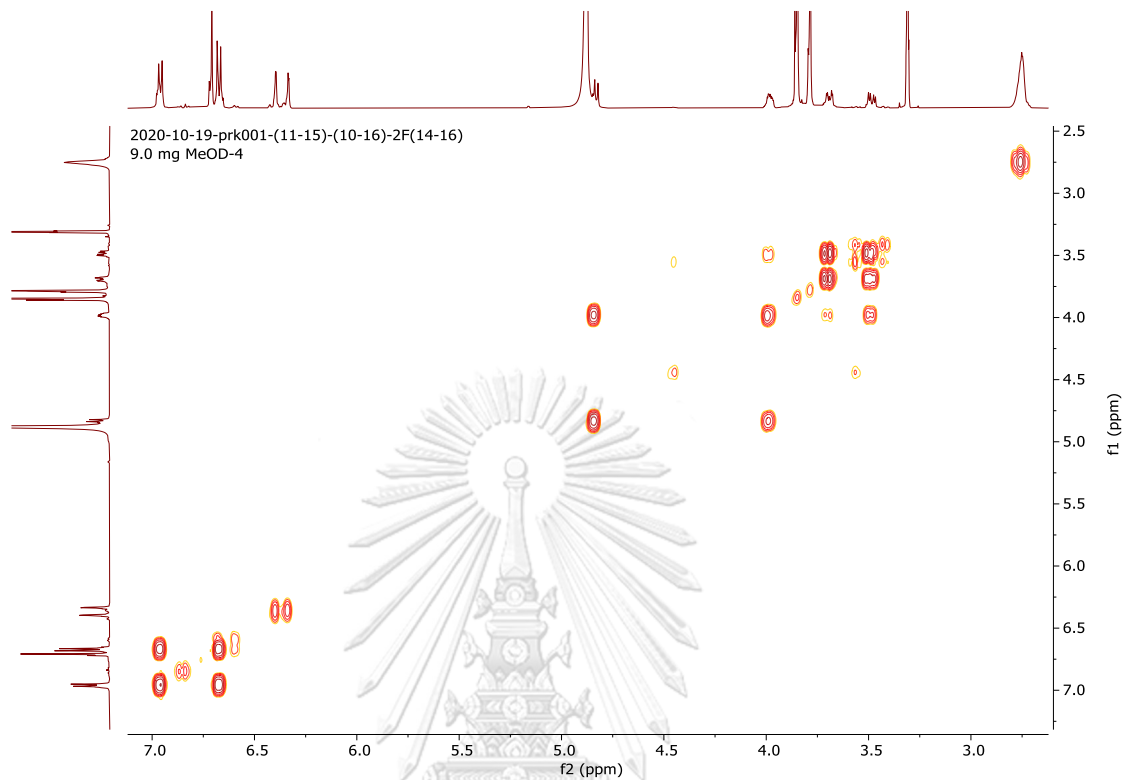
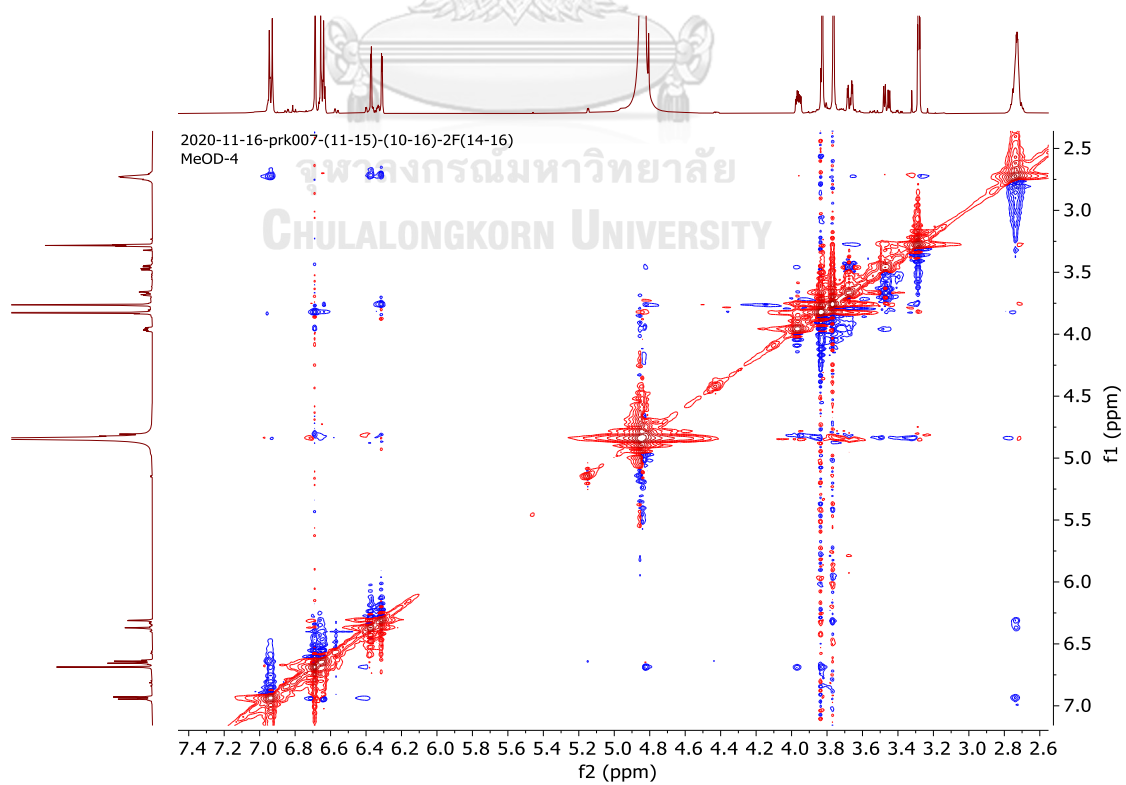
Figure S46. COSY spectrum of compound **7****Figure S47.** NOESY spectrum of compound **7**

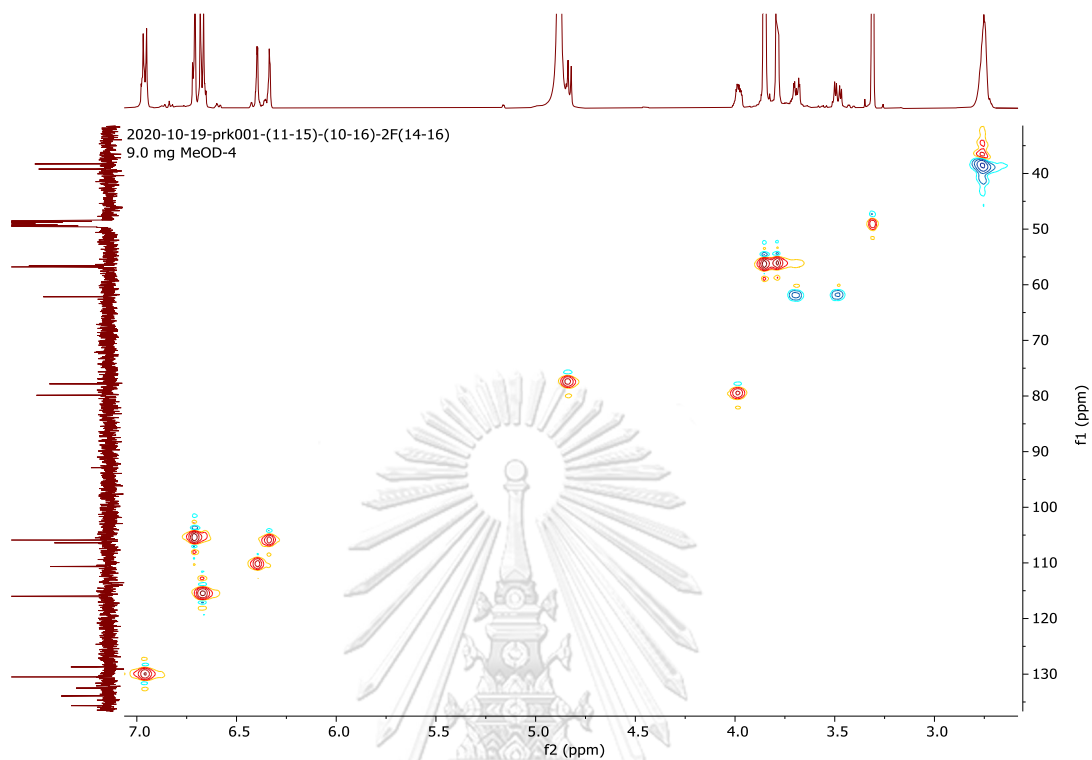
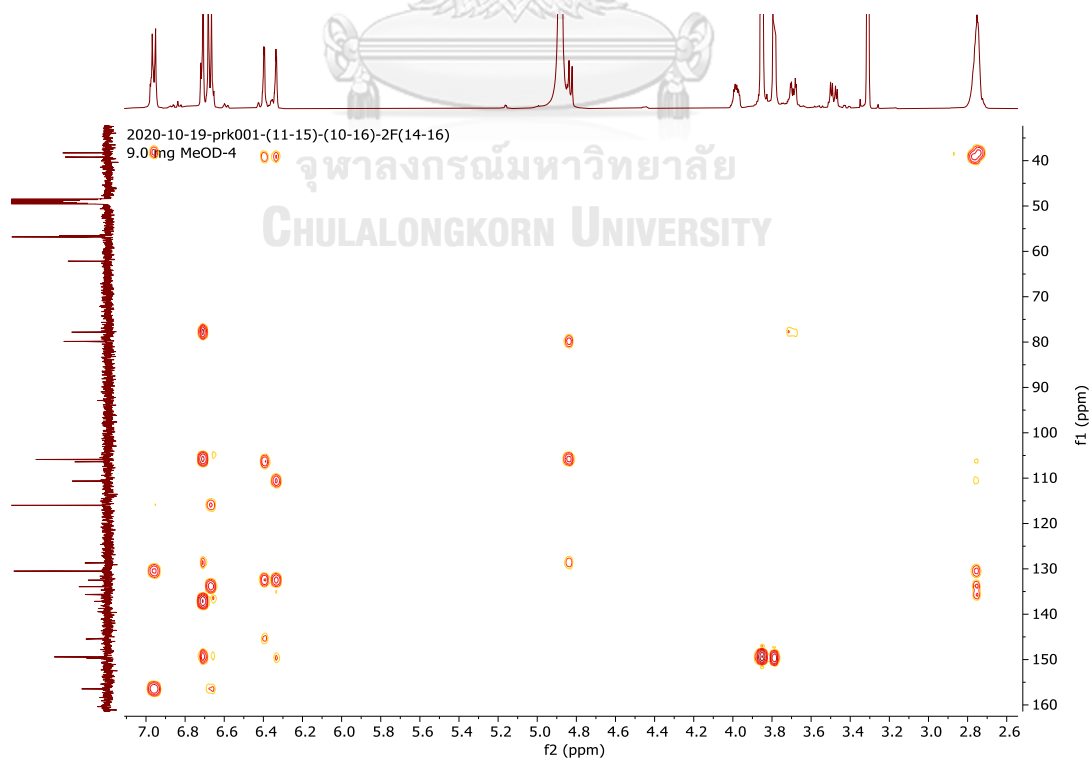
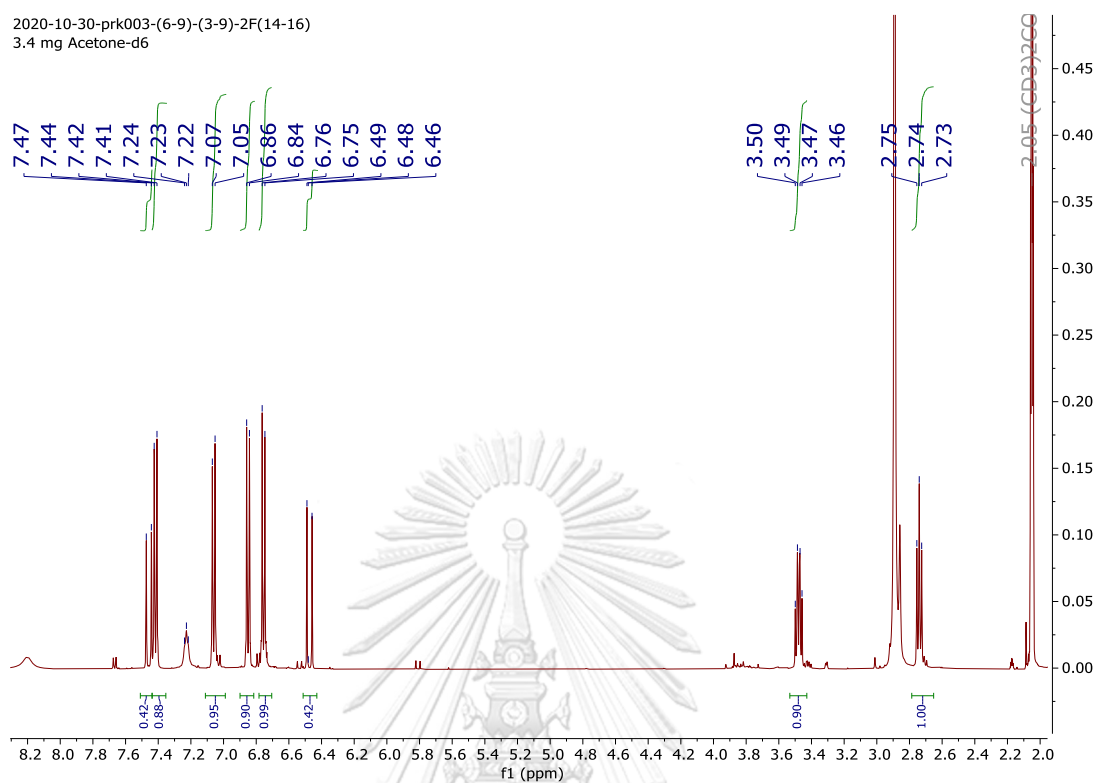
Figure S48. HSQC spectrum of compound **7****Figure S49.** HMBC spectrum of compound **7**

Figure S50. ^1H NMR spectrum (500 MHz, acetone- d_6) of compound **8**

2020-10-30-prk003-(6-9)-(3-9)-2F(14-16)
3.4 mg Acetone- d_6

**Figure S51.** ^{13}C NMR spectrum (500 MHz, acetone- d_6) of compound **8**

2020-11-30-prk001-(6-9)-(3-9)-2F(14-16)
6.0 mg Acetone d_6

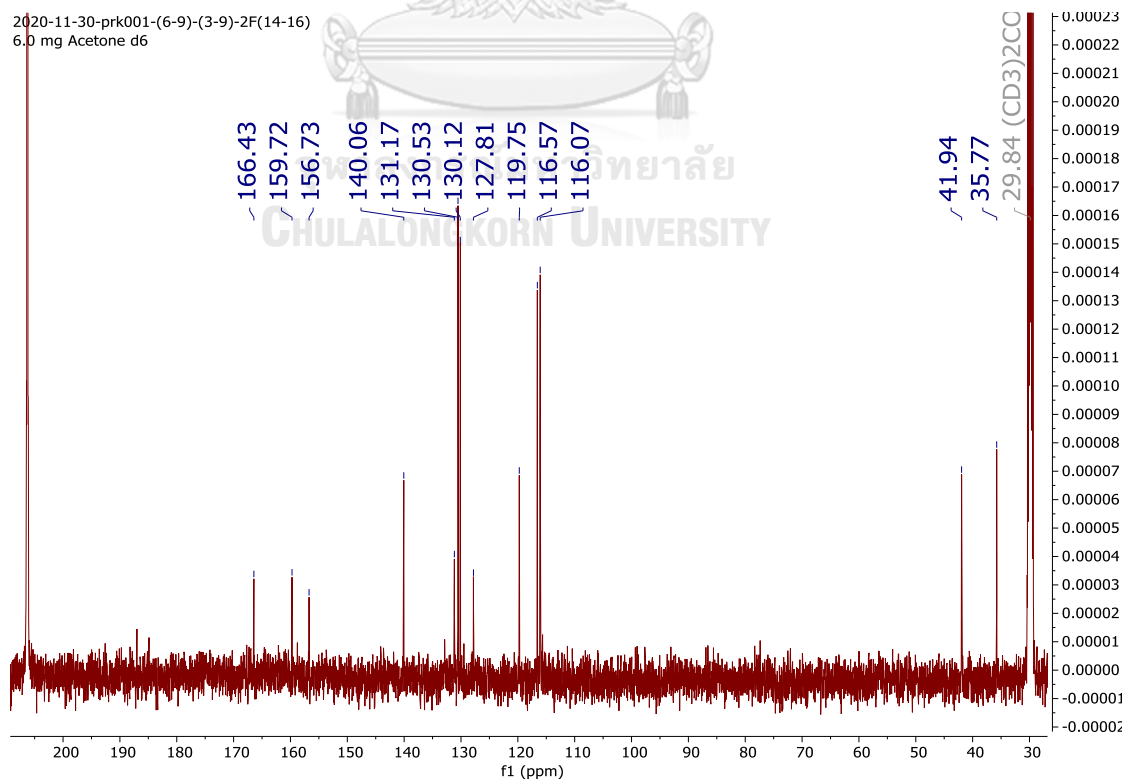


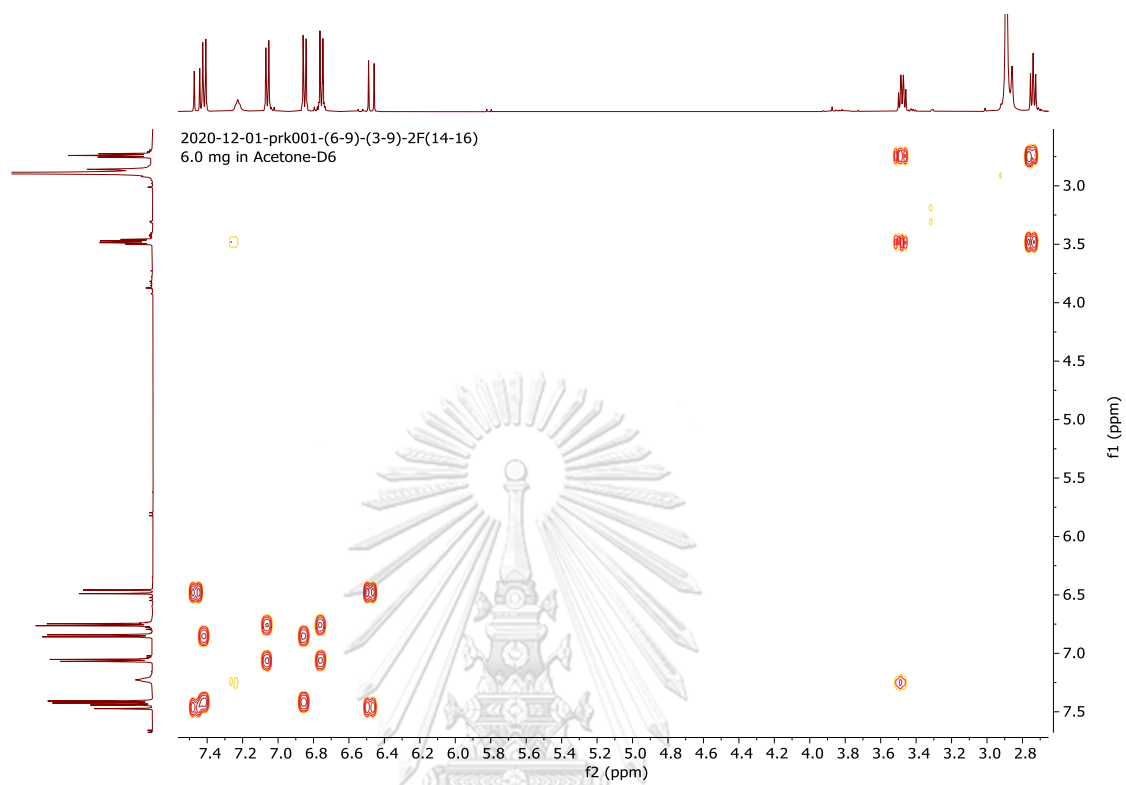
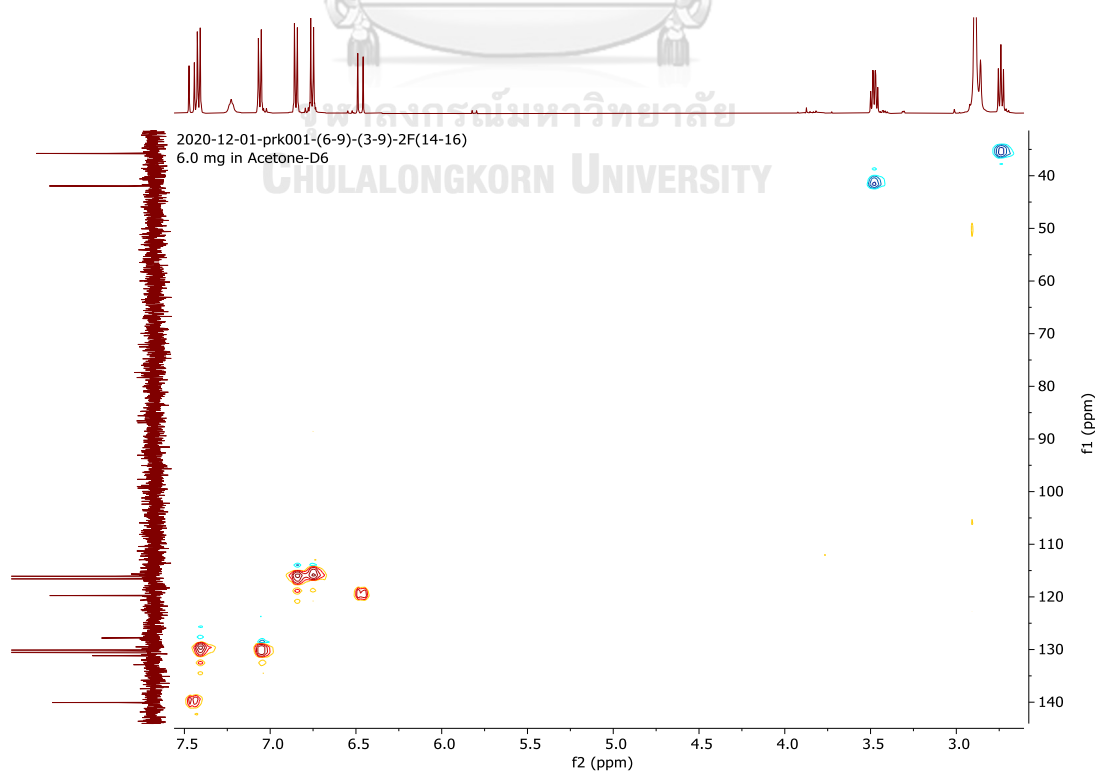
Figure S52. COSY spectrum of compound **8****Figure S53.** HSQC spectrum of compound **8**

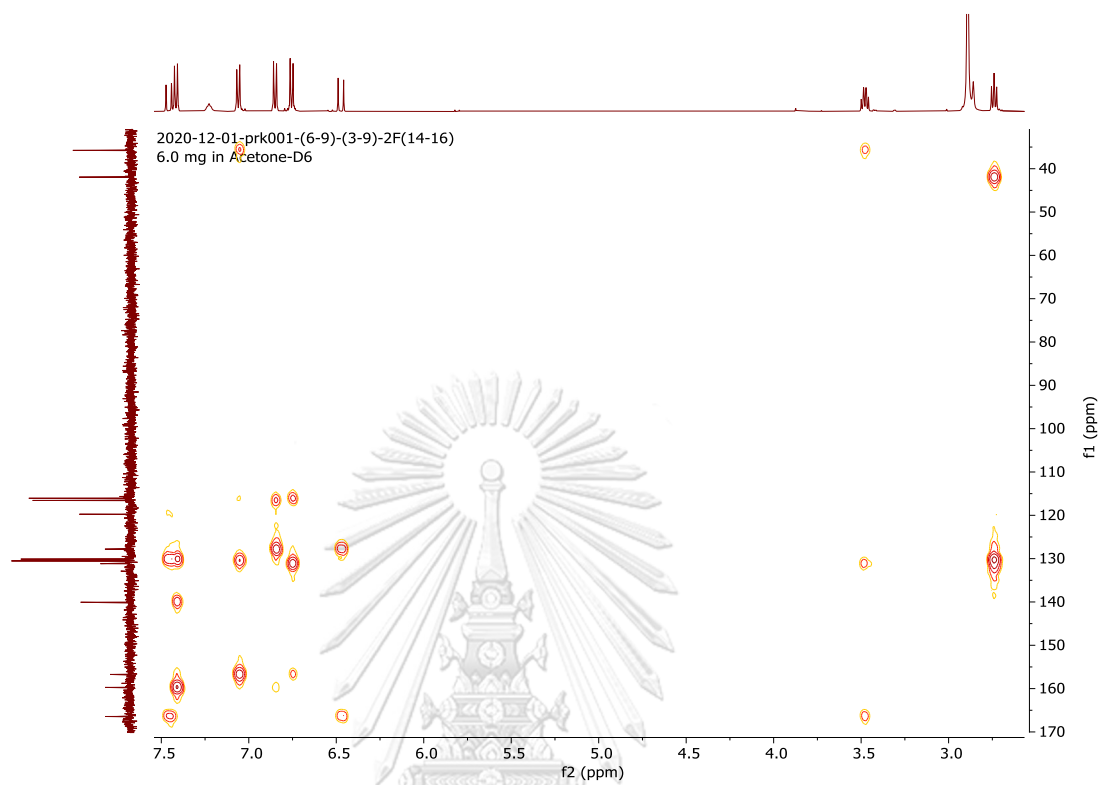
Figure S54. HMBC spectrum of compound **8**

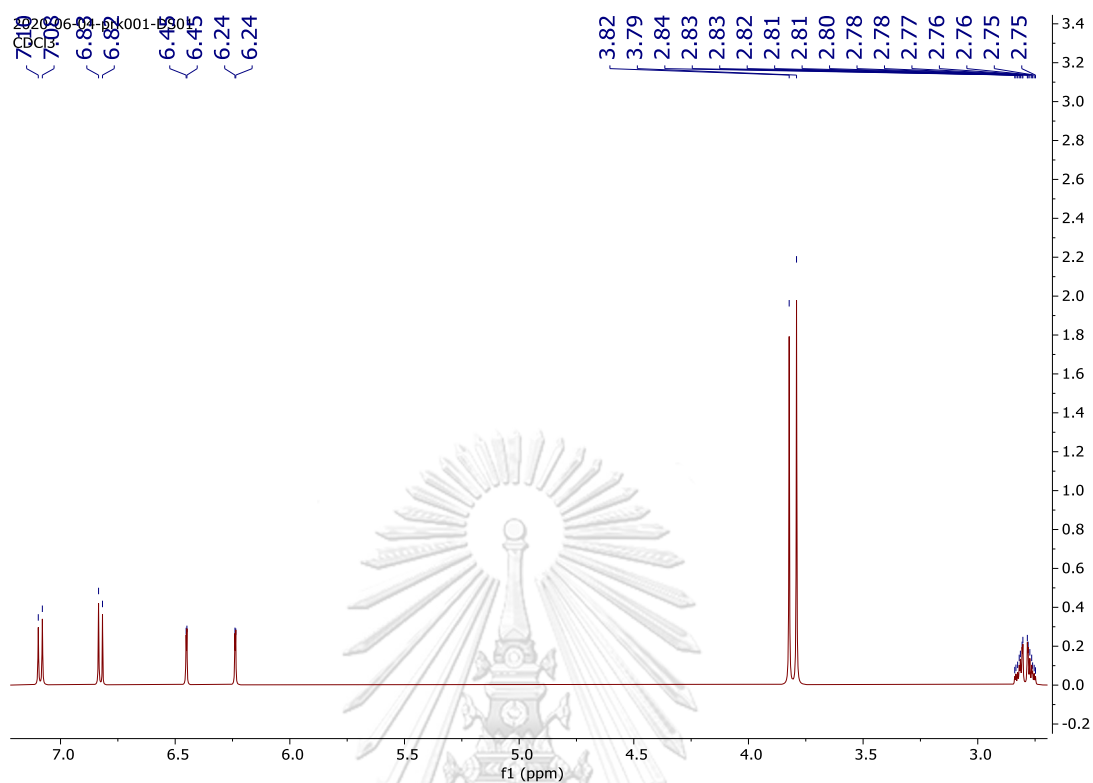
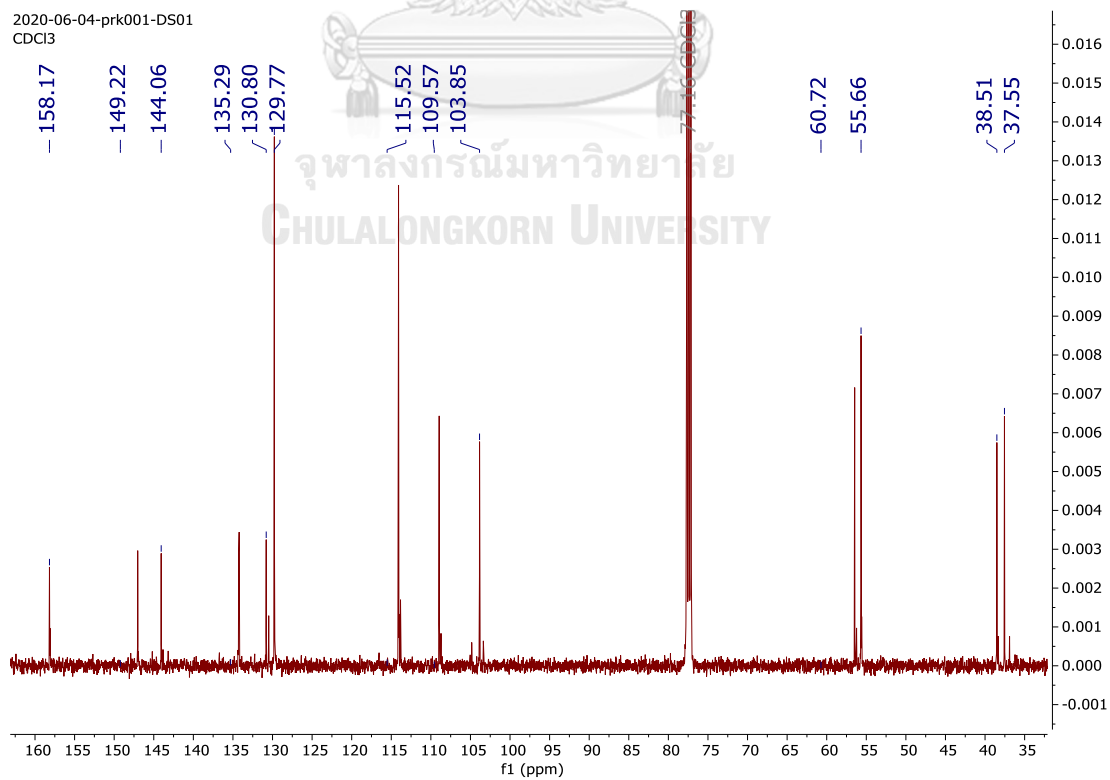
Figure S55. ^1H NMR spectrum (500 MHz, CDCl_3) of compound **9****Figure S56.** ^{13}C NMR spectrum (500 MHz, CDCl_3) of compound **9**

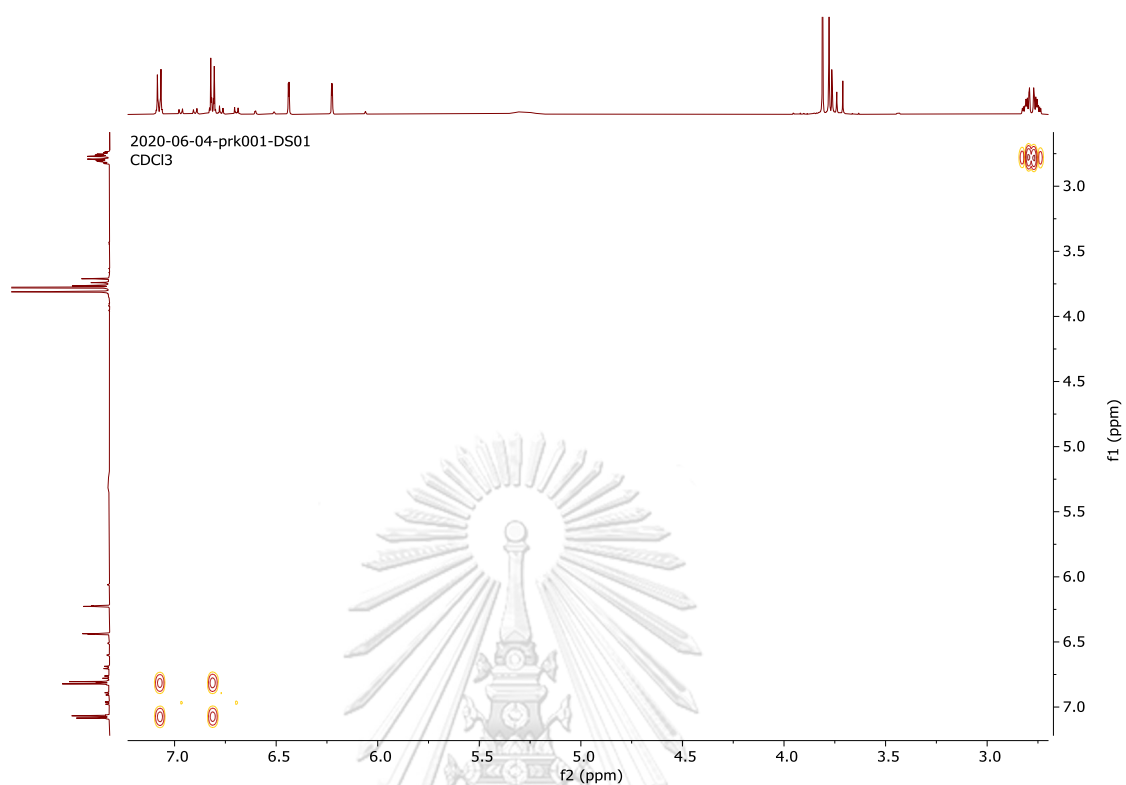
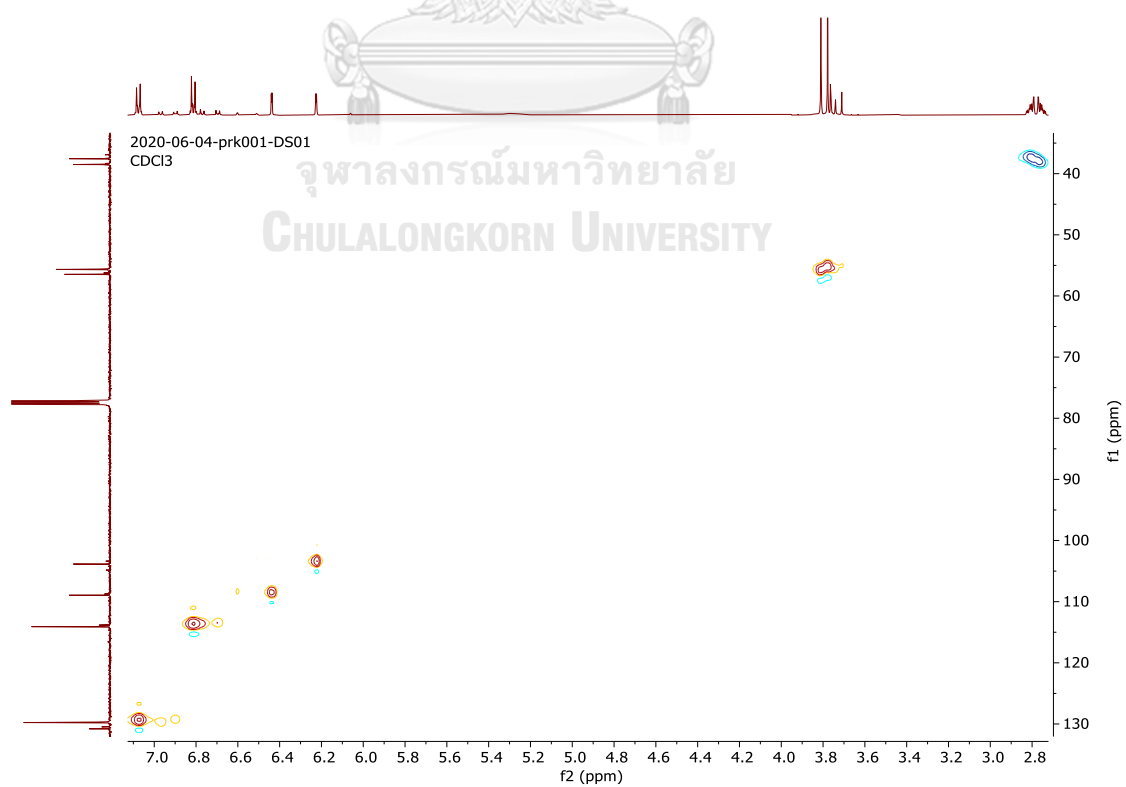
Figure S57. COSY spectrum of compound **9****Figure S58.** HSQC spectrum of compound **9**

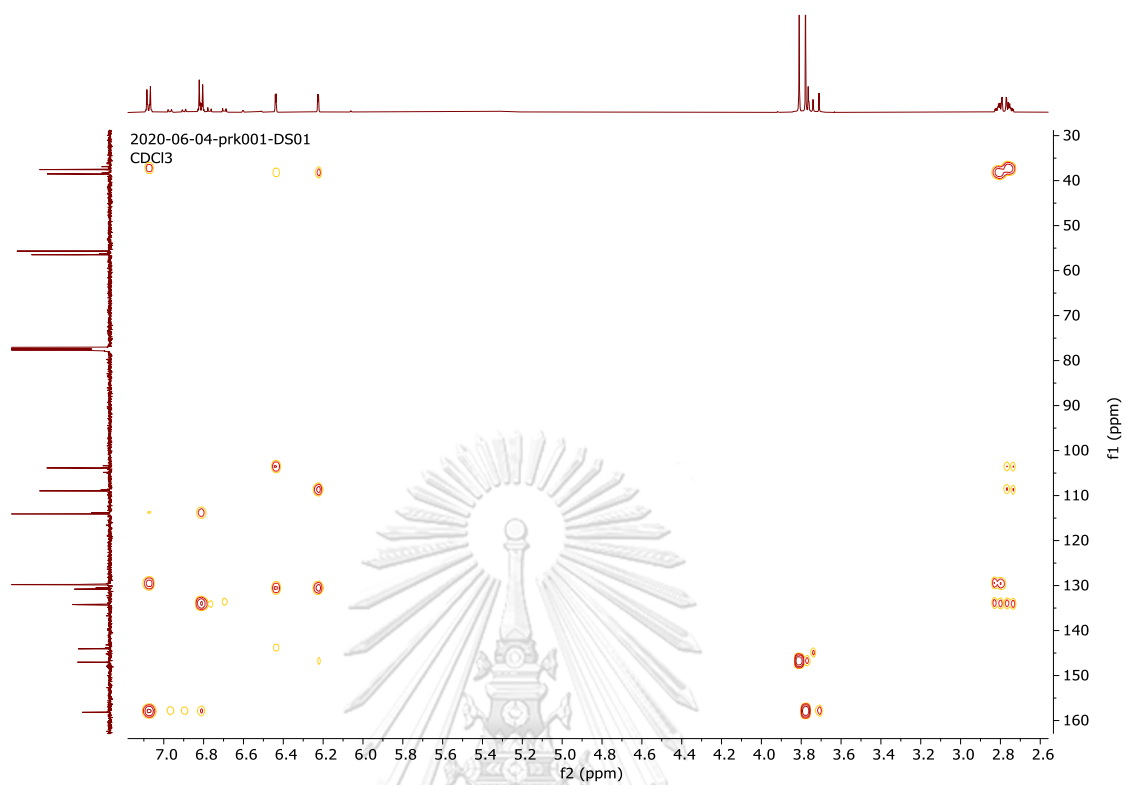
Figure S59. HMBC spectrum of compound **9**

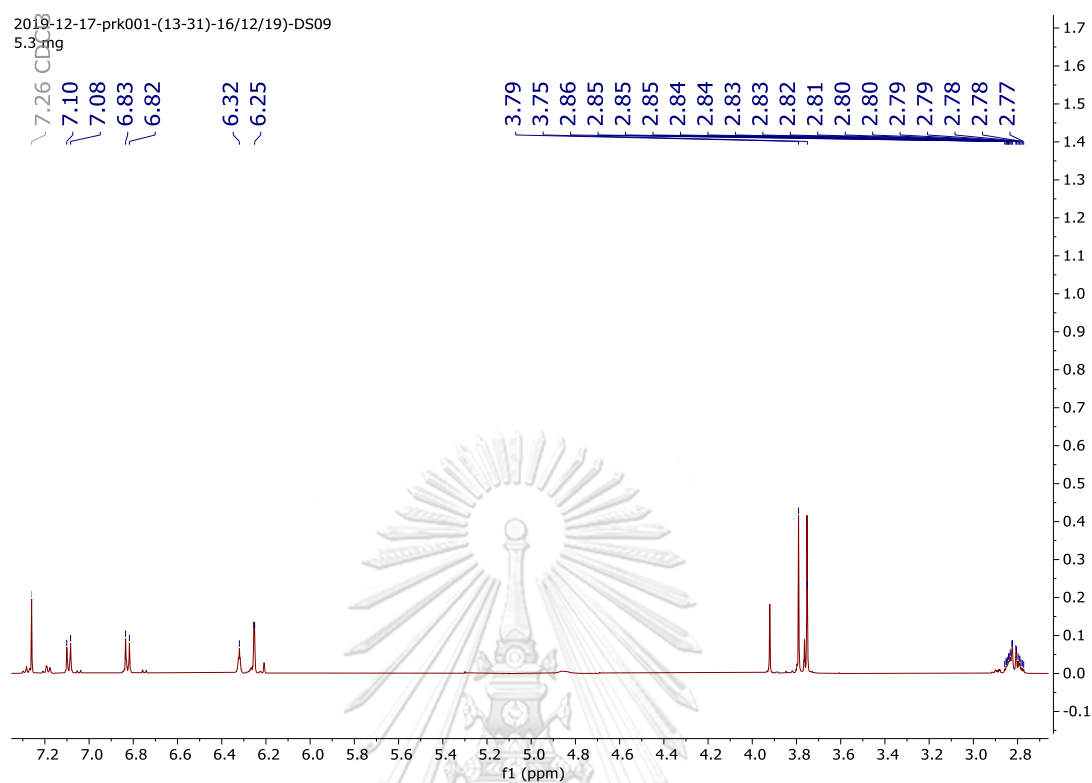
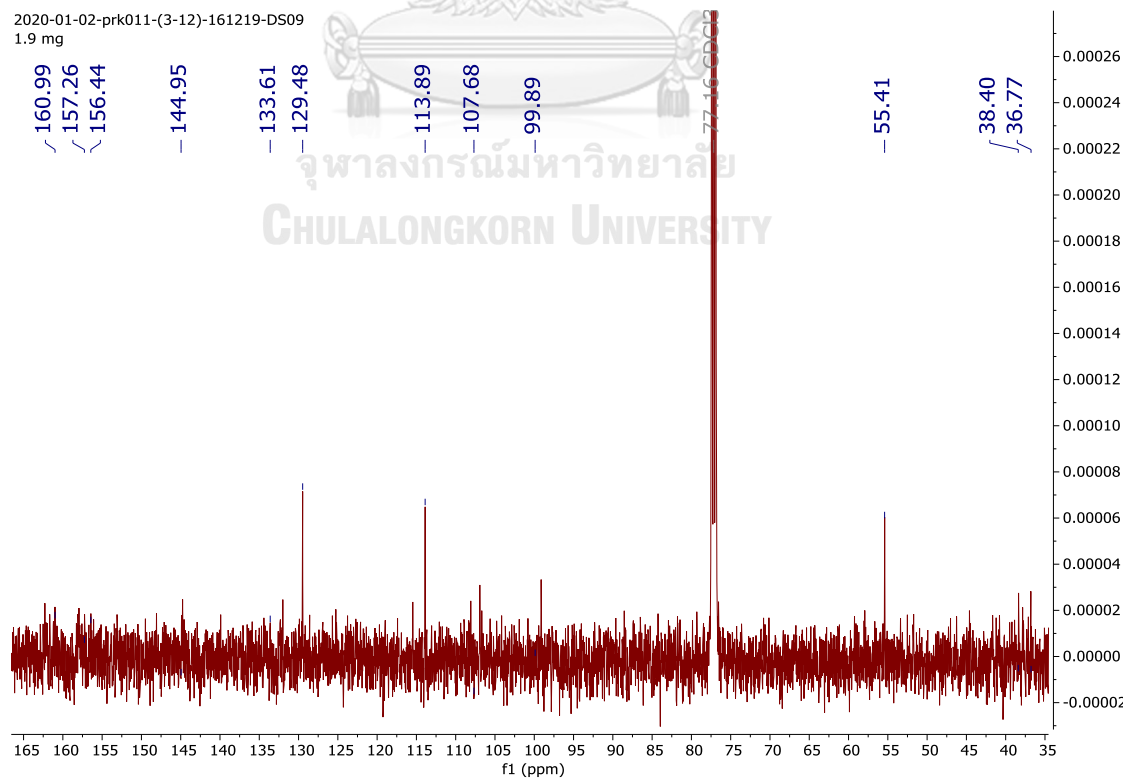
Figure S60. ^1H NMR spectrum (500 MHz, CDCl_3) of compound **10****Figure S61.** ^{13}C NMR spectrum (125 MHz, CDCl_3) of compound **10**

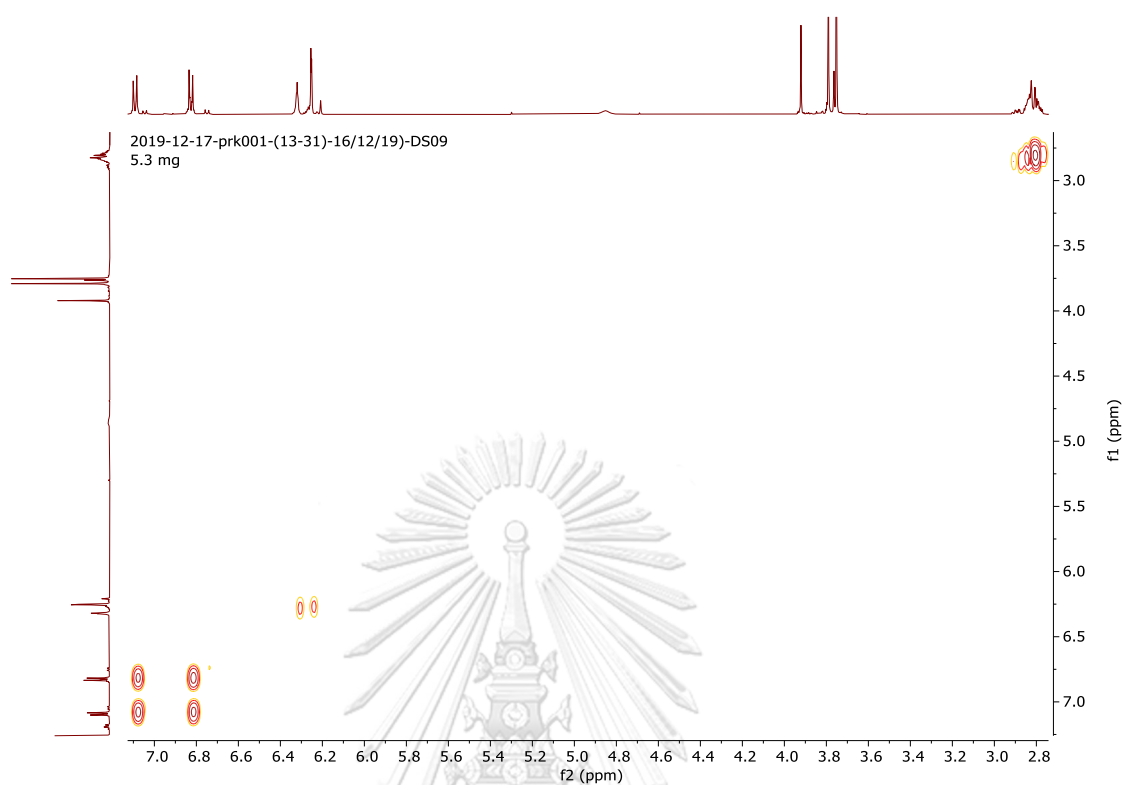
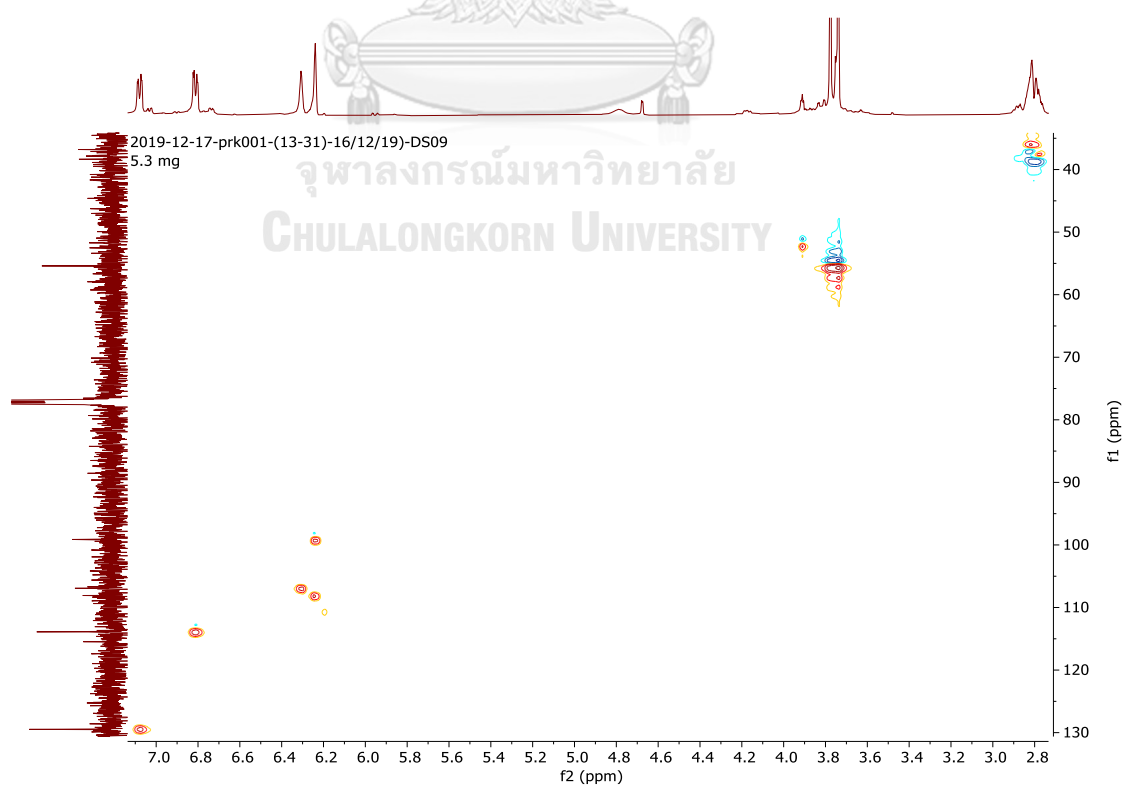
Figure S62. COSY spectrum of compound **10****Figure S63.** HSQC spectrum of compound **10**

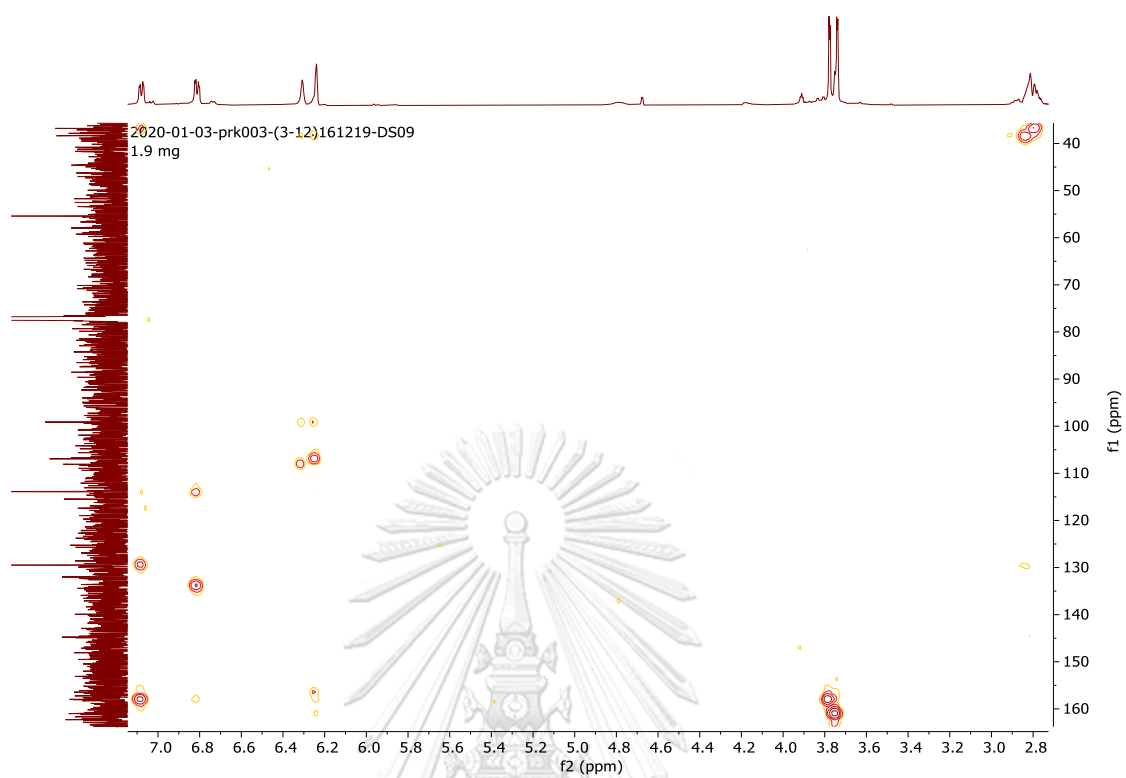
Figure S64. HMBC spectrum of compound **10**

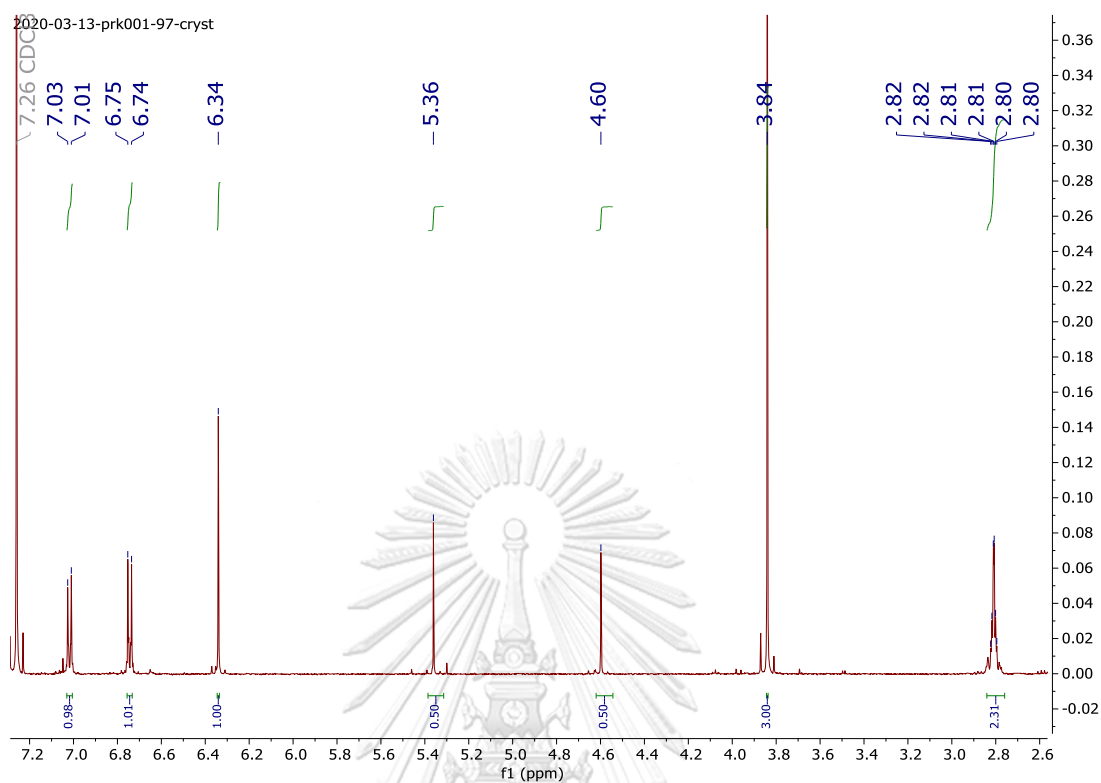
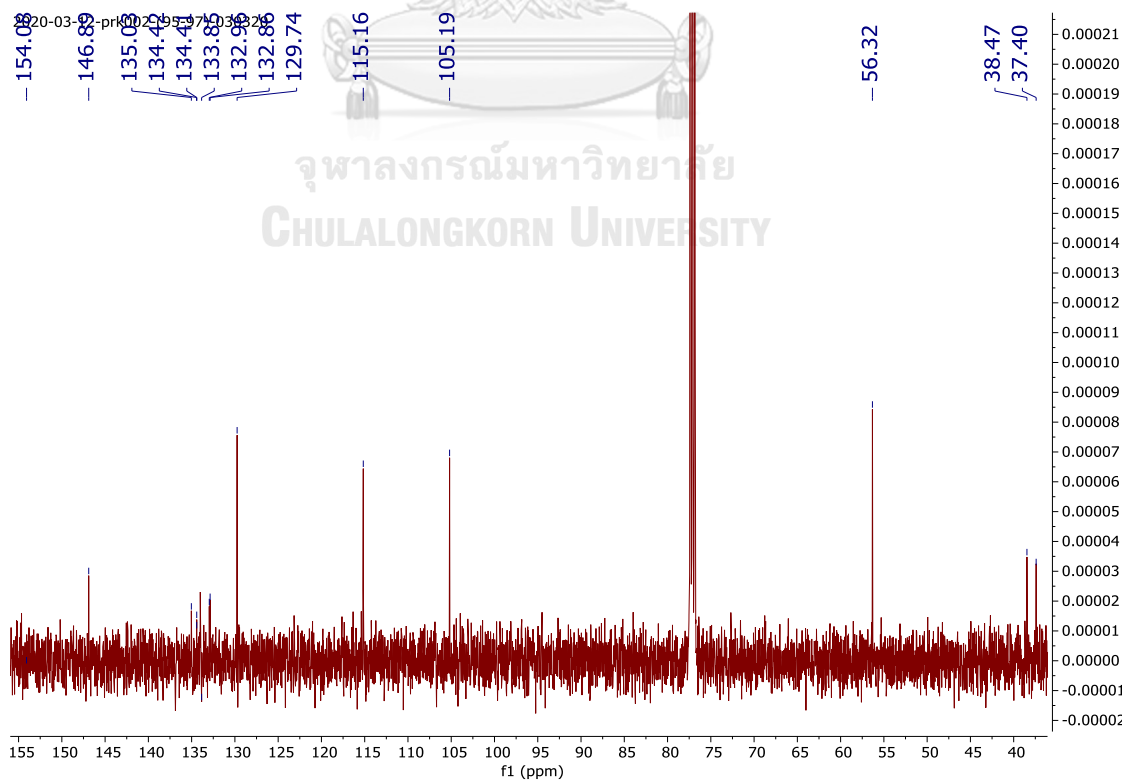
Figure S65. ^1H NMR spectrum (500 MHz, CDCl_3) of compound **11****Figure S66.** ^{13}C NMR spectrum (500 MHz, CDCl_3) of compound **11**

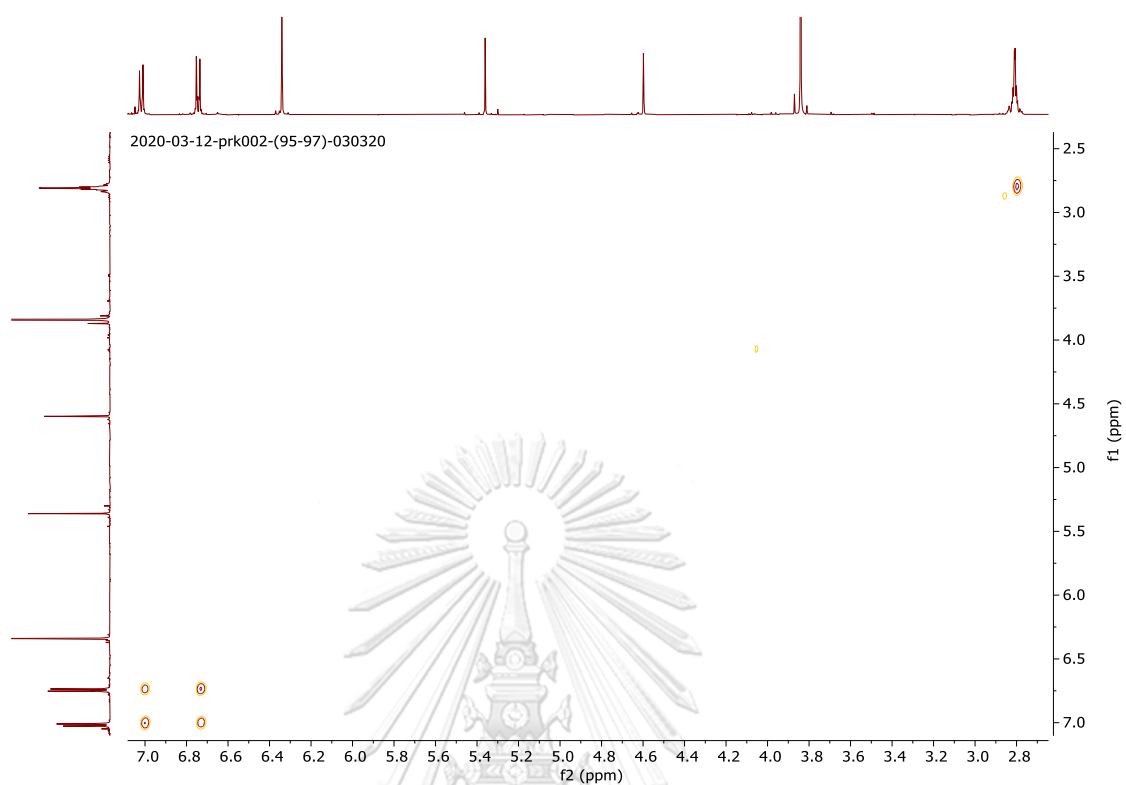
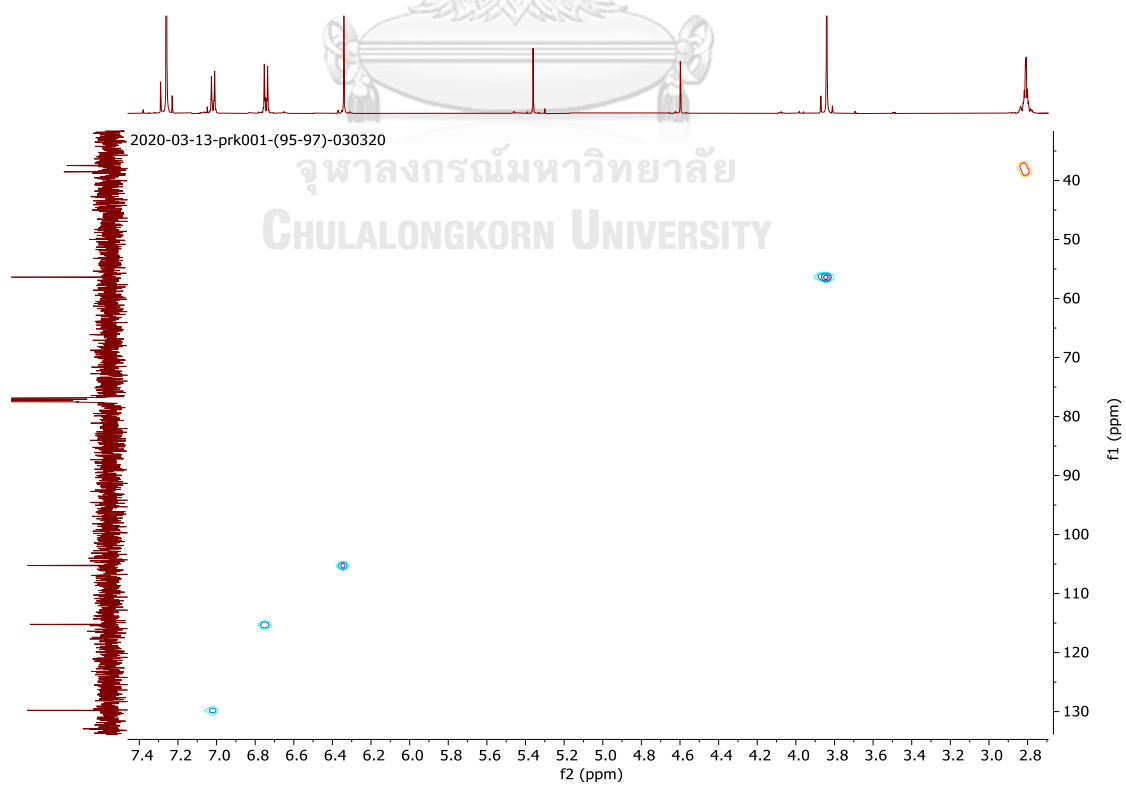
Figure S67. COSY spectrum of compound **11****Figure S68.** HSQC spectrum of compound **11**

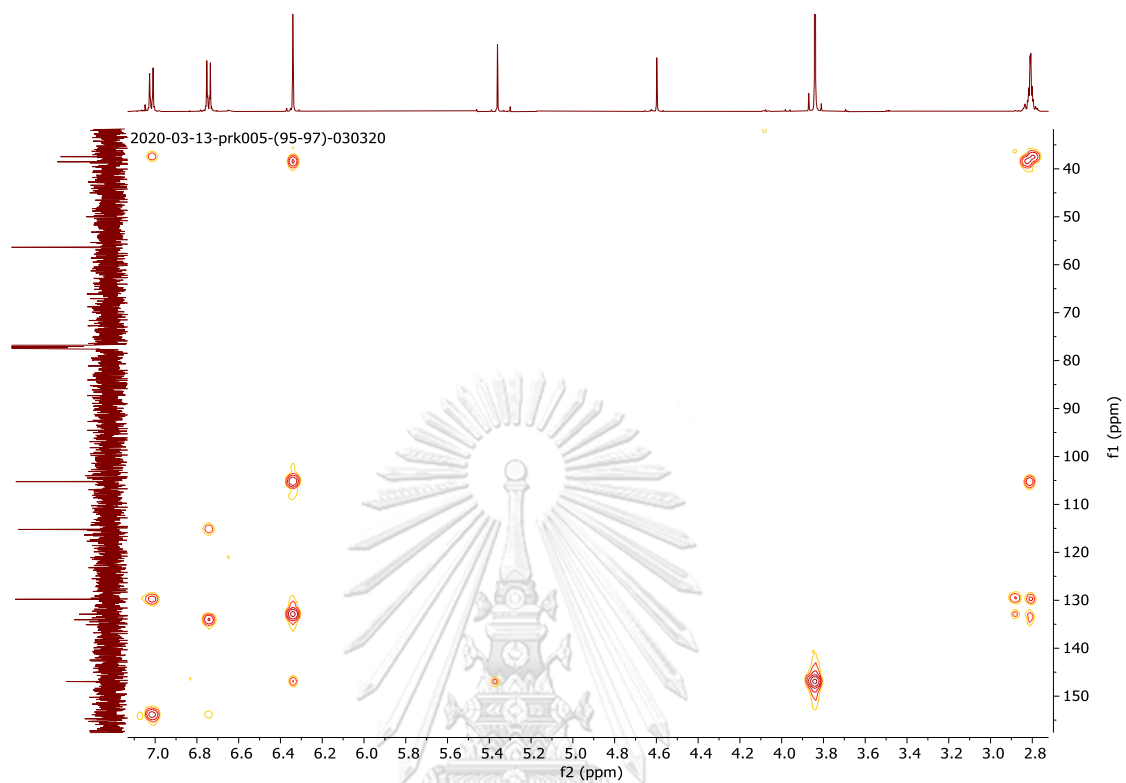
Figure S69. HMBC spectrum of compound **11**

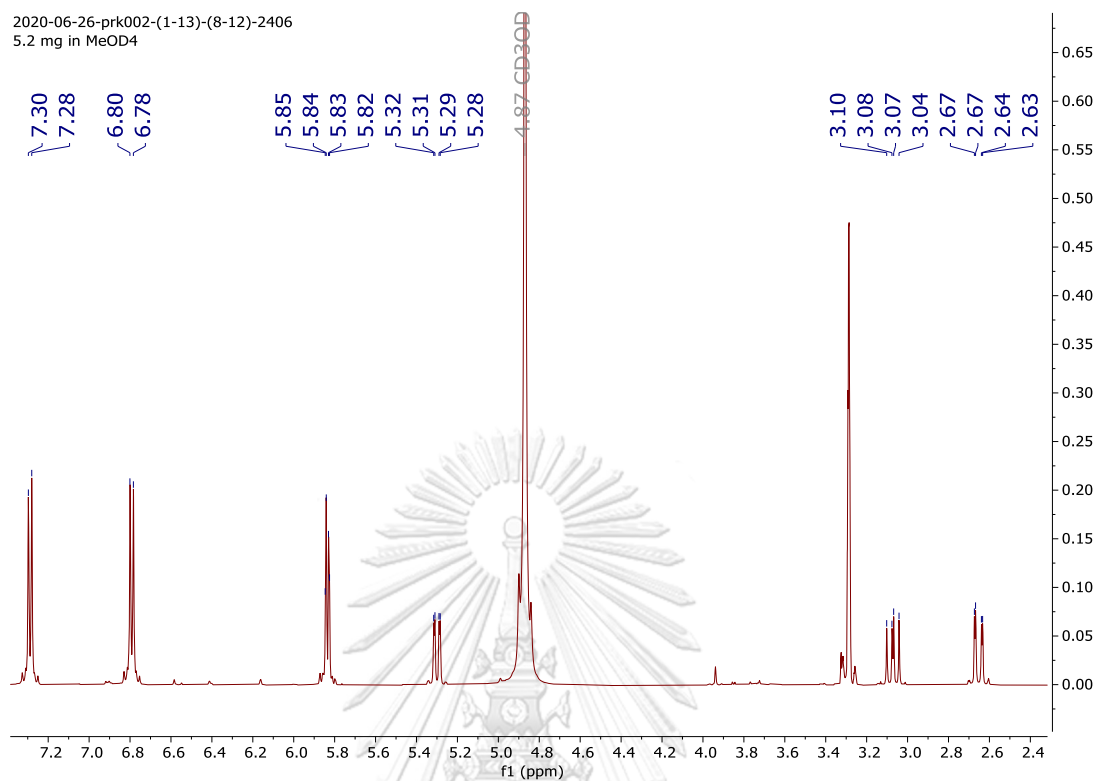
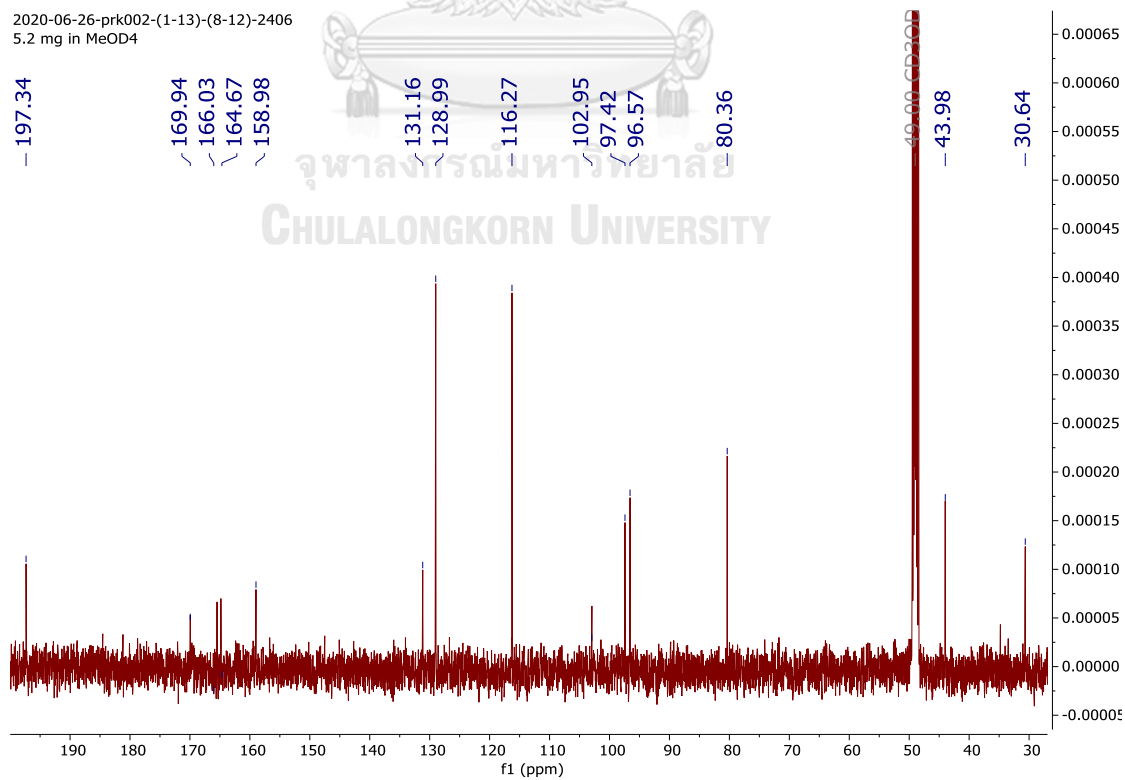
Figure S70. ^1H NMR spectrum (500 MHz, methanol- d_4) of compound **12****Figure S71.** ^{13}C NMR spectrum (125 MHz, methanol- d_4) of compound **12**

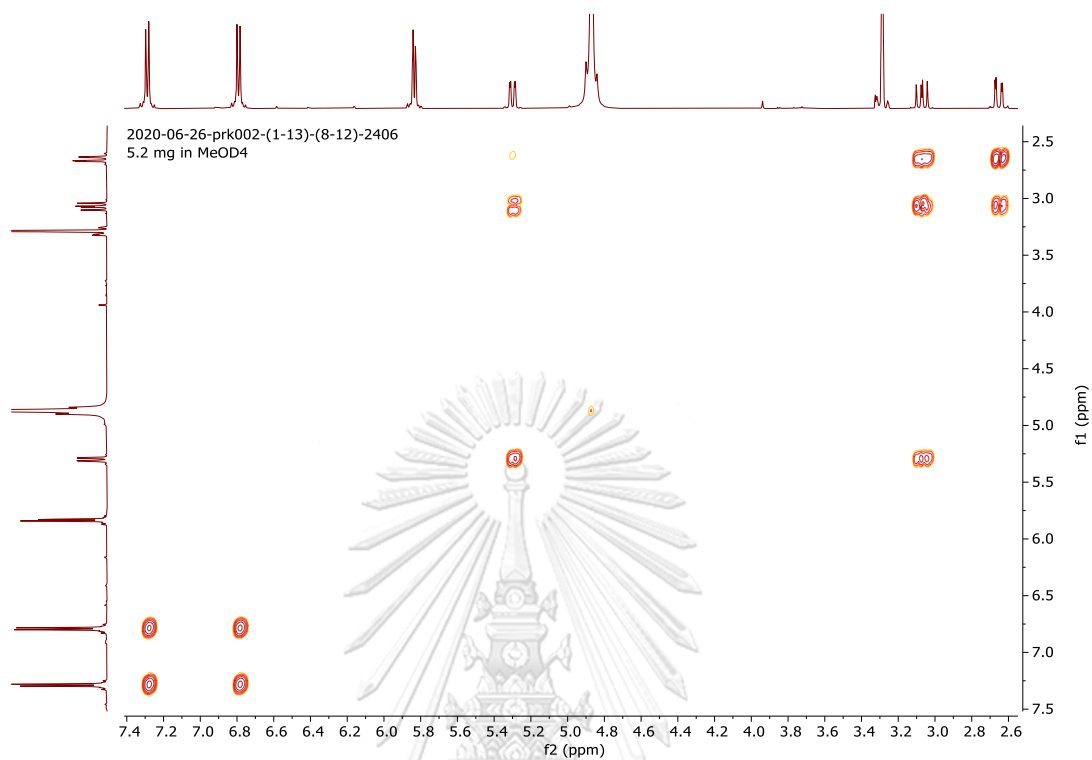
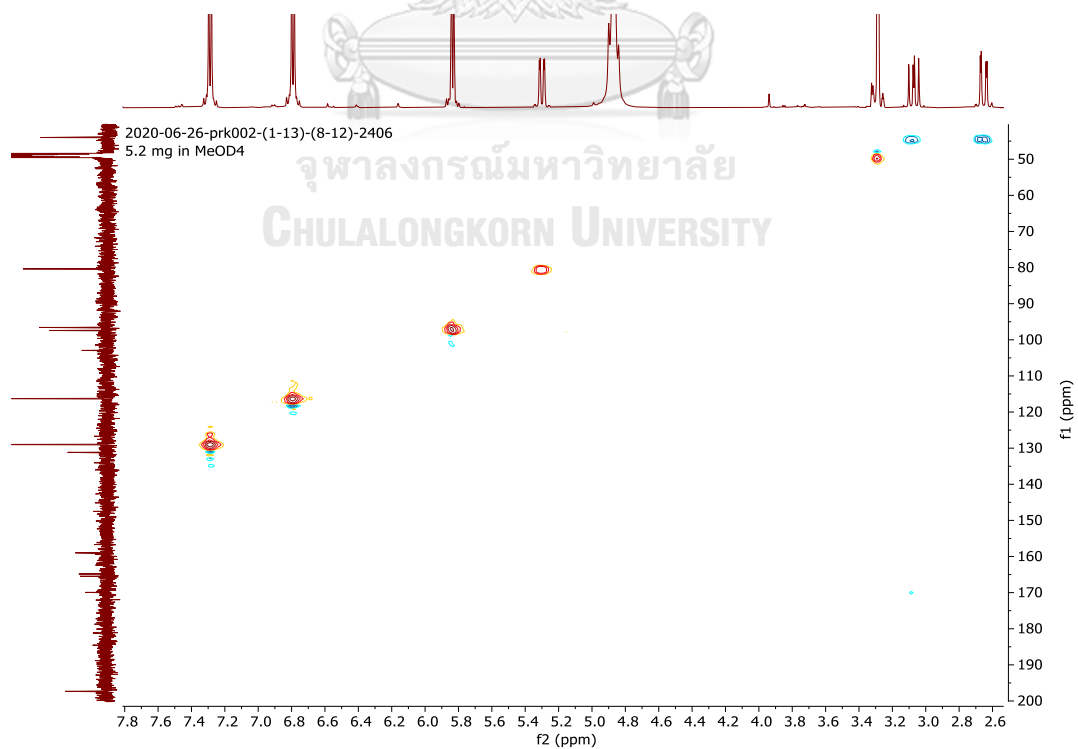
Figure S72. COSY spectrum of compound **12****Figure S73.** HSQC spectrum of compound **12**

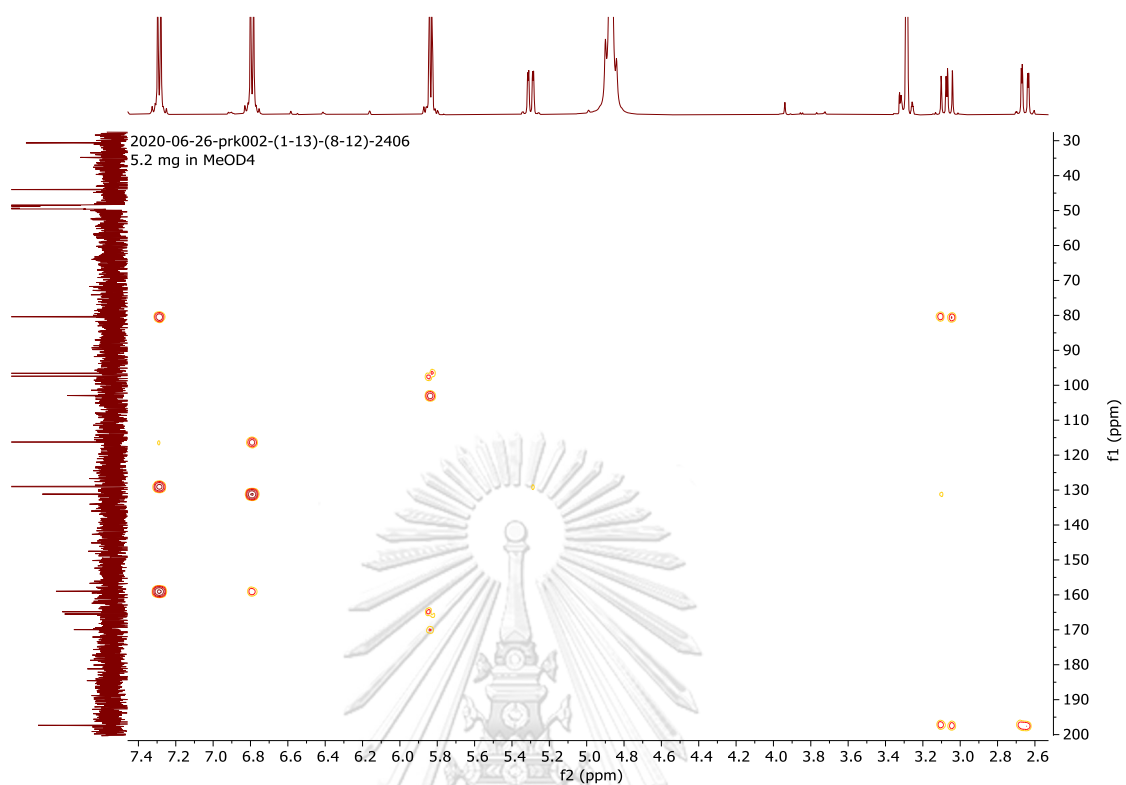
Figure S74. HMBC spectrum of compound **12**

Figure S75. ^1H NMR spectrum (500 MHz, acetone- d_6) of compound **13**

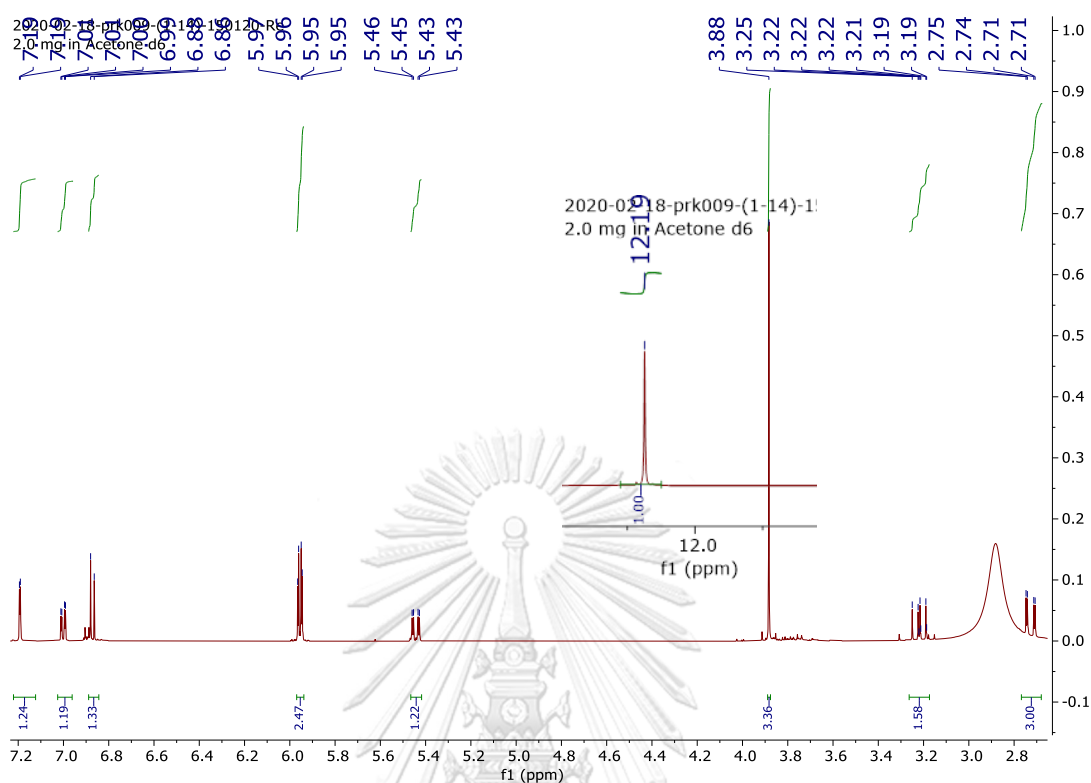


Figure S76. ^{13}C NMR spectrum (125 MHz, acetone- d_6) of compound **13**

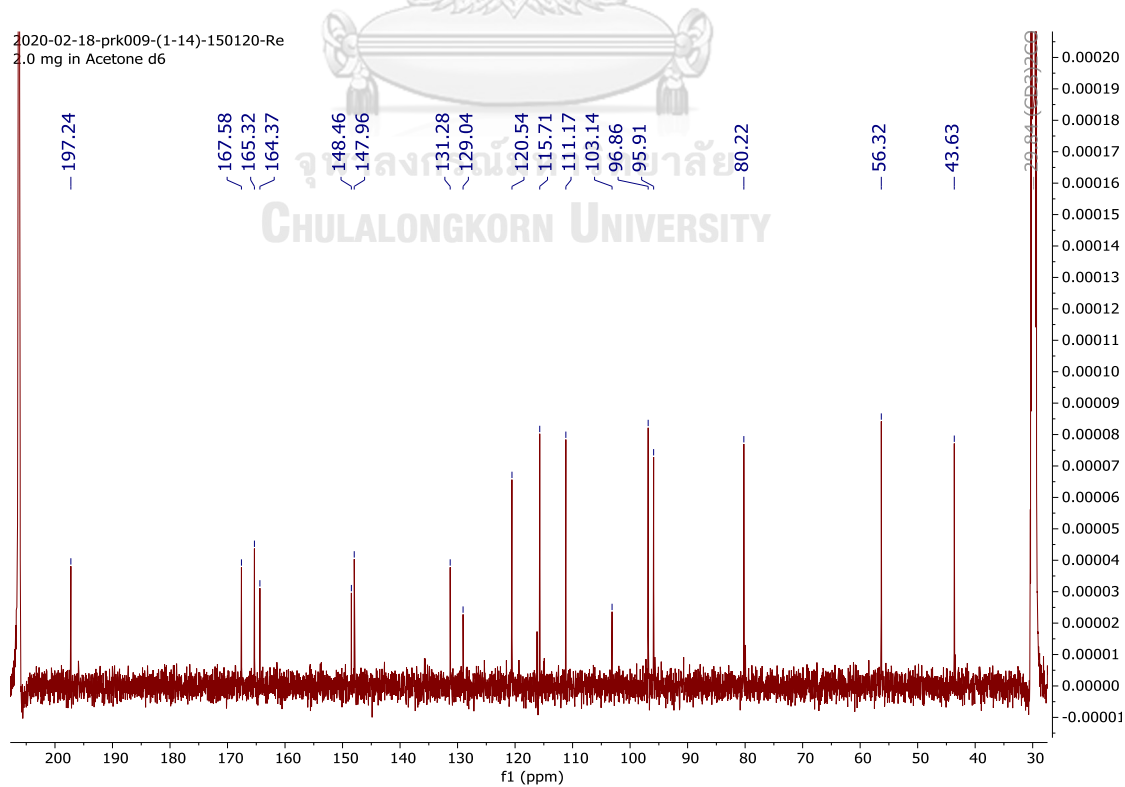


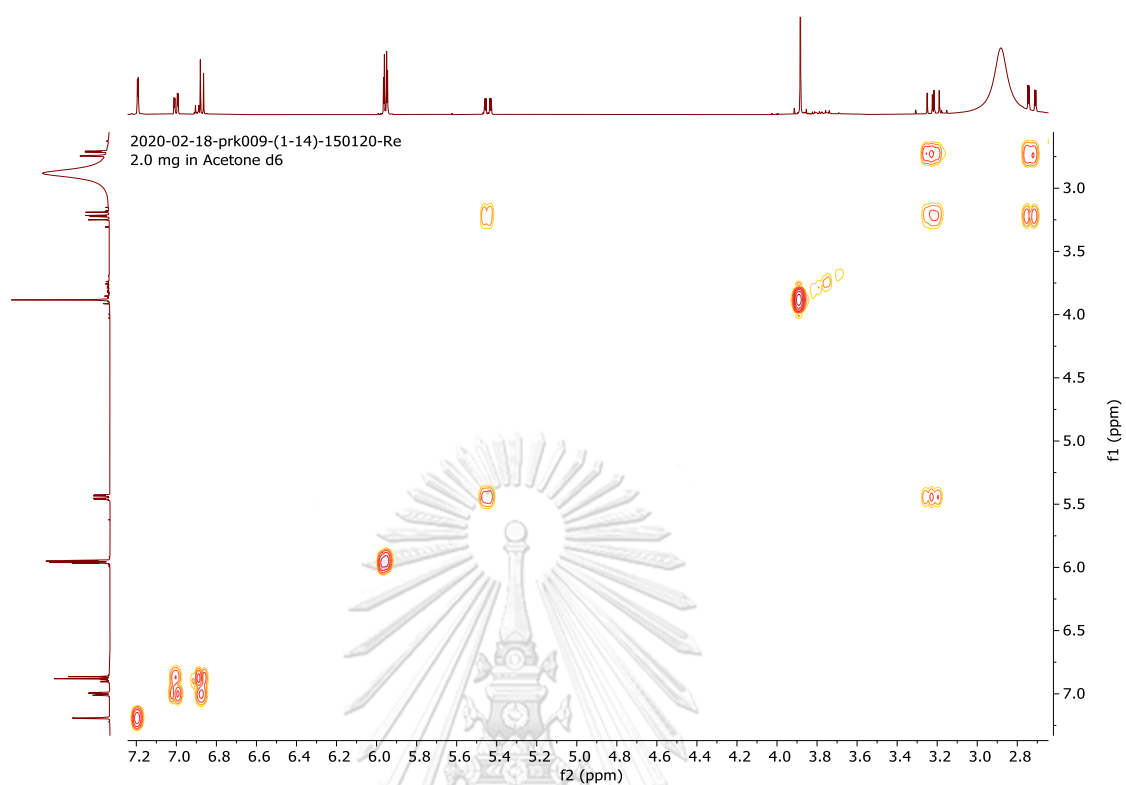
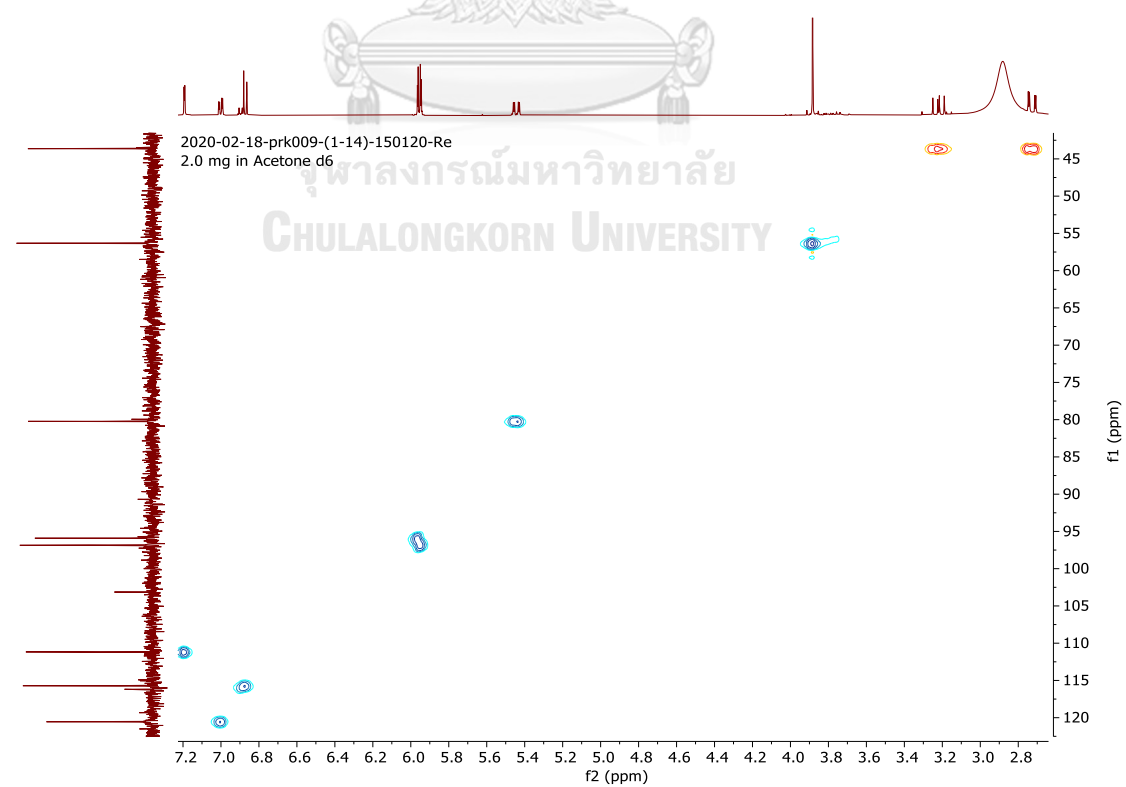
Figure S77. COSY spectrum of compound **13****Figure S78.** HSQC spectrum of compound **13**

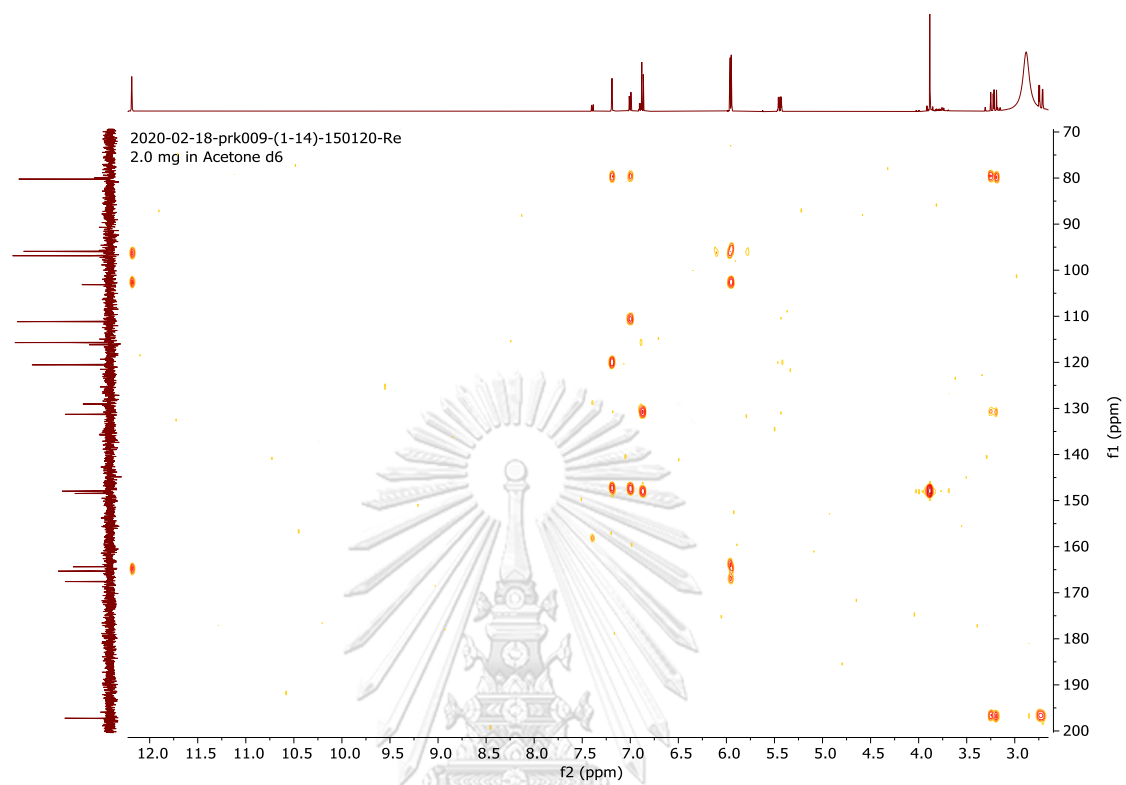
Figure S79. HMBC spectrum of compound **13**

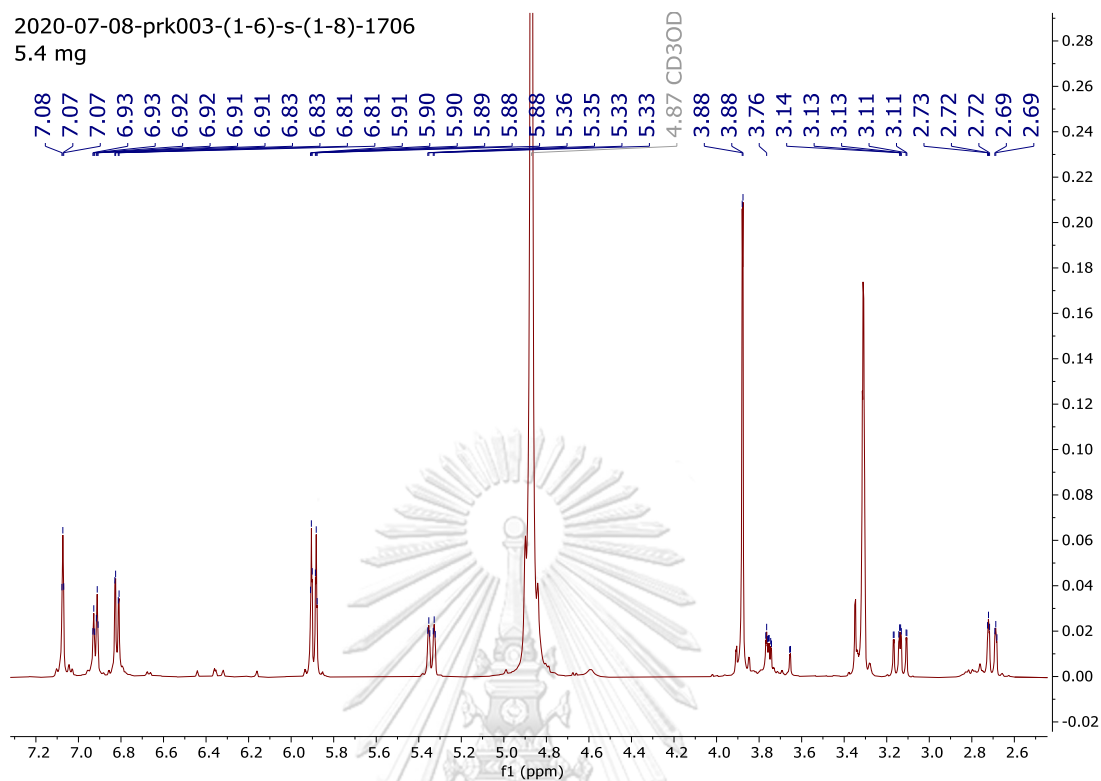
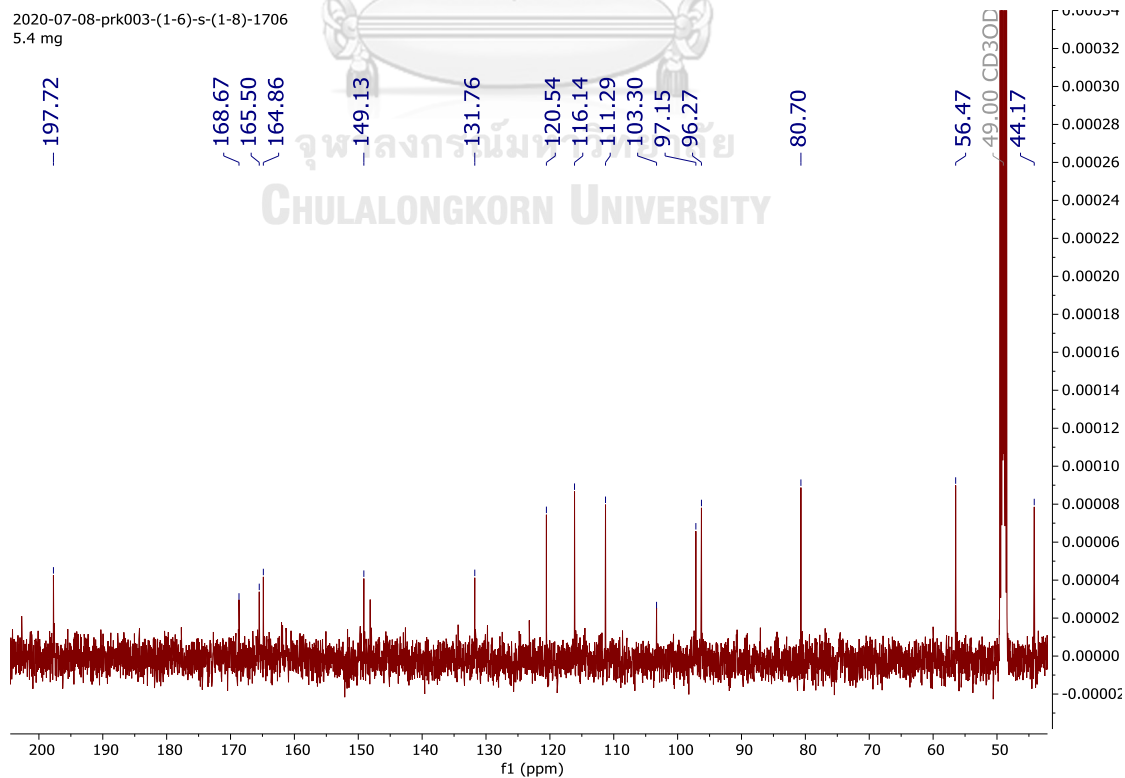
Figure S80. ^1H NMR spectrum (500 MHz, methanol- d_4) of compound **14****Figure S81.** ^{13}C NMR spectrum (125 MHz, methanol- d_4) of compound **14**

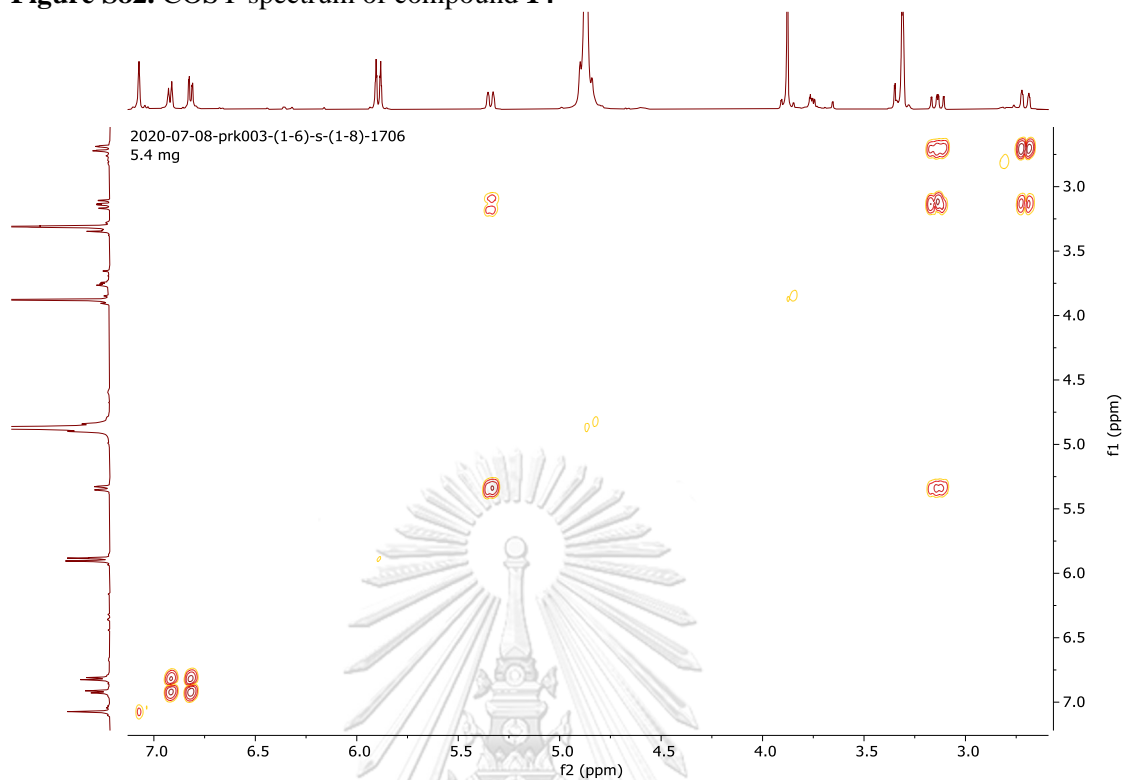
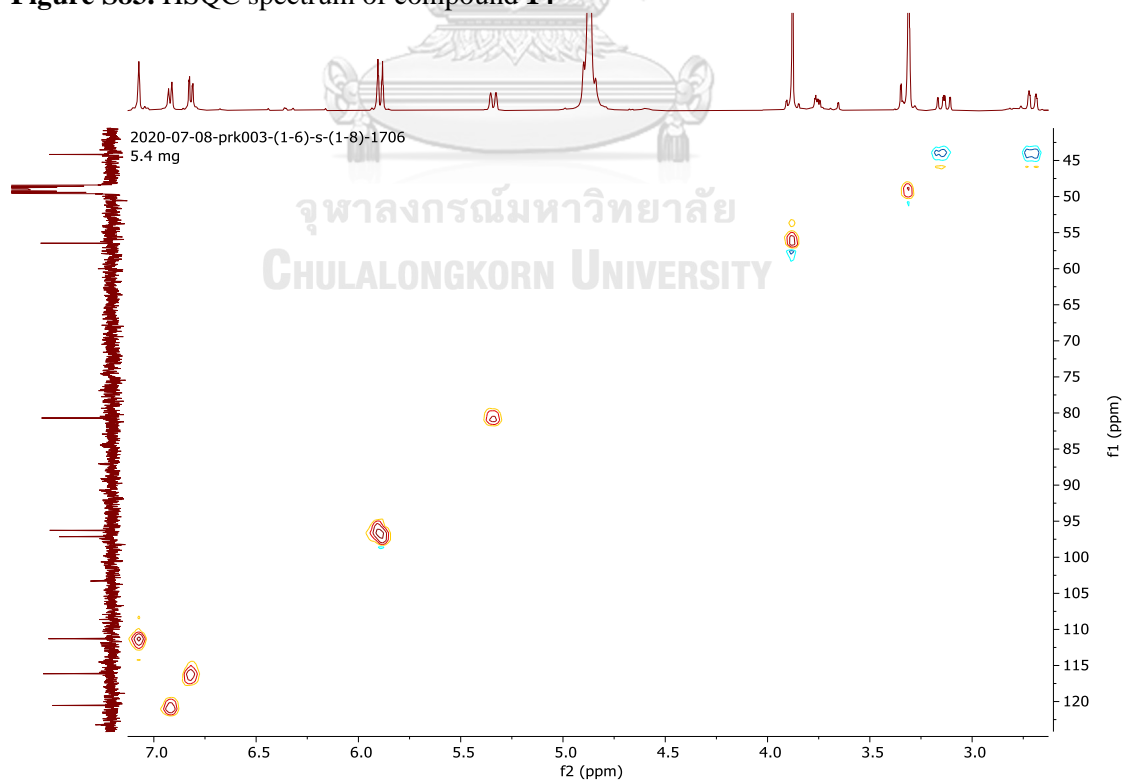
Figure S82. COSY spectrum of compound 14**Figure S83.** HSQC spectrum of compound 14

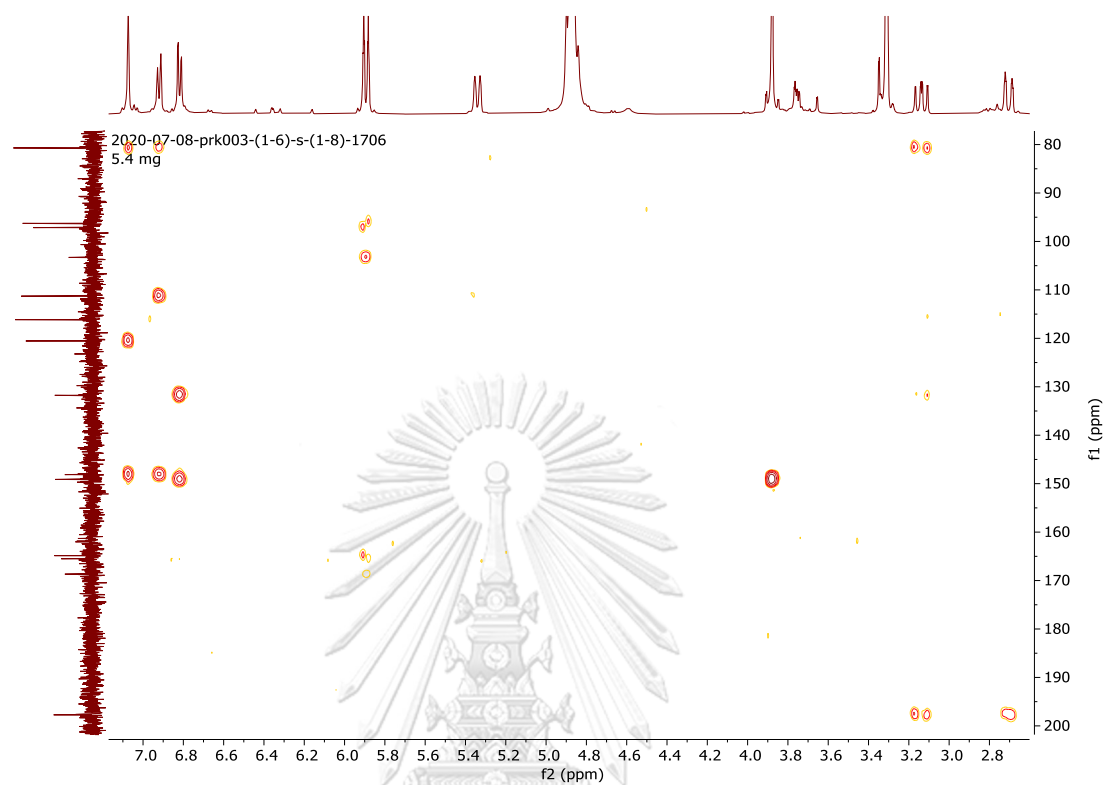
Figure S84. HMBC spectrum of compound **14**

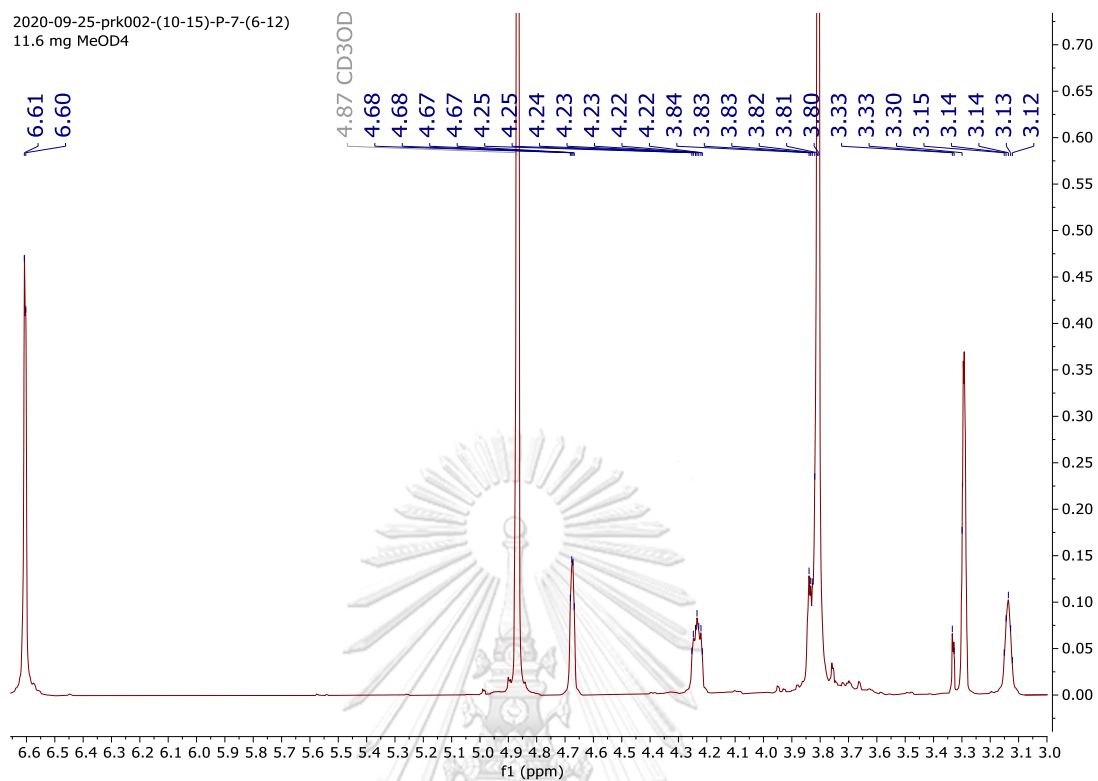
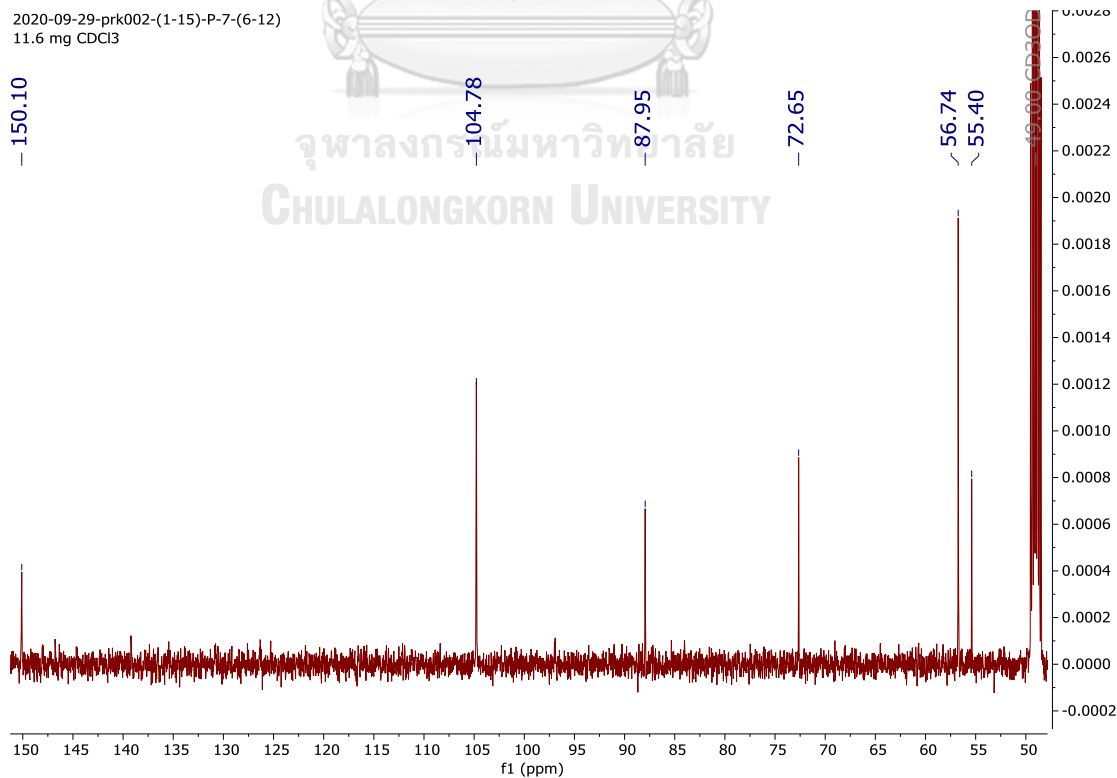
Figure S85. ^1H NMR spectrum (500 MHz, methanol- d_4) of compound **15****Figure S86.** ^{13}C NMR spectrum (125 MHz, methanol- d_4) of compound **15**

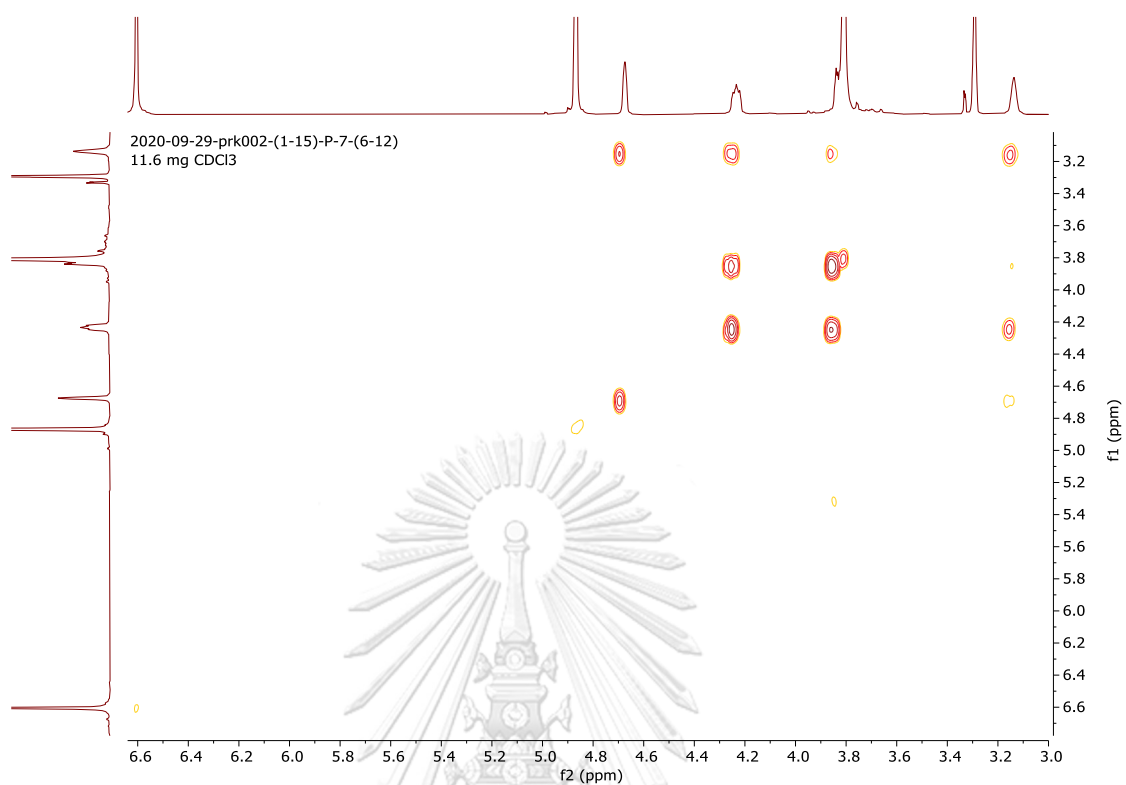
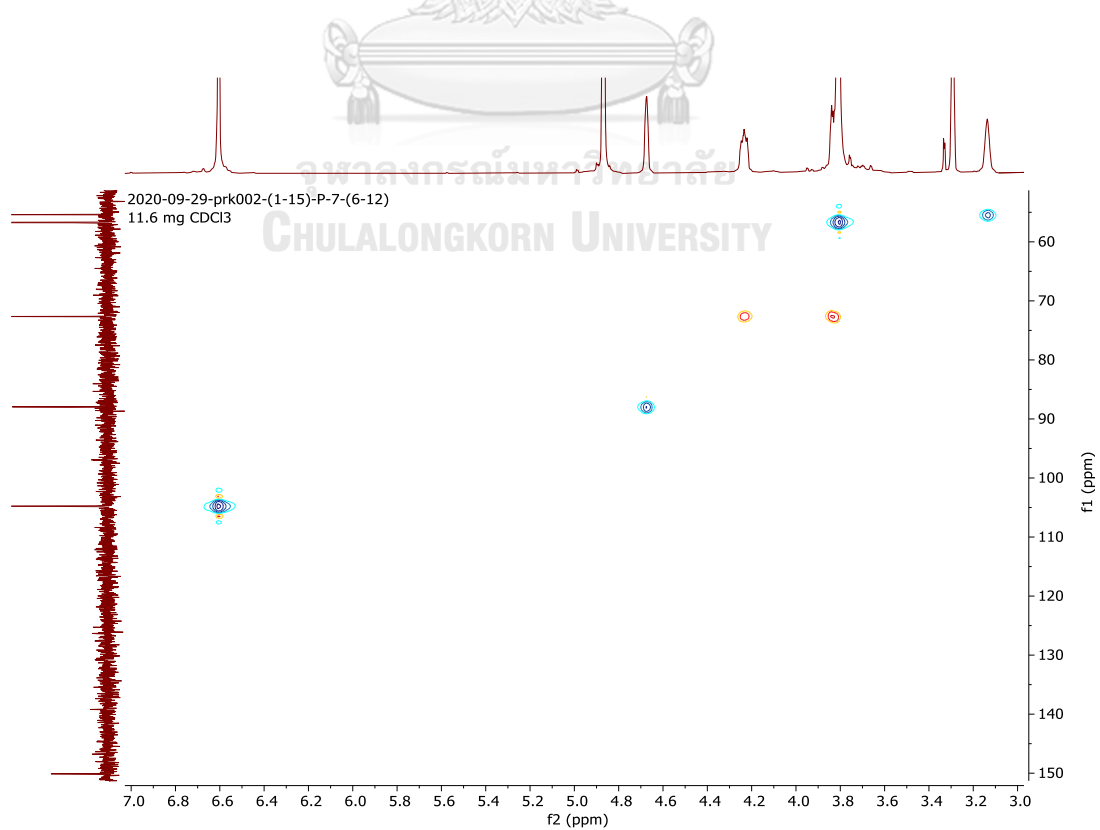
Figure S87. COSY spectrum of compound **15****Figure S88.** HSQC spectrum of compound **15**

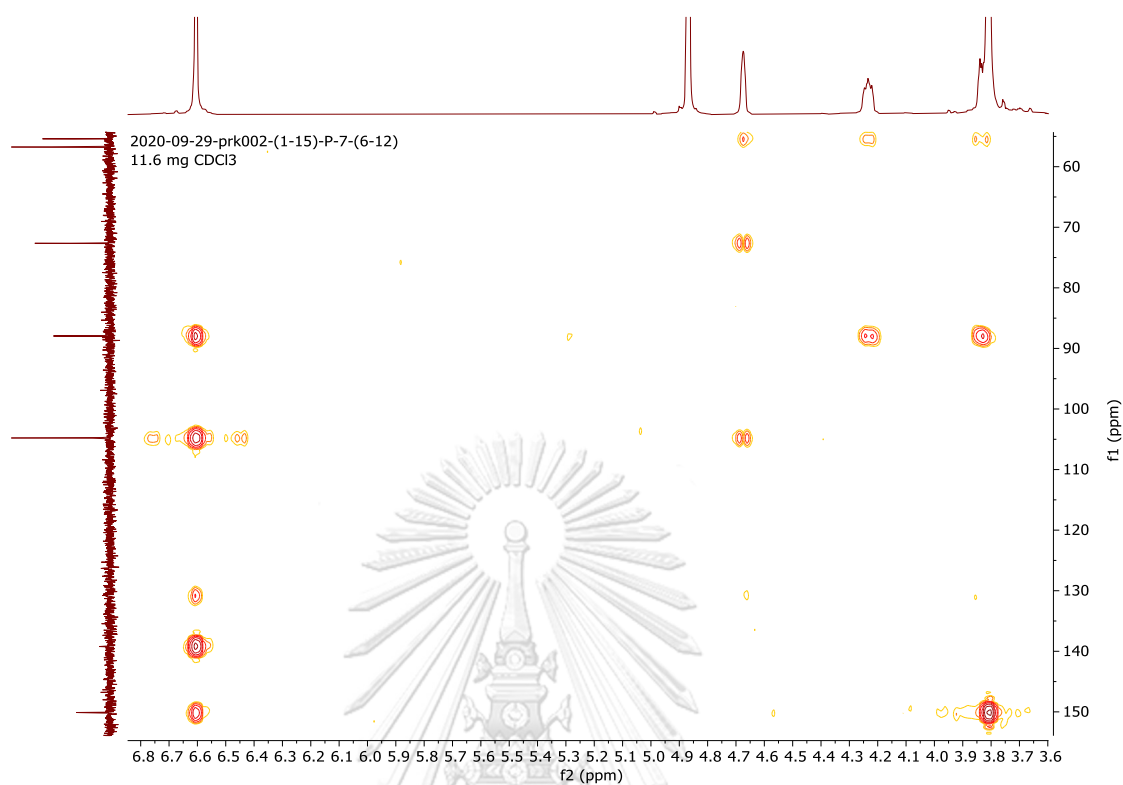
Figure S89. HMBC spectrum of compound **15**

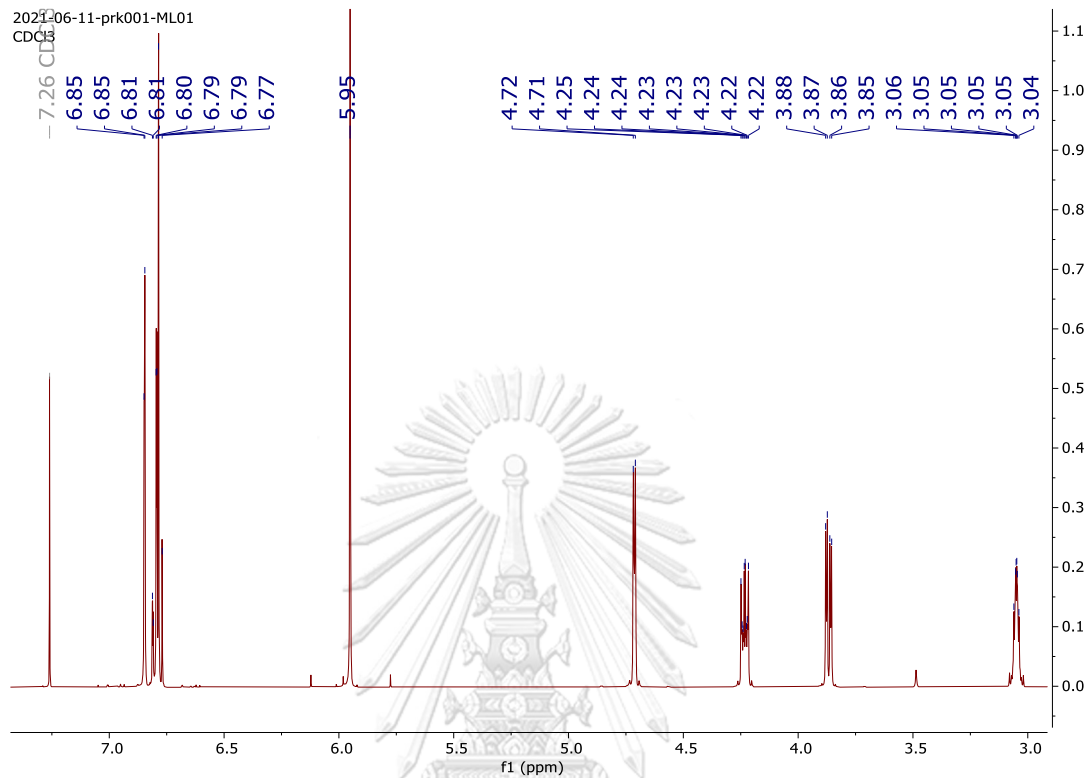
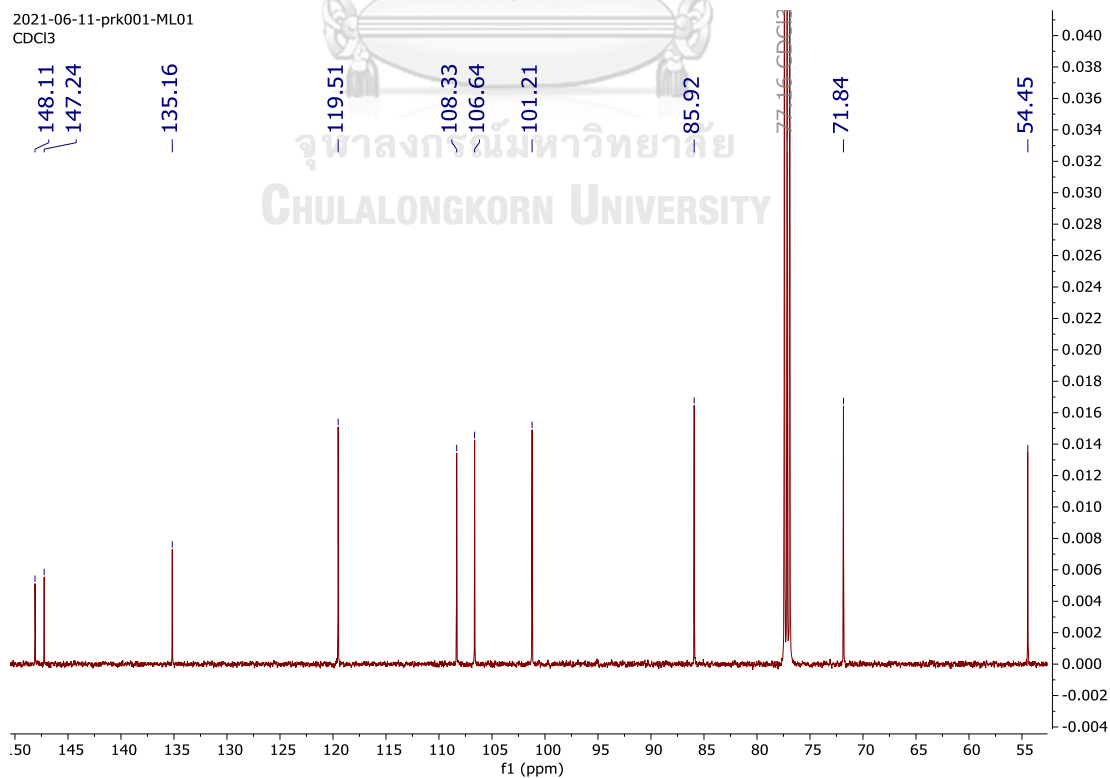
Figure S90. ^1H NMR spectrum (500 MHz, CDCl_3) of compound **16****Figure S91.** ^{13}C NMR spectrum (125 MHz, CDCl_3) of compound **16**

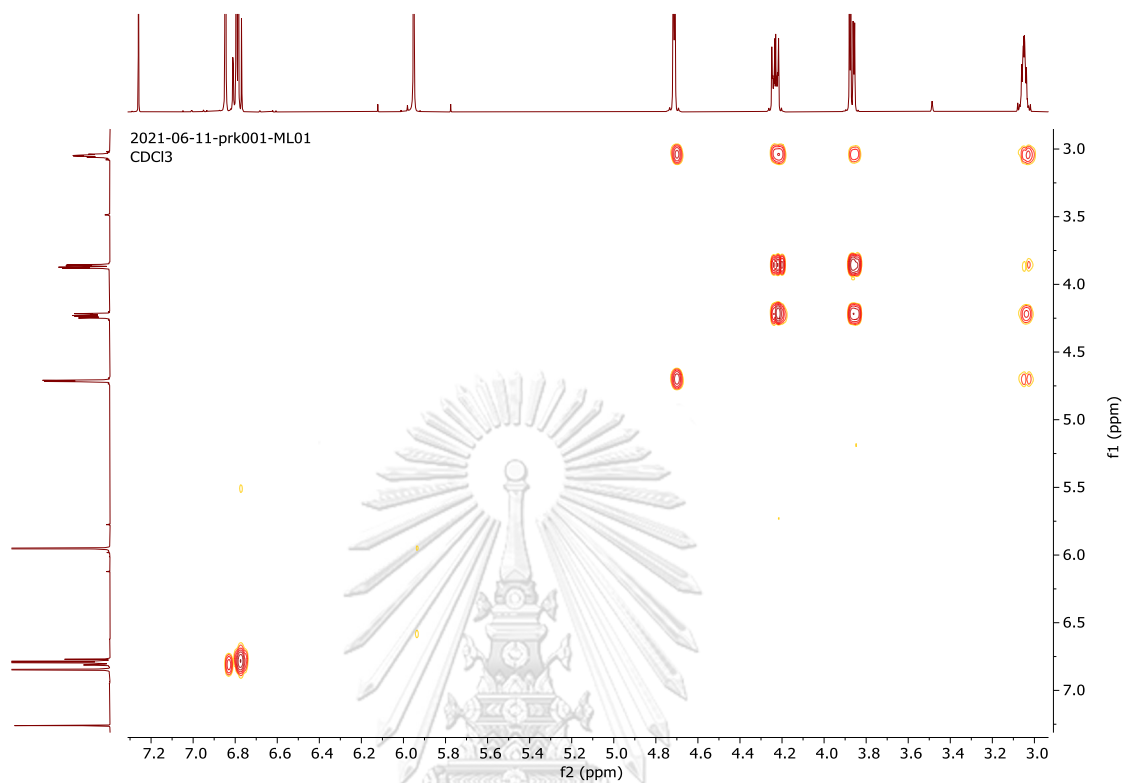
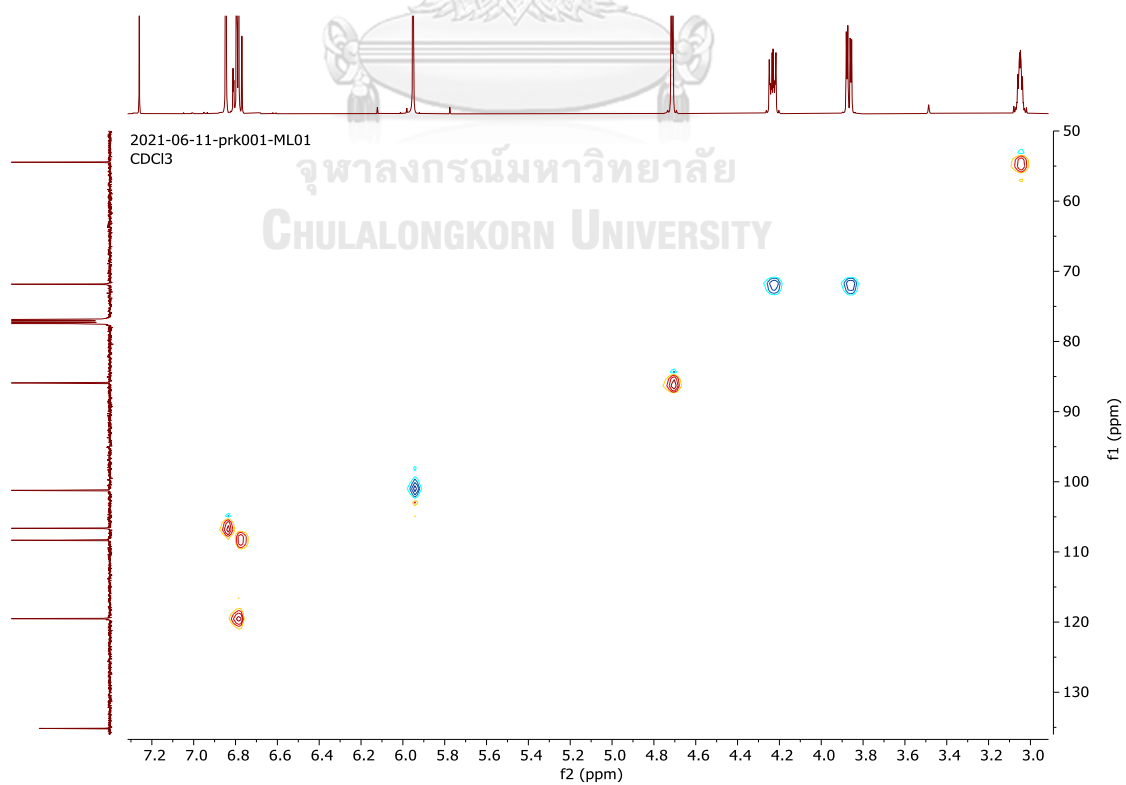
Figure S92. COSY spectrum of compound **16****Figure S93.** HSQC spectrum of compound **16**

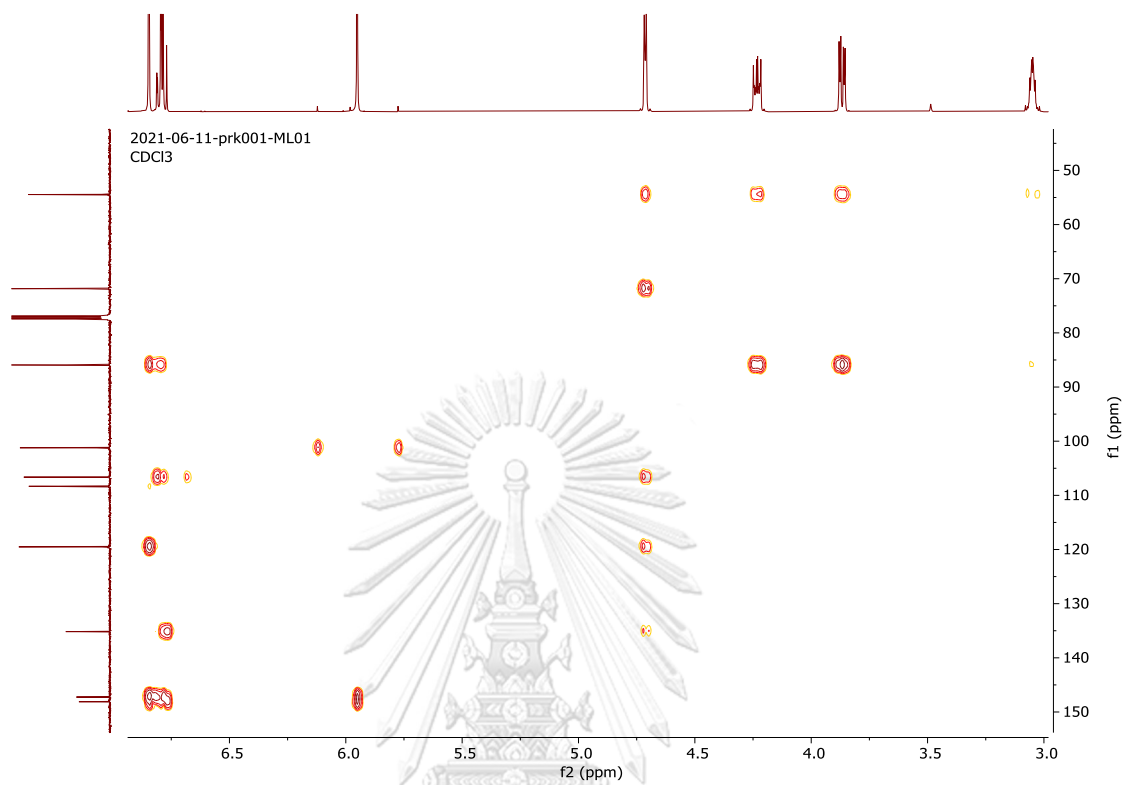
Figure S94. HMBC spectrum of compound **16**

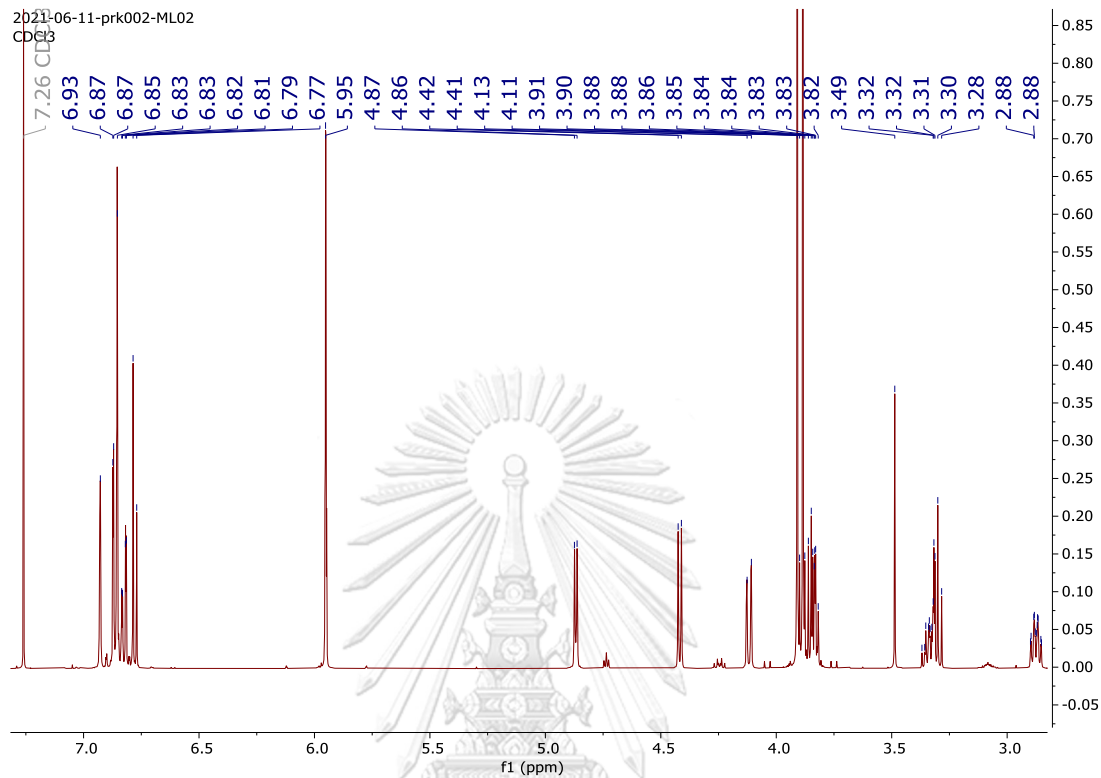
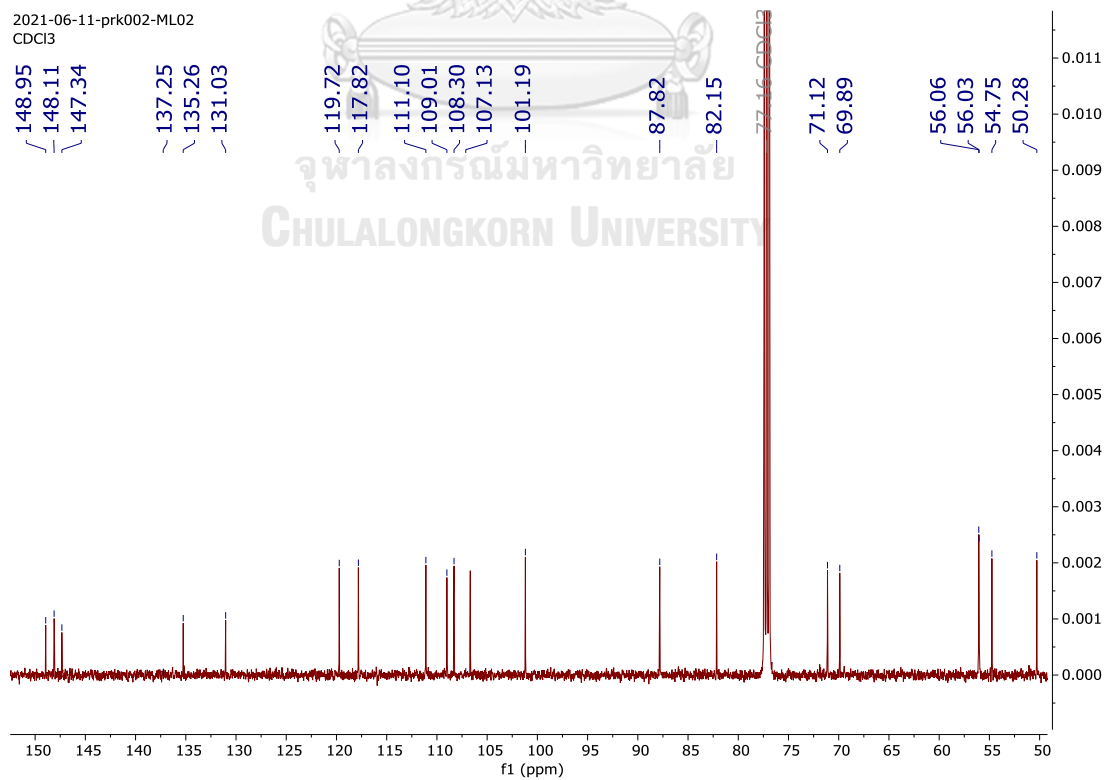
Figure S95. ^1H NMR spectrum (500 MHz, CDCl_3) of compound **17****Figure S96.** ^{13}C NMR spectrum (125 MHz, CDCl_3) of compound **17**

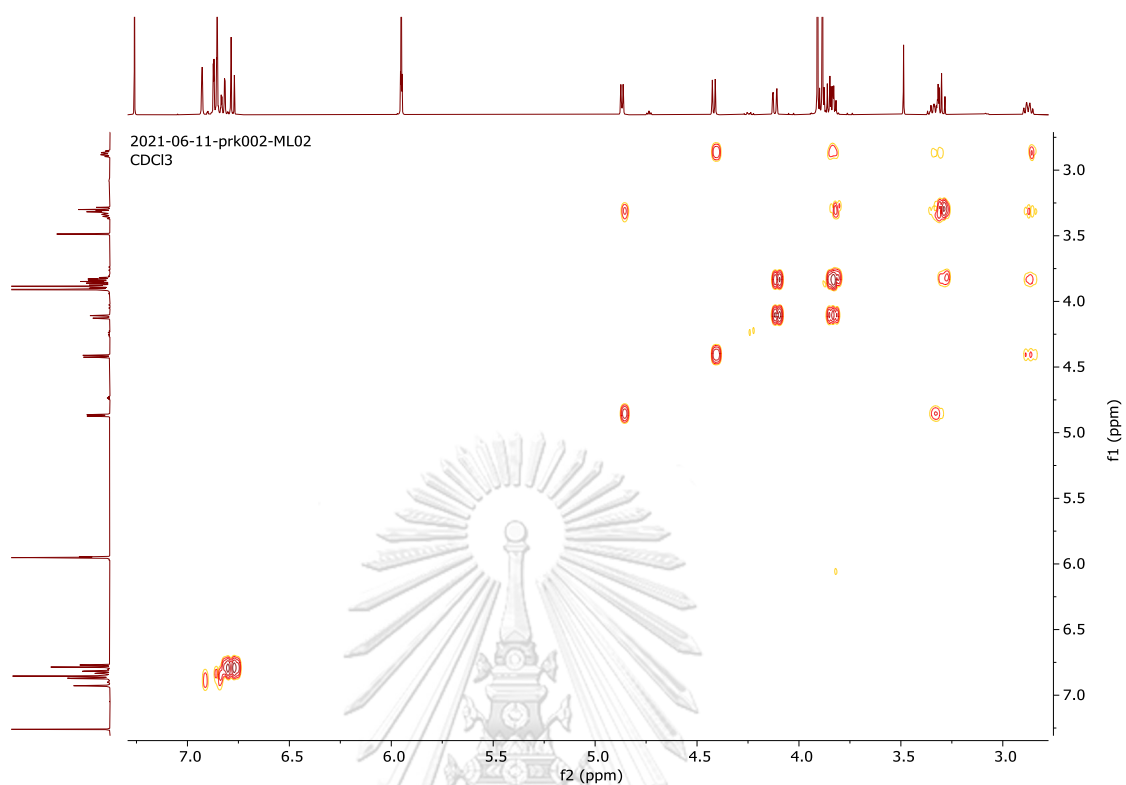
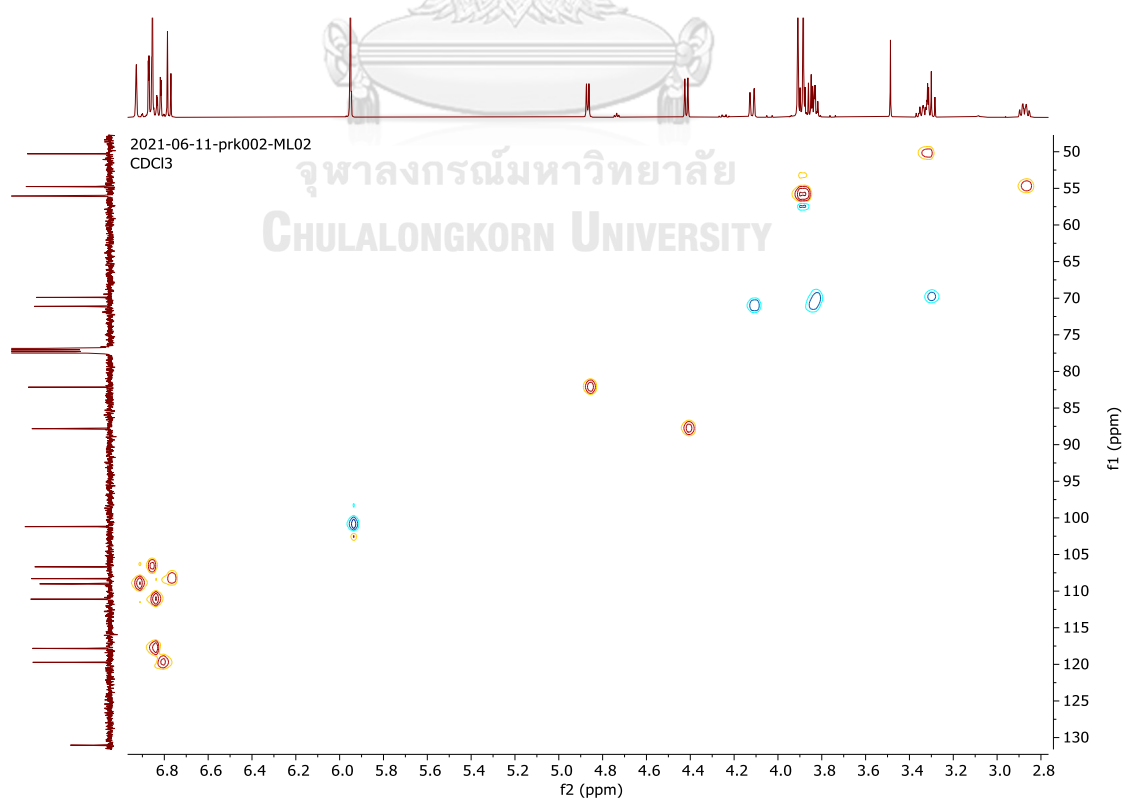
Figure S97. COSY spectrum of compound 17**Figure S98.** HSQC spectrum of compound 17

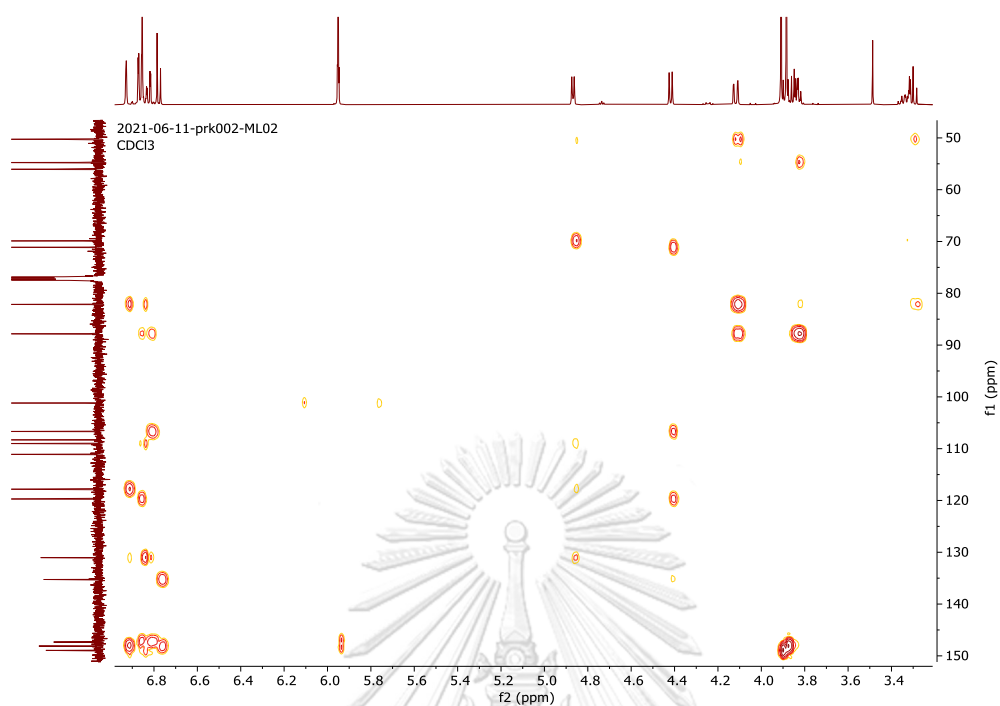
Figure S99. HMBC spectrum of compound **17**

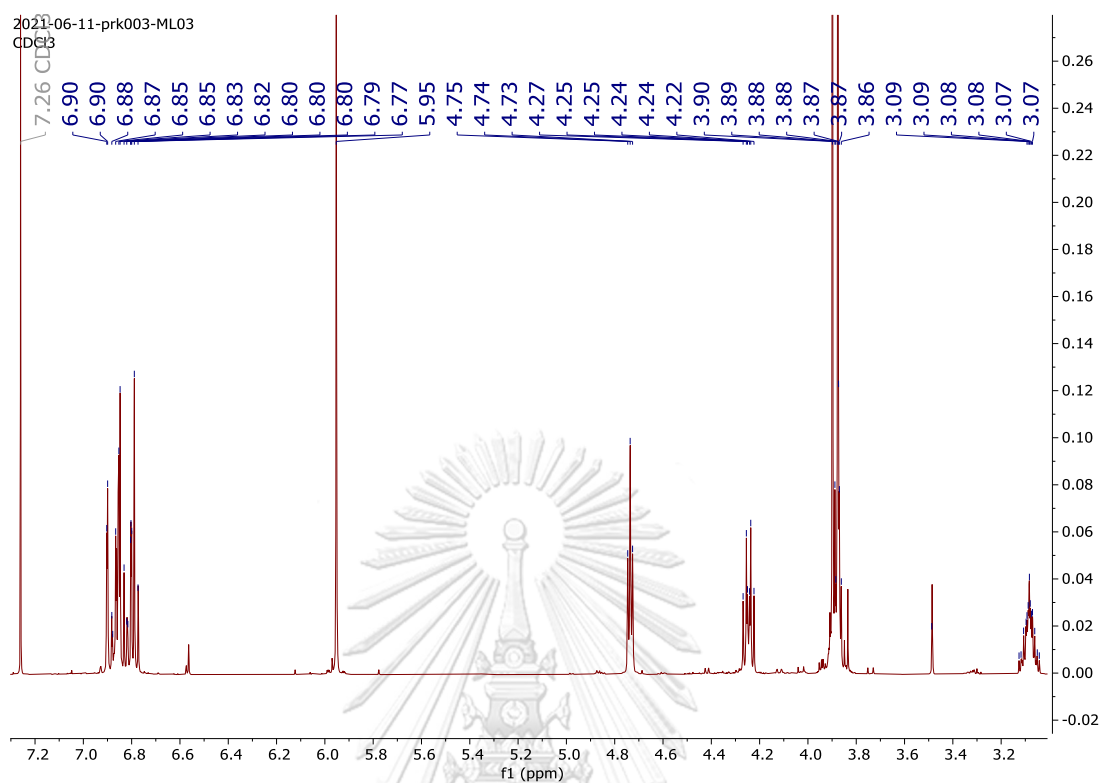
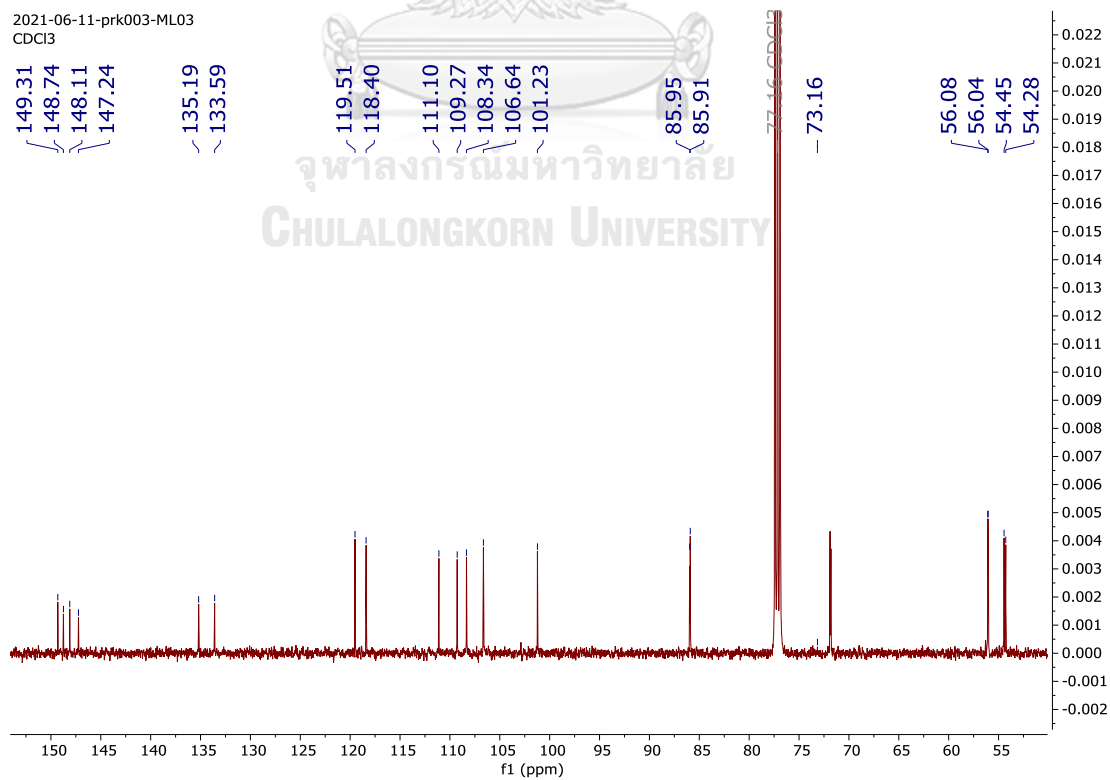
Figure S100. ^1H NMR spectrum (500 MHz, CDCl_3) of compound **18****Figure S101.** ^{13}C NMR spectrum (125 MHz, CDCl_3) of compound **18**

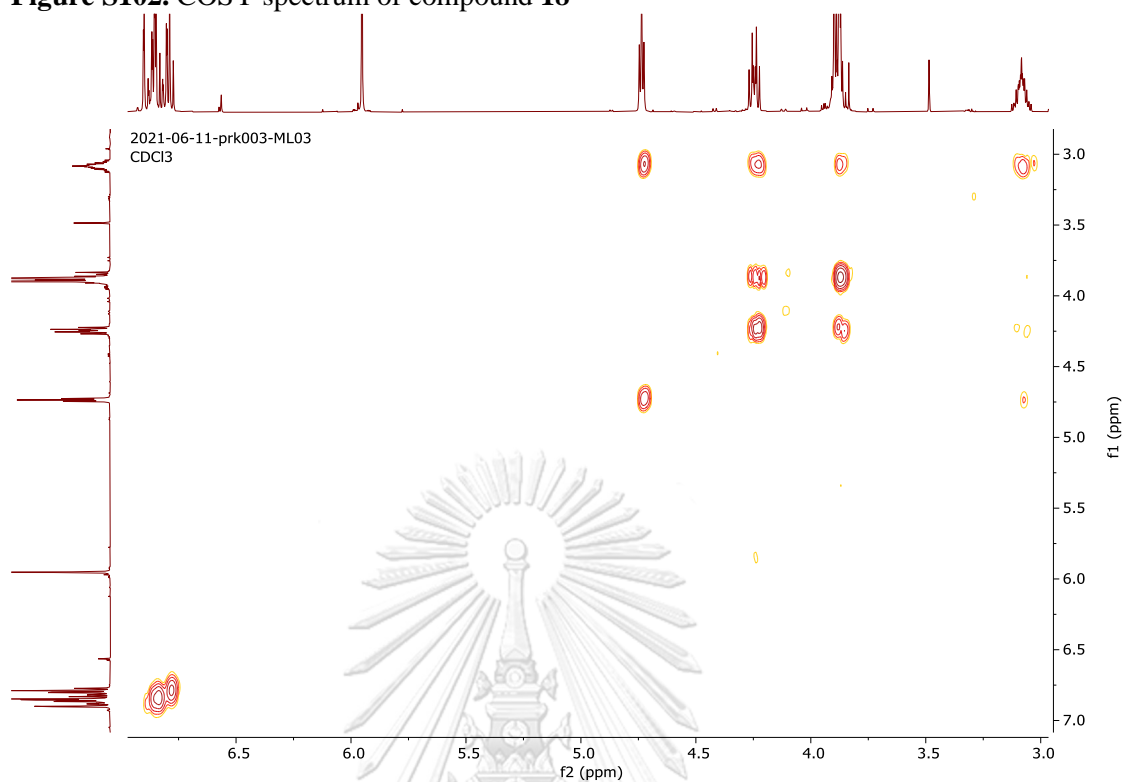
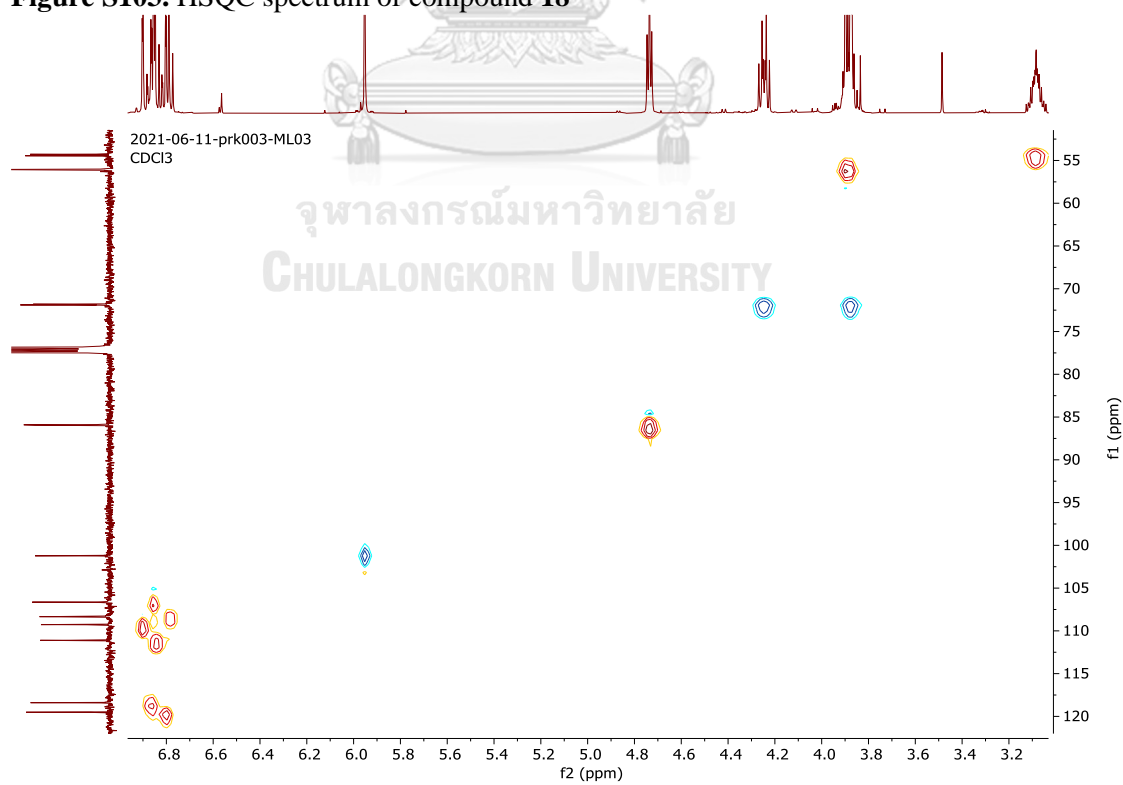
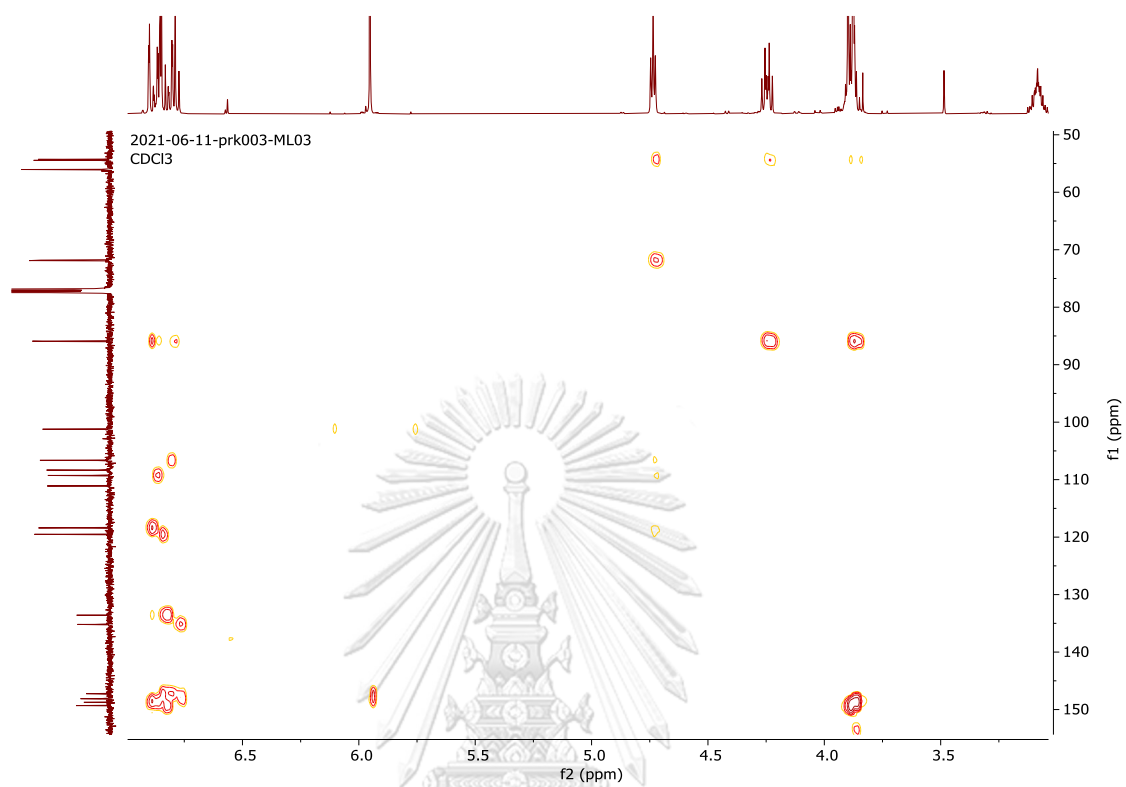
Figure S102. COSY spectrum of compound **18****Figure S103.** HSQC spectrum of compound **18**

Figure S104. HMBC spectrum of compound **18**

VITA

NAME Prajak Khumploy

DATE OF BIRTH 15 June 1995

PLACE OF BIRTH Angthong

INSTITUTIONS ATTENDED Satri Angthong School

HOME ADDRESS Residence of Chulalongkorn University, Phayathai Road,
Pathumwan, Bangkok Thailand, 10330

